The University Of Sheffield.

Post-translational regulation of C_4-related proteins and the regulation of C_4 photosynthesis in leaves of NADP-malic enzyme monocot grasses.

By:

Emmanuel González Escobar

A thesis submitted in partial fulfilment of the requirements for the degree of Doctor of Philosophy.

The University of Sheffield
Faculty of Science
Department of Animal and Plant Sciences

November, 2017

Abstract

C_4 photosynthesis is a complex trait that involves the efficient movement of carbon between mesophyll and bundle sheath cells, but gaps remain in our understanding on how protein phosphorylation regulates the relative flux through malate or aspartate in NADP-malic enzyme subtypes. Using mass spectrometry, 20 phosphosites in NADP-malic enzyme (ME), 9 phosphosites in aspartate aminotransferase (AAT) and 12 phosphosites in alanine aminotransferase were identified in the C_4 plant model *Setaria viridis*. *In silico* analysis shows that NADP-ME phosphorylation at Ser-343 may regulate $NADP^+$ binding.

NADP-ME from illuminated leaves of *Zea mays* exhibited a higher affinity for L-malate at pH 8.4. High *in vitro* activity at pH 7.4 in illuminated leaves of *Sorghum bicolor*, and no change in affinity for L-malate at pH 7.4 or pH 8.4 reveals dependence on enzyme activity immediately after the onset of light. It is speculated that the same protein may be differently regulated in each grass species. The activation of AAT by C_4-acids also differed among the NADP-ME subtypes. Light activation in the presence of L-alanine and L-malate was only evident in *Zea mays*, whereas L-malate and L-alanine inhibited the activity in *Sorghum bicolor* and L-malate inhibited activity in *Setaria viridis*. *In vitro* activity assays also demonstrated that the affinity for L-aspartate was higher in darkened conditions and this activity may not be associated with C_4 photosynthesis.

The work presented in this study shows that there are distinct interspecies differences in the properties of NADP-ME and AAT. These observations are discussed in terms of a regulatory mechanism that controls the relative flux through malate and aspartate in a dual-decarboxylation system of *Zea mays*, but not in *Sorghum bicolor*. Together, these findings add to our understanding of the regulation of C_4 photosynthesis, thereby advancing the wider objective of engineering the C_4 trait into existing C_3 crops.

Acknowledgements

I would like to thank Prof Richard Leegood for giving me the opportunity to conduct this research at The University of Sheffield. I am appreciative of his feedback and support throughout the PhD degree and the writing of this thesis. I am particularly grateful of his patience and constructive criticism, particularly when developing new ideas. I am also appreciative of Dr Karen Bailey, who trained me in immunoblotting. In addition, I would like to thank Prof Carl Smythe, who kept me motivated and invited me to present my work to his research group. I am also grateful of Dr Chatchawal Phansopa for his help in the laboratory, guidance when setting up experiments and reminding me that the PhD degree was not all about the experiments but also about the experience, the people met and the ideas that come from it. I want to thank Dr Richard Beniston and Dr Adelina E. Acosta Martin for their support and training in mass spectrometry. I also appreciate the L3 and L4 project students that helped at various stages of this project. Overall, this research was possible with the continuous support from these individuals, funding by the European Commission (FP7) and discussion meetings held with the 3to4 consortium members.

Declaration

I confirm that this work is all my own, except where clearly indicated. I have referenced all my sources properly.

Abbreviations

List of biological abbreviations and nomenclature

ABC	Ammonium bicarbonate
ACN	Acetonitrile
ADP	Adenosine diphosphate
APS	Ammonium persulfate solution
ATP	Adenosine triphosphate
BLAST	Basic Local Alignment Search Tool
BPB	Bromophenol blue
BSA	Bovine serum albumin
CHAPS	3-[(3-Cholamidopropyl) dimethylammonio]-1-propanesulfonate
CID	Collision induced dissociation
DTT	Dithiothreitol
EDTA	Ethylenediaminetetraacetic acid
FDR	False discovery rate
HEPES	4-(2-hydroxyethyl)-1-piperazineethanesulfonic acid
HPLC	High performance liquid chromatography
IAA	Iodoacetamide
IEF	Isoelectric focusing
IgG	Immunoglobulin G
IPG	Immobilized pH gradient
MOAC	Metal oxide affinity chromatography
MS	Mass spectrometry
NADH	Nicotinamide adenine dinucleotide (reduced form)
NADPH	Nicotinamide adenine dinucleotide phosphate (reduced form)
NCBInr	National Center For Biotechnology Information non-redundant
PAGE	Polyacrylamide gel electrophoresis
PPFD	Photosynthetic photon flux density
ppm	Parts per million
rpkm	Reads per kilobase million
PSM	Peptide spectrum match

SDS	Sodium dodecyl sulfate
TEMED	Tetramethylethylenediamine
TFA	Trifluoroacetic acid
TGS	Tris-glycine-SDS
TiO_2	Titanium dioxide
Tris-Base	Tris(hydroxymethyl) aminomethane
UniProtKB	Universal Protein Knowledgebase
UV	Ultra-violet

Enzymes

AAT	Aspartate aminotransferase
AlaAT	Alanine aminotransferase
GDC	Glycine decarboxylase complex
LDH	Lactate dehydrogenase
MDH	Malate dehydrogenase
ME	Malic enzyme
PEPC	Phospho*enol*pyruvate carboxylase
PEPCK	Phospho*enol*pyruvate carboxykinase (ATP)
PGM	Phosphoglycerate mutase
Rubisco	Ribulose-1,5-bisphosphate carboxylase/oxygenase

Metabolites

2-OG	2-oxoglutarate
Ala	Alanine
Asp	Aspartate
Glu	Glutamate
Mal	Malate
OAA	Oxaloacetate
PGA	Phosphoglycerate
Pyr	Pyruvate
RuBP	Ribulose-1,5-bisphosphate

List of Figures

List of Tables

Table of Contents

Chapter 1

1.1 Food for thought

1.1.1 Agricultural sustainability, energy harvesting and photosynthesis

Agricultural sustainability refers to the agricultural capacity of producing enough food to sustain the population at any given time, while reducing environmental impacts (Hansen, 1996; Mitchell and Sheehy, 2006; Pretty, 2008; Godfray *et al.*, 2010). The concept has received international attention in recent years due to a growing food crisis. As the global population rises, crop production must increase by at least 50% in the next 15 years to meet the minimum requirements to feed the population (Hibberd *et al.*, 2008; Peterhänsel and Offermann, 2012). Today, crop production faces extreme weather patterns brought on by climate change, such as high temperatures and increased rainfall variability (Rosenzweig *et al.*, 2001; McMichael *et al.*, 2006; Gornall *et al.*, 2010). It is evident that increased yields must be achieved using less land, which is declining due to urbanisation (Ramakrishnan, 2001; Zhu *et al.*, 2010) and less water, due to an increase in water demand from cities (Pimentel *et al.*, 1997; Postel, 2000; Pimentel *et al.*, 2004).

The global population has nearly doubled in the last 40 years (Tilman, 1998). During the Green Revolution (1960–2000), crop productivity was increased using improved breeding strategies (rather than genetic manipulation), modernised farming techniques and application of more fertilisers and improved pesticides (Mitchell and Sheehy, 2006), which also resulted in reduced global food prices (Tilman *et al.*, 2002; Evenson and Gollin, 2003). By the beginning of the 21st century, crop productivity rose 208% for wheat (*Triticum aestivum*), 109% for rice (*Oryza sativa*) and 157% for maize (*Zea mays*) (Pingali, 2012). However, at the rate that the current population is growing, projected yields are not enough to sustain developing countries. Furthermore, acquisition of farmland for bioenergy crop production (i.e. biofuels) will reduce the accessibility of land for agricultural use (Tokgoz *et al.*, 2012; Popp *et al.*, 2014; Vasile *et al.*, 2016). The future of agriculture relies on the improvement of farmland management, enhanced use of technology as well as genetically enhanced crops (Tilman *et al.*, 2002).

A consensus in the scientific community has called for a second Green Revolution, with hopes to create genetically enhanced crop plants. These should withstand the adverse effects of climate change, grow with fewer additives such as nitrogenous fertilisers and efficiently use photosynthetically active radiation (PAR) to assimilate CO_2 into carbohydrates during photosynthesis (Zhu *et al.*, 2010; Covshoff and Hibberd, 2012; Leegood, 2013).

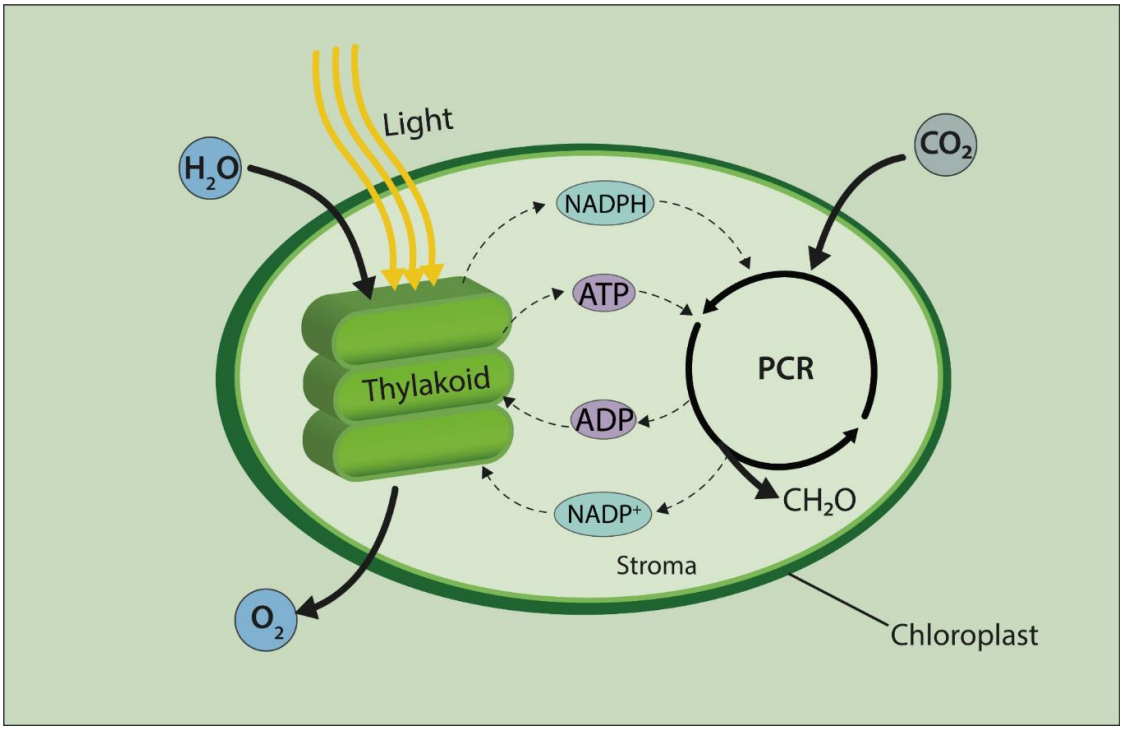

Fig. 1.1. Overview of photosynthesis in higher plants. In higher plants photosynthesis takes place inside chloroplasts. Captured energy is used to form ATP and NADPH. In the stroma of the chloroplast, ATP and NADPH are utilised by enzymes in the photosynthetic carbon reduction (PCR) cycle to fix CO_2 into carbohydrates (CH_2O).

Increasing the efficiency of photosynthesis in major food crops is the most feasible long-term solution that could mitigate the food crisis (Mitchell and Sheehy, 2006; Zhu *et al.*, 2010; Covshoff and Hibberd, 2012). Photosynthesis has two phases: the light harvesting and the photosynthetic carbon reduction (PCR) cycle (Figure 1.1). During the day, solar energy is intercepted by chlorophyll-containing, light-harvesting complexes embedded in chloroplast thylakoid membranes, resulting in the splitting of water and release of O_2 (Candau *et al.*, 1976; Kühlbrandt and Wang, 1991; McEvoy *et al.*, 2005). Harvested energy is then used for the formation of ATP and reducing equivalents, which are used in the PCR cycle for the formation of carbohydrates.

1.2 The inefficiency of C_3 photosynthesis

1.2.1 The problem with Rubisco and photorespiration

All photosynthetic species use ribulose-1,5-bisphosphate carboxylase/oxygenase (Rubisco) for carbon fixation. In C_3 plants, carbon fixation is limited by the inefficiency of Rubisco, which has a low turnover rate and competing specificity for CO_2 and O_2 binding (Portis and Parry, 2007; Raines, 2011). During photosynthesis, Rubisco fixes atmospheric CO_2 through the carboxylation of ribulose-1,5-bisphosphate (RuBP) forming two molecules of 3-phosphoglycerate (3-PGA) (Sage, 1999). Rubisco also catalyses the oxygenation of RuBP, in an unfavourable and unavoidable side reaction with O_2, forming 3-PGA and 2-phosphoglycollate, the latter which cannot be utilised in the PCR cycle (Figure 1.2) and may be toxic in high concentrations (Ogren, 1984; Andrews and Lorimer, 1987; Maurino and Peterhänsel, 2010). To prevent the accumulation of 2-phosphoglycollate, the compound is removed from the chloroplast and metabolised into organic compounds, using energy and 25% of assimilated carbon (Björkman *et al.*, 1969; Ehleringer and Björkman, 1977; Bauwe *et al.*, 2010), in the process of photorespiration (Figure 1.3). Most importantly, the carbon present on 2-phosphoglycollate must be recycled back to the PCR cycle as efficiently as possible.

Although Rubisco has a higher affinity for CO_2 (K_M 9.7 µM), than O_2 (K_M 244 µM) (Cousins *et al.*, 2010), the CO_2 concentration inside the chloroplast is about 1000-fold lower than that of O_2 (Ehleringer *et al.*, 1991). Furthermore, in warm climates, the oxygenase activity of Rubisco increases relative to the carboxylase activity, both because the relative solubility of dissolved O_2 is greater than that of dissolved CO_2, thus lowering the ratio of dissolved CO_2 to O_2 in the chloroplast and because the kinetic properties of Rubisco alter in response to increasing temperature, thereby increasing its affinity for O_2 (Ku and Edwards, 1977; Chen and Spreitzer, 1992; Tcherkez *et al.*, 2006; Leegood, 2013; Buchanan *et al.*, 2015). In addition, the diffusion of CO_2 to the site of Rubisco is reduced when stomata close to prevent the loss of water through transpiration in high temperatures (Sage, 2004; Schulze *et al.*, 2013). The loss of CO_2 near the site of Rubisco can reduce photosynthetic efficiency from 20–40% and increases in unfavourable

conditions such as warm temperatures (above 30 °C) and arid climates (Jordan and Ogren, 1984; Sharkey, 1988; Ehleringer *et al.*, 1991; Gowik and Westhoff, 2011).

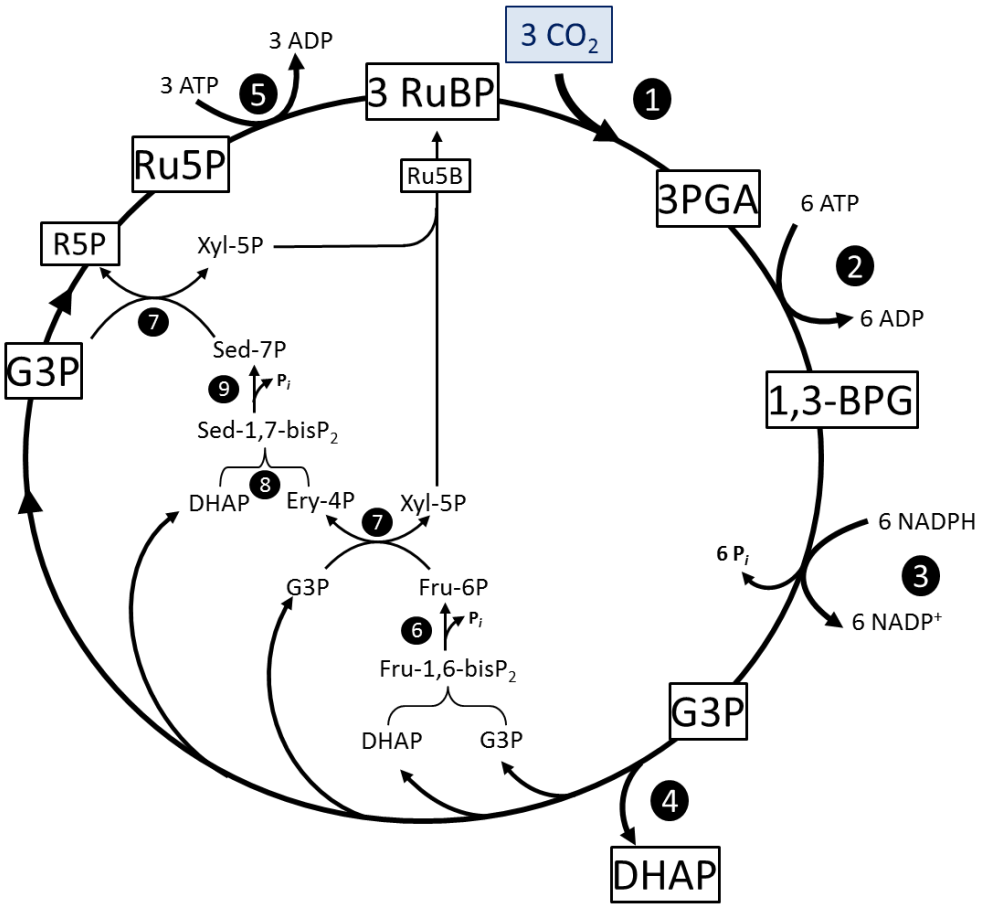

Fig. **1**.**2**. **Photosynthetic carbon reduction cycle in all photosynthetic organisms**. Enzymes: **1**, Rubisco; **2**, phosphoglycerate kinase; **3**, glyceraldehyde 3-phosphate (G3P) dehydrogenase, **4**, triose phosphate isomerase; **5**, phosphoribulokinase; **6**, fructose bisphosphatase; **7**, transketolase; **8**, fructose bisphosphate aldolase; 9, sedoheptulose-1,7-bisphosphatase. Metabolites: RuBP, ribulose 1, 5-P; Ru5P, ribulose 5-P; R5P, ribose 5-P; 1,3-BPG, glycerate 1,3 bisphosphate; *3PGA, glycerate 3-P; *G3P, glyceraldehyde 3-P; *DHAP, dihydroxyacetone-P (triose-P); Xyl, Xylulose; Ery, erythrose; Sed, sedoheptulose. *Diffuses from stroma to cytosol.

Photorespiration is a complex detoxification and recycling process that takes place in the chloroplasts, peroxisomes, mitochondria and cytosol of higher plants (Figure 1.3) (Bauwe *et al.*, 2010). Although it poses a problem for plants that solely rely on Rubisco for carbon fixation, photorespiration was not an issue when Rubisco first evolved around 3.5 billion years ago, due to an O_2-free atmosphere (Leegood, 2013), but as photosynthetic species populated the globe, O_2 became more readily available (Blankenship, 2010). This, however, was not a strong selective pressure to promote the

acquisition of a new carboxylase for carbon assimilation (Gowik and Westhoff, 2011). In fact, the bispecific nature of Rubisco evolved first and was subsequently maintained in all photosynthetic organisms, albeit preconditioned to operate in a high CO_2 atmosphere (Rachmilevitch *et al.*, 2004; Andersson, 2008). Consequently, it is likely that photorespiration co-evolved with oxygenic photosynthesis in cyanobacteria to recycle carbon and to prevent the accumulation of glycollate from the unavoidable oxygenase activity of Rubisco, protect against photoinhibition by supplying reducing equivalents to other metabolic pathways or produce essential amino acids, such as serine and glycine (Kozaki and Takeba, 1996; Rachmilevitch *et al.*, 2004; Bauwe *et al.*, 2010; Maurino and Peterhänsel, 2010; Peterhänsel *et al.*, 2012; Hagemann and Bauwe, 2016).

The reversible oxidation of glycine via the glycine decarboxylase complex (GDC), formed of glycine decarboxylase and serine hydroxymethyltransferase (SHMT) in the mitochondria (Figure 1.3, reaction 5), is an essential step in photorespiration (Walker and Oliver, 1986; Bauwe *et al.*, 2010). Firstly, glycine decarboxylation generates ammonia, which is necessarily and efficiently refixed through the interconversion of glutamate and glutamine during nitrate assimilation (Linka and Weber, 2005). Secondly, 3-PGA can be regenerated from serine via pyruvate and glycerate, but the phosphorylation of glycerate to form 3-PGA is ATP-dependent (Figure 1.3, reaction 8) (Weber and von Caemmerer, 2010). Finally, despite that CO_2 is eventually produced through the carboxylation of glycine in the mitochondria, the uptake efficiency of CO_2 back into the chloroplasts and its subsequent use in the carboxylation reaction is not significant to recover from the losses of photorespiration (Schulze *et al.*, 2013). Although loss of CO_2 through the photorespiratory pathway can have detrimental effects on C_3 plants by reducing nitrogen-use and water-use efficiency and limiting the regeneration of phosphate and RuBP, especially in warm and dry climates, photorespiration is important in all photosynthetic organisms (Rachmilevitch *et al.*, 2004; Sage and Kubien, 2007; Bloom *et al.*, 2010; Maurino and Peterhänsel, 2010; Bauwe *et al.*, 2012). In cyanobacteria, glycollate is metabolised using a plant-like mechanism (Bauwe *et al.*, 2010) or using a bacterial glycerate pathway, whereby glycollate is converted into glyoxylate, generating CO_2, but not ammonia, which does not need to be refixed through the ATP-dependent conversion of glutamate to glutamine (Figure 1.3, reaction 9) (Eisenhut *et al.*, 2008; Hagemann and Bauwe, 2016).

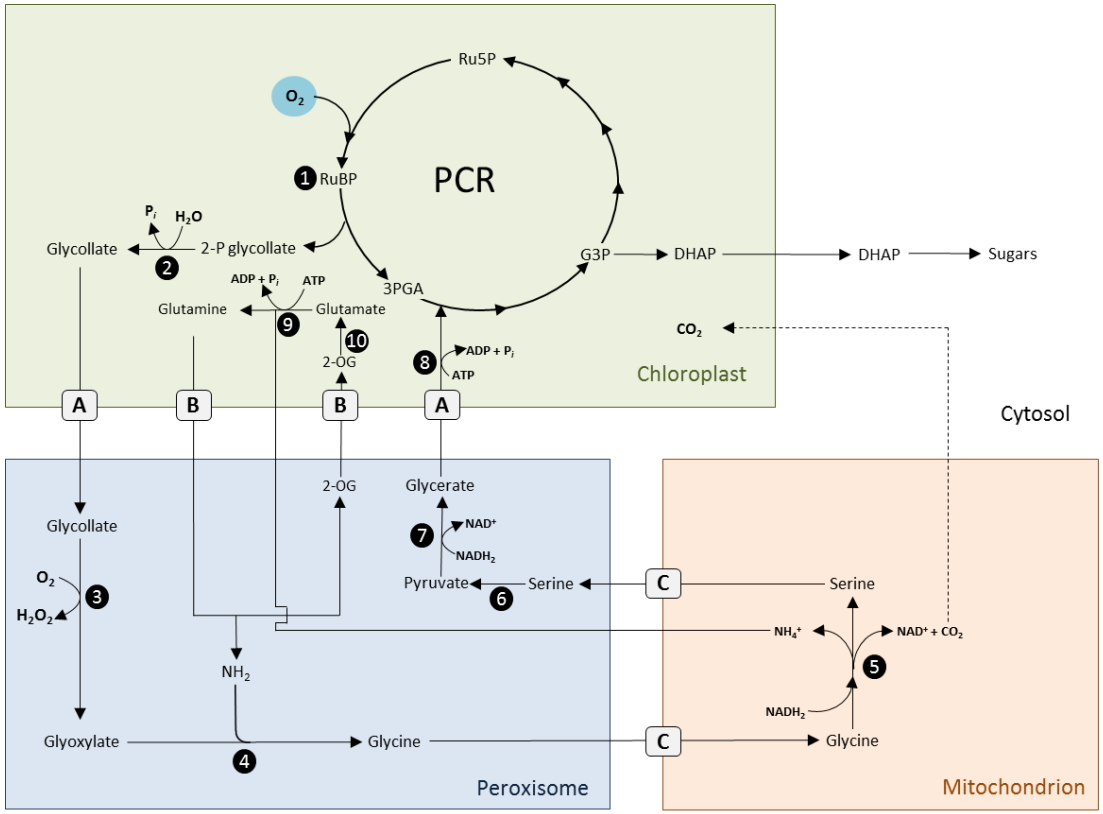

Fig. 1.3. Photorespiratory pathway recycles 2-phosphoglycollate between chloroplasts (green), peroxisomes (blue) and mitochondria (orange), eventually releasing CO_2. Enzymes: **1**, Rubisco; **2**, phosphoglycollate phosphatase; **3**, glycollate oxidase; **4**, glutamate-glyoxylate aminotransferase; **5**, glycine decarboxylase and serine hydroxymethyltransferase; **6**, serine-glyoxylate aminotransferase; **7**, pyruvate reductase; **8**, glycerate kinase; **9**, glutamine synthetase; **10**, ferredoxin-dependent glutamate synthase. Transporters: **A**, glycerate-glycollate translocator; **B**, malate-glutamate/2-oxoglutarate translocator; **C**, amino acid translocator. Metabolites: RuBP, ribulose-1,5-bisphosphate; Ru5P, ribulose 5-phosphate; 3PGA, 3-phosphoglycerate; G3P, glyceraldehyde-3-phosphate; DHAP, dihydroxyacetone phosphate. P_i, phosphate. Adapted from Bauwe *et al.* (2010).

Cyanobacteria mutants with the partial suppression of glycollate metabolism were found to have growth defects, while mutants completely lacking glycollate metabolism exhibited a lethal phenotype, suggesting that the removal of glycollate via photorespiration is essential (Eisenhut *et al.*, 2008). Moreover, *Zea mays* (C_4) mutants, grown in ambient CO_2, lacking glycollate oxidase activity did not exhibit a viable phenotype, despite that the rate of photorespiration is substantially lower than in C_3 plants (Zelitch, 1968; Zelitch *et al.*, 2009). Photorespiration is interwoven with other plant metabolic pathways of both C_3 and C_4 plants, and regardless of the amount of glycollate produced, and any disruption can have serious effects on the phenotype of photosynthetic species. The photorespiratory pathway may also play an intrinsic role in regulating the spatial availability of CO_2 and ammonia and mitigate the inhibition of photosynthesis by an excess of O_2 or phosphoglycollate (Chollet and Ogren, 1972; Ku and Edwards, 1977; Linka and Weber, 2005; Maurino and Peterhänsel, 2010; Weber and von Caemmerer, 2010).

1.2.2 C_3 photosynthesis will be limited by future climatic events

Since the evolution of oxygenic photosynthesis and increase in the atmospheric O_2, the rate at which Rubisco interacts with O_2 has increased, promoting photorespiration, which lowers photosynthetic efficiency and reduces carbon gain by at least 25% (Björkman *et al.*, 1969; Ehleringer *et al.*, 1991). Despite the competing carboxylase and oxygenase reactions, the reaction mechanism of Rubisco, with regards to structural differences and stabilisation during transition states, is optimised to differentiate between CO_2 and O_2 binding and maximise the rate of turnover (Lorimer *et al.*, 1993; Tcherkez *et al.*, 2006). However, Galmés *et al.* (2014) argues that the kinetic properties of Rubisco could still be improved such that its activity is optimised under future CO_2 concentrations. The efficiency of C_3 photosynthesis is not solely limited by the capacities of Rubisco. Transgenic plants with suppressed expression of Rubisco exhibited lower carbon fixation efficiencies when exposed to high light and temperature (Stitt and Schulze, 1994), but not if grown in high CO_2 (Masle *et al.*, 1993). These studies also show that factors such as increasing temperature and CO_2, which are within the context of climate change, may influence how C_3 plants will respond in future climates.

At the current atmospheric concentration of CO_2 and O_2, both carboxylation and oxygenation reactions occur at high rates (Leegood, 2013). In the next 50 years, the concentration of CO_2 is projected to double (from 360 to 600–1000 μmol mol^{-1}) , which may increase the carboxylase activity of Rubisco by at least 70% (Rachmilevitch *et al.*, 2004; Buchanan *et al.*, 2015). However, increasing CO_2 availability in the atmosphere does not imply that the efficiency of photosynthesis will increase in C_3 plants. Several studies have shown that plants grown in elevated CO_2 supress photorespiration and photosynthetic capacity increases by approximately 30% in the first instance (Björkman *et al.*, 1969; Woodward, 2002). However, photosynthesis is eventually limited because of the capacity of the PCR cycle to regenerate enough RuBP to maintain high carboxylase activity (Griffin and Seemann, 1996; Sage and Kubien, 2007). Moreover, plants acclimate to elevated CO_2 after prolonged exposure, due to the accumulation of carbohydrates, which desensitise CO_2 utilisation by Rubisco or other enzymes of the PCR cycle (Moore *et al.*, 1999; Rachmilevitch *et al.*, 2004; Buchanan *et al.*, 2015). In addition, prolonged exposure to high CO_2 can result in reduction of nitrogen-use efficiency, which could impair biomass production and photosynthesis (Smart *et al.*, 1998; Bloom *et al.*, 2002; Searles and Bloom, 2003).

Photosynthesis in plants can also be affected by temperature and it is one of many factors that can influence photosynthetic enzymes, plant development and leaf physiology (Berry and Bjorkman, 1980; Jordan and Ogren, 1984; Chen and Spreitzer, 1992; Leegood and Edwards, 1996; Bernacchi *et al.*, 2002; Sage and Kubien, 2007). Moreover, the life-cycle of plants grown for grain production rely on seasonal changes in weather and temperature (Hatfield *et al.*, 2011; Hatfield and Prueger, 2015). One of the suggestions to increase crop productivity is to extend the growing season, however, it is impractical because each crop species will have its optimum germination, maturation and harvest period, which is dependent on seasonal weather patterns (Covshoff and Hibberd, 2012). Certain crops, such as spinach (*Spinacia oleracea*), prefer cooler, winter temperatures (Hatfield and Prueger, 2015). Extreme weather patterns or fluctuation in minimum and maximum daily temperatures were found to perturb developmental timings of annual crops, like tomato (*Solanum lycopersicum*), and affected biomass production and seed viability (Ghosh *et al.*, 2000; Sato *et al.*, 2000; Pressman *et al.*, 2002; Sato, 2006). Some fruits, such as apple (*Malus domestica*) and grapes (*Vitis vinifera*) are perennial plants, which require a certain number of hours of exposure to cooler temperatures. If

temperatures continue to increase, pollen production of perennial crops will be impaired, thus disrupting fruit production (Hatfield and Prueger, 2015). Fujii and Kennedy (1985) showed that the rate of photosynthesis in apple trees was dependent on seasonal changes, particularly during fruit development, while the rates of dark respiration and photorespiration were unaffected. An increase in temperature may lower the photosynthetic capacity of these plants during specific seasons, as the combined rate of photorespiration and dark respiration may surpass the rate of net carbon assimilation. Some C_3 vegetative crops like the soybean plant (*Glycine max*) are sensitive to illumination and leaf temperature (Hatfield and Prueger, 2015). Studies have shown that leaf shading increases the rate of photosynthesis and promotes gas exchange by decreasing stomatal resistance, but the rate of photorespiration increases proportionally (Mondal *et al.*, 1978; Peet and Kramer, 1980). These effects could be more severe at higher temperatures and atmospheric CO_2 concentrations, and production yields may significantly suffer (Hatfield and Prueger, 2015). It is predicted that an increase in global temperatures will cause lower crop yields somewhere between 2.5% and 10% (Hatfield *et al.*, 2011; Lobell *et al.*, 2011) and these scenarios will be more prevalent if CO_2 emissions remain high (Schlenker and Roberts, 2009).

Increasing air temperature can also affect the rate of transpiration and energy balance of a leaf (Figure 1.4). High temperatures cause the exponential increase of atmospheric water vapour demand, which increases the rate at which water is transpired by the leaf until the rate of transpiration becomes limited by the rate of water absorption into the plant from the soil (Hatfield and Prueger, 2015). Increasing temperature can also limit photosynthesis, even when other conditions are at their optimum, by causing the premature closure of stomata in the daytime, thus increasing leaf temperature by at least 1 °C and decreasing the rate of gas exchange between the outside and inside of the leaf (Kimball *et al.*, 1993; Bernacchi *et al.*, 2002; Hatfield *et al.*, 2011; Schulze *et al.*, 2013; Hatfield and Prueger, 2015). Furthermore, the rate of evapotranspiration will drastically increase in extreme high temperatures, thus reducing the amount of water that the plant needs to absorb from the soil in order to meet the atmospheric evaporative demands (Hatfield and Prueger, 2011). In addition, altering the hydraulic conductance in plants may induce changes to the mechanisms that regulate the diurnal opening and closing of stomata, therefore limiting the rate of photosynthesis (Mathur *et al.*, 2014; Bellasio *et al.*, 2017).

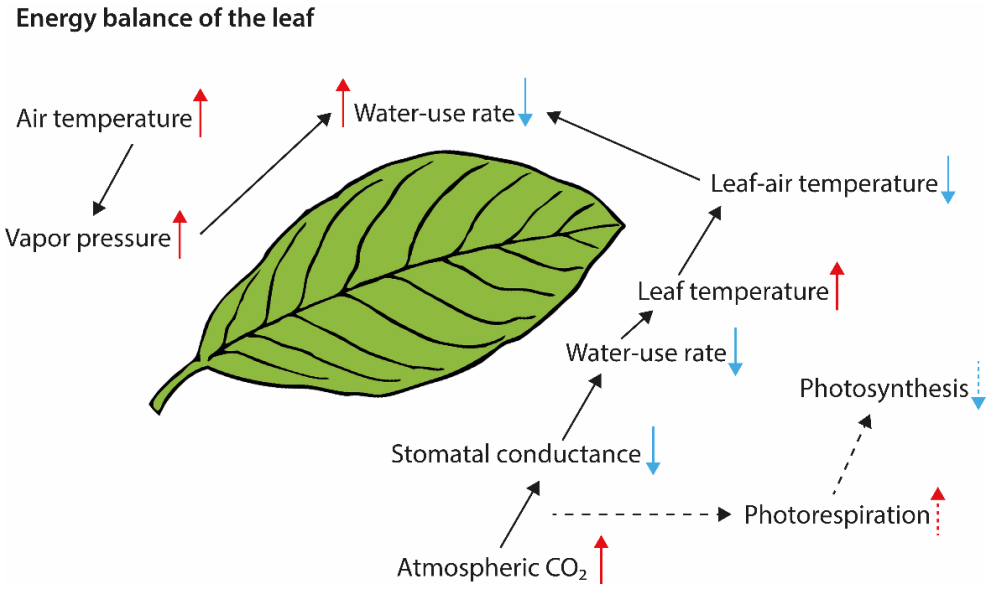

Fig. 1.4. Theoretical energy balance of a C_3 leaf in high atmospheric CO_2 and increase in air temperature. Black arrows indicate the direction of stress response in the leaf. Red arrows (pointing up) indicate an increase and blue arrows (pointing down) indicate a decrease. Dashed arrows show predicted events. Adapted from Hatfield and Prueger (2011).

The thermal optimum of C_3 plants is between 10–25 °C, depending on plant species (Hatfield and Prueger, 2011). In low atmospheric CO_2 and at higher temperatures, photosynthesis becomes limited as the activation state of Rubisco declines with increasing temperature (Crafts-Brandner and Salvucci, 2000; Sage *et al.*, 2002). Also, C_3 photosynthesis is limited by temperature only when atmospheric CO_2 concentration is high, because of a decline in the capacity to regenerate phosphate (Sage and Kubien, 2007). The thermal optima of C_3 plants can alter in response to increasing CO_2 concentration, thus increasing growth of certain plants in higher temperatures (Mawson and Cummins, 1989; Long, 1991; Ziska and Bunce, 1997; Atkin *et al.*, 2006). However, even if elevated CO_2 may increase the growth in certain C_3 crops, it may not be a substantial amount to increase the grain production (Amthor, 2001). C_3 crop plant interactions with CO_2, temperature and water availability can have serious implications for crop production. It is also evident that increasing CO_2 concentration does not improve C_3 photosynthesis efficiency, and even though photorespiration may be supressed by lowering the ratio of oxygenase to carboxylase activity. In summary, the inefficiency of C_3 photosynthesis poses a serious threat to C_3 crops grown for grain production if global temperatures and atmospheric CO_2 concentrations continue to increase. These effects will be more severe in drought-stricken regions.

1.2.3 Increasing crop productivity

Approximately 95% of land plants, including staple crops such as rice and wheat, use C_3 photosynthesis for carbon fixation (Sage, 2004). In these plants, CO_2 enters mesophyll cells and is directly fixed by Rubisco. However, maize is one of 4,500 grass species that use the alternative, and more efficient C_4 pathway (Sage, 1999). In the C_4-dicarboxylate cycle of C_4 photosynthesis, CO_2 is initially fixed by phospho*enol*pyruvate carboxylase (PEPC) in mesophyll cells, forming a C_4-acid that diffuses to and is decarboxylated in bundle sheath cells, concentrating CO_2 near Rubisco (Figure 1.5). C_4 crops are anatomically and biochemically superior to C_3 crops, and are capable of maintaining high rates of photosynthesis even in hot and dry climates (Berry and Bjorkman, 1980; Pearcy and Ehleringer, 1984; Sage, 1999; Lara and Andreo, 2011).

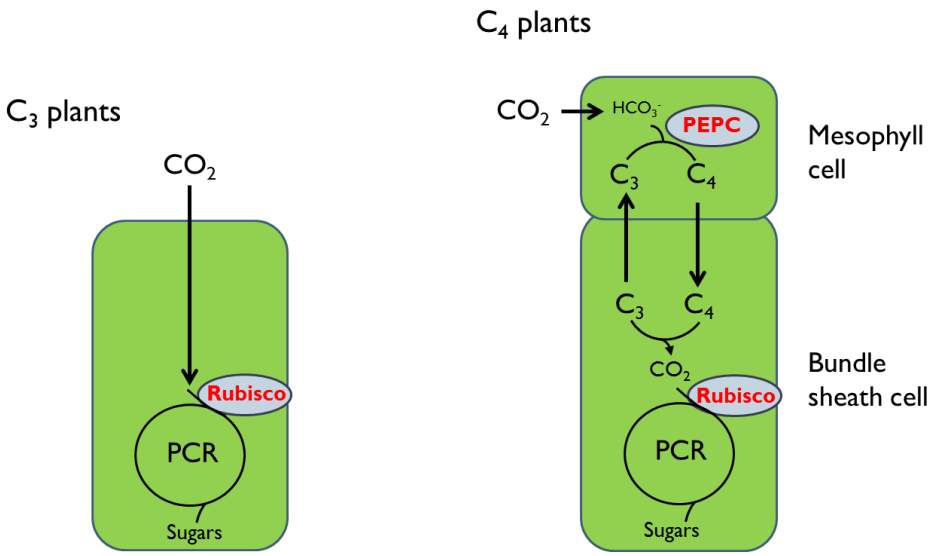

Fig. 1.5. Overview of the differences in the mechanism for carbon fixation in C_3 and C_4 plants. In C_3 plants (left), CO_2 is fixed by Rubisco in mesophyll cells. C_4 plants (right) operate a carbon concentrating mechanism between mesophyll and bundle sheath cells. PEPC, phospho*enol*pyruvate carboxylase.

With a global food crisis potentially developing by the end of this century, a great deal of attention has been given to the improvement of crop plants by converting to C_4 photosynthesis. Efforts to increase the photosynthetic potential of C_3 plants began after the realisation that plants operating the carbon concentrating mechanism of C_4 photosynthesis had a higher radiation use efficiency (RUE) than C_3 plants (Long *et al.*, 2006; Reynolds *et al.*, 2010; Zhu *et al.*, 2010; Covshoff and Hibberd, 2012).

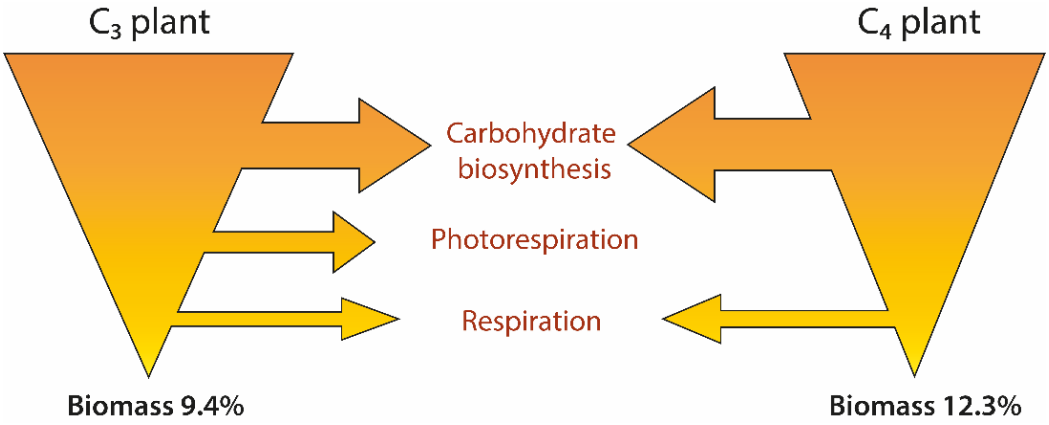

Fig. 1.6. Transduction of PAR in C_3 and C_4 plants in atmospheric CO_2 (400 ppm). Arrows show the cellular process where energy is being spent. The size of the arrow shows the relative difference in the amount of energy lost. Shading from orange to yellow shows the direction of energy transduction from harvested sunlight to plant biomass (given as a percentage of the theoretical maximal energy conversion efficiency). The higher the percentage, the more energy the plant has invested in biomass production. Figure adapted from Zhu *et al.* (2010).

Theoretical models predict that C_4-augemted crop plants could potentially perform 50% more efficiently than non-C_4 plants, which translates to increased crop production efficiency (Covshoff and Hibberd, 2012). Efficient crop production is defined as the ratio of energy output for carbohydrate biosynthesis to solar energy input (Monteith and Moss, 1977). Approximately 70% of solar energy is lost to the environment before it is intercepted by plants; the remainder is used for carbohydrate biosynthesis and respiration, or dissipated as heat (Zhu *et al.*, 2010). These models have also shown that C_4 plants, which have suppressed rates of photorespiration, can invest more energy into biomass production than C_3 plants (Figure 1.6). Therefore, converting C_3 crops to C_4 can potentially reduce the total amount of energy lost through photorespiration and increase photosynthetic efficiency by 30% (Zhu *et al.*, 2010). However, until this can be implemented, the factors that promote photosynthetic efficiency in C_4 plants must be understood. This Chapter will review past and ongoing C_4 photosynthesis research, outline important evolutionary adaptations and identify the key traits and characteristics of the C_4 phenotype.

1.3 The origins of C_4 photosynthesis

1.3.1 Natural bypass of photorespiration

Since Rubisco is the only enzyme involved in CO_2 fixation in the vast majority of photosynthetic organisms, major chemical alternations might not have been selected for during evolution (Sage, 2004; Gowik and Westhoff, 2011). The interaction with O_2 is an inevitable and unavoidable consequence in the reaction mechanism that occurs when the 2,3-enediol intermediate form of RuBP reacts with O_2 rather than CO_2, because of a higher free energy activation with O_2 (Chen and Spreitzer, 1992; Tcherkez *et al.*, 2006). Despite that different forms of Rubisco have evolved to respond better in low CO_2 to O_2 environments and increase the relative specificity for CO_2, some plants have found an alternative strategy for supressing the oxygenase reaction by compartmentalising Rubisco with physical barriers, thus creating a subcellular environment where the ratio of CO_2 to O_2 is higher (Badger and Andrews, 1987; Sage, 1999). Additionally, some C_3 plants can restrict GDC activity to the bundle sheath, by the selective loss of GDC in the mesophyll, allowing photorespired CO_2 to be recycled more efficiently (Monson, 1999). Anatomical variation and spatial availability of CO_2 in C_3 plants can also increase photosynthetic capacity. In several photosynthetic species, including cyanobacteria, aquatic and land plants, this can be achieved using compartments that concentrate CO_2 at the site of Rubisco (Leegood, 2013). In microalgae, such as *Chlamydomonas reinhardtii*, CO_2 is concentrated in specialised compartments (pyrenoids) that maintain the intracellular CO_2 concentration high to reach maximal carboxylase activity (Badger *et al.*, 1998; Mackinder *et al.*, 2017). This is similar to the strategy adopted by cyanobacteria, which operate a carbon concentrating mechanism in carboxysomes (Badger *et al.*, 2002). Changes to chloroplast positions can also affect the diffusion of CO_2 through the mesophyll of terrestrial C_3 plants (Tholen *et al.*, 2008). Recently, Busch *et al.* (2013) showed that rice and wheat can restrict the efflux of photorespired CO_2 in photosynthesising cells using air spaces as physical barriers for diffusion. Although Busch *et al.* (2013) argue that this adaptation could have contributed to reducing the wastage of CO_2 produced during photorespiration, the delivery of atmospheric CO_2 into the site of Rubisco can be restricted by such structural barriers, which cause the CO_2 partial pressure in the stroma to be several-fold lower than that of the atmosphere (Evans

et al., 2009; Tosens *et al.*, 2012). In rice, the entry of CO_2 may already be maximised as chloroplasts cover about 95% of the periphery of mesophyll cells, which increases the diffusion of CO_2 during high rates of photosynthesis (von Caemmerer and Evans, 1991; Tholen *et al.*, 2008; Evans *et al.*, 2009; Sage and Sage, 2009; Busch *et al.*, 2013). Rice has also considerably high variation in the number of chloroplasts in bundle sheath cells, some of which are deficient of chloroplasts (Leegood, 2008; Sheehy *et al.*, 2008). Theoretical models have also demonstrated that the diffusion efficiency and assimilation of CO_2 in tomato leaves correlates to the organisation and structure of mesophyll cells (Berghuijs *et al.*, 2015). However, anatomical variations, such as the difference in photosynthetically competent mesophyll and bundle sheath cells in C_3 plants, make it difficult to assess the factors that contribute to the transport and utilisation CO_2 within C_3 plant cells (Berghuijs *et al.*, 2016).

Before the elucidation of the C_4 photosynthetic pathway, Heinricher (1884) and Haberlandt (1904) noted that certain plant species of tropical origin had photosynthetically active chloroplasts in bundle sheath cells. In addition, chloroplasts found in bundle sheath cells of *Zea mays* were larger than those typically found in mesophyll cells of C_3 plants (Kiesselbach, 1916). Haberlandt (1904) originally suggested that the green parenchyma sheath cells in plants with wreath-like arrangement of mesophyll and bundle sheath cells (Kranz anatomy) might have specialised function. The accumulation of starch in bundle sheath cells (Rhoades and Carvalho, 1944), together with evidence that showed normal grana stacking in mesophyll chloroplasts but not bundle sheath chloroplasts in *Zea mays* (Hodge *et al*., 1955), further substantiated the biochemical specialisation of the bundle sheath. In light of these findings, Kortschak *et al.* (1965) demonstrated that radioactively labelled carbon in sugarcane was initially incorporated into malate and aspartate, but not 3-PGA, whereas 3-PGA in soybean plants accounted for 80% of the radioactively labelled carbon. These observations were consistent with those demonstrated by Karpilov (1960), which showed that radioactively labelled carbon was incorporated into malate and aspartate in *Zea mays*. Furbank (2016) argues that because of limitations of these labelling experiments at the time (Bassham, 2005), the published results may have been met with some degree of scepticism and delayed international recognition. However, upon further investigation Hatch and Slack (1966) demonstrated that 93% of radioactively labelled carbon was rapidly incorporated into malate and aspartate and that these were initial intermediates produced during

photosynthesis, with 3-PGA produced much later. Based on these observations, Hatch and Slack (1966) elucidated the C_4 dicarboxylic acid pathway of photosynthesis, termed C_4 photosynthesis.

1.3.2 The recurrent emergence of C_4 photosynthesis

The C_4 pathway is the most effective trait that evolved in certain plants to overcome photorespiration (Sage, 1999). It has evolved independently over 60 times in the last 35 million years, through gradual anatomical and biochemical adaptations that allow CO_2 to be concentrated at the site of Rubisco (Sage, 2004). This is usually achieved using concentric tubes of vascular tissue tightly packaged by specialised bundle sheath and mesophyll cells in Kranz anatomy (Figure 1.7D). In C_4 plants, CO_2 is initially fixed into a four-carbon organic compound, usually malate or aspartate (Hatch, 1987), in mesophyll cells by PEPC, transported to and decarboxylated in bundle sheath cells forming CO_2 and a three-carbon acid that is subsequently transported back to mesophyll cells completing the cycle (Figure 1.7C). Unlike C_3 leaves, Rubisco is localised in the bundle sheath, where CO_2 is concentrated (Kanai and Edwards, 1999). As a result, the ratio of CO_2 to O_2 in the bundle sheath increases, allowing the carboxylase reaction of Rubisco to operate at near CO_2 saturation (Hatch, 1987; Sage, 1999; von Caemmerer and Furbank, 1999). Although the dual-cell configuration of Kranz anatomy is an important characteristic for the assembly of C_4 photosynthesis and compartmentalisation of Rubisco, it is not a requirement for all C_4 organisms (Badger *et al.*, 1998; Edwards *et al.*, 2004; Leegood, 2013; Berry *et al.*, 2016). For instance, in a few single-cell chenopods such as *Bienertia sinuspersici*, C_4 photosynthesis operates by compartmentalising Rubisco within a specialised region in the cell, concentrating CO_2 in equal proportions as plants with fully established Kranz anatomy (Sage, 2004; Rosnow *et al.*, 2014).

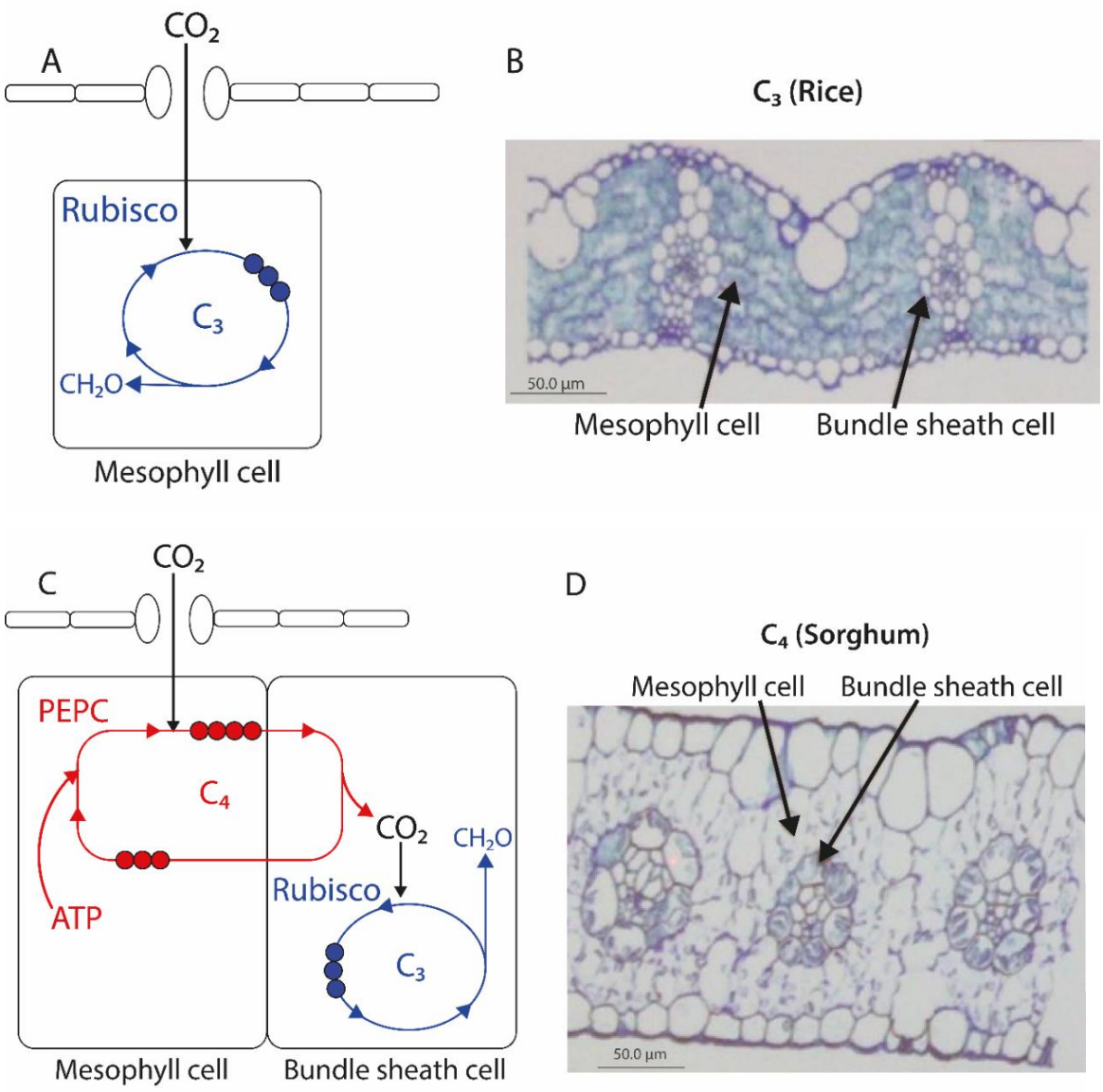

Fig. 1.7. Comparison between C_3 (A, B) and C_4 (C, D) anatomy in higher plants. Leave cross-sections show the arrangement of mesophyll and bundle sheath cells in C_3 rice **(B)** and C_4 Sorghum **(D)** plants. ATP is needed to regenerate PEP via PPDK (**C**). Transverse leaf sections acquired from RT Furbank and RF Sage.

C_4 photosynthesis evolved from the gradual specialisation of ancestral C_3 plant characteristics, which were predisposed to C_4 photosynthesis (Hibberd and Quick, 2002; Sage, 2004; Christin and Osborne, 2013). Furthermore, all C_4-related enzymes derived from C_3 isoforms, which are abundant in photosynthetic cells (Hibberd and Quick, 2002), albeit serve different cellular functions and are differently regulated (Sage, 2004). The acquisition of C_4-related traits has been extensively studied in several plant taxa (Figure 1.8), mainly to understand how the various biochemical variants of the C_4 pathway were assembled multiple times from separate origins. While it is generally accepted that the

evolution of C_4 photosynthesis was triggered, or at least favoured, by climatic events (i.e. decrease in atmospheric CO_2), Monson (2003) argues that its recurrent emergence was dependent on the genetic variability of C_3 lineages, mainly through genomic preconditioning such as gene duplications and neofunctionalisation.

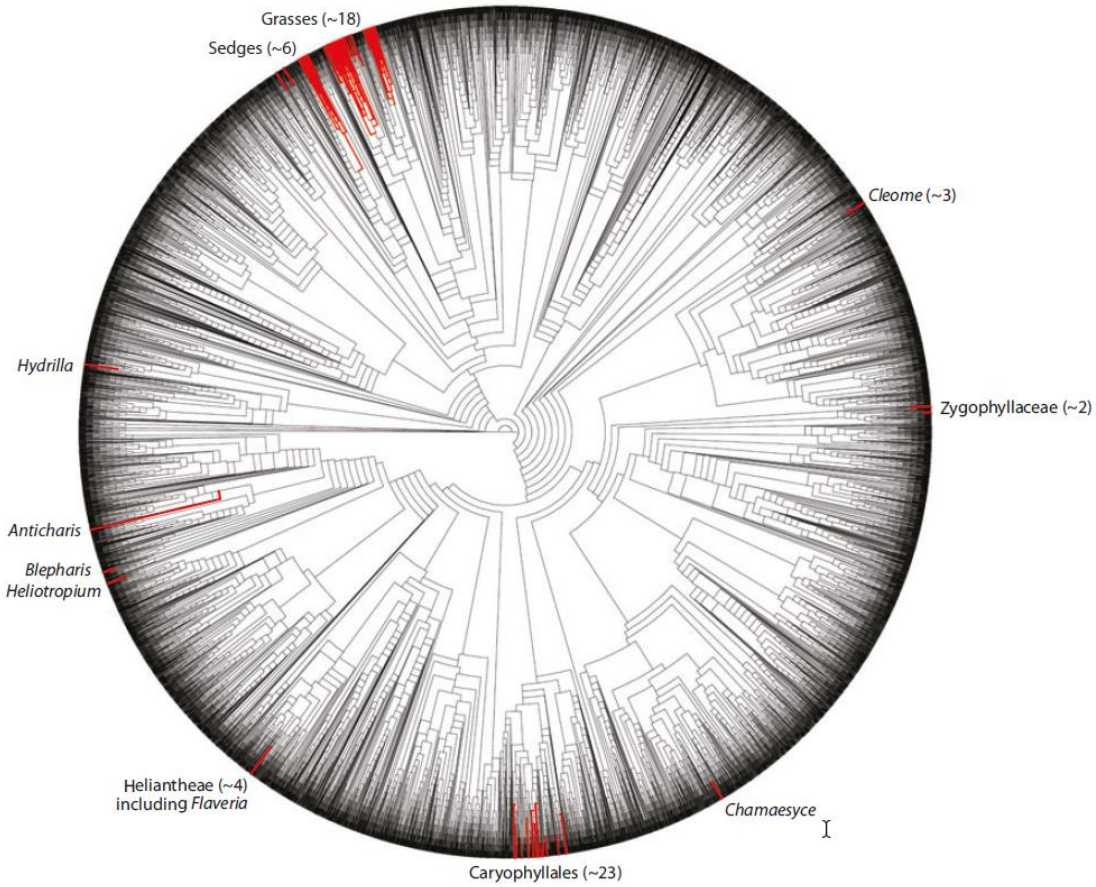

Fig. 1.8. The phylogenetic distribution of 47 angiosperm clades with C_4 photosynthesis. Red lines show C_4 lineages and grey lines show C_3 lineages. The number of independent origins are indicated to the right of genus names. Obtained from Sage *et al.* (2011).

From there, the C_4 pathway was assembled as an extension of the classical C_3 pathway, through two main phases (Figure 1.9): anatomical and biochemical specialisations (Monson *et al.*, 1986; Sage, 1999; Sage, 2004; Sage *et al.*, 2011). Comparative analyses in *Alloteropsis semialata* populations show that the convergent evolution of C_4 photosynthesis involved the optimisation of intermediary C_4 characteristics from C_4-like common ancestors, while others obtained C_4 features independently (Christin *et al.*, 2012; Dunning *et al.*, 2017). Furthermore, Gowik and Westhoff (2011) and Williams *et*

al. (2013) suggest that every transition into a C_4-like condition conferred certain advantages, and in some cases, certain species would not have necessarily continued to evolve C_4 photosynthesis, while others may still be evolving the C_4 pathway (Ludwig, 2012). Genomic and phylogenetic analyses predict that there are 4500 species in the grass family (Poaceae) that perform C_4 photosynthesis (equivalent to 60% of C_4 species), followed by 1500 species of sedges (Cyperaceae) and 1200 species of dicots, producing about a fourth of global O_2 (Sage, 2004; Edwards *et al.*, 2010; Sage *et al.*, 2012).

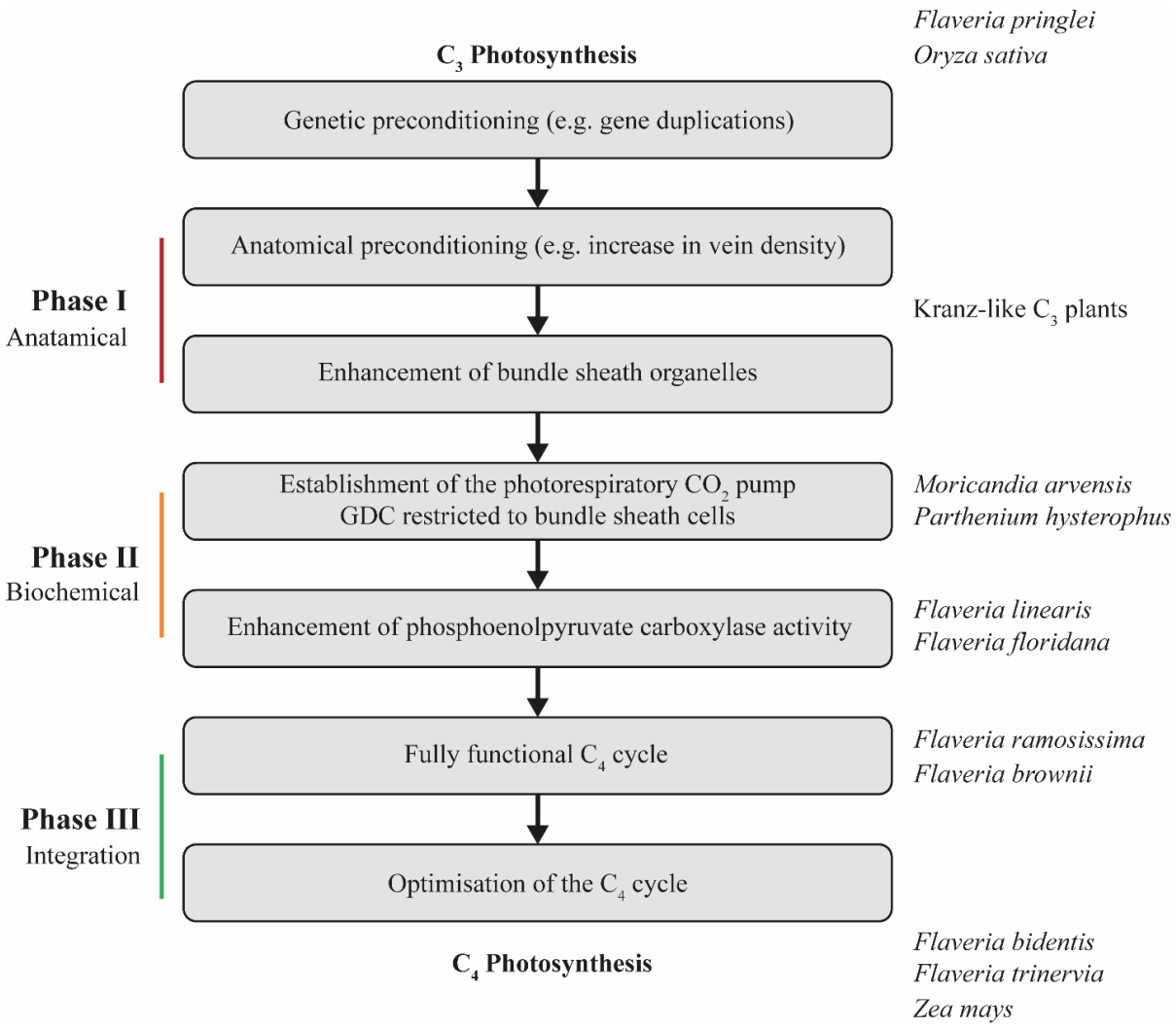

Fig. 1.9. The path to C_4 photosynthesis. Summary of the evolution of C_4 photosynthesis (in the direction of arrows). Example of C_3–C_4 intermediate species are shown to the right of each transition point. Figure adapted from Monson (1999), Monson and Rawsthorne (2000) and Gowik and Westhoff (2011).

1.3.3 Specialisation of mesophyll and bundle sheath cells

Trapping CO_2 at the site of Rubisco was accomplished by the development of a wreath-like arrangement of bundle sheath cells, spaced closely apart from neighbouring mesophyll cells and vasculature tissue. As a result, the intracellular CO_2 concentration in bundle sheath cells is about 10-fold higher than in mesophyll cells (Figure 1.10) (von Caemmerer and Furbank, 1999). Vein spacing in C_4 plants also facilitates the rapid diffusion of metabolites during photosynthesis (Osmond, 1971; Hatch and Osmond, 1976; Sage, 2004). Furthermore, C_4 plants typically have two mesophyll cells between veins, whereas C_3 plants can have more than five mesophyll cells between each vein (Figure 1.11) (Leegood and Walker, 1999; Ogle, 2003; Langdale, 2011).

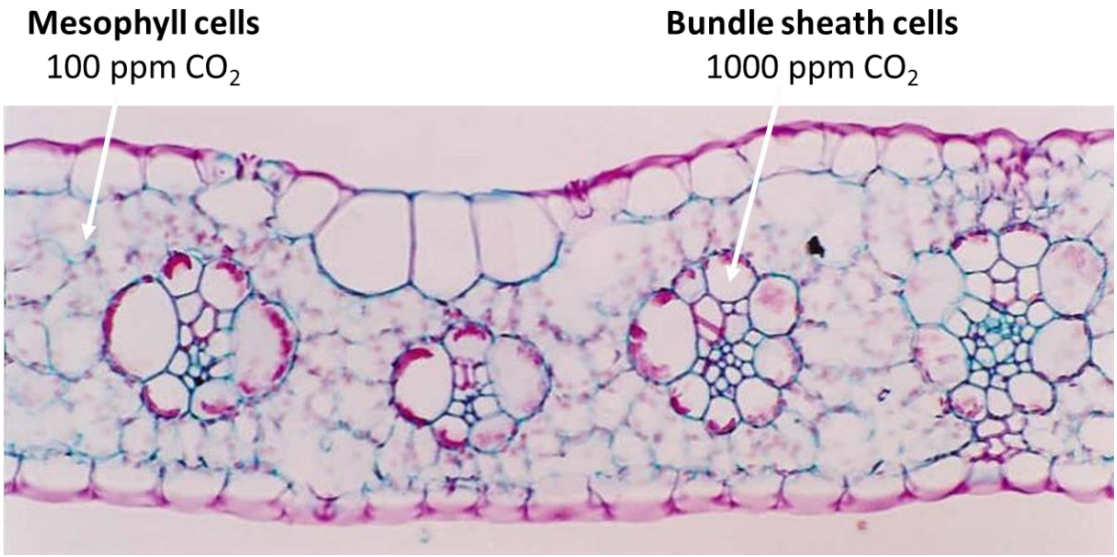

Fig. 1.10. Arrangement of mesophyll and bundle sheath cells in Kranz anatomy of C_4 plants. Kranz anatomy in a C_4 plant, such as *Zea mays*, is formed by specialised mesophyll and bundle sheath cells, which partition between carboxylation and decarboxylation reactions, respectively. CO_2 produced from the decarboxylation of the C_4-acid is concentrated in bundle sheath cells. Transverse leaf section provided by RC Leegood.

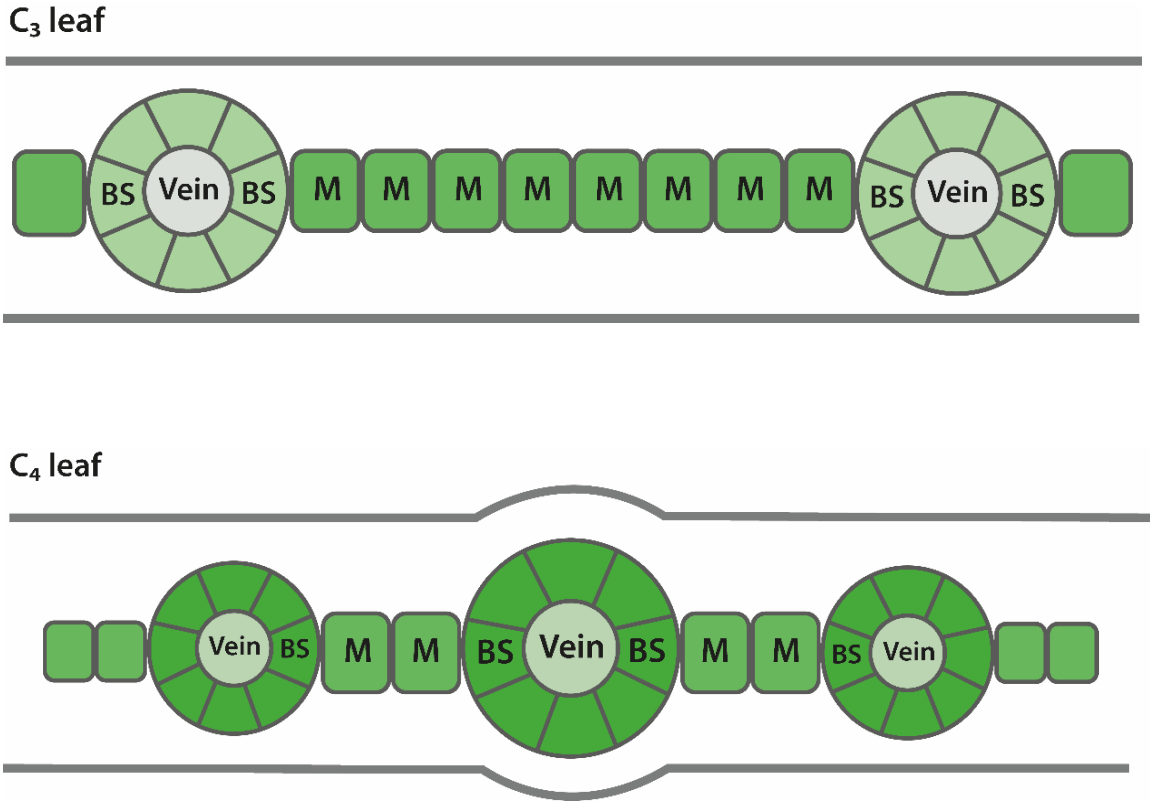

Fig. 1.11. Schematic showing interveinal distance comparison between C_3 (top) and C_4 (bottom) leaf cross-sections. Shorter interveinal distances in leaves of C_4 plants allow for the efficient movement of metabolites between mesophyll (M) and bundle sheath (BS) cells. Adapted from Langdale (2011).

The efficient transport of metabolites between mesophyll and bundle sheath cells is accomplished by exclusively using plasmodesmata, which are highly abundant in C_4 leaves (Evert *et al.*, 1977; Furbank, 2016). Enhancement of bundle sheath organelles was also necessary with the specialisation of the bundle sheath in leaves of C_4 plants. Unlike C_3 leaves, C_4 photosynthesis is partitioned between mesophyll and bundle sheath cells, and only bundle sheath cells have chloroplasts that are capable of operating the PCR cycle because of the cell-specific expression of Rubisco (Majeran and van Wijk, 2009). Moreover, the increased photosynthetic capacity of bundle sheath cells is likely to have been co-dependent with the increased number and size of chloroplasts during the development of Kranz anatomy (Sage, 2004). This is supported by *Flaveria* and *Moricandia* C_3–C_4 intermediates, which do not fully express Kranz anatomy, but have increased number of organelles in bundle sheath cells (Brown and Hattersley, 1989). Brown and Hattersley (1989) suggest that increased number of organelles in bundle sheath cells in some C_3–C_4 intermediates was enough to compensate for reduced

photosynthetic capacity due to bundle sheath cells resembling that of C_3 plants, which have reduced photosynthetic capacity and few chloroplasts (Leegood, 2008).

Photosystem activity in chloroplast thylakoid membranes is specific in C_4 plants, though varies in certain species due to the mechanism used for decarboxylation (Laetsch, 1968; Pfündel *et al.*, 1996; Kanai and Edwards, 1999). Photosystem activity also varies between mesophyll and bundle sheath cells in C_4 plants (Meierhoff and Westhoff, 1993; Pfündel *et al.*, 1996; Edwards *et al.*, 2001). For instance, *Sorghum bicolor* has bundle sheath cells with reduced grana stacking and lower photosystem II activity, but normal photosystem I activity, while mesophyll chloroplasts have comparable photosystem II and photosystem I activities with normal grana, resembling that of C_3 plants (Woo *et al.*, 1970; Edwards *et al.*, 2001; Majeran and van Wijk, 2009). By reducing photosystem II activity in bundle sheath cells, the intracellular O_2 concentration probably declines, thus preventing the unfavourable utilisation of O_2 by Rubisco (Chollet and Ogren, 1972; Chapman *et al.*, 1980). Also, enhancement of mitochondria along with peroxisomes and chloroplasts in precursors of C_4 species, would have been a requirement before the establishment of cell-specific enzyme expression and activity, and indicative of the decarboxylation mechanism that is evolving, though exceptions are known to exist (Hatch, 1978; Brown and Hattersley, 1989; Meierhoff and Westhoff, 1993).

1.3.4 Photorespiratory CO_2 pump in C_3–C_4 intermediates

The specialisation of bundle sheath chloroplasts was an important phase for the development of the photorespiratory CO_2 pump, since all dual-cell C_4 species use bundle sheath cells for the decarboxylation of the C_4-acid (Brown and Hattersley, 1989; Sage, 2004). The evolutionary trajectory of C_4 evolution has been explored in C_3–C_4 intermediate species, which possess some Kranz-like leaf characteristics and reduced rates of photorespiration, though C_4-specific enzymes are not regulated or achieve similar activities as in C_4-like or C_4 plants (Ku *et al.*, 1991). Furthermore, the photosynthetic CO_2 compensation point of *Flaveria* C_3–C_4 intermediates is between that of C_3 and C_4 plants, even under ambient O_2 concentration, suggesting a reduced rate of photorespiration (Ku *et al.*, 1983). One major development in C_3–C_4 intermediate species, which enhanced photosynthetic capacity by reducing photorespiration, was the

restriction of GDC to bundle sheath cells (Sage, 2004; Bauwe *et al.*, 2010; Sage *et al.*, 2012). This restricts glycine decarboxylation in mitochondria of bundle sheath cells (Figure 1.12), which release photorespired CO_2 at the site of Rubisco (Schulze *et al.*, 2013). Therefore, compartmentation of GDC increases the capacity to recycle photorespired CO_2 and reduces the loss of carbon through photorespiration or leakage from the cell periphery (Rawsthorne *et al.*, 1988; Bauwe *et al.*, 2010; Gowik and Westhoff, 2011).

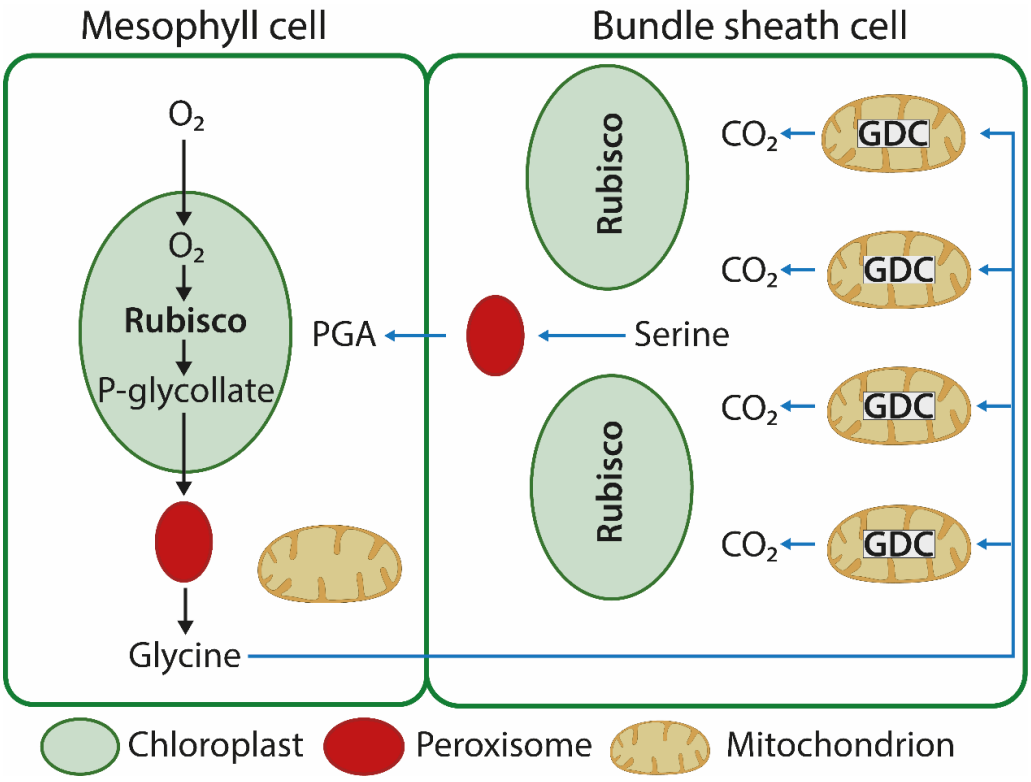

Fig. 1.12. GDC compartmentalisation and the photorespiratory CO_2 pump in C_3–C_4 intermediate species. Schematic showing the restriction of GDC in mitochondria of bundle sheath cells. In the CO_2 pump (blue arrows), all glycine produced by photorespiration must be transported to bundle sheath cells, where CO_2 is released, increasing the chance of its utilisation by Rubisco. Serine is transported back into mesophyll cells and converted into PGA. P-glycollate, phosphoglycollate; PGA, phosphoglycerate. Adapted from Rawsthorne *et al.* (1988).

Immunolocalisation experiments conducted in the C_3–C_4 intermediate species *Moricandia arvensis* showed that the P-protein subunit (encoded by *GLDP*) of GDC was solely expressed in bundle sheath cells, which resulted in the precursors of GDC in mesophyll cells to lose activity (Rawsthorne *et al.*, 1988; Morgan *et al.*, 1993). Loss of GDC activity in mesophyll cells is also evident in *Flaveria* C_3–C_4 intermediate species,

and was likely acquired by the gradual suppression of *GLDP* and GDC activity in mesophyll cells (Ku *et al.*, 1991; Schulze *et al.*, 2013), rather than rapid suppression as previously suggested (Sage, 2004; Sage *et al.*, 2012). Furthermore, the gradual transition of GDC activity from mesophyll to bundle sheath cells would have been advantageous to Kranz-like C_3 plants with C_3-like chloroplasts and mitochondria in bundle sheath cells, which would not have the capacity to perform all the required GDC activity (Bauwe, 2011; Muhaidat *et al.*, 2011; Schulze *et al.*, 2013). Therefore, certain lineages of C_3 species with Kranz-like anatomy or C_3–C_4 intermediates, in the early trajectory of C_4 evolution, which had the capacity to operate the glycine shuttle between mesophyll and bundle sheath cells would have been positively selected during evolution, whereas those with low capacity to remove phosphoglycollate would have probably not survived (Sage, 2004).

1.3.5 Establishing a fully functional C_4 cycle

C_3–C_4 intermediates typically show a distinct progression into C_4 characteristics, but do not have optimised enzyme activity to achieve similar photosynthetic capacity of C_4 plants (Engelmann *et al.*, 2003). Similar to C_3 plants, *Flaveria* C_3–C_4 intermediates have high concentration of PEPC and NADP-malic enzyme in photosynthetic cells, but the activities of these enzymes are not comparable to those found in C_4 plants (Ku *et al.*, 1991). The regulatory properties of PEPC evolved at a much later stage (Svensson *et al.*, 2003; Gowik *et al.*, 2004) and the significance of increased PEPC activity, with regards to C_4 evolution, is more evident when comparing the changes in activity between C_3 and C_3–C_4 intermediate species. For instance, the activity of PEPC from C_3–C_4 intermediates *Flaveria linearis* and *Flaveria ramosissima* is five and seven times higher than that of C_3 relatives, respectively (Monson and Moore, 1989). In addition, the activity of PEPC between C_4 *Flaveria* species can be up to 40 times higher than C_3 variants within the genus (Monson and Rawsthorne, 2000; Svensson *et al.*, 2003). Enhancement of PEPC activity in mesophyll cells was necessary to re-fix leaked CO_2 from the bundle sheath, which would have readily diffused along a concentration gradient through the chloroplast membrane (Monson, 1999; von Caemmerer, 2000; Gowik and Westhoff, 2011).

While *Flaveria* C_3–C_4 intermediates had elevated PEPC activity at this evolutionary stage, the C_4 pump would not have been fully established, firstly because the regeneration of PEP was not catalysed by the C_4-specific pyruvate, phosphate dikinase (PPDK), which was not acquired at the same time as PEPC activity increased in mesophyll cells (Sage, 2004). This is supported by C_3–C_4 *Flaveria* intermediates with C_3-characteristics that operated a pathway for the interconversion of 3-PGA and PEP (Monson and Moore, 1989). Secondly, CO_2 may not have been initially fixed by PEPC, since Rubisco activity was still prominent in mesophyll cells (Gowik and Westhoff, 2011). Thirdly, Rubisco acquired bundle sheath-specific expression much later in *Flaveria* species, possibly because of the glycine shuttle operating between mesophyll and bundle sheath cells in C_3–C_4 intermediates that efficiently recycled photorespired CO_2 (Monson and Rawsthorne, 2000). Carbon isotope analysis in *Flaveria* intermediates showed that a large quantity of assimilated carbon was transported through the glycine shuttle rather than the C_4 pump, suggesting that integration of C_3 and C_4 cycles would only be achieved if the activities of PEPC and Rubisco were equal and localised (Monson *et al.*, 1988).

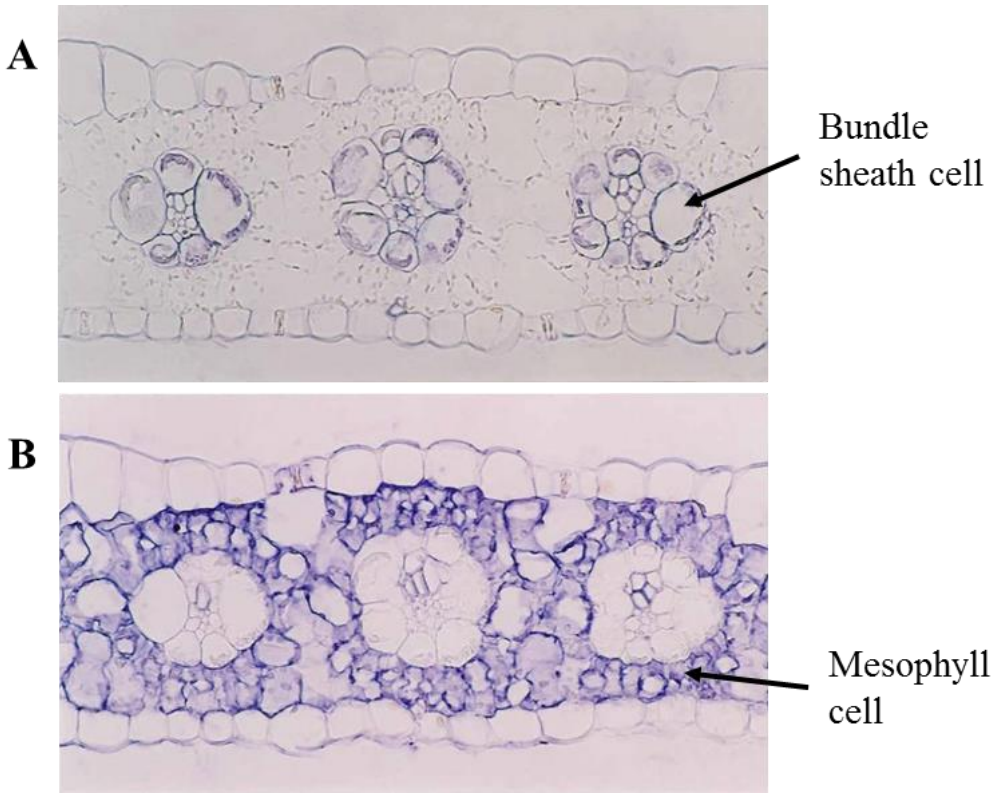

Fig. 1.13. C_4 leaf cross-section of *Zea mays* showing compartmentation of Rubisco (A) and PEPC (B). Rubisco is localised in bundle sheath cells and PEPC is localised in mesophyll cells of C_4 plants. Transverse leaf sections provided by RC Leegood.

1.3.6 Integration of C_3 and C_4 cycles

The spatial separation of Rubisco to bundle sheath cells (Figure 1.13A) and PEPC to mesophyll cells (Figure 1.13B) was the final requirement for the complete integration of C_3 and C_4 cycles (Sage, 2004). Differential gene expression patterns in *Sorghum bicolor* show the restriction of PEPC, PPDK, carbonic anhydrase and photosystem II proteins in mesophyll cells, while Rubisco activase, NADP-malic enzyme and other enzymes of the PCR cycle are exclusively expressed in bundle sheath cells (Wyrich *et al.*, 1998; Sage, 2004). In the *Flaveria* genus, the expression of Rubisco in mesophyll cells decreased along the evolutionary gradient of C_4 photosynthesis, with certain C_4-like species, like *Flaveria brownii*, exhibiting the preferential expression of Rubisco in bundle sheath cells, and *Flaveria* variants with C_3-characteristics and *Nicotiana tabacum* (C_3), expressing Rubisco in both mesophyll and bundle sheath cells (Bauwe, 1984; Reed and Chollet, 1985).

Once these restrictions were set, Rubisco would not compete with PEPC for carbon and the activity of PEPC would have been high enough to match the activity of Rubisco, creating a gradient of metabolites that diffused between C_3 and C_4 cycles and meet competing demands for ATP and CO_2 in mesophyll and bundle sheath cells, respectively (Monson, 1999; von Caemmerer and Furbank, 1999; von Caemmerer and Furbank, 2003; Gowik and Westhoff, 2011). Additionally, enhancement of mesophyll-specific carbonic anhydrase activity was necessary to generate enough bicarbonate for PEPC to avoid limiting the rate of photosynthesis (Hatch and Burnell, 1990). The reduction of carbonic anhydrase activity in bundle sheath cells was also an important step in C_4 evolution (Sage, 2004; Ludwig, 2012). As the intracellular concentration of CO_2 increases in bundle sheath cells, carbonic anhydrase would catalyse the conversion of CO_2 to bicarbonate, thus reducing the amount of substrate available for Rubisco (Burnell and Hatch, 1988). In C_4 species, carbonic anhydrase is expressed in large quantities in the cytosol of mesophyll cells, though the gene was acquired from a chloroplastic form (Ludwig, 2012), but lost its transit peptide due to a mutation to the sequence that encoded its chloroplastic expression (Tanz *et al.*, 2009).

While C_3 plants contain high amounts of decarboxylating enzymes (NADP- and NAD-malic enzyme), these were expressed in vascular tissues, and not in photosynthetic cells and had to acquire cell-specific expression patterns (Hibberd and Quick, 2002; Sage, 2004). Both PEPC and NADP-malic enzyme in C_4 *Flaveria* species acquired C_4 characteristics through the duplication of an ancestral C_3 gene followed by neofunctionalisation, which led to cell-specific gene expression (Hermans and Westhoff, 1990; Marshall *et al.*, 1996; Monson, 1999). Further establishment of the C_4 syndrome was dependent on substantial changes in gene expression patterns carried forward from ancestor C_3 species (Nelson and Dengler, 1992; Ku *et al.*, 1996), but only needed slight changes to regulatory elements to achieve C_4-specific function (Gowik and Westhoff, 2011). For instance, PEPC expression in C_4 plants is controlled by a transcriptional *cis*-regulatory element (mesophyll expression module1, MEM1), which encodes for the mesophyll-specific expression of the *ppcA* gene of PEPC in *Flaveria trinervia* (Gowik *et al.*, 2004). The MEM1 sequence is also found in the orthologous C_3 *Flaveria pringlei* gene, but it does not encode PEPC expression in mesophyll cells (Akyildiz *et al.*, 2007). It was shown that two discrete changes in the MEM1 sequence were substantial to generate the mesophyll-specific expression of PEPC in *Flaveria trinervia* (Akyildiz *et al.*, 2007). The cell-specific expression of the Rubisco found in C_4 plants is another well-documented example of subtle changes to gene expression. While most C_4-specific genes are regulated by transcriptional elements (Sheen, 1999), certain genes, like those in *Flaveria bidentis* encoding for bundle sheath-specific expression of the small subunit of Rubisco, are controlled by both transcriptional and posttranscriptional regulators (Patel *et al.*, 2006). Furthermore, despite cell-specific expression, the expression patterns of Rubisco genes in C_4 plants are very similar to those found in their C_3 relatives (Berry *et al.*, 2016). In both plant systems Rubisco genes are absent in non-photosynthetic tissues and ubiquitously expressed in photosynthetic tissues, where they are regulated by developmental signals, illumination or abiotic stress (Berry *et al.*, 2013; Berry *et al.*, 2016).

The eight large and small subunits of Rubisco are encoded by *rbcL* and *rbcS* genes, respectively (Patel *et al.*, 2006; Berry *et al.*, 2016). Despite that in the early stages of C_4 evolution these genes were expressed in both mesophyll and bundle sheath cells, Rubisco mRNAs were shown to only accumulate in the latter (Berry *et al.*, 2013). Furthermore, Berry *et al.* (2016) suggested that nucleic acid binding proteins, such as RLSB, could be

affecting the regulation of cell-specific Rubisco genes. Recently, highly conserved RLSB proteins, from C_3 ancestral *Flaveria* plants, were shown to accumulate in bundle sheath cells and bind *rbcL* mRNAs, in a mechanism that describes the regulation of cell-specific Rubisco expression in C_4 plants (Yerramsetty *et al.*, 2017). Changes to the sequence of RLSB was observed to occur gradually through the progression of C_3 to C_4-like to C_4 *Flaveria* plants, which suggest that RLSB co-evolved with C_4 photosynthesis, albeit the functional significance of these changes through the transition to C_4-characterstics is unclear (Yerramsetty *et al.*, 2017).

The light-dependent expression of the small subunit of Rubisco in bundle sheath cells is similar to the mechanism previously described for the cell-specific expression of NAD-malic enzyme in the C_4 plant *Amaranthus hypochondriacus*. In *Amaranthus hypochondriacus*, the functional subunit (α subunit) of NAD-malic enzyme is preferentially expressed in bundle sheath cells (Long *et al.*, 1994). During the early stages of leaf development, and induced by light, the mRNAs corresponding to the α subunit accumulate in bundle sheath cells in amaranth (Long and Berry, 1996). However, the NAD-malic enzyme bundle sheath-specific expression pattern in amaranth occurs earlier than that of Rubisco (Long and Berry, 1996). During the early stages of leaf development, mRNA products of the small and large subunits of Rubisco initially accumulate in mesophyll and bundle sheath cells, resembling the expression pattern of C_3 plants, and bundle sheath cell specificity is acquired later through metabolism cues (Wang *et al.*, 1992; Wang *et al.*, 1993). Furthermore, acquisition of a C_4-specific Rubisco might have occurred with fewer changes to regulation patterns, since it was acquired from a photosynthetic counterpart, whereas NAD-malic enzyme, PEPC and PPDK, were recruited from separate, non-photosynthetic origins (Hatch, 1987; Furbank and Taylor, 1995). This also suggests that the regulatory patterns for the three latter enzymes were recruited around the same time as C_4-specific function evolved and therefore share similar regulatory elements (Long and Berry, 1996; Gowik and Westhoff, 2011).

1.3.7 Fine-tuning C_4-specific enzyme activity

Once the C_4 cycle was fully established, the enzymes that were recruited from ancestral C_3 counterparts to serve a C_4-specific function were optimised for C_4 photosynthesis (Sage, 2004). In order to maintain the metabolite gradient that operates the C_4 cycle, the rate at which PEPC fixes CO_2 in mesophyll cells must be equivalent to the rate of diffusion into bundle sheath cells, utilisation by Rubisco and regeneration of PEP (Leegood and Walker, 1999). In contrast, the rate of transport is no higher than one-sixth of the steady-state CO_2 assimilation in C_3 leaves (Edwards and Walker, 1983). The kinetic properties of C_4-related enzymes were also optimised during this phase. For instance, the C_4-specific PEPC affinity for PEP is lower than that of its C_3 counterpart, while the affinity for bicarbonate is higher in the C_4-form (Chollet *et al.*, 1996; Gowik and Westhoff, 2011), and achieves higher maximum reaction rates than the C_3-form because PEP is available in larger quantities (Ku *et al.*, 1996). Also, the C_3 PEPC form is sensitive to inhibition by malate, but this is reduced in the C_4-form, so that it can remain active when large quantities of malate are produced during C_4 photosynthesis (Bläsing *et al.*, 2000; Svensson *et al.*, 2003; Jacobs *et al.*, 2008). Although the C_4-specific PEPC has evolved at least eight times through separate origins, all C_4 PEPCs share a large degree of similarity in *Flaveria* (Christin *et al.*, 2007; Gowik and Westhoff, 2011). Moreover, it is likely that these features were the last to evolve, based on the absence of these regulatory mechanisms in PEPC from *Flaveria* C_3–C_4 intermediates (Sage, 2004). Similarly, the C_4-specific Rubisco has a lower affinity for CO_2, relative to C_3 counterparts, but can achieve a higher turnover rate because CO_2 is more readily available (Seemann *et al.*, 1984). Similar to the regulatory features of the C_4 PEPC, Rubisco from *Flaveria* intermediates do not exhibit C_4-specific kinetic properties, but more closely resemble those of the C_3-form (Wessinger *et al.*, 1989), suggesting that these features also evolved in the final phases of C_4 evolution (Sage, 2004). NADP-malic enzyme also underwent slight changes to its kinetic properties when it was recruited for C_4-specific function. Unlike the C_3-form, NADP-malic enzyme in C_4 species exhibits a higher maximum activity and has a higher affinity for malate (Drincovich *et al.*, 2001). Also, unlike the C_4-specific PEPC, NADP-malic enzyme in *Flaveria* C_3–C_4 intermediates exhibited changes to affinity values for malate, somewhere between the

values of C_3 and C_4 variants (Sage, 2004), suggesting that some intermediates evolved these characteristics earlier than the regulatory properties PEPC or Rubisco evolved.

1.4 What does it mean to be C_4?

1.4.1 Variations of the C_4 pathway

During the evolution of the C_4 pathway, three decarboxylases were recruited (NAD(P)-malic enzyme and phospho*enol*pyruvate carboxykinase [PEPCK]), creating three distinct biochemical variations of the CO_2 concentrating mechanism of C_4 photosynthesis (Hatch, 1987). In the NADP-malic enzyme subtype (Figure 1.14A), malate is formed in mesophyll cell chloroplasts, whereas in NAD-malic enzyme (Figure 1.14B) and PEPCK subtypes (Figure 1.14C), both malate and aspartate are formed (Wang *et al.*, 2011). PEPCK operates as a secondary decarboxylase in several NADP- and NAD-malic enzyme subtypes, and does not appear to operate on its own (Walker *et al.*, 1997; Wingler *et al.*, 1999; Pick *et al.*, 2011; Bräutigam *et al.*, 2014). For instance, in NADP-malic enzyme subtypes, aspartate contributes to roughly 10–15% of assimilated carbon pool (Hatch and Mau, 1973; Hatch, 1987; Arrivault *et al.*, 2016).

The coordination of C_3 and C_4 pathways depends on the cooperate activity of carboxylation and decarboxylation reactions (Bailey *et al.*, 2007) and coordinate interaction of the C_4 pathway and mitochondrial metabolism (Leegood, 1985; Stitt and Heldt, 1985; Leegood and Walker, 1999). In PEPCK subtypes, for example, mitochondrial respiration generates the ATP required for the operation of PEPCK in bundle sheath cells (Hatch *et al.*, 1988). Moreover, NAD-malic enzyme decarboxylation activity in the mitochondria does not compete with PEPCK decarboxylation (Figure 1.13C), because the rate at which ATP is generated for PEPCK activity is limiting (Carnal *et al.*, 1993) and both decarboxylases contribute to the delivery of CO_2 at the site of Rubisco (Bräutigam *et al.*, 2014). In PEPCK type C_4 plants, PEP is regenerated in bundle sheath cells from the decarboxylation of oxaloacetate requiring one molecule of ATP, whereas in NADP- and NAD-malic enzyme subtypes, PEP is regenerated via PPDK in mesophyll cells using two molecules of ATP per molecule of CO_2 assimilated

(Bräutigam *et al.*, 2014). Theoretical models predict that the energetic costs of PEPCK subtypes are slightly lower than in NADP-malic enzyme subtypes, requiring less ATP per CO_2 molecule assimilated, although require one more molecule of ATP than C_3 plants (Kanai and Edwards, 1999; Bräutigam *et al.*, 2014).

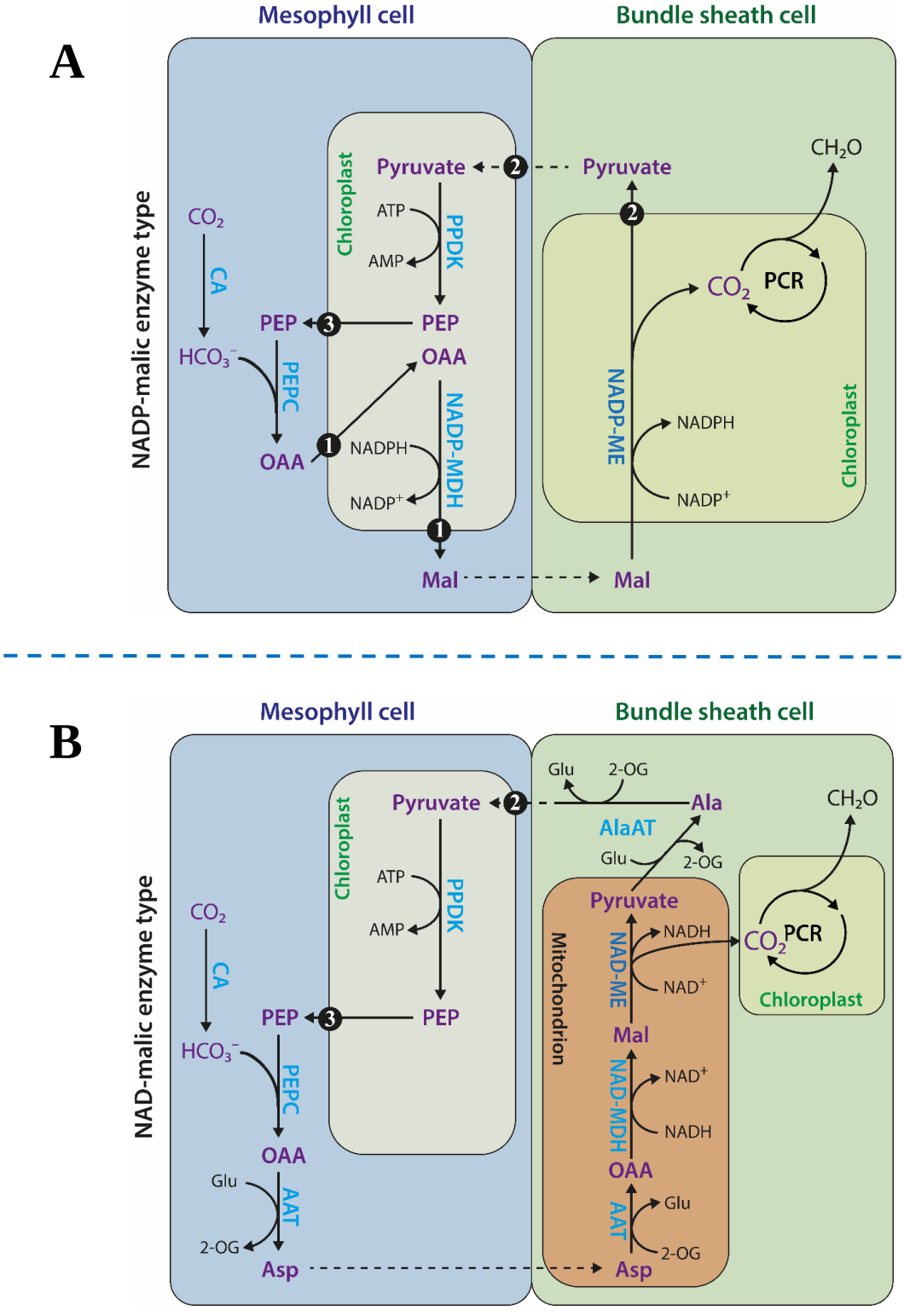

Fig. 1.14.

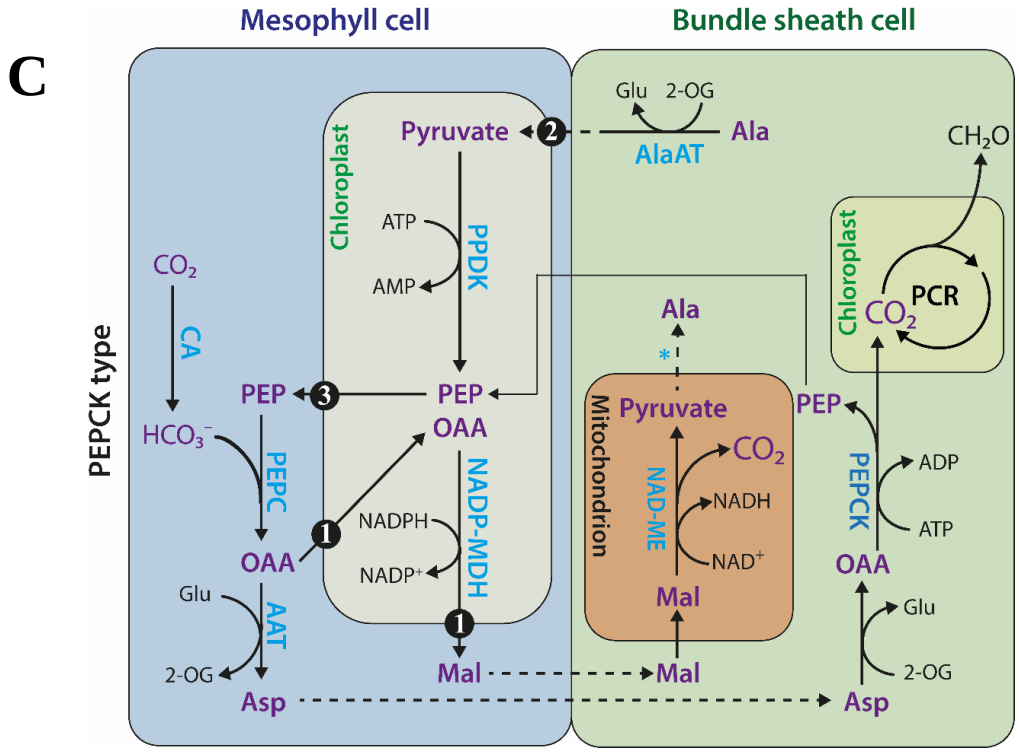

Fig. 1.14. Three biochemical variations of the C_4 pathway using the (A) NADP-malic enzyme, (B) NAD-malic enzyme or (C) PEPCK decarboxylase. C_4 photosynthesis is characterised by the primary decarboxylase (dark blue) operating in bundle sheath cells. Enzymes (light blue): CA, carbonic anhydrase; PEPC, phospho*enol*pyruvate carboxylase; AAT, aspartate aminotransferase; MDH, malate dehydrogenase; ME, malic enzyme; PEPCK, PEP carboxykinase; AlaAT, alanine aminotransferase. Metabolites (purple): OAA, oxaloacetate; Mal, malate; Asp, aspartate; Ala, alanine; Glu, glutamate; 2-OG, 2-oxoglutarate. Transporters: **1**, DiT1; **2**, BASS2/NHD1; **3**, PPT. PCR, photosynthetic carbon reduction cycle. Dashed lines show diffusion routes. *AlaAT. Adapted from Wang *et al.* (2011).

Aside from changes to the kinetic properties of Rubisco in C_4 plants, all other enzymes of the PCR cycle present in bundle sheath cells of C_4 plants are unchanged from their C_3 counterparts (Ashton *et al.*, 1990; Leegood and Walker, 1999). In C_3 leaves, triose phosphates that are generated in the PCR cycle in mesophyll cells are exported from the chloroplast, via a triose phosphate translocator, to be used in the cytosol for sucrose synthesis (Leegood and Walker, 1999). Since C_4 plants lack the ability to operate the PCR cycle in mesophyll cells due to the absence of Rubisco, phosphate, which is released from sucrose synthesis, is transported into bundle sheath chloroplasts and used for the regeneration of RuBP (Leegood and Walker, 1999). Triose phosphates accumulate in large quantities in C_3–C_4 intermediates *Flaveria floridana* and *Moricandia arvensis*, and the concentration is about 20-fold higher in C_4 plants than in C_3 plants (Leegood and von

Caemmerer, 1994). Movement of carbon through the 3-PGA/triose-phosphate shuttle (Figure 1.15) is another important feature in all C_4 plants and is likely to have evolved in C_3–C_4 intermediates to alleviate the burden on the PCR cycle in early developmental stages of C_4-competent bundle sheath chloroplasts (Leegood, 2013). In this shuttle, the concentration gradient of about 10 mM triose phosphate drives diffusion from mesophyll to bundle sheath cells, and in exchange return 3-PGA driven by a concentration gradient of about 9 mM (Stitt and Heldt, 1985).

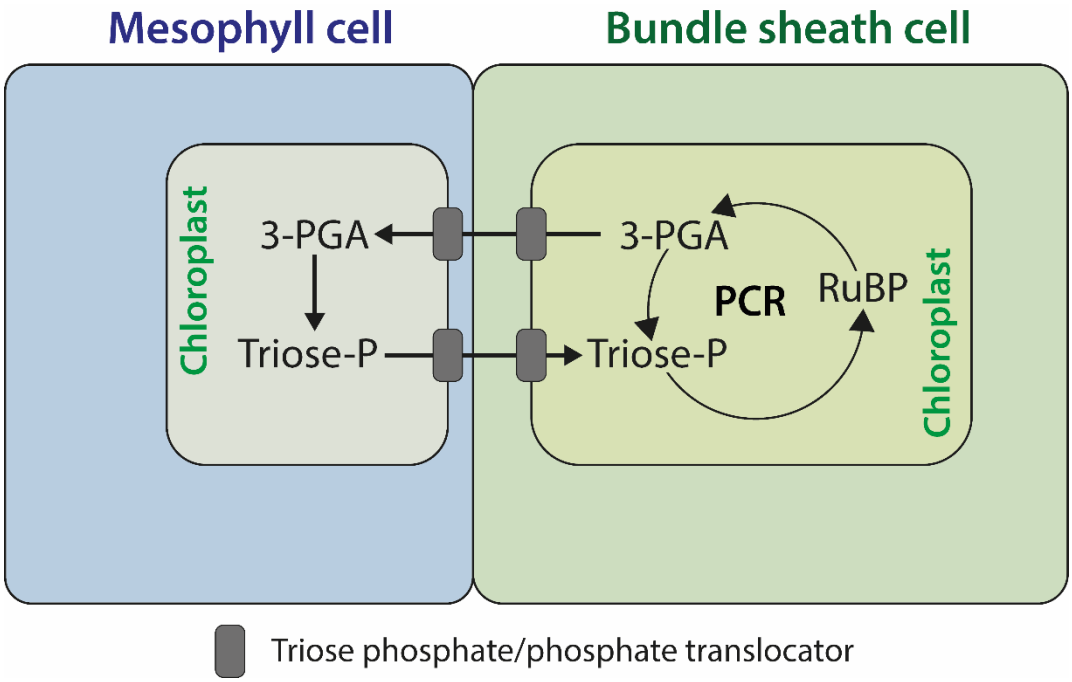

Fig. 1.15. 3-PGA/triose-phosphate shuttle operating between bundle sheath and mesophyll cells. The conversion of 3-PGA to triose phosphate requires three enzymatic reactions catalysed by phosphoglycerate kinase, glyceraldehyde-3-phosphate dehydrogenase and triose phosphate isomerase (see Figure 1.2).

1.4.2 Increased capacity of metabolite movement

The operation of the C_4 cycle depends on the efficient and rapid movement of metabolites through diffusion driven transport (Leegood, 1985; Leegood and von Caemmerer, 1989; Leegood and Walker, 1999). In C_4 plants, the capacity of these transport mechanisms are enhanced to move large quantities of metabolites between mesophyll and bundle sheath cells (Hatch and Osmond, 1976). In contrast to C_3 plants, which require one transport step to produce triose phosphates, C_4 plants require at least 30 steps (Weber and von Caemmerer, 2010). In NADP-malic enzyme subtypes, large quantities of oxaloacetate diffuse from the cytosol to chloroplasts of mesophyll cells via a translocator with high specificity for oxaloacetate but not malate (Hatch *et al.*, 1984). Another non-specific translocator with competing specificity for malate and oxaloacetate operates in mesophyll chloroplasts of *Zea mays* leaves, but is not efficient to operate under high load of C_4 photosynthesis when malate is in higher content than oxaloacetate (Day and Hatch, 1981; Hatch, 1987). During C_4 photosynthesis, a concentration gradient of about 18 mM malate drives diffusion from mesophyll cells to bundle sheath cells (Stitt and Heldt, 1985). In a recent study, however, Arrivault *et al.* (2016) noted that previous estimations were biased, since metabolite concentrations were determined from whole leaf tissue, instead of isolated mesophyll or bundle sheath cells.

These data also showed that malate, in *Zea mays*, contributes to the diffusion driven transport, and is about twofold more abundant in mesophyll than bundle sheath cells, resulting in a concentration gradient of 6 mM and not 18 mM as previously reported (Arrivault *et al.*, 2016). Furthermore, in NADP-malic enzyme subtypes, aspartate contributes to about 10% of the carbon pool and moves from mesophyll to bundle sheath cells in an estimated gradient of 0.96 mM (Kanai and Edwards, 1999; Arrivault *et al.*, 2016). In PEPCK subtypes, like *Megathyrsus maximus*, malate is imported into mitochondria in bundle sheath cells via a mitochondrial dicarboxylate carrier (DIC), but the transport of pyruvate from the mitochondrion to the cytosol has not been elucidated (Bräutigam *et al.*, 2011). Also, despite that the transport of pyruvate from bundle sheath to mesophyll cells via BASS2 (BILE ACID:SODIUM SYMPORTER FAMILY PROTEIN 2) and NDH1 (sodium:proton antiporter) has been elucidated in *Flaveria bidentis* (NADP-malic enzyme) and *Cleome gynandra* (NAD-malic enzyme), it has yet to be described in *Zea mays* (Furumoto *et al.*, 2011; Leegood, 2013).

1.4.3 Physiology and performance of C_4 plants

C_4 plants are characterised for their capacity to maintain high rates of photosynthesis in low CO_2 concentrations (Figure 1.16). This is because CO_2 can be concentrated around Rubisco, allowing Rubisco to operate under high CO_2 concentrations, thus suppressing the rate of photorespiration and inhibition by O_2 (Sage *et al.*, 2012). To allow such a response, membrane permeability has been increased to allow the rapid diffusion of metabolites, without compromising on the leakage of CO_2 or bicarbonate (Hatch, 1987).

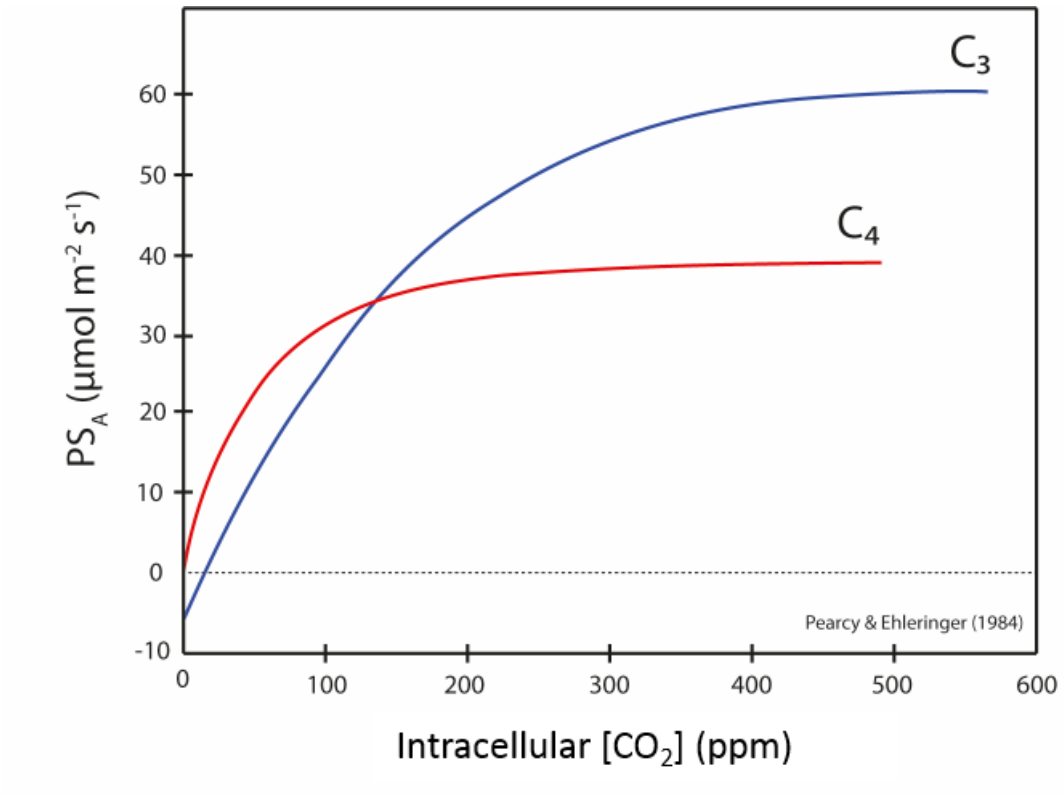

Fig. 1.16. Modelled relationship between the rate of photosynthesis (PS_A) and intracellular concentration of CO_2 in leaves of C_3 (blue) and C_4 plants (red). The initial slope of CO_2 assimilation in C_4 plants is greater than that of C_3 plants at a low intracellular CO_2 concentration, demonstrating the ability of C_4 plants to perform better in low CO_2. Redrawn from Pearcy and Ehleringer (1984).

The proportion of CO_2 leaked from C_4 leaves is minimised by the capacity of PEPC to rapidly assimilate CO_2 into the C_4-acid, along with the expression of Kranz anatomy (Hatch and Osmond, 1976; Hatch, 1987; Cousins *et al.*, 2007). However, the rate of photosynthesis in C_4 plants, at low CO_2, is limited by the rate at which bicarbonate is generated by carbonic anhydrase and delivered to PEPC (Sage and Kubien, 2007; Boyd

et al., 2015). Under such conditions, PEPC activity is independent of temperature unless the temperature falls below 10 °C, which increases the rate of PPDK inactivation (Shirahashi *et al.*, 1978; Hatch, 1979; Long, 1983; Ohta *et al.*, 2004) and the activity of PEPC becomes limited by the capacity of PPDK to regenerate PEP. In contrast and despite limited by low atmospheric CO_2, C_3 plants can achieve a higher maximal CO_2 assimilation rate because Rubisco is in higher content in C_3 leaves than in C_4 leaves (Ku *et al.*, 1996). However, nitrogen-use efficiency is increased in C_4 plants because less Rubisco is required to operate the PCR cycle (Brown, 1978; Schmitt and Edwards, 1981; Sage *et al.*, 1987).

C_4 grasses evolved under selective pressures such as increasing temperature, high light and declining CO_2 (Sage, 2004). A major characteristic of C_4 plants, especially those occupying open and arid grasslands, is to regulate the amount of water lost through transpiration by improving leaf hydraulics (Kocaçinar and Sage, 2004; Sack and Holbrook, 2006). As a result, stomata in C_4 plants can remain closed for longer during the daytime, when the light intensity is presumably higher, thus increasing water-use efficiency, which is at least twice as efficient as in C_3 plants (Hatch, 1987; Hatfield and Prueger, 2011). This is especially important in regions with higher temperatures and variable rainfall (Long, 1999; Gowik and Westhoff, 2011). There is also a distinct relationship between rate of assimilation and stomatal regulation. For instance, increased CO_2 fixation in C_4 grasses reduces stomatal conductance and minimises water loss (Osborne and Sack, 2012). A recent hydro-mechanical model of stomatal conductance of C_4 photosynthesis suggests that quicker responses in the mechanisms controlling stomatal opening and closure might have given C_4 plants the competitive advantage in achieving and maintaining high rates of CO_2 assimilation relative to C_3 plants (Bellasio *et al.*, 2017). An improved hydraulic design is likely to have co-evolved with the CO_2 concentrating mechanism of C_4 photosynthesis and would have served a significant role for the emergence of C_4 plants in arid zones (Osborne and Sack, 2012; Bellasio *et al.*, 2017).

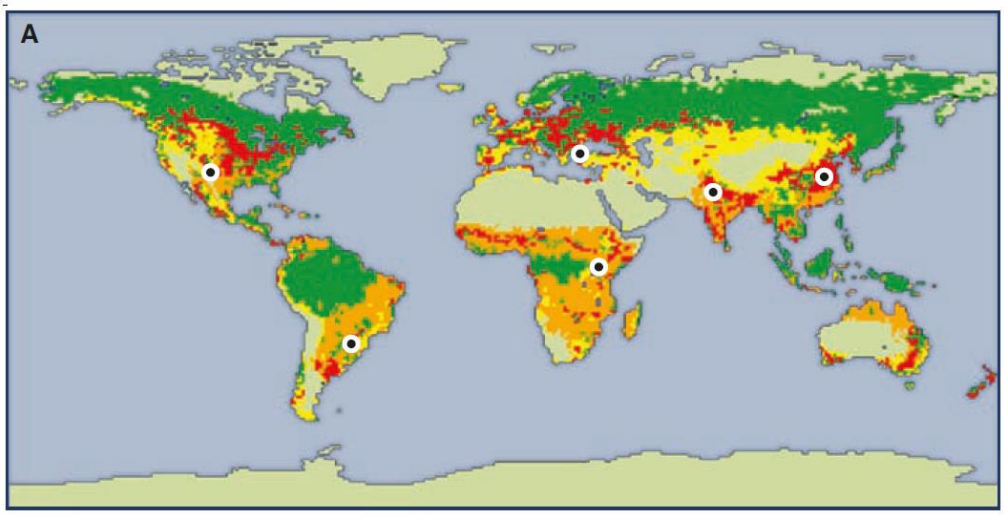

Fig. 1.17. Overview of the global distribution of higher plants dominated by either C_3 (yellow) or C_4 grasses (orange). Forests (green) and cropland (red) are also indicated. Figure does not consider the seasonal emergence of C_3 and C_4 plants in some grasslands. Black dots show the regions of C_4 grasslands whose geological history are best described. Figure and annotation obtained from Edwards *et al.* (2010).

In addition, the CO_2 compensation point of C_4 plants does not increase as much as it does in C_3 plants in response to high temperatures (Sage and Kubien, 2007). Therefore, C_4 leaves are less sensitive to leaf temperature, and better adapted for higher temperatures, somewhere in the 25 to 30 °C range (Ehleringer and Björkman, 1977). As a result, the landscape of grasses that populate the globe has drastically changed since the evolution of C_4 photosynthesis and it is believed that the C_4 syndrome was so successful that neighbouring ancestor C_3 grasses, mainly of tropical origin, were outcompeted as the atmospheric concentration of CO_2 decreased and temperatures increased (Sage, 1999; Edwards *et al.*, 2010; Sage *et al.*, 2012). C_4 grasses dominate in warm, tropical or subtropical environments (Figure 1.17), favouring higher daytime temperatures and lower altitudes, though need plenty of water and like their C_3 relatives are not adapted to drought-stress (Sage, 2004; Edwards *et al.*, 2010). Although the C_4 pathway was selected as an advantageous trait for increasing carbon gain through higher photosynthetic efficiency (Monson, 2003), higher energetic costs of C_4-related reactions, such as the ATP-dependent regeneration of PEP via PPDK or ATP-dependent decarboxylation by PEPCK, make C_4 plants less competitive in regions where C_3 photosynthesis is favoured (Bauwe *et al.*, 2010; Sage *et al.*, 2012; Lundgren *et al.*, 2016). It is likely, however, that the evolution of C_4 photosynthesis in grasslands allowed the broadening, rather than replacement, of existing ecological niches, thus allowing new C_4 populations to occupy

larger spaces, which gradually increased the ecological gap between C_3 and C_4 grasses (Edwards *et al.*, 2010; Lundgren *et al.*, 2015). The capacity of C_4 plants to operate at their optimum in regions with varying environmental conditions or extremes, such as temperature, water availability or soil salinity, which would otherwise directly promote photorespiration and dark respiration in C_3 plants (Brooks and Farquhar, 1985; Sharkey, 1988), have greatly contributed to C_4 evolution and the distribution of C_4 plants (Sage, 2004; Edwards *et al.*, 2010). Moreover, the diversity of these environmental conditions could promote evolution of C_4 photosynthesis in some taxa, but not others (Lundgren *et al.*, 2015). This is supported by the existence of several intermediate species, including *Flaveria* intermediates (Powell, 1978), in arid and saline habitats, which are zones where C_4 species originated from (Sage, 2004). However, there is still some doubt as to how much photorespiration is reduced in C_4 plants, and whether the three distinct subtypes of C_4 photosynthesis are truly representative or rather an oversimplification of the C_4 syndrome. We will understand the factors that contribute to the efficiency of carbon movement and assimilation in C_4 plants by investigating how the enzymes involved in C_4 photosynthesis are regulated (Furbank, 2011; Bellasio and Griffiths, 2014; Wang *et al.*, 2014; Arrivault *et al.*, 2016).

1.5 Aim of thesis and thesis structure

This research project was part of an international consortium which attempts to engineer characteristics of C_4 photosynthesis into existing C_3 crops in hopes to improve photosynthetic performance and crop yields (Leegood, 2013). However, the post-translational regulatory mechanisms of C_4-related proteins and how that regulation translates to the efficiency of carbon assimilation through a diurnal cycle remains unclear. Therefore, it is vital to identify the factors that contribute to the regulation C_4-related proteins prior to engineering artificial protein networks into existing C_3 crops, such that the efficiency of carbon fixation, water-use efficiency and nitrogen-use efficiency are achieved. Post-translational modifications (PTMs) play a crucial role in plant biology (Friso and van Wijk, 2015) and their extensive regulatory mechanisms remain largely undiscovered in C_4 plants. Characterising unknown PTMs of C_4-related enzymes can help to understand the regulation of C_4 photosynthesis, prior to incorporation into C_3 plants. With this information, artificial regulatory mechanisms can be implemented in C_4 crop plant transformants, thus maintaining the expected photosynthetic efficiency (Komatsu *et al.*, 2013; Furbank, 2016). Furthermore, exploiting these regulatory mechanisms can help maintain biochemical stability and increase abiotic stress tolerance of transformant crop plants grown in harsh nutrient-deficient environments (Hashiguchi and Komatsu, 2016).

The primary aim of this study was to identify light-dependent PTMs of key C_4-related proteins in leaves of *Setaria viridis* (NADP-malic enzyme subtype). Protein phosphorylation plays an important role in regulating the diurnal activity of PEPC, PEPCK and PPDK and it is hypothesised that several other C_4 enzymes, including NADP-dependent malic enzyme, aspartate aminotransferase and alanine aminotransferase undergo light-dependent phosphorylation. It is expected that not every phosphorylation site that is identified is under regulation or contributes to enzyme activity. However, identifying novel phosphorylation sites might provide some indication to undiscovered phosphoregulatory mechanisms that induce distinct changes to diurnal enzyme activity.

The secondary aim of this project was to ascertain whether NADP-malic enzyme, aspartate aminotransferase and alanine aminotransferase have similar kinetic properties across three C_4 NADP-malic enzyme monocot grasses, as well as explore the dual-decarboxylase system in NADP-malic enzyme subtypes and determine if there are distinct variations in the properties of aspartate and alanine aminotransferase in *Setaria viridis*, *Sorghum bicolor* and *Zea mays*. In the dual-decarboxylase system, C_4-acid decarboxylation is partitioned between NADP-malic enzyme and PEPCK or NAD-malic enzyme (Wang *et al.*, 2014). However, whether these pathways are differently regulated in closely related C_4 grasses is unclear. The C_4 grasses used in this study were chosen because they use NADP-malic enzyme as the primary decarboxylase, though have varying amounts of PEPCK activity (Hatch, 1987; Bräutigam *et al.*, 2014). Furthermore, *Sorghum bicolor* and *Zea mays* share a common ancestor whereas *Setaria viridis* evolved C_4 photosynthesis through a separate origin (Christin *et al.*, 2009). While it is accepted that NADP-malic enzyme activity is pH-dependent across C_4 species (Johnson and Hatch, 1970), it is hypothesised that each of the C_4 grasses in this study regulate NADP-malic enzyme differently and dependence on pH varies in dark and light conditions. Finally, it is hypothesised that there are interspecies differences in the kinetic properties of NADP-malic enzyme, aspartate aminotransferase and alanine aminotransferase.

The novel findings of this project are presented in Chapter 3, Chapter 4 and Chapter 5 of this thesis. A summary of our current understanding of the regulation of C_4-related proteins is presented in Chapter 3, followed by novel light-dependent phosphorylation sites identified in *Setaria viridis* (supplementary data in Appendix A). In Chapter 4, the light and dark *in vitro* activities and the corresponding Michaelis-Menten constants (K_M) of NADP-malic enzyme from *Setaria viridis*, *Sorghum bicolor* and *Zea mays* are presented and discussed. In Chapter 5, novel findings will show that the activity of aspartate aminotransferase is sensitive to dark and light changes and only aspartate aminotransferase in *Zea mays* is activated by L-malate and L-alanine. In Chapter 5 and 6, the implications of these findings will be discussed, with emphasis towards a putative, regulatory mechanism, which controls the flux of carbon, formation of PEP and efficiency of carbon assimilation in C_4 photosynthesis and sugar homeostasis during illuminated and darkened conditions.

Chapter 2 – Methods

2.1 Proteomics and Mass Spectrometry

2.1.1 Growth of plant material

Setaria viridis seeds accession A10 (harvested on April 2013) were received from Dr Asaph Cousins' Lab (Washington State University, Pullman, WA, USA) in early 2014. Seed dormancy was overcome by cold stratification (Brutnell *et al.*, 2010) or incubation at 45 °C prior to sowing (Rizal *et al.*, 2013).

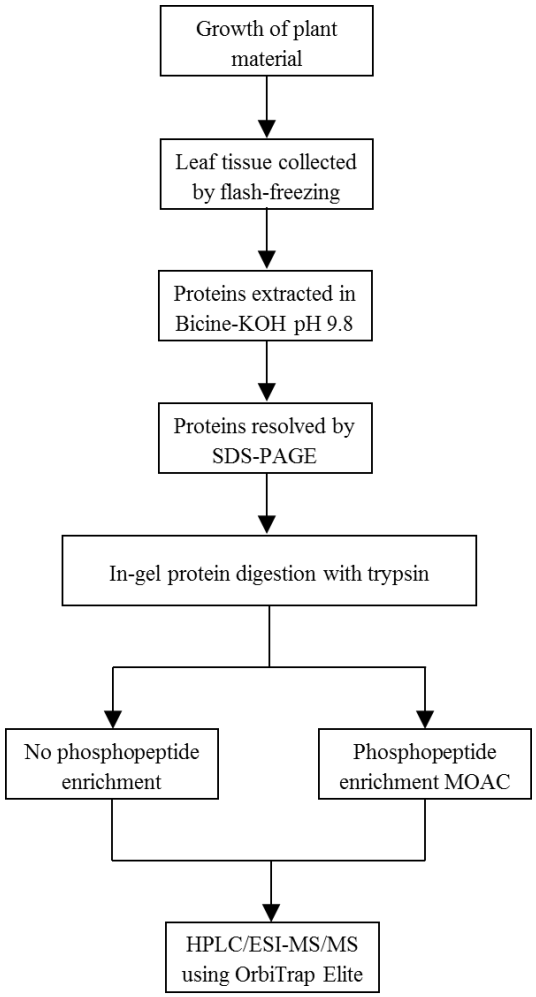

Fig. 2.1. General workflow for the extraction of leaf proteins, sample processing and analysis by mass spectrometry. Mass spectrometry method optimised for in-gel digestion of plant proteins. Samples were analysed using electrospray ionisation LC-MS/MS with ultra-sensitive Orbital Trap mass spectrometer.

Plants were grown for seed production and seeds were harvested from one-month old plants. To increase seed viability upon collection from bristles, seeds were dried at 40 °C for five days then stored at room temperature. Ten-month old *Setaria viridis* seeds were culled and sown into large trays containing nutrient rich M3 compost (ICL Levington, Ipswich, UK), supplemented with nitrogen (144 mg L^{-1}), phosphorus (73 mg L^{-1}) and potassium (239 mg L^{-1}) and covered with a thin layer of compost, following the planting method described by Jiang *et al.* (2013). Trays were watered with distilled water and propagator lids were fixed onto potting trays. Lids were covered with a sheet of black cloth for no more than 36 h to allow for dark germination. Plants were grown in an environment controlled growth chamber using a 16 h photoperiod (28 °C/26 °C light/dark), maintaining 350 µmol m^{-2} s^{-1} photosynthetic photon flux density (PPFD), 70% relative humidity and CO_2 not exceeding 600 ppm. A week after germination, seedlings were transplanted into individual 7 cm pots and grown until the 6th leaf was fully emerged, equivalent to 2.5 weeks after germination (Figure 2.2).

Fig. 2.2. 2.5-week old *Setaria viridis* photographed before the harvesting of leaves. During the harvest, cuts were made approximately half way from the tip and base of the leaf, indicated by the dashed line. One half-leaf section was collected per plant. 20 half-leaves were used for each time-point.

2.1.2 Extraction of leaf proteins for mass spectrometric analysis

All mass spectrometry protocols were performed under sterile conditions using proteomic-grade reagents and MilliQ water (18.2 MΩ cm^{-1}). To assess changes in protein post-translational modifications during the dark–light transition, 20 half-leaf sections from different 2.5-week old *Setaria viridis* plants (Figure 2.2) were harvested and flash-frozen in liquid nitrogen at 4 time-points: 2 h and 7.5 h into the dark period, 4 h and 15.5 h into the photoperiod. Frozen leaf tissue was ground to a fine powder in liquid nitrogen using a pestle and mortar, homogenised in 200 mM Bicine-KOH, pH 9.8 and 50 mM dithiothreitol (DTT) containing 1× ethylenediaminetetraacetic acid (EDTA)-free protease and PhosSTOP phosphatase inhibitors (Roche, Mannheim, Germany) (Figure 2.3). Crude extracts were cleared by centrifugation in Eppendorf tubes at 16,800 × *g*. Protein concentrations were determined spectrophotometrically at 595 nm following Bradford (1976) using bovine serum albumin (BSA) standards. Crude extracts were solubilised and boiled in sodium dodecyl sulfate (SDS) solubilisation buffer containing 100 mM Tris-HCl pH 6.8, 200 mM DTT, 20% (v/v) glycerol, 4% (w/v) SDS, 0.2% (w/v) bromophenol blue (BPB).

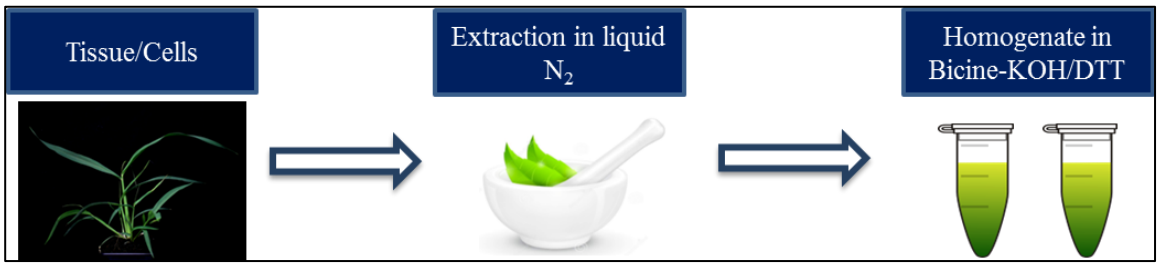

Fig. 2.3. Classical method for the extraction of proteins from plant leaves using liquid nitrogen. Proteins were extracted by grinding leaf tissue in liquid nitrogen using a pestle and mortar and homogenising in Bicine-KOH/DTT extraction buffer. Plant lysate was collected in Eppendorf tubes and cleared by centrifugation.

2.1.3 In-gel tryptic digestion

To analyse proteins by mass spectrometry, protein extracts were resolved by one-dimensional (1D) SDS polyacrylamide gel electrophoresis (PAGE) using 4–20% gradient pre-cast SDS-gels (Bio-Rad, Hertfordshire, UK). Gels were run at 180 V for 40

min in a Bio-Rad electrophoresis gel tank containing 1× Tris-Glycine-SDS (TGS) running buffer. After electrophoresis, gels were stained with Expedeon InstantBlue™ (Expedeon, Harston, UK). Bands were excised, placed into Eppendorf Lo-Bind microtubes (Figure 2.4) and destained at 37 °C in a solution containing 200 mM ammonium bicarbonate (ABC) and 40% acetonitrile (ACN). Gel pieces were dried down at 45 °C in a vacuum concentrator (Eppendorf, Stevenage, UK), and then reduced for 1 h at 56 °C with 200 µL 10 mM DTT and 50 mM ABC. Proteins were then alkylated in the dark at room temperature in a solution containing 55 mM iodoacetamide (IAA) and 50 mM ABC. Gel pieces were briefly washed with 50 mM ABC and 50% ACN then dried down. Tryptic digestion reactions were performed at 37 °C using 0.4 µg of trypsin from porcine pancreas (Sigma-Aldrich, Saint Louis, USA) in 70 µL containing 1 mM HCl, 40 mM ABC and 9% ACN. The following day, peptides were transferred to collection Lo-Bind microtubes and gel pieces were treated with 100% ACN and 5% formic acid to protonate and extract remaining peptides. Extracted peptides were slowly dried at 30 °C to remove interfering organic solvents, and stored at –20 °C until use.

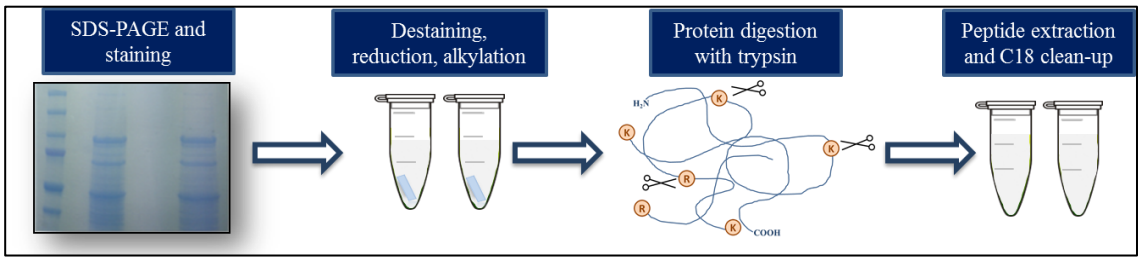

Fig. 2.4. General workflow for sample processing using an in-gel tryptic digestion approach, prior to analysis by mass spectrometry. First, proteins were resolved on 4–20% or 4–12% pre-cast SDS Bis-Tris gel and stained with Coomassie InstantBlue™. Proteins in the SDS matrix were washed, reduced and alkylated to linearise peptides. Finally, proteins were treated with trypsin. Scissor symbols indicate trypsin cleavage sites at amino acids (orange circles) lysine (K) and arginine (R) within the protein (represented by the blue line). Peptides were de-salted using C18 spin tips to remove detergents and organic contaminants prior to analysis by mass spectrometry.

2.1.4 C18 column clean-up

To increase peptide recovery and spectrum resolution, dried down peptides were desalted using Pierce C18 spin columns (ThermoFisher Scientific, Waltham, USA). Spin columns were activated with 50% methanol and washed with 0.5% trifluoroacetic acid (TFA) and 5% ACN (equilibration buffer). Peptides were reconstituted in 50 µL equilibration buffer, applied to the C18 resin and centrifuged at 1000 × *g*, following manufacturer's protocol (Pierce Biotechnology, Rockford, USA). Peptides were eluted in 70% ACN containing 0.1% formic acid.

2.1.5 Phosphopeptide enrichment by titanium dioxide

To enrich for phosphopeptides by titanium dioxide (TiO_2) metal oxide affinity chromatography (MOAC), dried down peptides were reconstituted in 150 µL 26% lactic acid, 0.4% TFA and 80% ACN (Buffer A) and applied to the surface of the activated TiO_2 resin (Figure 2.5) and centrifuged at 1000 × *g*. The flow-through was reapplied to the resin to maximise phosphopeptide binding. TiO_2 columns were washed with Buffer A at 3000 × *g*, and peptides were eluted in 1.5% ammonium hydroxide and 5% pyrrolidine. Samples were desalted using a graphite clean-up kit.

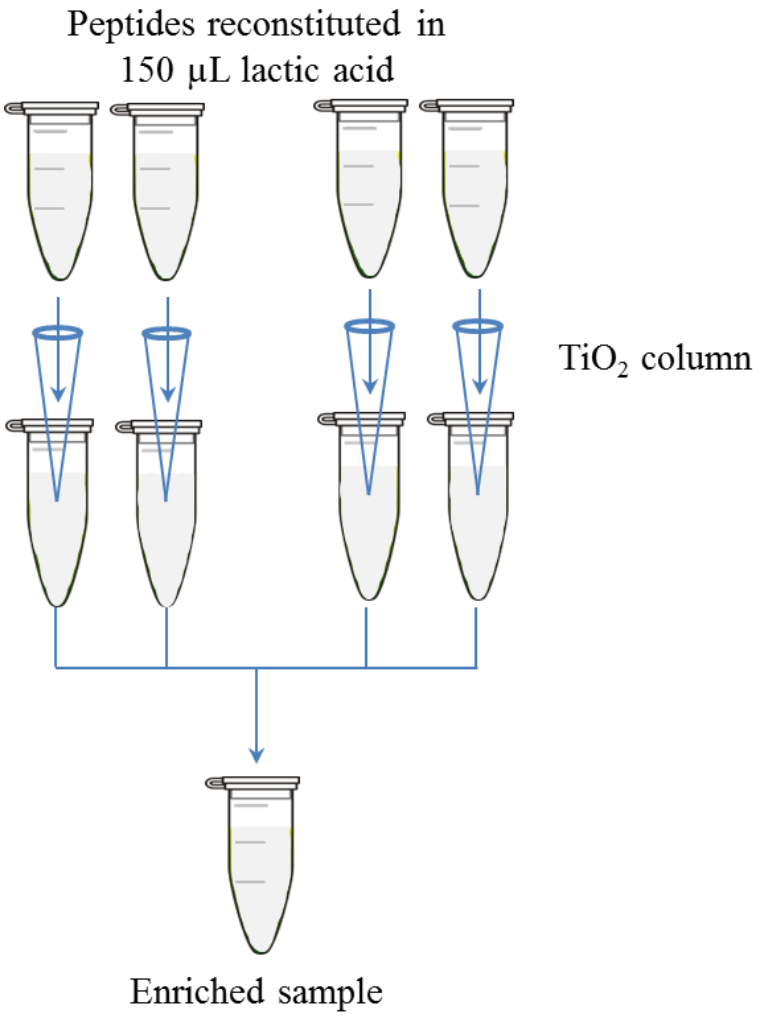

Fig. 2.5. Workflow schematic illustrating the basic flow of analyte through TiO_2 phosphopeptide enrichment columns. Four Eppendorf tubes per time-point, containing dried down peptides, were removed from the –20 °C freezer and equilibrated to room temperature. Peptides were reconstituted in 150 µL lactic acid and run through activated TiO_2 resins (blue cones) by centrifugation at low speed. Phosphopeptides were eluted into a new Eppendorf tube with 1.5% ammonium hydroxide and 5% pyrrolidine.

2.1.6 Mass spectrometry analysis

Mass spectrometry analyses, using a high-performance liquid chromatography (UHPLC) MS/MS Orbital Trap Elite mass spectrometer, were performed by Dr Richard G. Beniston (Senior Scientific Officer, biOMICS, The University of Sheffield) from February 2014 to November 2015 and Dr Adelina E. Acosta Martin (Facility Manager, biOMICS, The University of Sheffield) from April 2016 to June 2017. The protocols for in-gel protein digests, instrument calibration, sample injection and data analysis were issued and performed as a service by biOMICS and optimised through communication with Dr R. G. Beniston and Dr A. E. Acosta Martin.

2.1.7 General mass spectrometry protocol

Dried down peptides were reconstituted in 0.1% formic acid and 2% ACN and injected into a Dionex Ultimate 3000 UHPLC using a PepMap100 C18 trap column at a constant rate of 10 µL min^{-1}. The separation phase was performed over a 71 min gradient with increasing ACN concentrations from 2.4% to 72%, using a 15 cm PepMap100 C18 analytical column (2 µm particle size, 100 Å pore size, 75 µm I.D) (ThermoFisher Scientific, Waltham, USA) at a rate of 250 nL min^{-1}, at 35 °C. Nanospray ionization was performed at 2.0 kV, with the ion transfer capillary at 250 °C and S-lens setting of 60%. MS1 spectra ranging from 350–2000 *m*/*z* were acquired at a resolving power of 60,000. Following MS1 analysis, the top ten most abundant precursors were selected for MS2 analysis using collision induced dissociation (CID).

2.1.8 Immunoblotting

Immunoblots were performed using PEPC and NADP-malic enzyme antibodies raised from C_4 sequences, as described in Lundgren *et al.* (2016). Polypeptides were visualised with their appropriate Immunoglobulin G (IgG) secondary antibody grown in rabbit (polyclonal) or mouse (monoclonal) (Sigma-Aldrich, St. Louis, USA), in conjunction

with an enhanced chemiluminescence (ECL) blotting kit and Hyperfilm ECL (GE Healthcare, Buckinghamshire, UK).

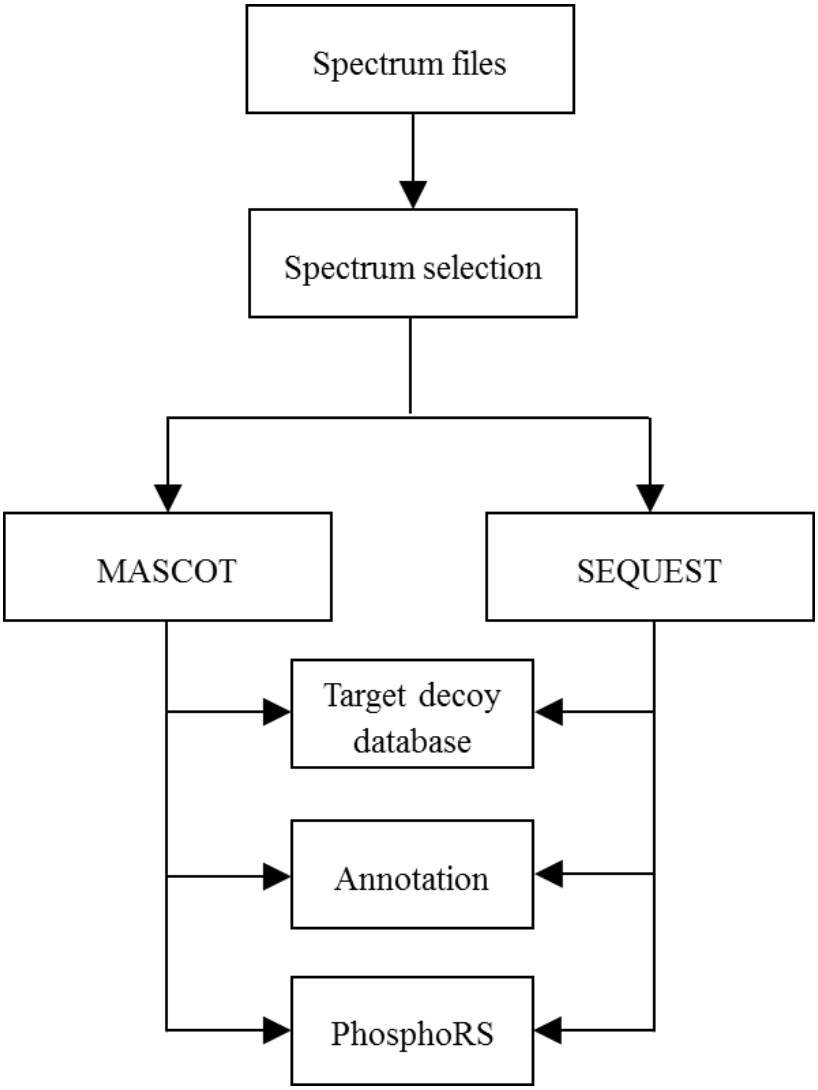

Fig. 2.6. Proteome Discoverer workflow used for identifying novel phosphorylation sites. Resulting spectrum files were searched against spectral libraries using MASCOT and SEQUEST and validated using a target decoy database. Phosphorylations were determined using the PhosphoRS algorithm in Proteome Discoverer.

Table 2.1. **MS/MS search engines used during the study**. The main MS/MS search engines that were available during the study. All search engines score protein matches as a measure of how similar experimental spectra are to theoretical peptide spectrum files.

Search Engine	Developer	Reference
MASCOT	Matrix Science	http://www.matrixscience.com
SEQUEST	ThermoFisher Scientific	http://www.thermo.com/com/cda/product/detail/0,1055,22209,00.html
MaxQuant	Max Planck Institute	http://www.biochem.mpg.de/5111795/maxquant

2.1.9 Data acquisition and analyses

The resulting peptide spectra were searched against target databases (Table 2.1), or theoretical spectral libraries from the National Center for Biotechnology Information non-redundant (NCBInr) and the Universal Protein Knowledgebase (UniProtKB) protein sequence databases using MASCOT or SEQUEST. Peptide spectrum match (PSM) validation was performed using decoy amino acid sequences assembled from the target database during each analysis. Search parameters set as follows: digestion with trypsin with a maximum of two missed cleavages, MS1=5 ppm, MS2=0.2 Da, carbamidomethylation of cysteine (57.02 Da) as a static modification and serine (Ser, S) and threonine (Thr, T) phosphorylation (79.97 Da, HPO_3; 97.99 Da, H_3PO_4) and methionine oxidation (15.99 Da) as variable modifications. Phosphorylations were determined using PhosphoRSv3.1. PhosphoRS site probabilities were set to a minimum of 0.75 to compensate for poor PSM scores and due to the high degree of automation of PTM prediction algorithms (Zhao and Jensen, 2009). Low scoring phosphorylation sites were only considered if the phosphorylation was repeatedly assigned in subsequent experiments. For statistical confidence, accepted spectra were searched against decoy amino acid sequences. The false discovery rate (FDR) was defined at two stringencies (1% and 5%), requiring a minimum of two peptides per protein match, filtered above 95% confidence. Candidate phosphopeptide significance was determined at $P \leq 0.05$ (*E*-value) in MASCOT and the cross-correlation value (Xcorr) in SEQUEST, where Xcorr ≥ 2.15 is significant.

Table 2.2. Online protein sequence databases used for MS/MS analyses. To increase the number of peptide spectrum matches, observed peptide spectra were searched against several plant protein databases. Uncharacterised proteins were subsequently searched against green plant protein sequences using BLAST.

Target Database	Online Directory	FASTA
NCBInr	ftp.ncbi.nlm.nih.gov/blast/db/FASTA/nr.gz	All Green Plants *Viridiplantae*
UniProtKB/Swiss-Prot UniProtKB/TrEMBL	ftp.uniprot.org/pub/databases/uniprot/uniref/uniref100	*Setaria italica* *Zea mays* *Sorghum bicolor*

Protein matches, which remained uncharacterised due to unreviewed protein accessions in UniProtKB, were searched against green plant protein sequences using the Basic Local Alignment Search Tool (BLAST). For consistency and due to uncharacterised matches from protein sequence repositories, along with the use of protein sequences from related species, differences in protein amino acid sequences of inferred proteins of multiple accession numbers and multiple protein isoforms, phosphorylation sites were annotated by the position of the modified residue in the phosphopeptide and not the amino acid number in the protein sequence, unless specifically indicated. UniProt accession numbers are indicated in the text (Table 3.3).

Full length protein sequences and structural information were obtained from the UniProtKB database and annotated using *FASTA*nnotate. Alignments were performed using Clustal Omega (http://www.ebi.ac.uk/Tools/msa/clustalo/). Protein schematics were drawn to scale using Adobe Illustrator and annotated with experimental data obtained (Appendix A). Peptide spectrum annotation was performed using pFind Studio (Fu *et al.*, 2004; Li *et al.*, 2005; Wang *et al.*, 2007). Protein structure information was acquired from the Protein Data Bank (https://www.rcsb.org/) and proteins were modelled using PyMol (https://pymol.org). Additional protein information was acquired from BRENDA (http://www.brenda-enzymes.org/). Monoisotopic masses were calculated using the Peptide Mass Calculator (http://www.peptidesynthetics.co.uk).

2.1.10 Phosphopeptide validation

Novel phosphorylation sites were validated using a modified in-gel tryptic digestion. Half-leaves from 2.5-week old *Setaria viridis* and *Sorghum bicolor* plants were harvested at 7.5 h into dark and *Megathyrsus maximus* leaves were harvested at 7.5 h into the dark and 4 h into the light. Leaves were ground to a fine powder in liquid nitrogen, then homogenised in 200 Bicine-KOH, pH 9.8 and 40 mM DTT containing EDTA-free protease and phosphatase inhibitors. Lysate was centrifuged at 4 °C and aliquots pipetted into 0.5 mL Eppendorf tubes. Protein concentrations were determined following Bradford (1976).

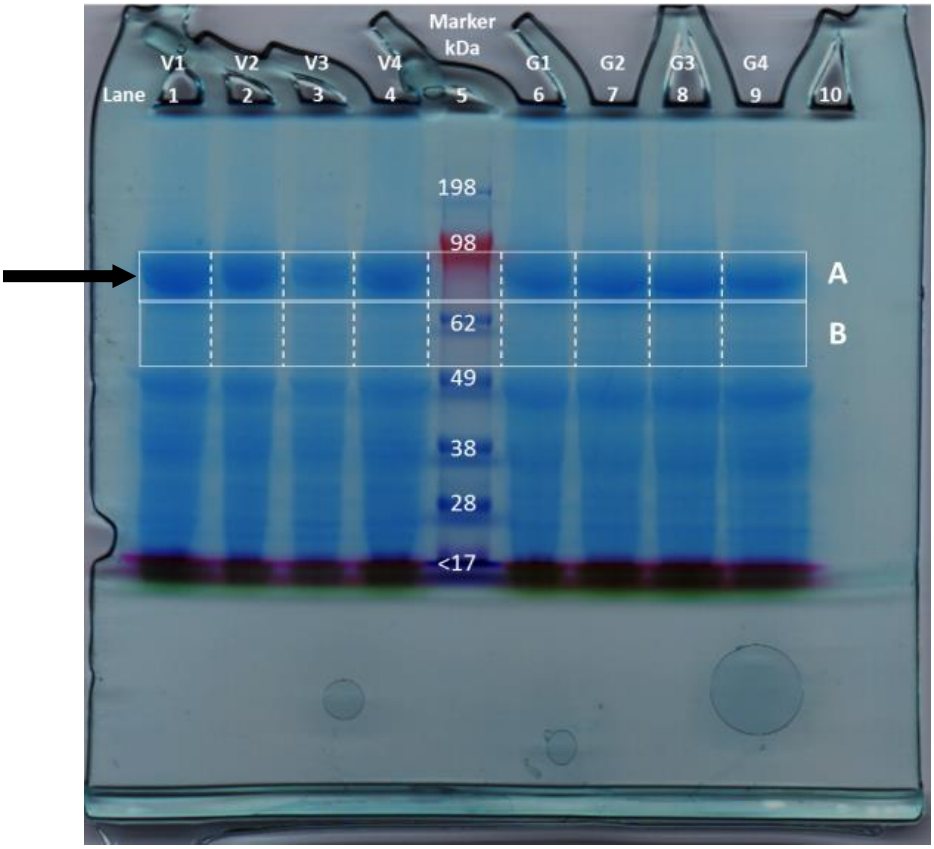

Fig. 2.7 Stained protein gel containing four replicates of *Setaria viridis* (lane 1–4, V1–V4) and *Sorghum bicolor* (lane 6–9, G1–G4) protein extracts from 7.5 h darkened leaves. 50 µg of protein was loaded into each lane of a 4–12%, 1.5 mm Bis-Tris SDS gel (NuPAGE), adding 15 µL of protein ladder into lane 5. Lane 10 was left empty. Gel was stained with InstantBlue™ stain for 15 min. Two sections (A and B) of the gel were excised per lane, per replicate, along the dashed lines. Dark band indicated by the black arrow below 98 kDa in Section A across eight samples is a combination of PEPC (109 kDa native) and PPDK (108 kDa native).

Protein extracts were solubilised in 4× lithium dodecyl sulfate (LDS) buffer and reduced using 10 mM DTT at 70 °C for 15 min then alkylated with 55 mM IAA for 15 min with dark incubation. 150 µg of protein was resolved using a 4–12% NuPAGE Bis-Tris 1.5 mm gel and subsequently stained with Coomassie dye, InstantBlue™ stain for 15 min. After staining, gel pieces were excised from two regions of the gel, between 110 kDa and 50 kDa, as indicated on Figure 2.7. Gel pieces were destained at room temperature and incubated overnight with 0.15 µg of trypsin at 37 °C. The following day, peptides were extracted in ACN and 5% formic acid by gentle agitation at room temperature, dried down using a SpeedVac at 45 °C and stored at –20 °C before use.

2.2 Protein Isoform and Phosphoproteome Analysis

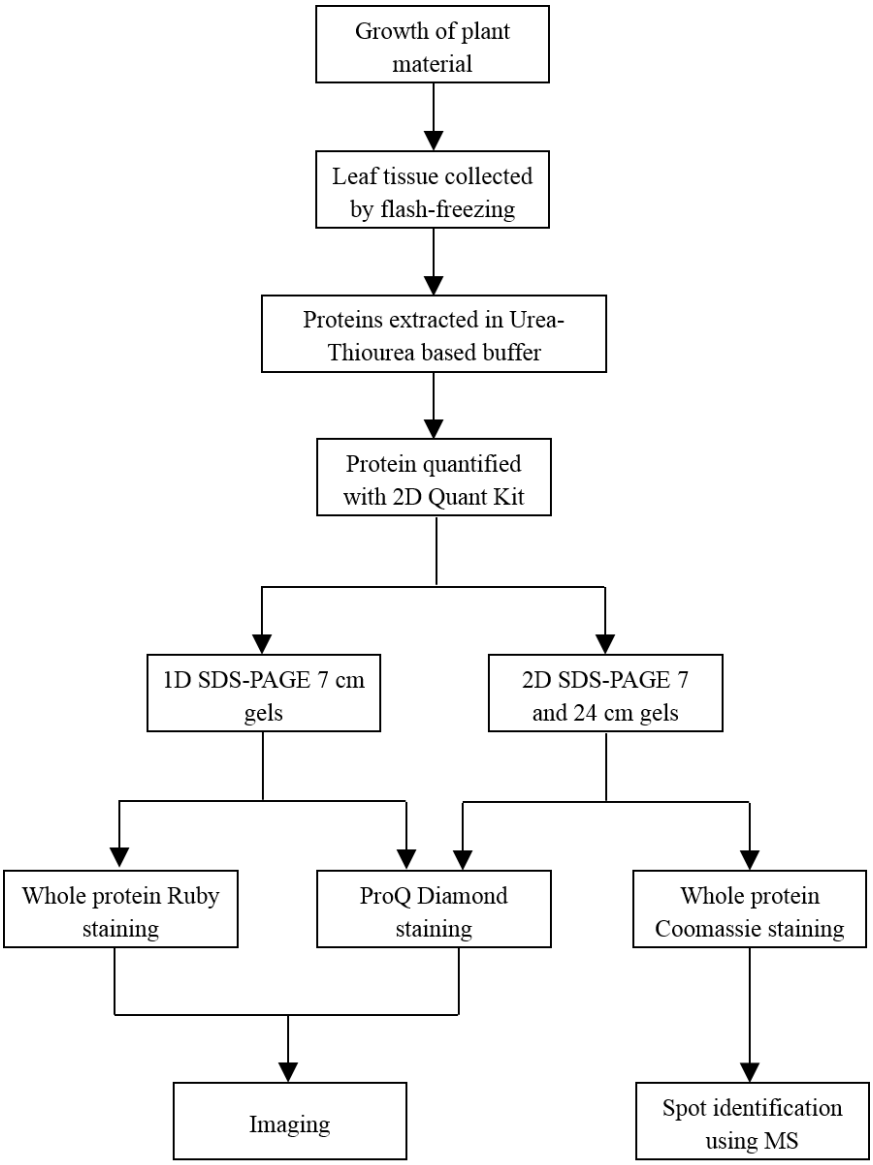

Fig. 2.8. *Setaria viridis* sample preparation workflow for protein isoform analysis. *Setaria viridis* plants were grown in a controlled environment and harvested at four time-points by flash-freezing in liquid nitrogen. Proteins were extracted using a urea-thiourea based buffer. Gels were either stained for whole protein or phosphoprotein, and the former subjected to analysis by mass spectrometry.

2.2.1 Sample preparation

To analyse protein isoforms by 2-dimensional (2D) SDS-PAGE, 350 mg of plant tissue from four specific time-points (2 h and 7.5 h into dark; 4 h and 15.5 h into light) was homogenised in a concentrated lysis buffer containing 8.2 M urea, 2.3 M thiourea, 35 mM Tris-base ((hydroxymethyl)aminomethane), 4.7% 3-[(3-cholamidopropyl)dimethylammonio]-1-propanesulfonate (CHAPS), 1 μM pepstatin, 1× nuclease mix, EDTA-free protease and PhosSTOP phosphatase inhibitors (Roche, Mannheim, Germany). Crude extracts were transferred into Eppendorf tubes, incubated on ice for 30 min with agitation every ten min for the complete removal of nucleic acids, and centrifuged at 4 °C at 16,800 × *g* until liquid fraction appeared clear. The supernatant was collected, and proteins were quantified using the 2D Quant Assay Kit (GE Healthcare, Buckinghamshire).

2.2.2 Two-dimensional SDS-PAGE

Protein extracts were subjected to analysis by two-dimensional (2D) gel electrophoresis on 7 and 24 cm resolving gels using a 29:1 acrylamide:bisacrylamide solution containing 1.5 M Tris-HCl pH 8.8, 10% SDS, 0.5% (v/v) ammonium persulfate solution (APS) and 0.05% (v/v) tetramethylethylenediamine (TEMED). Proteins in native conditions were solubilised in rehydration buffer (lysis buffer, BPB and 1.6% (v/v) DeStreak) containing 1.6% (v/v) immobilized pH gradient (IPG) buffer (pH 4–7) and 20 mM DTT, vortexed and centrifuged at 13,300 × *g* for 5 min. 80 or 450 μg of protein for 7 or 24 cm 10% SDS gels, respectively, was fixed onto a pH 4–7 Immobiline DryStrip Gel (referred hereafter as IPG strip) (GE Healthcare, Buckinghamshire, UK) by passive rehydration. Isoelectric focusing (IEF) for 7 cm IPG strips was performed using a 12.5 h protocol (Table 2.3) at 300–2000 volts (V), 50 μA and 24 cm IPG strips were focused using a protocol at 750–10,000 V over the course of 15 h (Table 2.4).

Table 2.3. **Programme for 7 cm IEF**. Small format protocol used for isoelectric focusing of *Setaria viridis* proteins using 7 cm 10% SDS gels.

Step	Task	Voltage (V)	Duration
1	Gradual voltage increase	300V	1h30
2	Gradual voltage increase	500V	3h
3	Voltage hold	500V	0h30
4	Gradual voltage increase	2000V	1h
5	Voltage hold	2000V	6h30

Table 2.4. **Programme for 24 cm IEF**. Large format protocol used for isoelectric focusing of *Setaria viridis* proteins using 24 cm 10% SDS gels. 24 cm gels were used for subsequent spot analysis and protein identification using tandem mass spectrometry.

Step	Task	Voltage (V)	Duration
1	Gradual voltage increase	750	1h
2	Gradual voltage increase	2000	5h
3	Voltage hold	2000	2h
4	Gradual voltage increase	8000	2h
5	Voltage hold	8000	3h
6	Gradual voltage increase	10000	0h30
7	Voltage hold	10000	1h30

After IEF, IPG strips were immediately stored in plastic containers at –20 ˚C. Before the second dimension, IPG strips were immersed in 1× TGS containing 1% (w/v) DTT for 15 min then alkylated with 2.5% (w/v) IAA. Strips were then positioned on 7 or 24 cm SDS gels and stabilised using 1% (w/v) agarose. 7 cm gels were run at 25 V for 15 min, then at 200 V until bands migrated to the bottom of the gel. 24 cm gels were run at 600 V for 6.25 h with a maximum current of 10 µA for the first 3 h, then 40 µA per gel, while maintaining 20 °C.

2.2.3 ProQ Diamond phosphoprotein staining

For phosphoprotein profiling, 7 cm SDS-PAGE gels were fixed in 50% (v/v) methanol and 10% (v/v) acetic acid, then left to stain in the dark on a rocker for 2 h in 65 mL 3-fold diluted ProQ Diamond phosphoprotein gel stain (ThermoFisher Scientific, Weltham, USA), following Agrawal and Thelen (2009). After staining, gels were destained in 20% ACN and 5% sodium acetate, pH 4.0. ProQ Diamond stained gels were visualised with a FLA-5100 (FUJIFILM Life Science, Stamford, USA) using a 532 nm laser at 740 V intensity. Phosphoprotein signal was tuned against a PeppermintStick™ phosphoprotein standard (ThermoFisher Scientific, Weltham, USA).

2.2.4 Coomassie staining

7 and 24 cm 2D gels were stained using Coomassie Simply Blue (ThermoFisher Scientific, Weltham, USA) with gentle agitation at 4 °C. Stained gels were washed twice with ultra-pure water and imaged using the FLA-5100 at 500 V with 635 nm laser excitation.

2.3 Determining Enzyme Kinetics

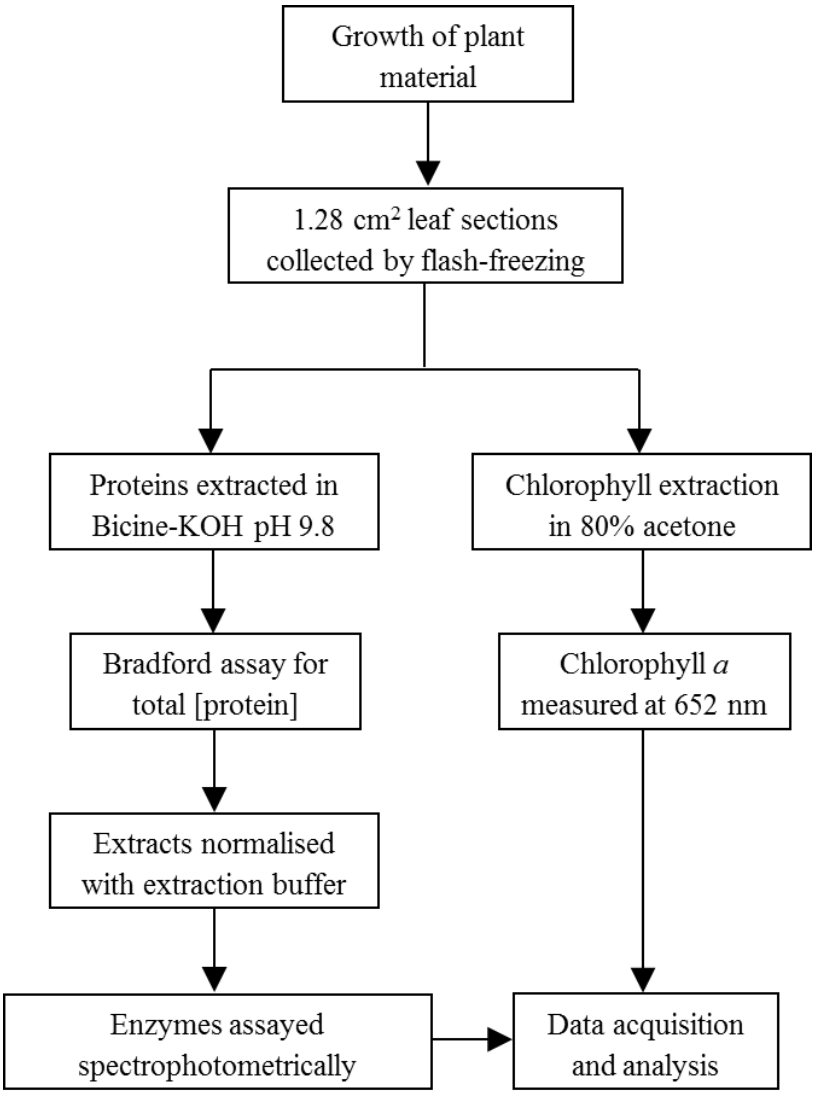

Fig. 2.9. Schematic showing the workflow for protein assays using *Setaria viridis*, *Sorghum bicolor* and *Zea mays* leaf proteins. Plants were grown in four sets of 20 replicates in a controlled chamber under ambient CO_2 (400 ppm), long days at 28 °C and 900 µmol m^{-2} s^{-1} PPFD. Leaf tips of 2.5-week old plants were harvested by flash-freezing in liquid nitrogen. Proteins were extracted, quantified and normalised prior to measurement.

2.3.1 Preparation of leaf homogenates for enzyme measurement

To determine the enzymatic properties of PEPC, NADP-malic enzyme, aspartate aminotransferase and alanine aminotransferase in response to the dark to light transition, two 16 mm × 8 mm sections (Figure 2.10) were cut no more than 2 cm from each leaf tip of mature *Setaria viridis* and *Sorghum bicolor* plants at four time-points (2 h and 7.5 h into dark; 4 h and 15.5 h into light) and *Zea mays* at two time-points (7.5 h into dark and 15.5 h into light), placed into a microtube and flash-frozen in liquid nitrogen. Leaf proteins were extracted from the leaf section closer to the leaf tip, as detailed in Chapter 2, Methods Part I, using 1 mL of 200 mM Bicine-KOH, pH 9.8, including protease inhibitors. Crude extracts were cleared by centrifugation in Eppendorf tubes at 16,800 × *g* at 4 °C, then 250 µL aliquots were stored at –80 °C.

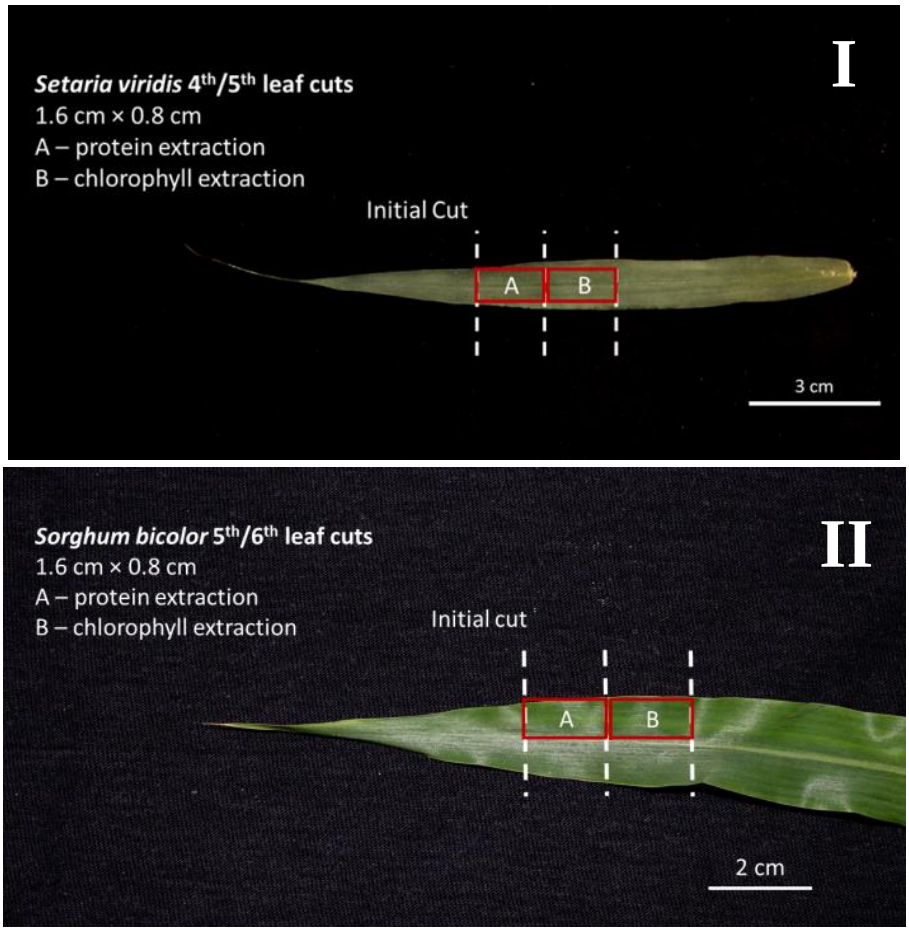

Fig. 2.10. 2.5-week old *Setaria viridis* (I) and *Sorghum bicolor* (II) leaves photographed before harvests. Proteins for enzyme assays were extracted from leaf section **A**. Chlorophyll content was measured in the adjacent leaf section (**B**). The 16 mm × 8 mm leaf sections were accurately cut using a metal template.

2.3.2 Protein quantification

Protein concentrations were determined for leaf homogenates spectrophotometrically at 595 nm using a BSA standard curve (Figure 2.11) following Bradford (1976).

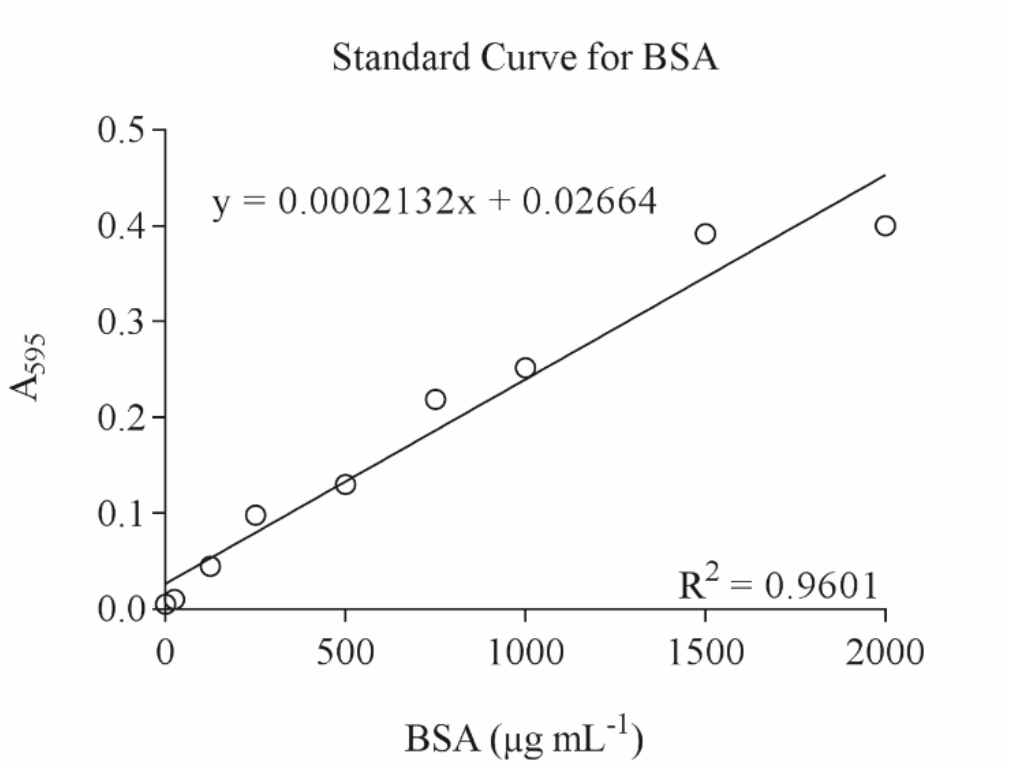

Fig. 2.11. The BSA standard curve that was used to determine protein concentration in leaf homogenates. Absorbance of bovine serum albumin standards (0–2000 µg), in solution, was determined spectrophotometrically. Linear regression analysis was performed, and the equation was used to calculate total protein concentration in leaf lysates.

Prior to each assay, crude extracts were normalised against the lowest protein concentration using equation 1,

$$\left(\frac{A_n}{A_x} - 1\right) \times U_i = U_F \qquad (1)$$

where A_n is the absorbance of a sample, A_x is the absorbance of the least concentrated sample, U_i is the initial crude extract volume (mL) and U_F is the volume (mL) of buffer to add each extract to normalise them against the least concentrated extract.

2.3.3 Measurement of enzymes

Rapid-assays are summarised in Table 2.8. Each enzyme assay consisted of six biological replicates across ten substrate concentrations (5000 range fold), each including three technical replicates on a 96-well microtitre plate (Figure 2.12). Reactions were initiated by the addition of 5 µL of leaf lysate (150 µL final volume) and monitored over 15 cycles (20 min) or until reaction reached saturation. For each assay, no leaf protein and no substrate controls were used to subtract non-enzyme mediated reaction background signals. Reaction rate given in terms of the amount of NADP (Figure 2.13A) or NADPH (Figure 2.13B) formed, per amount of protein used to initiate the reaction, per unit time.

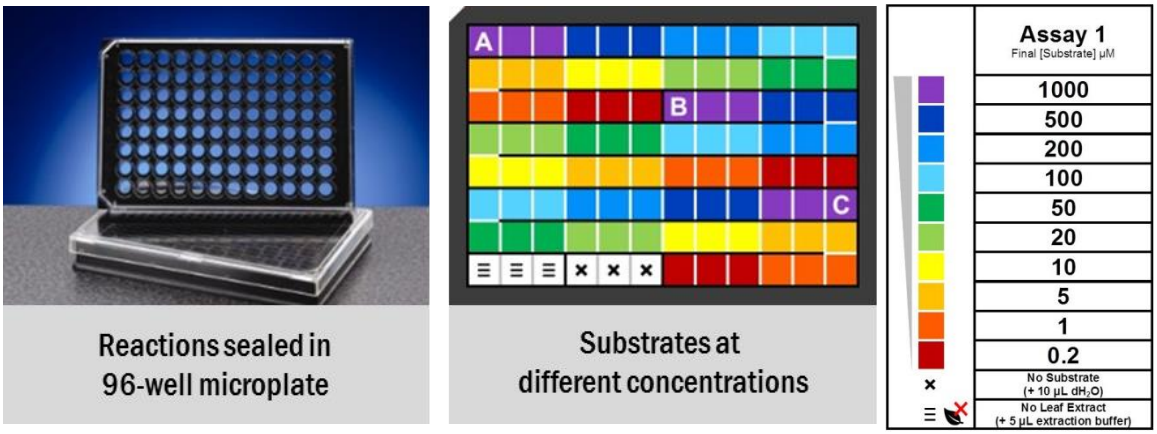

Fig. 2.12. Example of a 96-well microtitre plate assay design used for determining Michaelis-Menten kinetics. Each plate contained three biological replicates (A, B and C), no substrate (≡) and designated controls (×), across ten substrate concentrations to determine K_M constants. Reactions were initiated by adding 5 µL of normalised protein extract to 145 µL of mastermix, giving a final volume of 150 µL and monitored spectrophotometrically over time in a continuous assay at 25 °C.

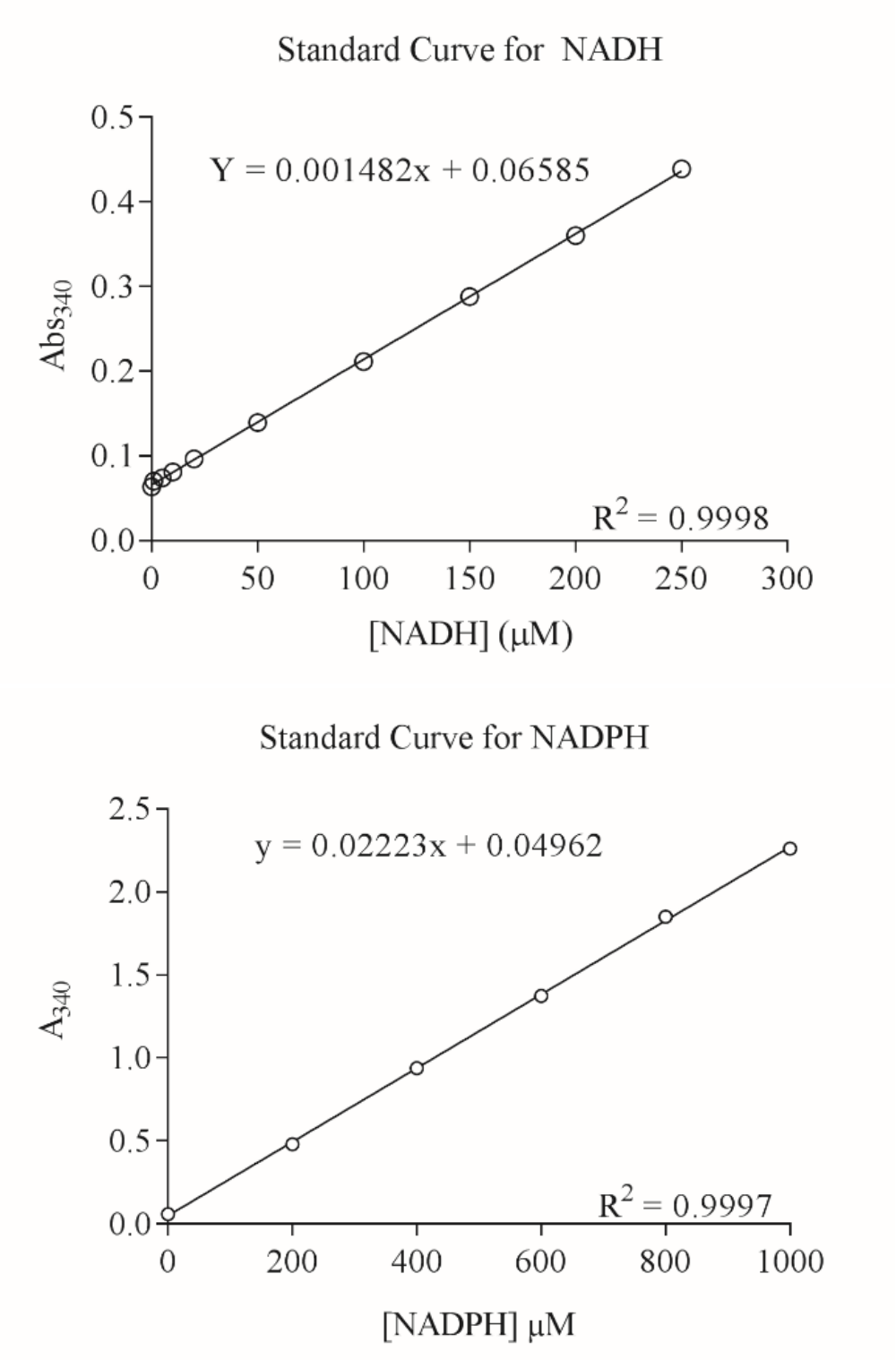

Fig. 2.13. NADH (A) and NADPH (B) standard curves for determining enzyme reaction rates. The assay was performed using serial dilutions of a freshly made NADH or NADPH stock solutions. Linear regression analysis was performed, and the goodness of fit was determined. NADH curves were used for PEPC, PEPCK and aminotransferase assays. NADPH used for the NADP-malic enzyme assays.

2.3.4 Phosphoenolpyruvate carboxylase assay

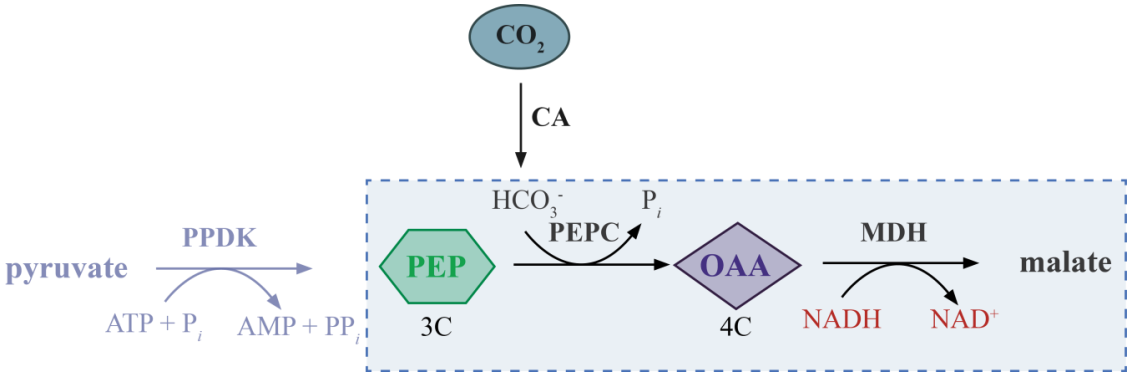

Fig. 2.14. Reaction mechanism showing the carboxylation of phospho*enol*pyruvate (PEP) to oxaloacetate (OAA) catalysed by PEPC in C4 photosynthesis. Highlighted region in blue box indicates the direction of the *in vitro* reaction, monitoring the reduction of OAA to malate via MDH. The number of carbons is indicated below each metabolite. CA, carbonic anhydrase; PPDK, pyruvate phosphate dikinase; P_i, phosphate.

Phospho*enol*pyruvate carboxylase (PEPC; EC 4.1.1.31) was assayed at 340 nm, 25 °C, following the reduction of oxaloacetate (OAA) by nicotinamide adenine dinucleotide (NADH) (Figure 2.14). 150 µL reaction mixtures contained 97.32 mM 4-(2-hydroxyethyl)-1-piperazineethanesulfonic acid-potassium hydroxide (HEPES-KOH), pH 7.5, 10 mM $NaHCO_3$, 5 mM glucose-6-phosphate (G6P), 5 mM $MgCl_2$, 0.2 mM NADH and 6 units of malate dehydrogenase (MDH) (Table 2.5). Absorbance signals of reaction mixtures containing no leaf protein were used to correct for non-enzymatic oxidation of NADH.

Table 2.5. PEPC mastermix.

Stock Concentration	Reagent	Final Concentration
0.1 M	HEPES-KOH, pH 7.5	97.32 mM
1 M	$NaHCO_3$	10 mM
1 M	G6P	5 mM
0.5 M	$MgCl_2$	5 mM
0.25 M	NADH	0.2 mM
1200 U mg^{-1} (5 mg mL^{-1})	MDH	6 U mL^{-1}

2.3.5 NADP-malic enzyme assay

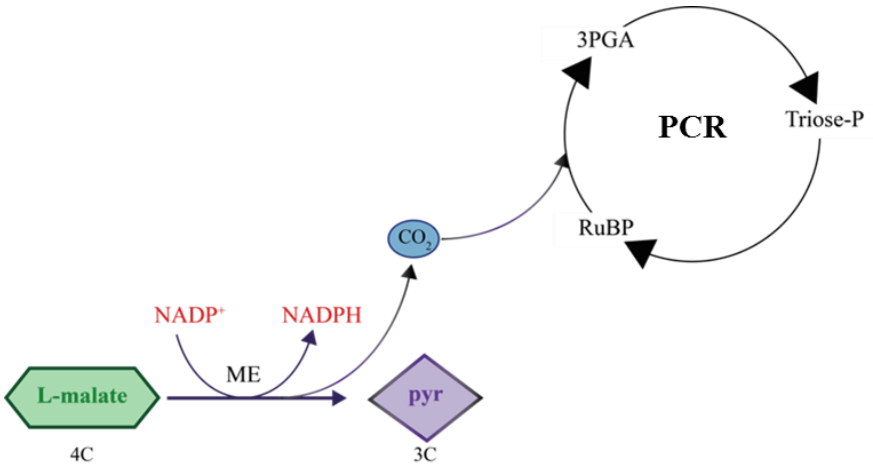

Fig. 2.15. Reaction mechanism showing the decarboxylation of L-malate by NADP-malic enzyme (ME) in bundle sheath chloroplasts of C_4 plants. The *in vitro* assay monitors the formation of NADPH (in red) following the decarboxylation of L-malate by the NADP-dependent malic enzyme. In bundle sheath chloroplasts of C_4 plants, malate is oxidised to pyruvate (pyr), forming NADPH and CO_2. CO_2 then enters the PCR cycle. The number of carbons is indicated below each metabolite. RuBP, ribulose-1,5-bisphosphate; 3-PGA, 3-phosphoglycerate.

NADP-dependent malic enzyme (NADP-ME; EC 1.1.1.40) was spectrophotometrically assayed in the forward direction (decarboxylating), at 340 nm at 25 °C, following the reduction of $NADP^+$ (Figure 2.15). The reaction mixture contained 98.90 mM Tris-HCl, pH 8.0, 5 mM $MgCl_2$ and 0.5 mM nicotinamide adenine dinucleotide phosphate ($NADP^+$) (Table 2.6). The pH and concentration of $MgCl_2$, required to achieve optimal rates of reaction, were determined for NADP-malic enzyme from darkened and illuminated leaves.

Table 2.6. NADP-malic enzyme mastermix.

Stock Concentration	Reagent	Final Concentration
0.1 M	Tris-HCl, pH 8.0	98.90 mM
0.5 M	$MgCl_2$	5 mM
0.5 M	$NADP^+$	0.5 mM

2.3.6 Aspartate and alanine aminotransferase assay

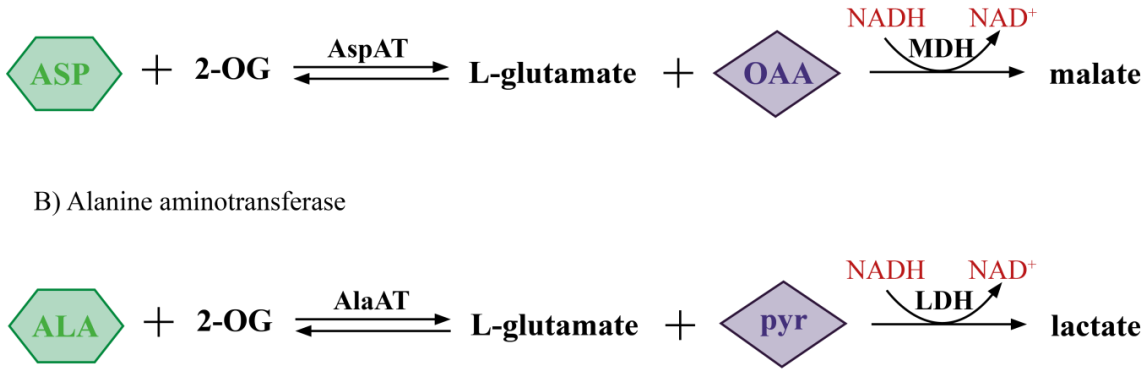

Fig. 2.16. Reaction mechanism for the aspartate (Asp) and alanine (Ala) aminotransferase assays. Aminotransferases were assayed by coupling to malate dehydrogenase (MDH) or lactate dehydrogenase (LDH). 2-OG, 2-oxoglutarate; OAA, oxaloacetate.

Aspartate aminotransferase (EC 2.6.1.1) was assayed spectrophotometrically at 340 nm by coupling to MDH (Table 2.7), following the oxidation of NADH to NAD^+ (Figure 2.16) at pH 8.0. The range of L-aspartate and 2-oxoglutarate concentrations used in this assay was 0-25000 µM and 0–2000 µM, respectively. The activity of aspartate aminotransferase was assayed in the presence of L-malate, L-alanine, 3-PGA, PEP, pyruvate and dimethyl-2-oxoglutarate, an analogue of 2-oxoglutarate.

Alanine aminotransferase (EC 2.6.1.2) was assayed in the presence of L-alanine towards the formation of lactate at pH 7.5, by coupling to LDH. L-Alanine and L-aspartate were used as the negative control for aspartate and alanine aminotransferase, respectively.

Table 2.7. Aminotransferase mastermix. Mastermix used for aspartate and alanine aminotransferase assays. † Indicates alanine aminotransferase reagents.

Stock Concentration	Reagent	Final Concentration
1 M	Tris-HCl, pH 8.0 or 7.5†	50 mM
50 mg mL^{-1}	Pyridoxal phosphate	10 µg mL^{-1}
0.5 M	EDTA	2 mM
0.5 M	NADH	0.2 mM
6000 U mg^{-1} (1.0 mg mL^{-1})	MDH	4 U mL^{-1}
1000 U mg^{-1} (9.3 mg mL^{-1})	LDH†	4 U mL^{-1}

Table 2.8. Summary of enzyme assays.

Assay	Wavelength	Spectroscopy
PEPC	**340**	Measures the concentration of NADH. Abs should ***decrease*** over time due to oxidation to NAD^+.
PEPCK	**340**	Measures the concentration of NADH. Abs should ***decrease*** over time due to oxidation to NAD^+.
NADP-ME	**340**	Measures the concentration of NADPH. Abs should ***increase*** over time due to $NADP^+$ reduction to NADPH.
AspAT AlaAT	**340**	Measures the concentration of NADH. Abs should ***decrease*** over time due to oxidation to NAD^+.
Bradford	**595**	Measures the concentration of total protein present in the crude extract (Beer-Lambert Law).
Chlorophyll	**652** (Sample) **750** (Blank)	Measures the concentration of chlorophyll *a* (mg L^{-1}) in 80% ethanol or 80% chilled acetone (Appendix B).

2.3.7 Determining Michaelis-Menten kinetics

Raw data was analysed in Microsoft Excel and enzyme reaction rates were graphed using Prism 7 (GraphPad Software) and the Michaelis-Menten constants (K_M) were determined using a curve fitting algorithm in GraphPad, using the Michaelis-Menten model (2),

$$V_0 = V_{max} \cdot \frac{[S]}{[S] + K_M} \qquad (2)$$

where V_0 is equal to the velocity of the reaction, V_{max} is the maximum reaction rate, [S] is the substrate concentration and K_M is the Michaelis-Menten kinetics constant. Initial velocity is given as an arbitrary unit of absorbance (Abs) change over time (min).

NB. V_{max} cannot be reported because enzyme assays were conducted using enzyme in crude leaf lysates and not purified protein. Also, for simplicity, K_M will be referred to as affinity. However, it should be noted that K_M and affinity are not interchangeable due to limitations of the Michaelis-Menten model. To properly discuss substrate affinity for an enzyme, the structural properties and binding interactions must be known.

Affinity fold change (i.e. increase or decrease) was calculated as a ratio of two K_M values using equation (3),

$$\text{Fold change} = \frac{{K_M}^2}{{K_M}^1} - 1 \qquad (3)$$

where K_M^2 is the new value (in response to a variable, for example light) and K_M^1 is the original value. An increase in K_M corresponds to a decrease in affinity (positive fold change) and decrease in K_M corresponds to an increase in affinity (negative fold change).

Chapter 3 – Identification of novel light-dependent phosphorylation sites of C_4-related enzymes

3.1 Introduction

C_4 photosynthesis has evolved independently in over 60 plant lineages from the classical C_3 pathway, involving the gradual transition to Kranz anatomy and recruitment of C_3 genes for C_4 function (Sage *et al.*, 2012). The genetic mechanisms that underpinned the regulation of mesophyll- or bundle sheath-cell specific gene expression evolved in parallel across multiple C_4 origins (Sinha and Kellogg, 1996; Brown *et al.*, 2011; Williams *et al.*, 2013). C_4 plant lineages have also shared mechanisms for determining C_4-specific enzyme function through changes to amino acid sequences, though the degree of parallelism depends on the selective pressures acting on specific residues. For instance, the acquisition of the C_4-specific PEPC, through the evolution from the ancestral non-C_4 PEPC, occurred repeatedly across several independent C_4 lineages (Christin *et al.*, 2007). Furthermore, Christin *et al.* (2007), also showed that particular PEPC codon mutations, at positions 517, 577, 579, 761 and 780 for serine and threonine amino acids, were under positive selection in independent C_4 lineages and may be determinants of C_4 characteristics. These amino acid substitutions, namely the A780S transition in *Zea mays*, have been shown to be contenders associated with the regulatory properties and kinetics of C_4-specific PEPCs (Dong *et al.*, 1998; Bläsing *et al.*, 2000; Svensson *et al.*, 2003). The amino acids that evolved in parallel across independent lineages may be indications of the adaptations that were advantageous in determining C_4 function (Williams *et al.*, 2013), but the significance of these residue mutations, with regards to the phosphoregulatory mechanisms underlying the kinetic properties of C_4-related enzymes, have not been studied in detail.

In plants, serine and threonine residues are frequently phosphorylated (Friso and van Wijk, 2015) and are prominent sites of regulation for C_4-related enzymes like PEPC, PPDK and PEPCK. These mechanisms of regulation are often complex, and may be dependent on illumination or circadian controllers (Jiao and Chollet, 1988; Jiao *et al.*, 1991; Wilkins, 1992; Nimmo, 1998; Hartwell *et al.*, 1999). The light-dependent phosphorylation of PEPC is well documented at the invariant *N*-terminal serine across

grass species (Jiao and Chollet, 1988; Jiao and Chollet, 1991), however despite evidence of the selection pressures of serine and threonine residues in C_4 lineages presented by Bläsing *et al.* (2000) and Christin *et al.* (2007), little is known about the regulatory characteristics that span across the C_4-specific PEPC sequence. Furthermore, the phosphoregulatory properties of other essential C_4-related proteins that evolved C_4-specific function, like aspartate and alanine aminotransferase (Hatch and Mau, 1973) or NADP-malic enzyme (Christin *et al.*, 2009; Saigo *et al.*, 2013), have not been described in C_4 plants.

3.1.1 The role and diversity of post-translational modifications in plants

Post-translational modifications (PTMs) play a pivotal role in the regulation of proteins and contribute to the functionality of the proteome (Figure 3.1). The diversity of PTMs, together with their reversible, dynamic nature, contribute to protein function, which is essential for the regulation of metabolic pathways, protein-protein interactions or activation of signal transduction pathways (Karve and Cheema, 2011). However, these tightly regulated, dynamic mechanisms are often overshadowed by spontaneous enzymatic reactions induced by reactive species such as free radicals or redox potentials, which non-specifically modify amino acids and result in irreversible changes to protein structure and function (Friso and van Wijk, 2015).

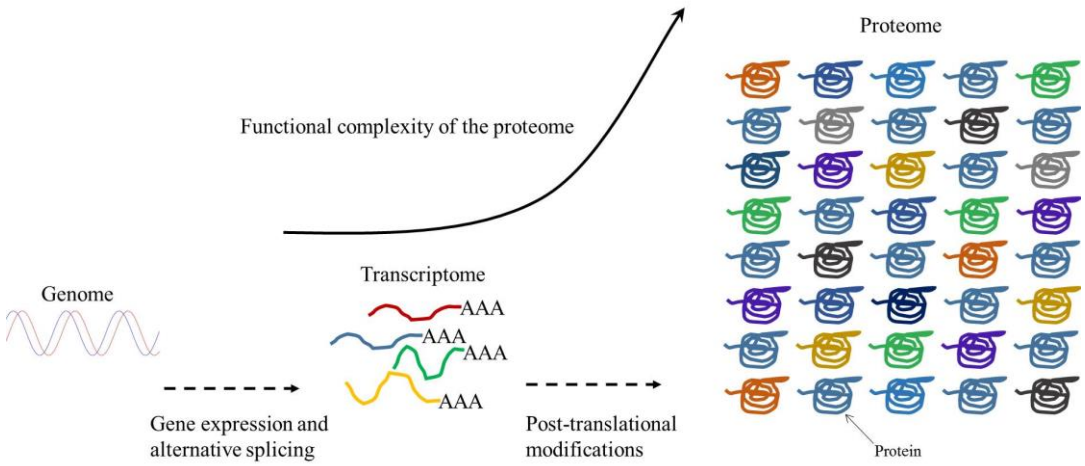

Fig. 3.1. Schematic showing the role of PTMs on the functional complexity of the proteome. Expressed genes undergo splicing mechanisms creating polyadenylated gene transcripts (coloured lines, –AAA). Proteins shown as multi-coloured swirls.

Table 3.1. **Reversible post-translational modifications that regulate the activity of plant proteins**. Common PTMs found in plant cells, structural characteristics and their general role in biology. Binding interactions between the amino acid and the PTM are highlighted in orange. Adapted from Friso and van Wijk (2015).

PTM observed *in vivo*	Modifiable amino acid	Monoisotopic mass (Da)	General role in biology	Structure	Binding notes
Acetylation	Cysteine, Lysine	42.01056	Protein localisation Protein-protein interactions	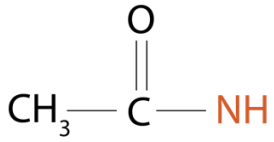	An acetyl group (CH_3–CO) binds to the *N*-terminal (NH_3^+) of an amino acid.
Methylation	Lysine, Cysteine, Arginine, Glutamic acid	14.01565	Transcriptional regulation Protein expression	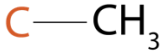	A methyl group (CH_3) reacts with side-chains or *C*-terminals of target amino acids.
Oxidation	Methionine	15.99491	Protein stability and interactions		An oxygen atom binds to the sulphur atom in methionine.
Phosphorylation	Serine, Threonine, Tyrosine, Histidine (rare)	79.96633	Signal transduction Protein activity Protein interactions	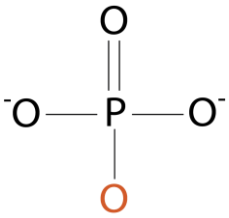	A phosphate group $(PO_4)^{3-}$ reacts with a side chain hydroxyl group (–OH) of a serine, threonine or tyrosine residue (Figure 3.2).
Ubiquitination	Lysine	114.04292	Development Signal transduction Protein activity Cross-talk	Ubiquitinations are identified by a characteristic diglycine substituent conjugated with a lysine residue.	Ubiquitin protein binds to a lysine residue forming an isopeptide bond between lysine and a glycine residue on ubiquitin.

In plants, proteins may be phosphorylated, ubiquitinated, acetylated or methylated (Table 3.1, 3.2) by enzymatic reactions mediated by regulatory enzymes (Friso and van Wijk, 2015). In the event of phosphorylation (Figure 3.2) protein kinases transfer the γ-phosphate of ATP onto tyrosine, threonine or serine residues (Hunter, 2007). Histidine and aspartate residues can also undergo phosphorylation, but at low frequencies (Friso and van Wijk, 2015).

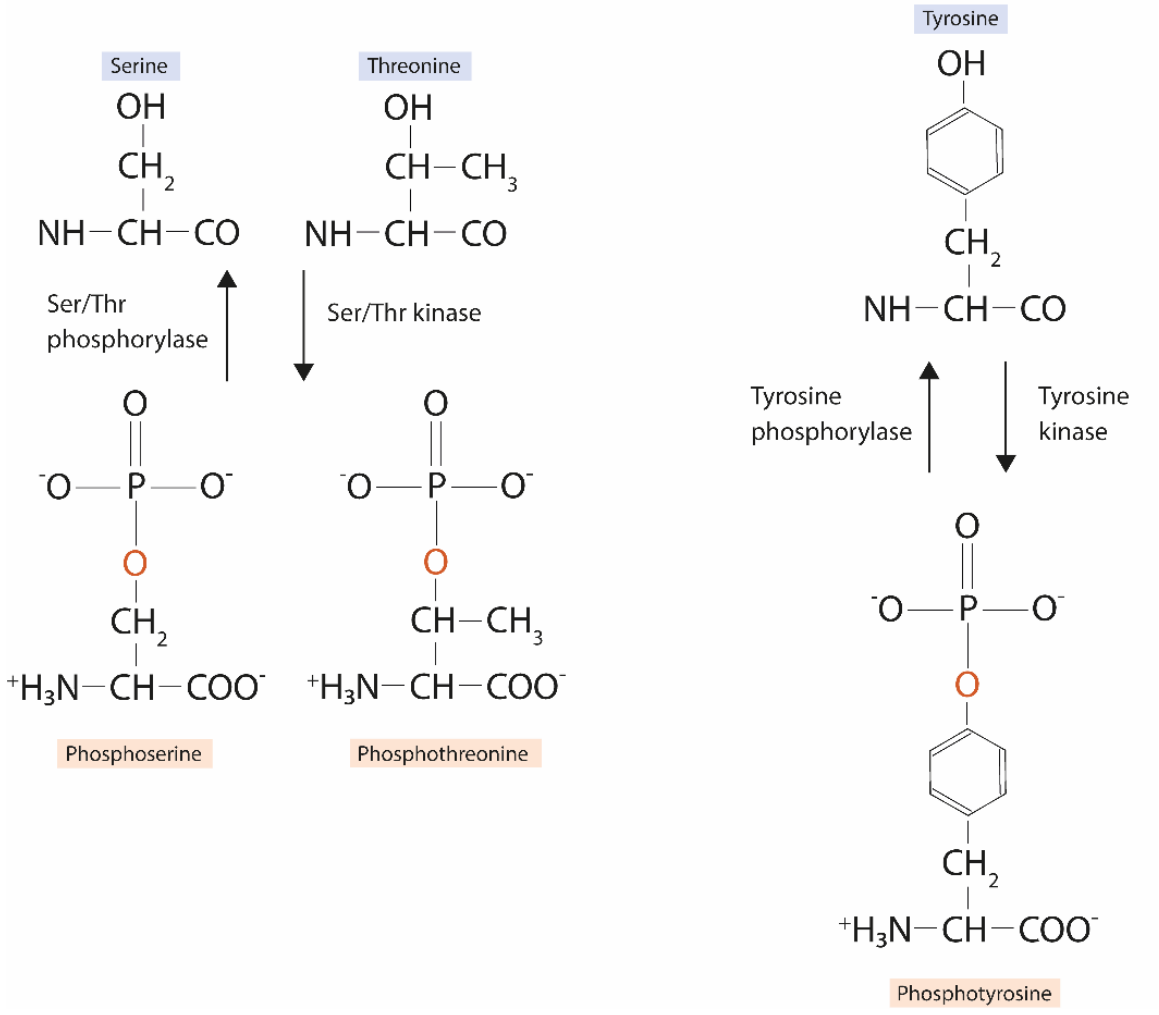

Fig. 3.2. *In vivo* reversible phosphorylation mechanism of serine, threonine and tyrosine residues. Protein kinases and phosphorylases regulate the reversible phosphorylation of serine, threonine and tyrosine residues (only functional groups shown), whereby phosphate groups are linked by phosphoester bonds (bottom) via an oxygen atom (in orange), resulting in an 80 Da mass shift in the target protein (top). Arrows show the direction of phosphorylation by protein kinases and dephosphorylation by phosphorylases.

Reversible modifications, such as phosphorylation, typically regulate protein activity through the diurnal cycle, but PTMs in plants like acetylation, play another crucial role in determining protein localisation for organelle-specific reactions. Carbon fixation in plants depends on cytosolic protein activity as well as protein activity in subcellular compartments such as chloroplasts, mitochondria and peroxisomes (Hodges *et al.*, 2013). However, the PTM diversity of plastidic proteins and how they regulate plant metabolism is unclear (Lehtimäki *et al.*, 2015). Additionally, proteins may undergo non-specific modifications, which may affect other PTMs on the same protein or nearby proteins. A single PTM can serve as a signal promoting the binding of regulator proteins that mediate subsequent specific or non-specific modifications (Hunter, 2007). Direct competition between PTMs can result in the blocking of amino acid side chains preventing site-specific modifications. For instance, cysteine residues are essential for plant development, immunity, pathogen defence, protein stability and enzyme activity (Kim *et al.*, 2015) but are prone to non-specific PTMs typically by redox regulation (Michelet *et al.*, 2013), due to a highly reactive thiol group in the side-chain. Under specific conditions, such as oxidative stress, cysteine residues are susceptible to spontaneous, non-enzymatic modifications, which block sites of regulation (Marino and Gladyshev, 2012; Chung *et al.*, 2013; Bhattacharjee *et al.*, 2015; Friso and van Wijk, 2015).

Enzymes involved in carbon fixation, such as Rubisco, PEPCK and NADP-malate dehydrogenase (MDH), as well as enzymes in the PCR cycle, are regulated by redox mechanisms (Table 3.2) (Ashton and Hatch, 1983; Drincovich and Andreo, 1994; Raines *et al.*, 2000; Schürmann and Buchanan, 2008; Michelet *et al.*, 2013; Gütle *et al.*, 2016). These regulatory mechanisms are widespread in plants and other biological systems. For instance, in *Mycobacterium tuberculosis*, PEPCK preferentially catalyses the conversion of oxaloacetate to PEP, but under hypoxic and growth-limiting conditions, the anaplerotic reaction (in the reverse direction) towards the formation of oxaloacetate is favoured (Machová *et al.*, 2014). These changes are controlled by the reduction of disulphide bridges forming between cysteine residues, either by maintaining reducing intracellular environments, or interaction with reducing agents, such as thioredoxin (Machová *et al.*, 2014). It was shown that the formation of disulphide bridges in PEPCK resulted in the loss of enzyme activity (Carlson *et al.*, 1978; Krautwurst *et al.*, 1995), but such modifications can have more intrinsic effects on tertiary protein structures. It was recently shown that the interaction between Cys-391 and Cys-397, via a disulphide

bridge, induced changes to the structure and function of PEPCK from *Mycobacterium tuberculosis*, whereas the reduced form of these residues stabilised PEPCK and influenced the anaplerotic function (Machová *et al.*, 2017).

In C_4 plants, NADP-MDH is activated in illuminated and reducing conditions. In *Zea mays*, NADP-MDH is inactive in darkened leaves, but when transferred from darkness to illumination, activity can be restored (Johnson and Hatch, 1970). In addition, when NADP-MDH from darkened leaves was subjected to 5 mM DTT, enzymatic activity was fully restored, suggesting that the reduced form of the enzyme was essential for catalysis (Johnson and Hatch, 1970). Furthermore, NADP-MDH was inactivated when extracted in the absence of thiol-reducing agents such as DTT or thioredoxin (Jacquot *et al.*, 1981; Ashton and Hatch, 1983). The light activation of NADP-MDH is regulated by the reduction of a disulphide bridge occurring between Cys-10 and Cys-15 within the *N*-terminal of NADP-MDH (Decottignies *et al.*, 1988).

3.1.2 Phospho*enol*pyruvate carboxylase

PEPC (EC 4.1.1.31) plays a pivotal role in C_4 photosynthesis, catalysing the irreversible *β*-carboxylation of PEP to oxaloacetate (OAA) by utilising bicarbonate (HCO_3^-) (Figure 3.3) in mesophyll cells of C_4 plants (Chollet *et al.*, 1996; Cousins *et al.*, 2007) and is by far one of the best characterised enzymes of the C_4 pathway. The active form of PEPC consists of four identical 109 kDa subunits (Hatch, 1978; Matsumura *et al.*, 2002) and *in vivo* catalysis is dependent on a divalent cation, usually Mg^{2+}, though Mn^{2+} and Co^{2+} can be replaced *in vitro* (O'Leary *et al.*, 1981).

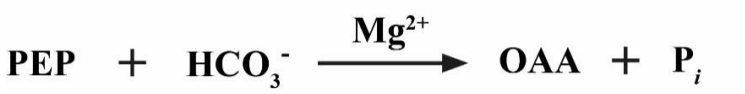

Fig. 3.3. Irreversible *β*-carboxylation of PEP to OAA by PEPC.

In C_4 plants, PEPC is activated by glucose-6-phosphate and allosterically inhibited by malate and aspartate (Huber and Edwards, 1975; Andreo *et al.*, 1987). Inhibition by malate is less pronounced when assayed at pH 8.0, rather than in physiological pH 7.3 and sensitivity to inhibition by malate is reduced with increasing concentration of Mg^{2+}

(Hatch, 1978; Wedding *et al.*, 1990; Echevarría *et al.*, 1994; Duff and Chollet, 1995). Sensitivity to feedback inhibition by malate or activation by glucose-6-phosphate is regulated by light-dependent reversible phosphorylation (Jiao and Chollet, 1991; Chollet *et al.*, 1996). The underlying mechanism was first described by Nimmo *et al.* (1984), demonstrating that the PEPC from Crassulacean acid metabolism (CAM) species was more sensitive to inhibition by malate during illumination than in the dark period, when PEPC is active. Furthermore, when the phosphorylated night form was purified and dephosphorylated *in vitro*, the sensitivity to malate inhibition increased (Nimmo *et al.*, 1986).

Using the ^{32}P-phosphorylation system, the C_4-form of PEPC from *Zea mays* was shown to undergo phosphorylation *in vitro* (Budde and Chollet, 1986). Consistent with the CAM-form, the phosphorylation of the C_4-specific PEPC was determined to occur predominantly at a single serine residue within the *N*-terminal of PEPC from *Zea mays* (Ser-15) and *Sorghum bicolor* (Ser-8) during illumination, when PEPC from C_4 plants is active (Jiao and Chollet, 1988; Jiao and Chollet, 1990; Jiao *et al.*, 1991). The relationship between phosphorylation and sensitivity to malate inhibition was substantiated in phosphomimetic mutants of the *Sorghum bicolor* PEPC expressed in *Escherichia coli*, which showed that substituting the Ser-8 with aspartate (S8D) resulted in reduced inhibition by malate (Wang *et al.*, 1992), whereas substitution to cysteine (S8C) showed no reduced sensitivity (Duff *et al.*, 1993). Also, while the phosphorylation of the C_4-specific PEPC decreases sensitivity to inhibition by malate during illumination and causes about a two-fold increase in V_{max}, it does not alter the its affinity for bicarbonate or PEP (Vidal and Chollet, 1997). The phosphorylation of PEPC is essential to maintain high nocturnal carboxylase activity in CAM plants (Boxall *et al.*, 2017), while in *Flaveria bidentis* (C_4), phosphorylation of PEPC is not essential to maintain high CO_2 assimilation rates during illumination (Furumoto *et al.*, 2007).

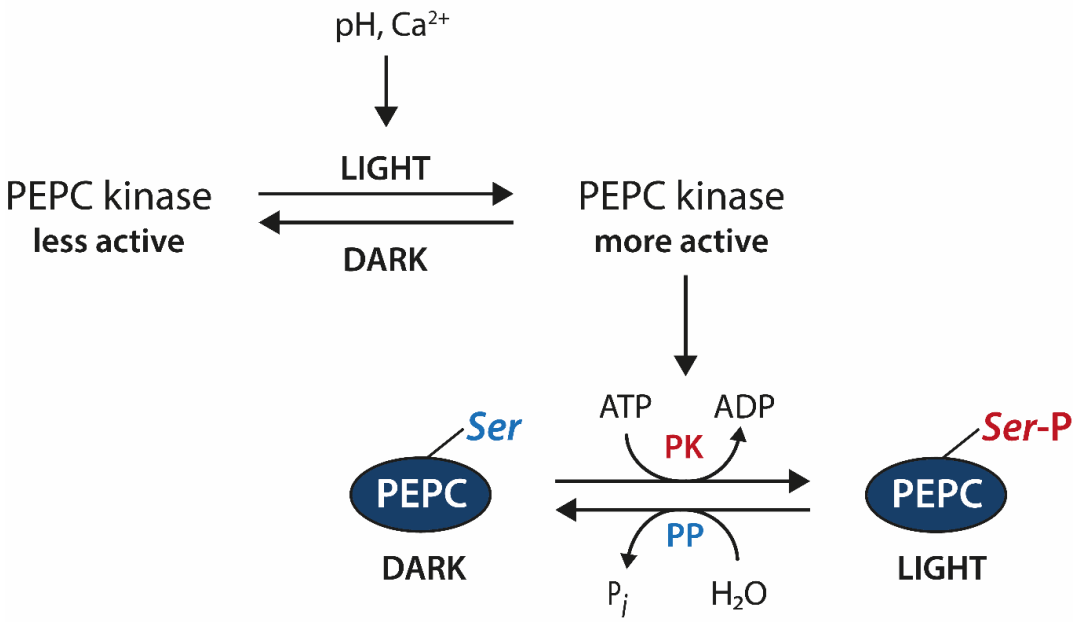

Fig. 3.4. Regulation of C_4-specific PEPC activity by *in vivo* serine phosphorylation. Light-dependent PEPC phosphorylation (serine in red) is regulated by PEPC kinase (PK), which is more active in the light. PEPC kinase is regulated by cytosolic pH and Ca^{2+}. Dephosphorylation (serine in blue) is mediated by protein phosphatase 2A (PP). Phosphorylated PEPC can maintain higher maximal activity due to a decrease in sensitivity to inhibition by malate. Figure adapted from Chollet *et al.* (1996).

PEPC is maximally phosphorylated within one hour of illumination by PEPC kinase (Vidal and Chollet, 1997; Bailey *et al.*, 2007) and dephosphorylated by a type 2A protein phosphatase shortly before the dark period in C_4 plants (Carter *et al.*, 1990; Vidal and Chollet, 1997; Dong *et al.*, 2001). Another study showed that the phosphorylation of PEPC in *Zea mays* occurred before the onset of light and was dephosphorylated before the dark period (Ueno *et al.*, 2000), suggesting that to some degree, C_4 photosynthesis is controlled by circadian mechanisms (Wang *et al.*, 2011). In fact, the activity of PEPC is largely dependent on the light-dependent activation of PEPC kinase (Figure 3.4) rather than changes of protein phosphatase 2A activity (Echevarría *et al.*, 1990; Carter *et al.*, 1991; McNaughton *et al.*, 1991). Moreover, two protein kinases can phosphorylate PEPC at the *N*-terminal serine residue, but only the Ca^{2+}-dependent protein kinase shows light dependency (Jiao and Chollet, 1988; McNaughton *et al.*, 1991; Li and Chollet, 1993; Wang and Chollet, 1993). In the C_4-form, PEPC kinase is regulated by metabolic factors, such as protein turnover, photosynthesis and pH (Jiao *et al.*, 1991; Jiao and Chollet, 1992; Li and Chollet, 1993), whereas activation of the CAM-form PEPC kinase is controlled by a circadian oscillator, rather than light to dark transitions (Duff *et al.*, 1996; Giglioli-

Guivarc'h *et al.*, 1996; Vidal and Chollet, 1997). At the protein level, the activity of PEPC kinase is also regulated by ubiquitination mediated degradation (Agetsuma *et al.*, 2005). In relation to PEPC, the PEPC kinase is also preferentially expressed in mesophyll cells in *Zea mays*, suggesting the existence of additional regulatory controls at the gene level (Li *et al.*, 2010).

Recent studies have suggested that the activation mechanism of the C_4-form PEPC is dependent on cross-talk between phosphorylation and lysine ubiquitination. Lysine ubiquitination has received attention in recent years, because, like phosphorylation, it is reversible, widespread in eukaryotic cells, occurs at relatively higher frequencies and mediated by a myriad of regulator enzymes (Hunter, 2007; Huber, 2011; Friso and van Wijk, 2015). Monoubiquitination was first described by Uhrig *et al.* (2008), demonstrating that the non-photosynthetic PEPC was modified at Lys-628 in germinating castor oil seeds. Ruiz-Ballesta *et al.* (2014) demonstrated that PEPC monoubiquitination occurred at Lys-624 in developing *Sorghum bicolor* seeds, and proposed a novel network of regulatory mechanisms contributing to PEPC activity. In addition to this, recent evidence suggests that the activation cascade of PEPC depends on several modifications, other than phosphorylation. This is supported in maturing phosphate-deficient roots of *Hakea prostrata*, where PEPC deubiquitination was followed by phosphorylation, promoting enzyme activity *in vivo* (Shane *et al.*, 2013).

3.1.3 Pyruvate, phosphate dikinase

PPDK (EC 2.7.9.1) catalyses the ATP-dependent regeneration of PEP from pyruvate in mesophyll chloroplasts of C_4 plants (Figure 3.5). Similar to PEPC, the active form of PPDK is a homotetramer made up of four 94 kDa subunits (Hatch, 1978).

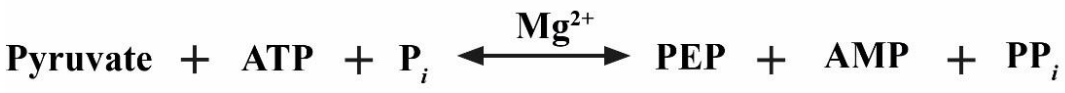

Fig. 3.5. Regeneration of PEP from pyruvate by PPDK in C_4 plants.

The reaction mechanism of the C_4-specific PPDK involves two steps. The reaction begins when PPDK binds two ATP and phosphate to form a phosphohistidine intermediate,

AMP and diphosphate, and is subsequently followed by a ping-pong mechanism for the addition of phosphate to pyruvate to form PEP (Hatch, 1978; Roeske *et al.*, 1988). PPDK is inhibited by PEP, AMP and PP_i, but these products are readily utilised by high activities of PEPC, adenylate kinase and pyrophosphatase in mesophyll cells, thus the C_4-specific PPDK reaction is favoured towards the formation of PEP (Hatch and Slack, 1968; Hatch, 1978). Mg^{2+} is also essential for catalysis and the increasing concentration of Mg^{2+} in the stroma during illumination correlates to the light activation mechanism of PPDK (Leegood and Walker, 1999).

An early study demonstrated that PPDK was less active in darkened leaves than illuminated leaves of *Amaranthus palmeri* (Slack, 1968). This study also showed that the *in vitro* activity of PPDK declined after transferring light-grown sorghum and sugarcane plants to a period of darkness. In addition to this, PPDK is activated *in vitro* with treatment by a stromal regulatory protein and phosphate and deactivated by a regulatory protein and ADP (Budde *et al.*, 1985). To determine the activation properties of PPDK from *Zea mays*, PPDK was assayed *in vitro* using radioactively labelled phosphate. In this approach, it was demonstrated that PPDK underwent phosphorylation at a threonine residue by an ADP-dependent regulatory protein, resulting in the deactivation of the enzyme (Ashton and Hatch, 1983). Furthermore, the activity of PPDK depends on the degree of phosphorylation. It was shown that one 94 kDa subunit from the inactive form of PPDK contained two-fold higher content of phosphate than one subunit from the active form (Budde *et al.*, 1985).

In *Zea mays*, PPDK is inactivated in the dark by phosphorylation at the active site (Thr-456) and re-activated by dephosphorylation (Roeske *et al.*, 1988). Both the phosphorylation and dephosphorylation of PPDK are uniquely regulated by a single bifunctional regulatory protein (PPDK-RP) (Figure 3.6) (Chastain *et al.*, 1997; Chastain *et al.*, 2000). Although PPDK-RP is active in mesophyll cell chloroplasts where PPDK is localised, transcripts of PPDK-RP were predominantly found in bundle sheath cells of *Zea mays* (Li *et al*., 2010). Also, despite its essential role in the regulation of PPDK, PPDK-RP appears to be in low abundance in mesophyll chloroplasts (Wang *et al.*, 2011). However, being localised in the stroma of the chloroplast, PPDK-RP is regulated by light-dependent changes in ADP, which increases after the light to dark transition, resulting in higher PPDK-RP activity and PPDK phosphorylation in darkened leaves (Chastain and Chollet, 2003). Conversely, the phosphatase reaction of PPDK-RP is

favoured in illuminated conditions, when ADP is limiting, resulting in fewer copies of PPDK being phosphorylated.

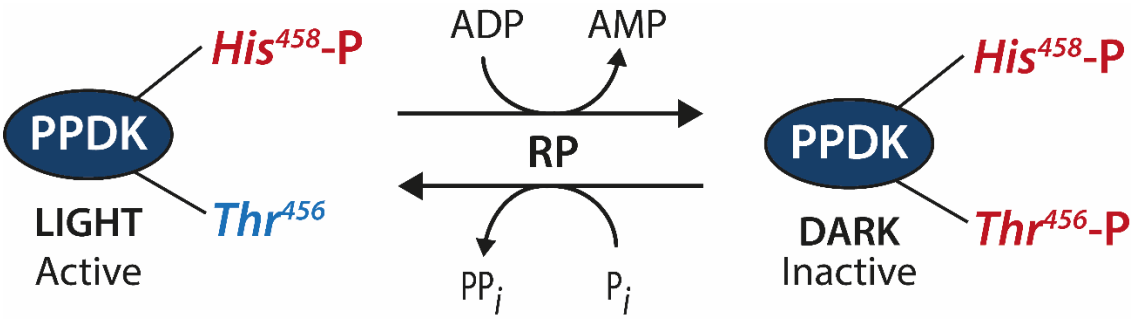

Fig. 3.6. Light activation mechanism of the C₄-specific PPDK by reversible phosphorylation. Phosphorylation (in red) and dephosphorylation (in blue) is regulated by a bifunctional ADP-dependent regulator protein (PR). PPDK is inactivated by phosphorylation in the dark and activated by dephosphorylation. Figure adapted from Chastain *et al.* (1997).

The catalytic effect of phosphothreonine-456 of PPDK from *Zea mays* was determined by direct mutagenesis in *Escherichia coli*, using serine (also a target for phosphorylation), valine and aspartate substitutions (Chastain *et al.*, 1997). In this study, it was shown that a threonine to serine substitution at position 456 (T456S) did not hinder the phosphorylation of PPDK nor affected catalysis, but resulted in less effective enzyme inactivation, whereas the substitution to aspartate (T456D), mimicking a non-labile phosphorylation, resulted in complete enzyme inactivation (Chastain *et al.*, 1997). Chastain *et al.* (1997) also showed that the dephosphorylated form (T456V) remained active. Further analysis also showed that a second phosphomimetic mutant (T456E) abolishes catalytic activity, while substitutions to tyrosine (T456Y, another target for phosphorylation) and phenylalanine (T456F) substantially decreases activity (Chastain *et al.*, 2000).

In a study to determine the tolerance of low temperatures on the photosynthetic activity in *Zea mays* showed that the accumulation of PPDK in mesophyll chloroplasts decreased by 50% when plants were grown in low temperature, though transcript amounts were unchanged, suggesting that low temperature had little effect on gene expression (Naidu *et al.*, 2003). While there are no other known regulatory sites on the C₄-specific PPDK, Wang *et al.* (2011) speculates that PPDK may be controlled by more complex mechanisms, thus explaining the difference between gene expression and accumulation

of PPDK in mesophyll chloroplasts. In fact, it has been recently demonstrated that the PPDK regulatory mechanism at Thr-527 in *Zea mays* is strictly controlled by light intensity rather than by the dark to light transition (Chen *et al.*, 2014). It is important, however, that inactivation by decreasing light intensity had been previously noted (Burnell *et al.*, 1986), but had not been attributed to a single residue. In the recent study, it is suggested that increasing the expression of PPDK in mesophyll cells does not imply an increase enzymatic activity and there could be other regulatory controls or regulatory sites that are still unaccounted for (Chen *et al.*, 2014).

3.1.4 Phospho*enol*pyruvate carboxykinase

Compared to PEPC and PPDK, the light-dependent phosphorylation of PEPCK (4.1.1.49) is the most recent to be elucidated in C_4 plants, yet other C_4-related proteins have not been shown to be regulated by phosphorylation (Table 3.2). In PEPCK- and NAD-malic enzyme subtypes and certain NADP-malic enzyme C_4 plants, such as *Zea mays* (Walker *et al.*, 1997), PEPCK catalyses the cytosolic ATP-dependent decarboxylation of oxaloacetate (OAA) in bundle sheath cells, forming CO_2 and PEP (Figure 3.7) (Hatch, 1978).

Fig. 3.7. ATP-dependent decarboxylation of OAA by PEPCK in C_4 plants.

Initial observations noted that the activity of PEPCK and accumulation in bundle sheath cells changed very little between light and dark conditions (Walker *et al.*, 2002) and regulating the activity PEPCK would be essential to prevent depletion of ATP or oxaloacetate during the light to dark transition of C_4 photosynthesis (Carnal *et al.*, 1993). The light-dependent phosphorylation of PEPCK was first described in cucumber cotyledons by feeding seedlings with radioactively labelled phosphate (Walker and Leegood, 1995). In this study, the native form of PEPCK was purified and shown to undergo phosphorylation by treatment with PEPC kinase from *Zea mays*. Also, the larger and native 74 kDa protein was phosphorylated, whereas the truncated form (62 kDa) was not phosphorylated, suggesting that the phosphorylation site was in the *N*-terminal

extension that had been proteolysed (Walker and Leegood, 1995). Walker and Leegood (1995) also showed that upon the removal of ATP in the reaction assay, the phosphorylation of PEPCK was reversible by treatment with protein phosphatase 2A.

In C_4 plants, such as the PEPCK-type *Megathyrsus maximus* (previously *Panicum maximum*), PEPCK is phosphorylated in darkened leaves and dephosphorylated in illuminated leaves, in a regulatory mechanism that leads to PEPCK activation in illuminated leaves (Walker and Leegood, 1996; Walker *et al.*, 2002). The role of phosphorylation in this mechanism was studied by Bailey *et al.* (2007), with emphasis towards the coordination between carboxylation by PEPC and decarboxylation by PEPCK in darkened and illuminated leaves of *Megathyrsus maximus*. In this study, the authors showed that PEPCK activation at full sunlight correlated to a decrease in its phosphorylation state, whereas the phosphorylation state of PEPC during illumination correlated with the light-induced activation of PEPC (Bailey *et al.*, 2007). Recently, the phosphoregulatory site of PEPCK from *Zea mays* was determined by mass spectrometry. In *Zea mays*, PEPCK was shown to undergo phosphorylation at Ser-55, Thr-58, Thr-59 and Thr-120, though phosphorylation at Ser-55 showed a higher degree of light-dependency (Chao *et al.*, 2014). Furthermore, the study showed that in *Zea mays* seedlings, Ser-55 was phosphorylated in illuminated leaves and dephosphorylated in darkened leaves, which is the opposite of what had previously been reported (Walker and Leegood, 1995; Walker and Leegood, 1996; Bailey *et al.*, 2007). Differing from previous findings, the activity of PEPCK was shown to be lower in illuminated leaves and higher in darkened leaves (Chao *et al.*, 2014).

Table 3.2. Summary of known post-translational modifications of plant proteins involved in carbon fixation. For each protein, the type of PTM is indicated (p, phosphorylation; ub, ubiquitination) and relevant references are cited.

Protein	Biological process	Post-translational regulation	Modifications	References
Phospho*enol*pyruvate carboxylase EC 4.1.1.31	C_4 photosynthesis	Light-dependent reversible phosphorylation decreases sensitivity to malate inhibition Mono-ubiquitination cross-talk with phosphorylation	pSer-15 ub-Lys-624	(Ruiz-Ballesta *et al.*, 2014) (Shane *et al.*, 2013) (Uhrig *et al.*, 2008) (Jiao and Chollet, 1991) (Huber and Edwards, 1975)
Phospho*enol*pyruvate carboxylase kinase EC 2.7.11.1	C_4 photosynthesis	Ubiquitination mediated degradation		(Agetsuma *et al.*, 2005)
Glycerate kinase EC 2.7.1.31	Photorespiration	Thioredoxin regulated disulphide bridge (S-S)		(Bartsch *et al.*, 2010)
Pyruvate, phosphate dikinase EC 2.7.9.1	C_4 photosynthesis	Light-intensity mediated reversible phosphorylation by PPDK-RP kinase-phosphatase	pThr-527 pSer-528	(Chen *et al.*, 2014) (Chastain *et al.*, 2011) (Roeske *et al.*, 1988)
NADP-malic enzyme EC 1.1.1.40	C_4 photosynthesis	None documented in C_4 plants	–	–
NADP-malate dehydrogenase EC 1.1.1.82	C_4 photosynthesis	Thioredoxin regulated disulphide bridge (S-S)	67 ↔ 72	(Decottignies *et al.*, 1988) (Leegood and Walker, 1983) (Jacquot *et al.*, 1981)
Phospho*enol*pyruvate carboxykinase EC 4.1.1.49	C_4 photosynthesis	Light-dependent reversible phosphorylation	pSer-55	(Chao *et al.*, 2014) (Bailey *et al.*, 2007)

Protein	Biological process	Post-translational regulation	Modifications	References
Carbonic anhydrase EC 4.2.1.1	C_4 photosynthesis	None documented in the C_4 photosynthesis protein	–	–
Alanine aminotransferase EC 2.6.1.2 **Aspartate aminotransferase** EC 2.6.1.1	C_4 photosynthesis	None documented in the C_4 photosynthesis protein	–	–
Pyruvate dehydrogenase EC 1.2.4.1	Respiration	Reversible phosphorylation		(Tovar-Méndez *et al.*, 2003) (Thelen *et al.*, 2000)
Sucrose phosphate synthase EC 2.4.1.14	Sucrose metabolism	Reversible light-regulated phosphorylation in maize	pSer-162	(Huber and Huber, 1996)
Rubisco EC 4.1.1.39	C_3 photosynthesis	Disulphide bridge Phosphorylation, methylation, acetylation	Cys-247	(Friso and van Wijk, 2015) (Hodges *et al.*, 2013) (Houtz *et al.*, 2008)
Transketolase EC 2.2.1.1	Pentose-phosphate pathway	Phosphorylation	Ser-428	(Rocha *et al.*, 2014)

3.1.5 Identifying novel phosphorylation sites using LC-MS/MS

The adaptation of proteomic pipelines for large-scale studies has grown in recent years through the technological advances of high-throughput mass spectrometry. Proteomics, along with genomics and metabolomics, has become a powerful tool for identifying proteins and characterising protein function and is essential for elucidating the factors that contribute to the complexity of the proteome (Porubleva and Chitnis, 2000; Park, 2004). Using high resolution mass spectrometry, not only can proteins be inferred from peptide spectra, but post-translational modifications (PTMs) can be accurately identified to amino acid specificity. The analysis of complex mixtures is most frequently achieved by coupling mass spectrometry to high performance liquid chromatography (Pitt, 2009), as in the case of the Orbital Trap mass spectrometer (Aebersold and Mann, 2003; Hu *et al.*, 2005; Perry *et al.*, 2008), in which ions can be separated on a liquid elution gradient prior to injection into the instrument. However, success in proteomic studies, such as phosphoproteomics, depends on several factors that may outweigh the technological improvements and optimisations during analysis. Phosphoproteomic studies are hindered by experimental challenges such as sample preparation, which may affect phosphopeptide recovery and yield computational challenges, like poorly annotated protein databases (Ma, 2010). In plants, these challenges are more pronounced due to incomplete genome sequences and uncharacterised protein entries. Furthermore, proteins from plant samples may be underrepresented due to incomplete protein extraction from various specialised cell types or organelles (Jorrín *et al.*, 2007), presence of nucleic acids and non-protein contaminants that affect subsequent analysis (Haynes and Roberts, 2007), high concentration of in-soluble membrane proteins, which are lost during detergent-free extractions using non-volatile buffers and high content of hydrophobic molecules that may block analytical columns (Abdallah *et al.*, 2012; Bagag *et al.*, 2013).

The success in proteomic studies relies on increased resolution, sensitivity and accuracy of analytical protocols. Early proteomic experiments were designed to understand cellular function at the protein level by mapping proteins using 2D protein gels, which were limited to small-scale experiments due to the increased difficulty in identifying multiple proteins in more complex mixtures (O'Farrell, 1975; Mann *et al.*, 2001; Graves and Haystead, 2002). This was overcome by the development of mass spectrometry technology, which had the necessary sensitivity and resolution to accurately identify

proteins in complex mixtures. The study of proteins by mass spectrometry became capable after the development of ionisation strategies, which transfer the protein analyte from the liquid to the gas phase, maintaining ions in their charged state. There are two commonly used methods for ionisation: 1) matrix-assisted laser desorption/ionization (MALDI) and 2) electrospray ionisation (ESI); the latter ionisation source is used in OrbiTrap-based mass spectrometers (Aebersold and Mann, 2003; Hu *et al.*, 2005). During the first stage of analysis (MS1), ions (peptides) are accelerated through positively and negatively charged plates, separated and selected by their mass-to-charge ratio (*m*/*z*) using an electromagnetic field. In tandem mass spectrometry, ions are isolated in a collision chamber and fragmented with an inert gas during collision-induced dissociation (CID) (Marcotte, 2007; Dephoure *et al.*, 2013), which breaks down peptides into smaller fragments, most commonly at the peptide bond, resulting in b-ions (*N*-terminal fragments) and y-ions (*C*-terminal fragments), which are analysed, during the second stage of analysis (MS2) (Aebersold and Mann, 2003).

For rapid protein identification, the resulting peptide spectra are searched against theoretical mass spectra, which are generated from the computational digestion of protein sequence databases (Zhang *et al.*, 2013). For phosphopeptide determination, observed spectra are searched against theoretical peptide spectra generated assuming all possible serine, threonine or tyrosine phosphorylation events (Dephoure *et al.*, 2013). Phosphorylated peptides bearing a phosphate group (80 Da), unlike dephosphorylated peptides, behave differently during CID fragmentation. The behaviour of the labile phosphoester bond during fragmentation can affect phosphorylation site assignment due to peptide spectra generated from multiple fragment ion products, often from the partial neutral loss of phosphoric acid (H_3PO_4; 98 Da), through the gas-phase β-elimination of phosphoserine or phosphothreonine (Schweppe *et al.*, 2003; Thingholm *et al.*, 2009; Solari *et al.*, 2015). The neutral loss of phosphoric acid from phosphoserine or phosphothreonine is a favourable event during CID, unlike phosphotyrosine which is resistant to gas-phase β-elimination due to stabilisation of β-protons in the benzene ring (Figure 3.2) (Mann *et al.*, 2002; Schweppe *et al.*, 2003). Moreover, the neutral loss of water (18 Da), along with the loss of phosphate competes with mass spectra for the loss of phosphoric acid, which, under specific conditions, can hinder phosphorylation site assignment (Cui *et al.*, 2014). Although these complex chemical interactions pose challenges for neutral loss scanning methods and subsequent mass spectrum analysis, the

versatility of new proteomic approaches, as well as, tailored prediction algorithms and mass spectra visualisation tools have enhanced the accuracy of PTM identification by mass spectrometry (Kwon *et al.*, 2006; Audagnotto and Dal Peraro, 2017).

To understand the significance of convergent C_4-related enzyme evolution and identify the determinants for C_4-specific enzyme activity, the phosphorylation of C_4 proteins in three NADP-malic enzyme C_4 subtypes was studied using high-resolution tandem mass spectrometry. Recent large-scale phosphoproteomic studies in C_3 plant models have demonstrated that several metabolic proteins undergo phosphorylation, regardless of their subcellular compartmentation, indicating that phosphoregulatory mechanisms are ubiquitous in C_3 plant organelles and in the cytosol (Nakagami *et al.*, 2010; Hodges *et al.*, 2013; Liu *et al.*, 2014; Lv *et al.*, 2014; Ye *et al.*, 2016). The enzymes that are involved in carbon fixation and photorespiration in C_4 plants operate between two specialised cell types (Hatch, 1987; Kanai and Edwards, 1999), in the cytosol, as well as in chloroplasts, mitochondria and peroxisomes (Hatch and Osmond, 1976; Hodges *et al.*, 2013), and may be, like their C_3 counterparts, subjected to PTMs. However, the diversity of these modifications and how they regulate C_4-specific protein activity across subcellular compartments as well as how they contribute to the efficiency of C_4 photosynthesis is unclear. High-resolution mass spectrometry has been previously used in targeted studies to describe the light-dependent phosphorylation sites on PEPCK (Chao *et al.*, 2014) or light-intensity dependent phosphorylation sites on PPDK in *Zea mays* (Chen *et al.*, 2014). However, there have not been any large-scale phosphoproteomic experiments in C_4 grasses, so the underlying regulatory properties of C_4-related proteins involved in C_4 photosynthesis are unaccounted for. The aim of this investigation was to determine novel phosphorylation sites on key C_4-related proteins from darkened and illuminated leaves of *Setaria viridis*, as well as in *Sorghum bicolor* and *Megathyrsus maximus*. In this Chapter, novel light-dependent phosphorylation sites identified on C_4-related proteins are presented and discussed. This was the first attempt to analyse the phosphoproteome in *Setaria viridis*, with hopes to elucidate novel phosphoregulatory mechanisms and further understand the role of phosphorylation and how changes of protein activity, through a diurnal cycle, are regulated. The comprehensive list of novel phosphorylation sites identified are listed in Appendix A.

3.2 Results – Novel phosphorylation sites of C_4-related enzymes

3.2.1 Identifying key C_4 photosynthesis proteins in *Setaria viridis*

To determine novel phosphorylation sites in the C_4 model *Setaria viridis*, proteins were extracted from 2.5-week old leaves 30 min before the onset of light and 4 h and 15.5 h into the photoperiod. Leaf extracts were subjected to 1D SDS-PAGE and stained with Coomassie Blue protein dye (Figure 3.8). Two bands above 100 kDa were excised to identify previously described phosphorylation of PEPC (phosphoserine at position 15, residues 12–20, HHSIDAQLR) and PPDK (phosphothreonine at position 527, residues 524–535, GGMTSHAAVVAR) in *Zea mays* (Roeske *et al.*, 1988; Jiao *et al.*, 1991). The tolerances for subsequent MS/MS spectra validations were established against the aforementioned phosphopeptide controls. Twenty-three proteins involved in carbon fixation were identified, of which seven were specific to C_4 photosynthesis (Table 3.3). 1,702 spectra were matched from 155 observed peptides of PEPC at 7.5 h into the dark compared to 1,669 peptide spectrum matches (PSMs) from 131 observed peptides of PPDK. The number of PEPC PSMs increased to 1,983 at 15.5 h into the light and amino acid sequence coverage increased by 16%. Similarly, PPDK sequence coverage increased by 41% between 7.5 h into the dark and 15.5 h into the light, resulting in 2,358 PSMs.

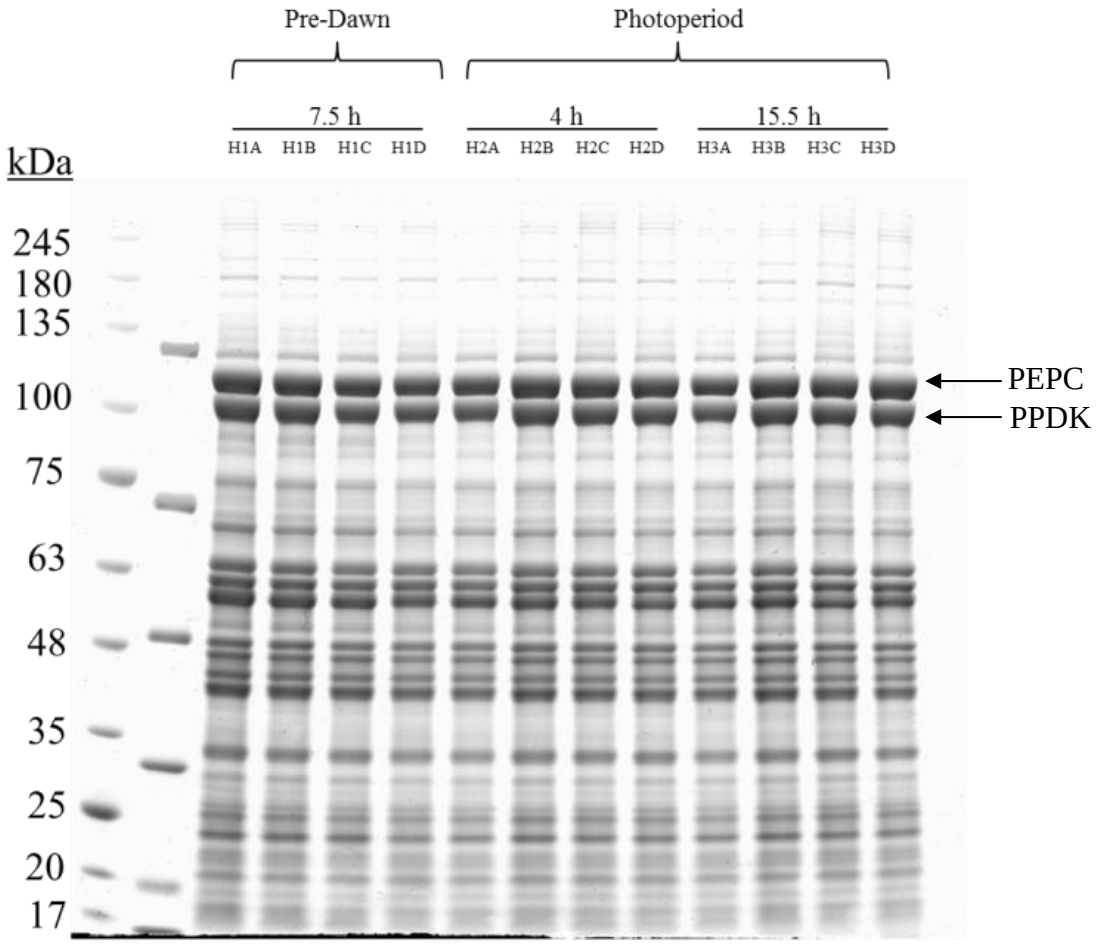

Fig. 3.8. ***Setaria viridis*** **whole leaf proteins resolved by 1D SDS-PAGE**. The 4–12% SDS gel was stained with Coomassie Blue protein dye. Lane 1 and lane 2 contained protein and phosphoprotein standards, respectively. 10 µg of protein was loaded into each lane, across four replicates (A–D) at three time-points: 7.5 h into the dark (H1A–H1D, lane 3–6), 4 h into the light (H2A–H2D, lane 7–10) and 15.5 h into the light (H3A−H3D, lane 11–14). Lane number 15 did not contain any protein. The gel was imaged using a FLA-5100 with 635 nm laser excitation. PEPC and PPDK are indicated at 109 kDa and 102 kDa, respectively.

Unlike PEPC and PPDK, the recovery of NADP-malic enzyme in *Setaria viridis* was less consistent, but protein sequence coverage increased by 58% after the dark to light transition. From the total 143 theoretical peptides, assuming a maximum of two missed cleavages filtered above 500 Daltons, 48 peptides were identified in NADP-malic enzyme from the 7.5 h into dark extracts; this increased by 13% after plants were illuminated for four hours, and then again by 2% towards the end of the photoperiod. The number of PSMs increased 4-fold from 228 to 1,179 after 15.5 h illumination; however, this large difference was due to the increased resolution of observed peptide spectra rather than an increased number of total observed peptides.

Table 3.3. Summary of proteins involved in C_4 photosynthesis identified by MS/MS. Accession numbers, protein mass (kDa) and the calculated isoelectric point (pI) obtained from the UniProtKB protein database.

Protein name	UniProt Accession	Mass (kDa)	Calc. pI
Alanine aminotransferase	K4A868	59.3	8.09
	K3ZSX0	53.2	7.64
Aspartate aminotransferase	K3YSB2	50.2	8.63
	K3XHJ0	50.2	8.68
	K4AG31	16.1	5.01
	K3Z6L1	44.6	6.28
	K3YSM6	47.6	6.84
	K3XHZ4	47.3	8.22
Enolase	K3XWW9	47.9	5.31
	K3Z681	47.9	5.81
	P42895	48.1	5.97
	P26301	48.0	5.33
NADP-dependent malate dehydrogenase	K3YHB4	52.8	6.68
	K3ZT87	49.3	6.35
NAD-dependent malate dehydrogenase	K4ACE3	35.5	6.09
	K3ZU36	40.8	7.59
	K3Z7W1	34.3	7.39
	K3XJN7	35.5	7.85
	K3Z7Q4	35.5	8.10
NADP-dependent malic enzyme	K3XG11	63.8	7.15
	K3XFW4	65.1	6.16
	K3XFH6	70.0	6.77
	K3ZRI5	69.4	6.51
Phospho*enol*pyruvate carboxylase	K3XV32	109.9	6.34
	K3YPN6	109.8	6.20
Pyruvate, phosphate dikinase	K3Z3Q6	95.7	5.12

Smaller sized or less abundant proteins in the leaf at the time of harvesting showed a lower number of PSMs and below 50% sequence coverage on average, suggesting that analyte recovery may have been overwhelmed by large quantities of more abundant ions (peptides) from PEPC and PPDK. PEP carboxykinase (PEPCK) was not identified in any of the *Setaria viridis* leaf lysates, but 38% of the total sequence was observed in *Megathyrsus maximus* at 7.5 h into the dark and 4 h into the light (Table 3.7) using a similar experimental approach. To evaluate the subset proteins that undergo *in vivo* phosphorylation, gels were stained with ProQ Diamond phosphoprotein gel stain. The

light-dependent phosphorylation of PEPC was evident in illuminated leaf lysates, whereas no banding was observed in darkened leaves (Figure 3.9). Conversely, the phosphorylation of PPDK was more prominent at 7.5 h into dark. The phosphorylation pattern of PEPC and PPDK at 4 h and 15.5 h into the light was less consistent across the biological replicates, and there was no distinguishable pattern of light-dependency between the light time-points. Phosphoprotein profiling using 2D gels (Figure 3.10) concurred with Figure 3.9 and showed that PEPC phosphorylation increased from dark to light, while PPDK phosphorylation remained constant throughout the 16h light and 8h dark cycle.

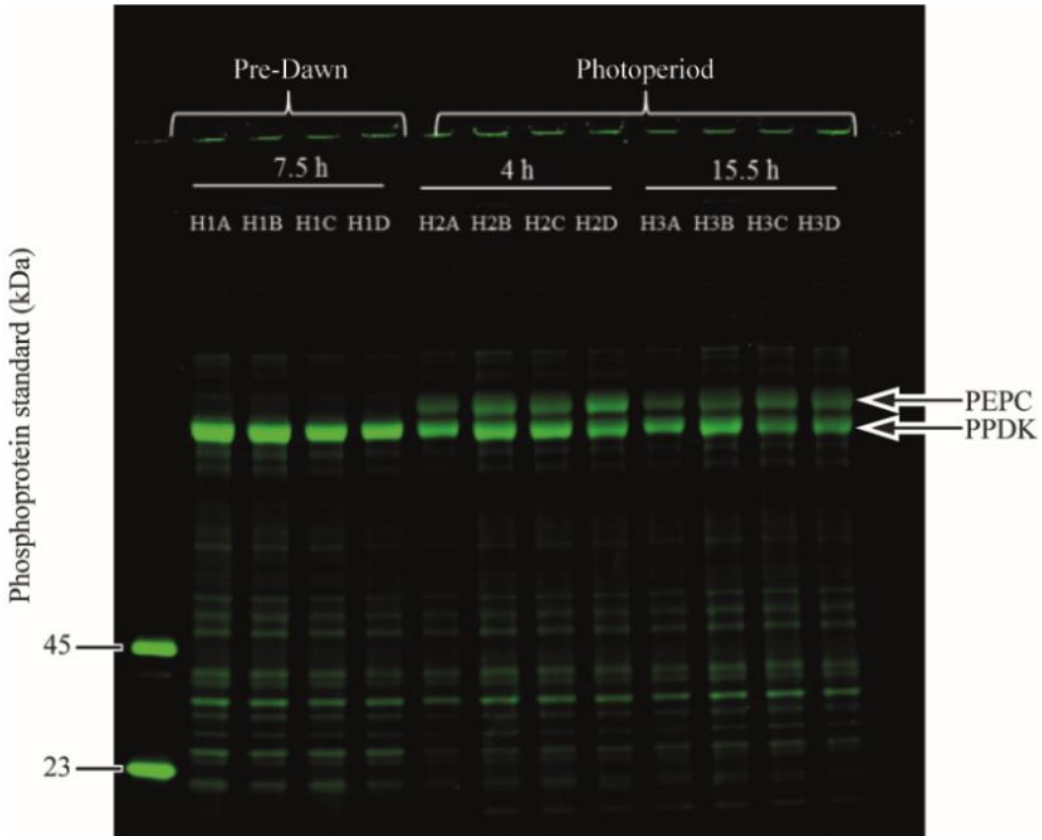

Fig. 3.9. Fluorescence stained gel showing phosphorylated proteins in *Setaria viridis*. 10 µg of protein from 7.5 h into the dark, 4 h and 15.5 h into the light were resolved using a 12% SDS gel. After electrophoresis, the gel was stained with ProQ Diamond phosphoprotein fluorescent gel stain. 8 µL of PeppermintStick™ phosphoprotein standard was loaded into lane 2 (lane 1 is not shown). Phosphorylation of PEPC and PPDK is indicated. The gel was visualised with 532 nm laser excitation.

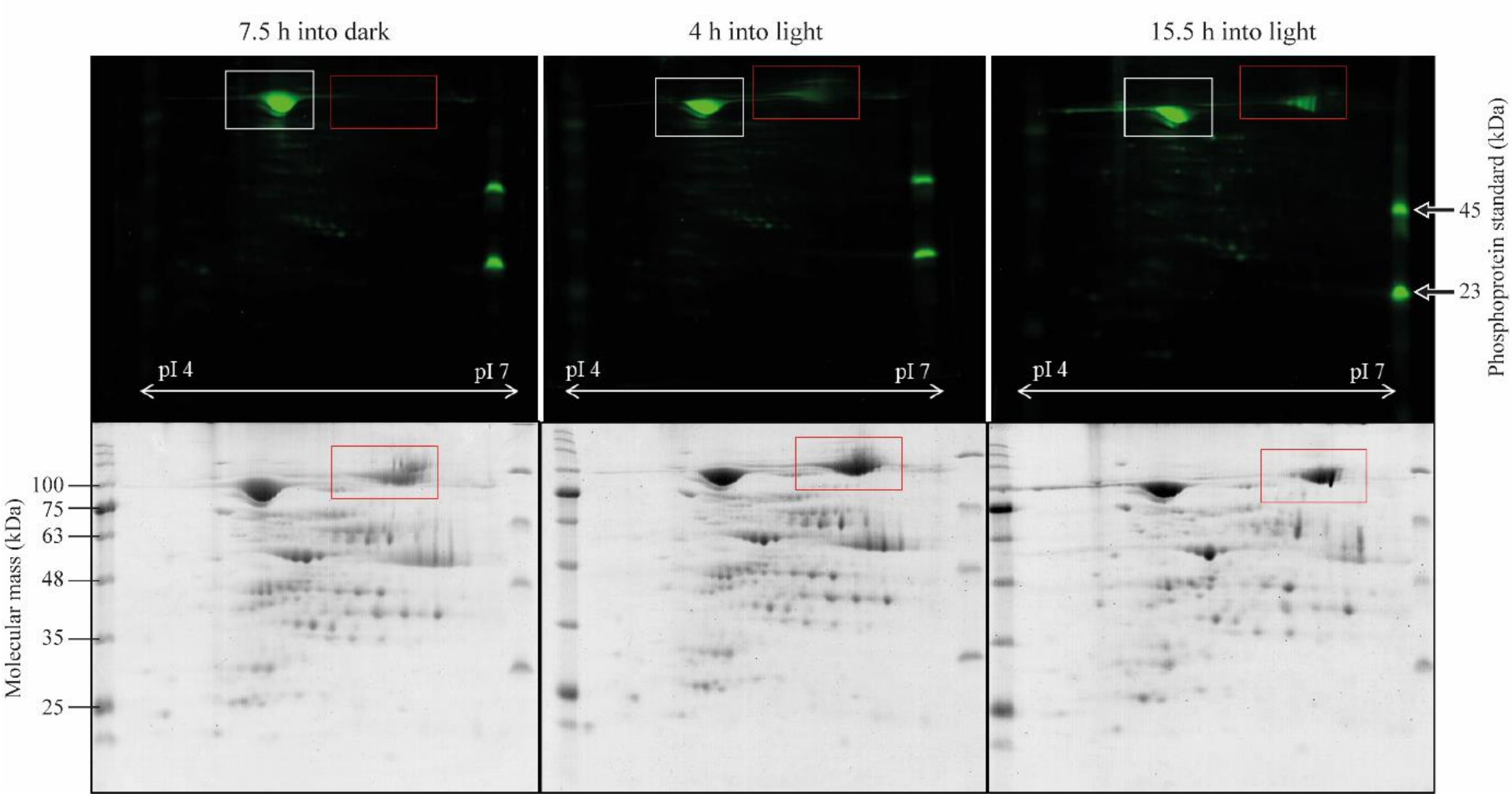

Fig. 3.10. 7 cm stained gels showing *Setaria viridis* whole leaf proteins resolved by 2D SDS-PAGE. 80 µg of protein was fixed onto a pH 4–7 IPG strip by passive rehydration, followed by IEF. After IEF, proteins were resolved on 10% SDS gels and stained with ProQ Diamond (top) or Coomassie InstantBlue™ (bottom). PEPC and PPDK are indicated by the red and white rectangles, respectively.

Using tandem mass spectrometry, PEPC was confirmed to undergo phosphorylation at Ser-11 (Figure 3.12A, residues 9–17, HHSIDAQLR), strictly after leaves were illuminated. However, during validation experiments, a triply charged phosphopeptide ion (residues 2–17, ASKPVE-KHHSIDAQLR, *m*/*z* 604.99) was observed four times in 7.5 h into the dark protein extracts (Table 3.7). The phosphorylation of PEPC at 7.5 h into the dark was not evident from the phosphoprotein stained gel (Figure 3.10) and presumably remained present in the dark period as an intermediate PEPC isoform during the light to dark transition. While the phosphorylation at Ser-11 in PEPC generally exhibited a strict light-dependent regulatory mechanism, PPDK phosphorylation at Thr-462 (Figure 3.15, residues 459–470, GGMTSHAAVVAR) was identified in every leaf sample mixture, irrespective of the harvesting time-point in *Setaria viridis* and *Sorghum bicolor* leaf lysates. Additionally, the phosphorylation at Ser-463 was detected four times, although in low confidence, at 7.5 h into dark in validation experiments using a 1% FDR (Table 3.6). The phosphorylation of Ser-463 had not been identified in *Setaria viridis* protein extracts. In total, 69 putative phosphorylation sites from key C_4 photosynthesis enzymes in *Setaria viridis* were identified by LC-MS/MS (Appendix A): 12 sites in alanine aminotransferase, 9 sites in aspartate aminotransferase, 13 sites in malate dehydrogenase, 20 sites in NADP-malic enzyme, seven sites in PEPC including the identified phosphorylation at Ser-15 in *Zea mays*, and eight sites in PPDK, including the phosphorylation identified at Thr-527 in *Zea* mays.

Table 3.4. Novel phosphopeptides identified in *Setaria viridis* leaf lysates using phosphopeptide enrichment. Phosphorylation sites identified in 7.5 h darkened (A) and 15.5 h illuminated (B) *Setaria viridis* by TiO_2 enrichment. The resulting spectra were searched against UniProtKB *Setaria italica* protein sequences using SEQUEST. The percentage of the protein sequence that was experimentally observed is given for each protein match. Phosphorylation site localisation probabilities (*P*) are indicated in parentheses to the right of the modified amino acid ($P > 0.75$ is significant). Statistical confidence is given by Xcorr, where Xcorr $\geq$ 2.15 is significant.

Table 3.4A. Novel phosphorylation sites identified in 7.5 h darkened *Setaria viridis* leaves.

Protein	Accession	Coverage (%)	Phosphopeptide	Position in peptide	MH^+ (Da)	Monoisotopic mass (Da)	Xcorr
PPDK	K3Z464	25.27	NDNDLTAS(0.99)DLKELVAQYK	Ser-8	2116.98	2035.99	3.99
			GGMT(0.97)SHAAVVAR	Thr-4	1252.55	1155.57	3.80

Table 3.4B. Novel phosphorylation sites identified in 15.5 h illuminated *Setaria viridis* leaves.

Protein	Accession	Coverage (%)	Phosphopeptide	Position in peptide	MH^+ (Da)	Monoisotopic mass (Da)	Xcorr
PGM	K3XFX0	8.69	AHGTAVGLPSDDDMGNS(1)EVGH NALGAGR	Ser-17§	2801.18	2704.21	3.48
PEPC	K3XV32	38.90	RGDFADEGFAATES(0.95)DIEET LKR	Ser-14	2537.12	2456.13	4.17
			LLAPGKVS(1)EDDKLVEYDALLI	Ser-8§	2652.36	2571.37	3.50
			FTAATLEHGMHPPVS(1)PKPEWR	Ser-15§	2484.15	2387.17	1.99
			RVDT(1)ALKNIGIDER	Thr-4	1679.85	1598.86	1.86
			NQTVDLVFTAHPTQS(0.99)VRR	Ser-15	2149.05	2068.07	1.50
			HHS(1)IDAQLR	Ser-3§	1156.53	1075.54	1.28

3.2.2 Phospho*enol*pyruvate carboxylase phosphorylation

Seven phosphorylation sites (Figure 3.11) were identified in *Setaria viridis* PEPC (K3XV32), including the phosphoserine described in *Zea mays* PEPC (P04711). PEPC-2 (K3YPN6) was also identified in *Setaria viridis*, but despite conserved active site residues, the extent of similarity between PEPC-2 and the C_4 PEPC was not investigated. Furthermore, the *N*-terminal phosphopeptide was not detected in PEPC-2. Based on the phosphoproteomic data and information obtained from the UniProtKB database, candidate protein K3XV32 was selected as the true counterpart to *Zea mays*' C_4 PEPC primarily because of 1) the fully conserved *N*-terminal phosphopeptide which bears the phosphorylated regulatory site described in *Zea mays*, 2) higher sequence similarity to *Zea mays* PEPC and 3) more substantial peptide recovery, suggesting that PEPC is relatively more abundant in leaf lysates than PEPC-2 (Table 3.5).

PEPC sequence information was obtained from the UniProtKB database, aligned using Clustal Omega and illustrated to scale as Figure 3.11. Sequence similarity between C_4 PEPC in *Zea mays* (P04711) and PEPC in *Setaria viridis* (K3XV32) is 84% covering 814 identical positions, which is close to the 83% similarity between PEPC and PEPC-2, whereas similarity between PEPC-2 and P04711 is slightly lower at 80%, based on 781 identical positions. All phosphorylated residues, except for Ser-378 in K3XV32, are conserved in the *Zea mays* C_4 PEPC. PEPC in *Setaria viridis* was phosphorylated at Ser-11 (Figure 3.12A, residues 9–17, HHSIDAQLR) after the onset of light and remained phosphorylated until the end of the photoperiod (Table 3.4B). While Ser-12 (PEPC-2, residues 9–18, HQSIDAQLR) corresponds to Ser-11 in PEPC, it was not phosphorylated. The phosphorylation of Ser-25 of PEPC occurred strictly after the onset of light and corresponds to Ser-26 in PEPC-2, which was phosphorylated at the same time-point.

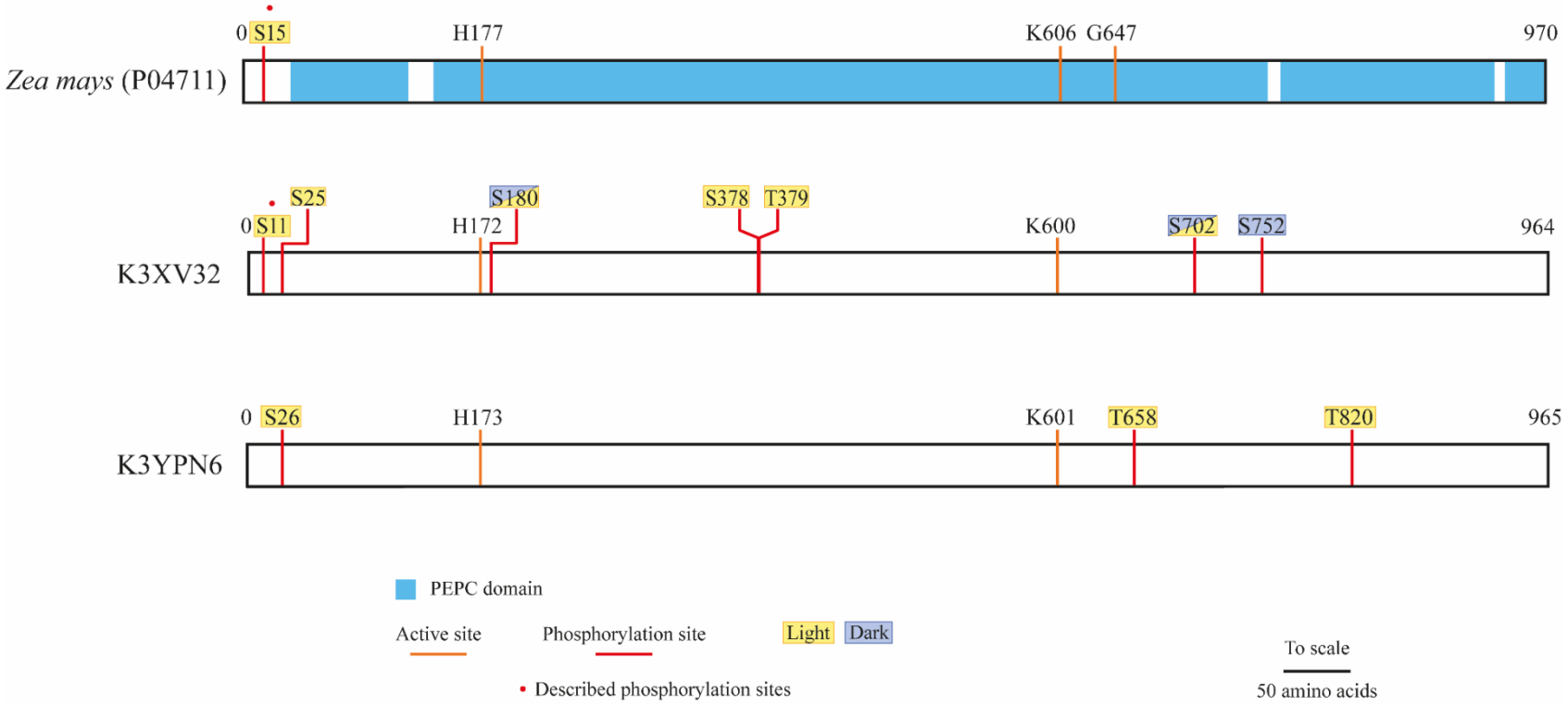

Fig. 3.11. Protein schematic showing the similarities between PEPC P04711, K3XV32 and K3YPN6. Proteins sequences are represented by rectangles and the number of amino acids in the sequence is indicated at the far right of each protein. Light or dark phosphorylation sites are highlighted in yellow or blue boxes, respectively. Phosphorylation sites present in darkened and illuminated leaves are shown in half-yellow-half-blue boxes. The regulatory site at Ser-15 in *Zea* mays, corresponding to Ser-11 in K3XV32, is indicated by a red dot above the modified residue. PEPC structural data for *Zea mays* obtained from Matsumura *et al.* (2002).

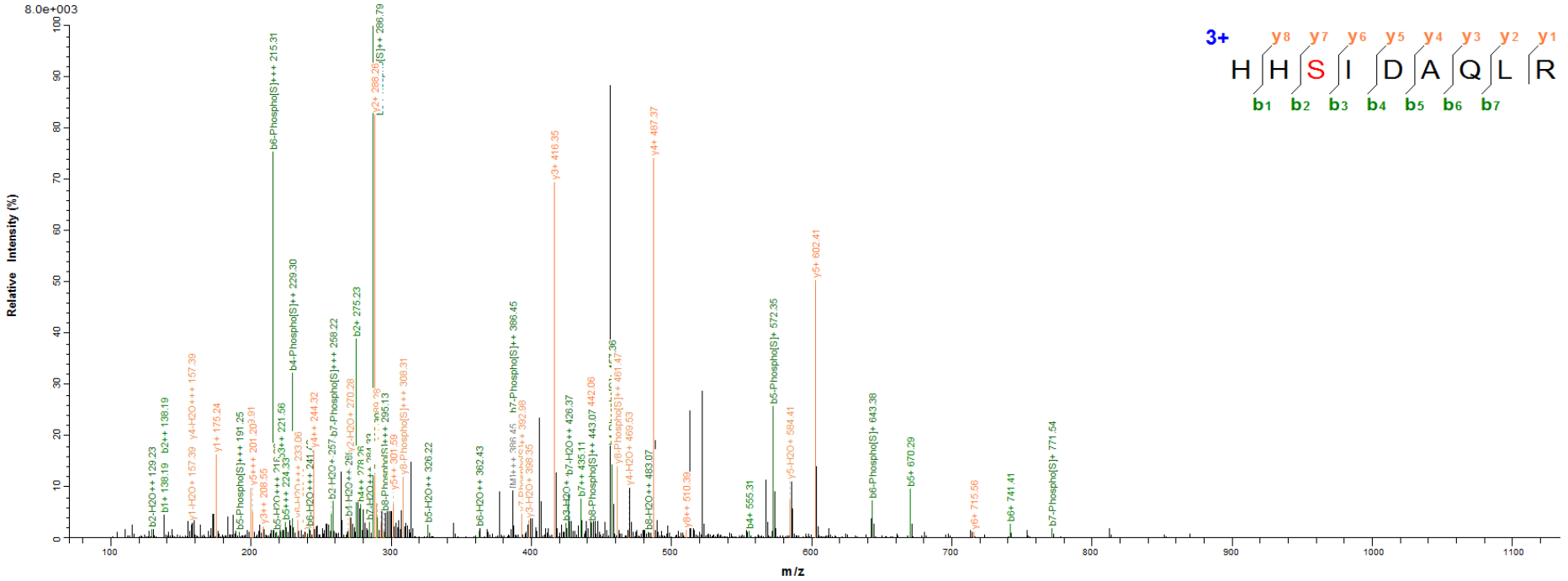

Fig. 3.12A. Phosphorylation at Ser-11 occurred after illumination. PEPC peptide spectra showing the ion fragmentation pattern of residues 9–17 (above spectrum) along its mass-to-charge (*m*/*z*) ratio.

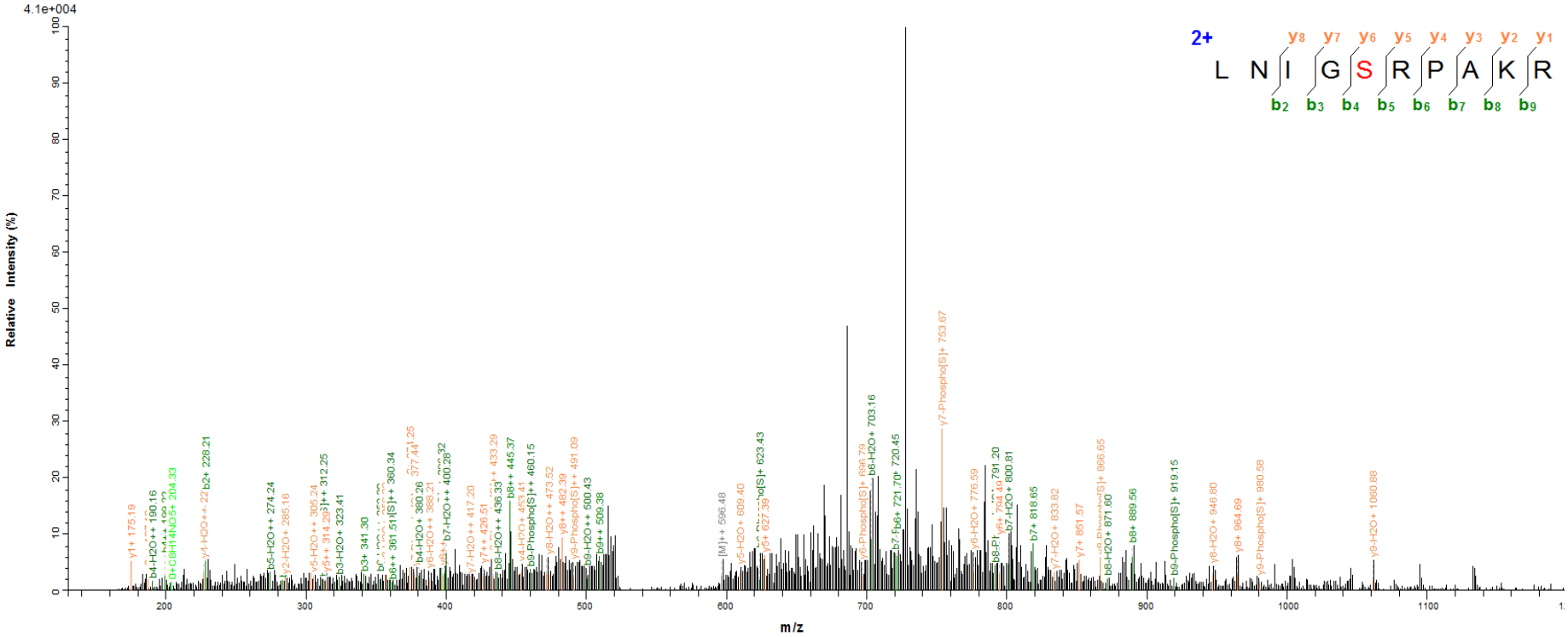

Fig. 3.12B. Phosphorylation at Ser-752 occurred in darkened leaves. PEPC peptide spectra showing the ion fragmentation pattern of residues 748–757 (above spectrum) along its mass-to-charge (*m*/*z*) ratio. Charge of the peptide is indicated by the blue number above the peptide sequence. The detected b- and y-ions (including loss of H_2O, 18 Da and loss of $(PO_4)^{3-}$, 80 Da) are indicated in green and yellow, respectively. Spectrum quality is determined by the total number of b- and y-ions observed along the peptide sequence and the size of peaks (relative intensity, %).

The phosphorylations at Ser-25, Ser-378 and Thr-379 were present in illuminated conditions, but absent in darkened leaves. Conversely, the phosphorylation at Ser-752 (Figure 3.12B, residues 748–757, LNIGSRPAKR) solely occurred in darkened leaves and was not identified in illuminated leaves. As shown in Figure 3.9, the phosphorylations at Ser-180 (Figure 3.13A, residues 180–189, SLLQKHARIR) and Ser-702 (Figure 3.13B, residues 688–708, FTAATLEHGMHPPVSPKPEWR) occurred in darkened and illuminated leaves and showed no light-dependent regulation. Additionally, the light-dependent phosphorylations of Thr-658 and Thr-820 occurred in PEPC-2, but the corresponding residues in PEPC were not phosphorylated.

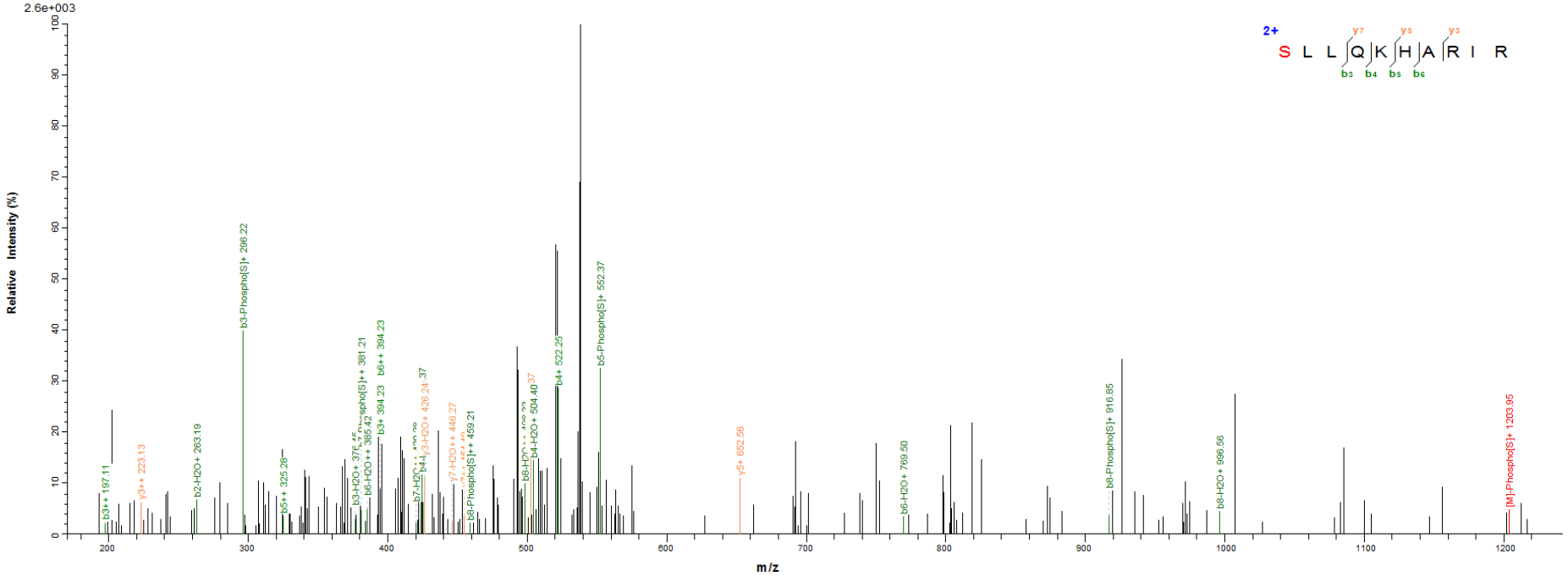

Fig. 3.13A. Phosphorylation at Ser-180 occurred in darkened and illuminated leaves of *Setaria viridis*. PEPC peptide spectra showing the ion fragmentation pattern of residues 180–189 (above spectrum) along its mass-to-charge (*m*/*z*) ratio. Protonated precursor ion in red (ca 1200 *m*/*z*).

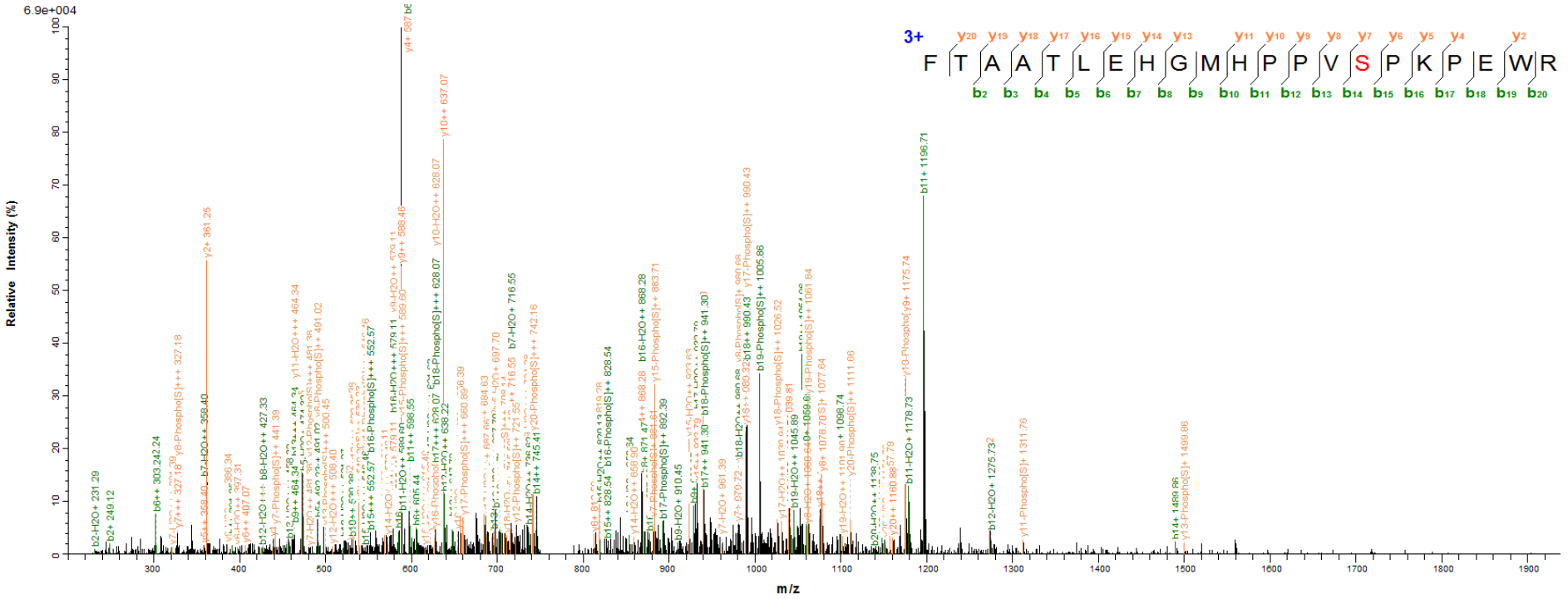

Fig. 3.13B. Phosphorylation at Ser-702 occurred in darkened and illuminated leaves of *Setaria viridis*. PEPC peptide spectra showing the ion fragmentation pattern of residues 688–708 (above spectrum) along its mass-to-charge (*m*/*z*) ratio. Charge of the peptide is indicated by the blue number above the peptide sequence. The detected b- and y-ions (including loss of H_2O, 18 Da and loss of $(PO_4)^{3-}$, 80 Da) are indicated in green and yellow, respectively. Putative phosphorylation sites highlighted in red.

Table 3.5. Protein isoforms identified in 7.5 h darkened *Setaria viridis* leaves. Information acquired from the validation of phosphopeptides in *Setaria viridis* at 7.5 h into dark from four biological replicates (R1-R4) using MaxQuant. Unique peptides are unique to the protein group indicated by the protein accession, whereas all other peptides, which exist in related proteins, are labelled as razor peptides. Sequence coverage is given as a percentage of the total number of amino acids present in the sum of the experimentally observed unique peptides and razor peptides against the total number of amino acids in the protein sequence. The intensity-based absolute quantification value (iBAQ) is a mathematical approximation used to compare the relative amount of one protein to another within the same complex mixture.

		Number of razor peptides				Number of unique peptides						
Protein	**Accession**	**R1**	**R2**	**R3**	**R4**	**R1**	**R2**	**R3**	**R4**	**Mass (kDa)**	**Coverage (%)**	**iBAQ**
AlaAT	K3ZSX0	0	0	0	0	4	3	2	2	53.2	20.5	366910
AlaAT	K4A8B1	0	0	0	0	1	0	0	0	58.2	3.0	3011
Enolase 1	K3XWW9	7	7	5	5	9	10	9	6	47.9	45.3	1202000
Enolase 2	K3Z681	0	0	0	0	7	7	7	4	47.9	38.2	2003400
NADP-malic enzyme	K3XG11	3	3	3	3	38	39	34	38	63.9	56.7	2208700
NADP-malic enzyme	K3XFW4	0	1	1	0	3	4	2	2	65.1	13.4	412370
NADP-malic enzyme	K3ZRI5	0	0	0	0	19	13	16	22	69.5	49.9	3637300
PEPC	K3XV32	14	16	18	21	120	12	133	141	109.98	75.2	5812700
PEPC	K3YPN6	3	1	2	3	3	5	6	8	109.82	27.6	790010

3.2.3 Pyruvate, phosphate dikinase phosphorylation

Eight phosphorylation sites were identified in *Setaria viridis* pyruvate, phosphate dikinase (PPDK, K3Z3Q6), including the previously described phosphopeptide at position Thr-527 in *Zea mays* (Roeske *et al.*, 1988), which corresponds to Thr-462 in *Setaria viridis* (Figure 3.14). The extent of sequence similarity between K3Z3Q6 and P11155 is 83% covering 786 identical amino acid positions, including all identified phosphorylated residues. The phosphorylation at Thr-462 (Figure 3.15, residues 459–470, GGMTSHAAVVAR) occurred at 7.5 h into the dark and 4 h and 15.5 h into the light, suggesting that PPDK phosphorylation at Thr-462 may be under more extensive regulation rather than being simply induced by the dark to light transition. Based on the ratio between the phosphopeptide and its unmodified counterpart, as a relative quantitative measure, the phosphorylated phosphopeptide was observed in higher amounts in 7.5 h darkened leaves than in illuminated leaves. Aside from Thr-462, phosphorylations at Ser-104, Ser-394 and Thr-593 (Figure 3.16, residues 584–597, AVRQMIMAPTLELR) occurred at 7.5 h into dark, whereas the phosphorylations at Thr-557, Thr-704, Thr-721 and Thr-753, occurred strictly after the onset of light. Additionally, the phosphorylations at Thr-753 and Thr-462 were identified in the phosphopeptide enrichment experiments.

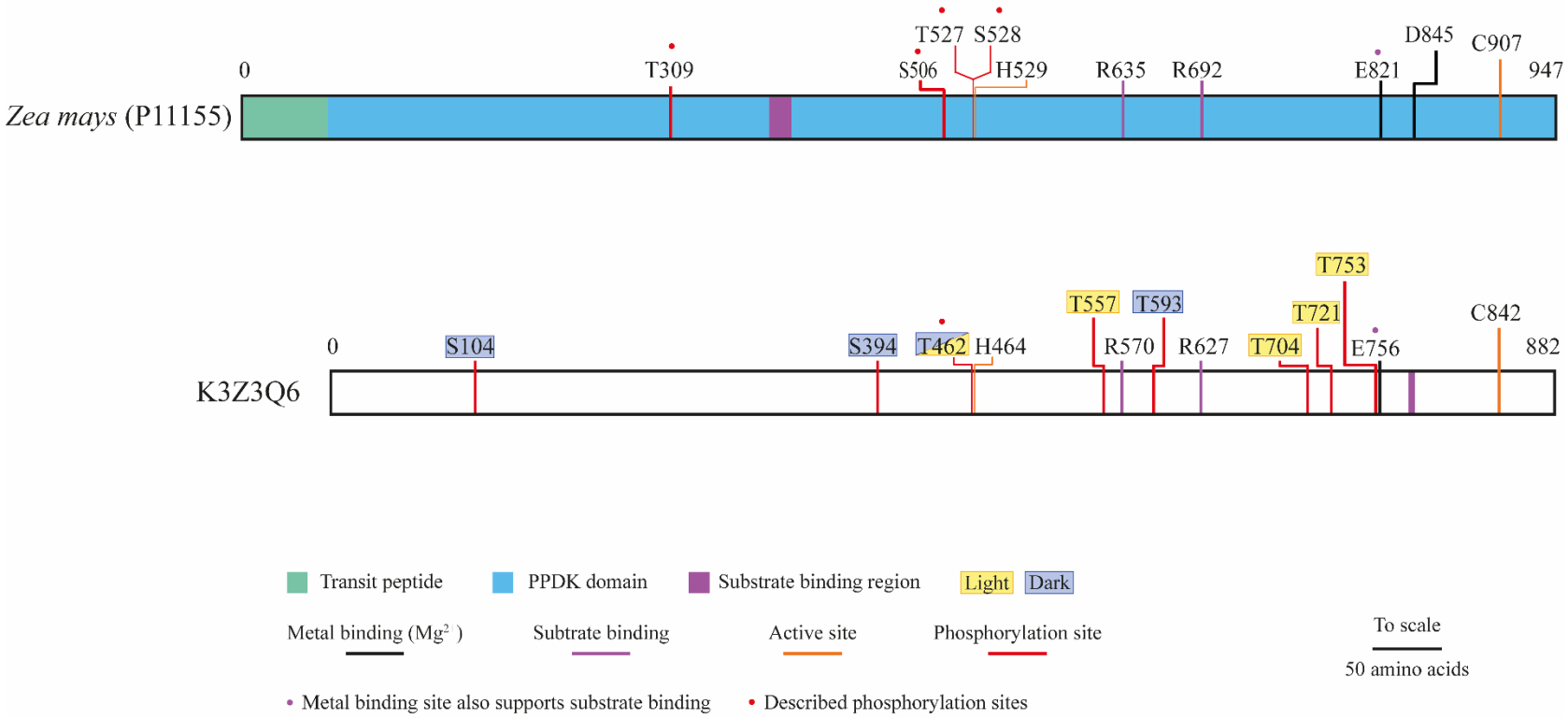

Fig. 3.14. Phosphorylation of PPDK (K3Z3Q6) in leaves of *Setaria viridis* compared to *Zea mays* PPDK. Proteins sequences (rectangles) are annotated based on information obtained from UniProtKB. Light and dark phosphorylation sites identified in K3Z3Q6 are highlighted in yellow or blue boxes, respectively (light-independent phosphosites are highlighted in blue and yellow). Described phosphorylation sites are indicated by a red dot above the modified residue. Purple dots above residues indicate metal and substrate binding sites.

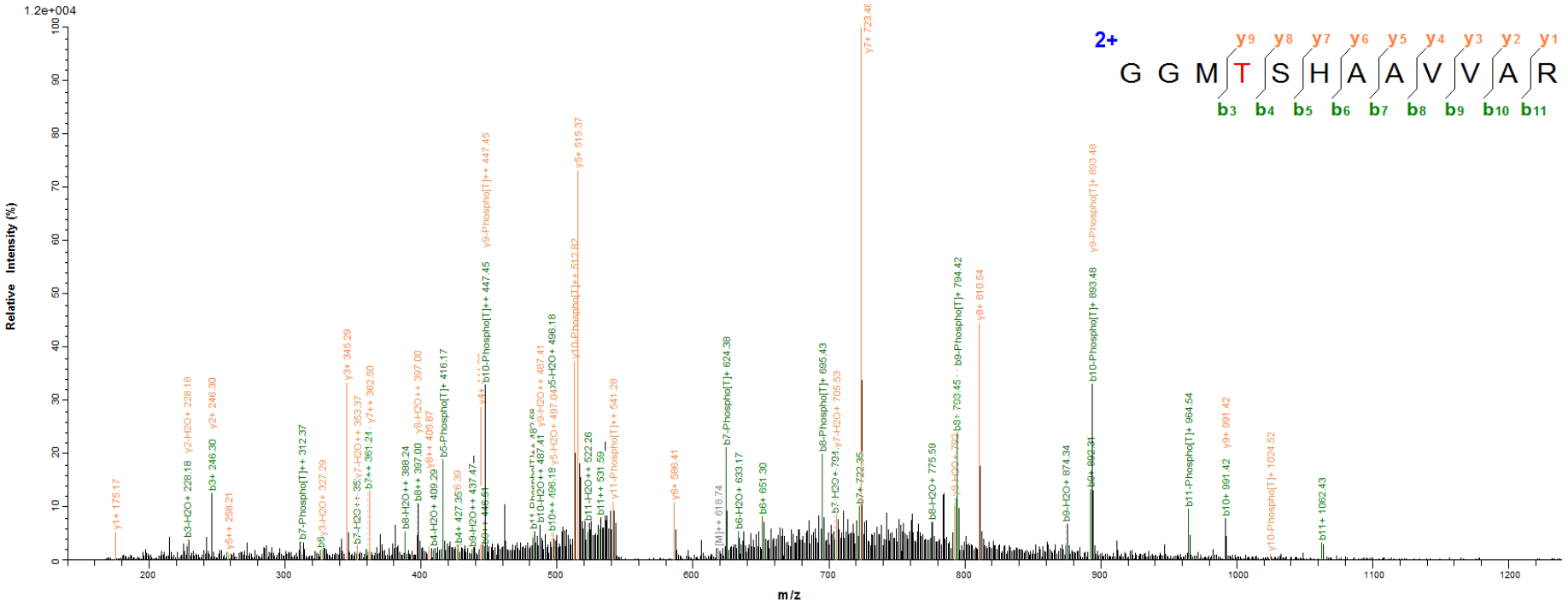

Fig. 3.15. PPDK phosphorylation at Thr-462 in *Setaria viridis*. PPDK peptide spectrum showing the ion fragmentation pattern of residues 459 –470 (above spectrum) along its mass-to-charge (*m/z*) ratio. Charge of the peptide is indicated by the blue number above the peptide sequence. The detected b- and y-ions (including loss of H_2O, 18 Da and loss of $(PO_4)^{3-}$, 80 Da) are indicated in green and yellow, respectively. Putative phosphorylation sites highlighted in red. Protonated precursor ion indicated in red.

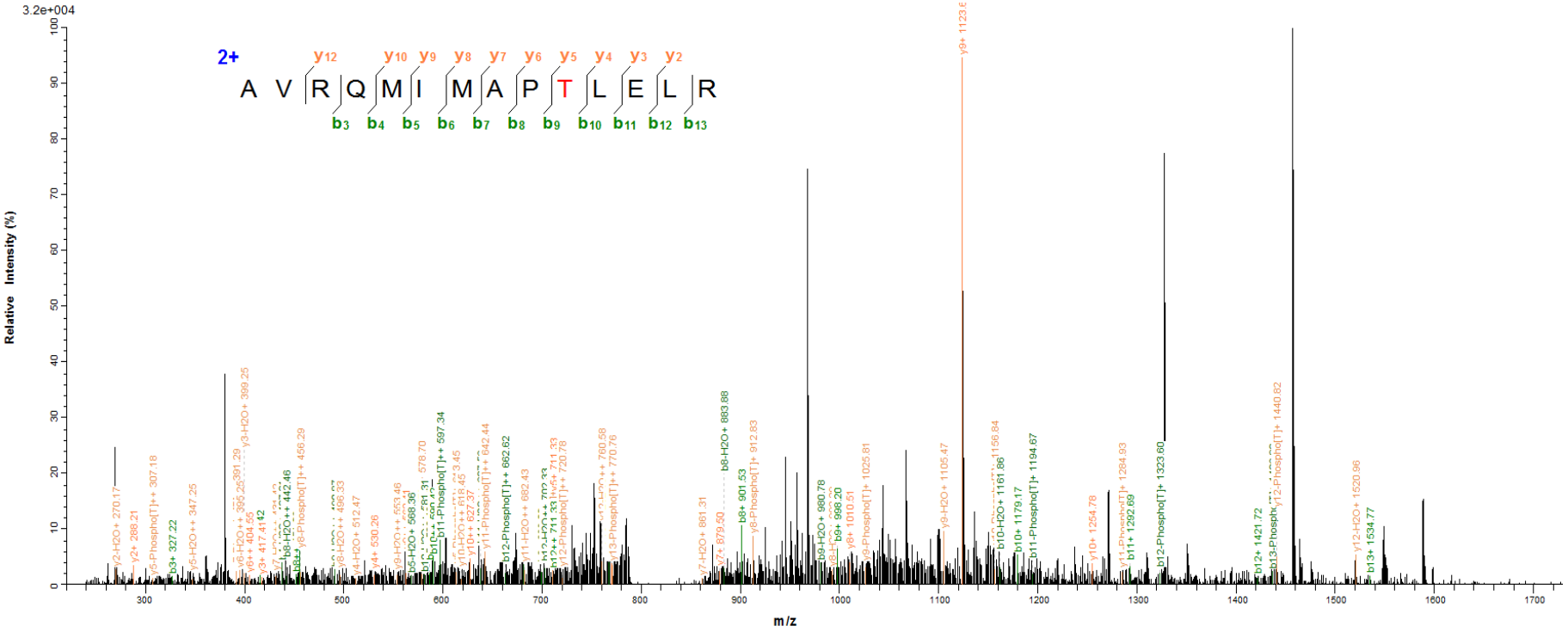

Fig. 3.16. Phosphorylation at Thr-593 occurred strictly in darkened leaves of *Setaria viridis*. PPDK peptide spectrum showing the ion fragmentation pattern of residues 584–597 (above spectrum) along its mass-to-charge (*m*/*z*) ratio. Charge of the peptide is indicated by the blue number above the peptide sequence. The detected b- and y-ions (including loss of H_2O, 18 Da and loss of $(PO_4)^{3-}$, 80 Da) are indicated in green and yellow, respectively. Putative phosphorylation sites highlighted in red.

3.2.4 NADP-dependent malic enzyme phosphorylation

Four NADP-dependent malic enzyme proteins were identified in *Setaria viridis*: K3XFH6, K3XFW4, K3XG11 and K3ZRI5 (Table 3.3). Compared to the primary NADP-malic enzyme in *Zea mays* (P16243), K3ZRI5 is 36% identical, while the protein sequence similarity between P16243 and K3XFH6, K3XFW4 and K3XG11 is higher at 83%, 70% and 75%, respectively. In addition, NADP-malic enzyme K3XG11 was approximately 60-fold and 535-fold more abundant in darkened leaf lysates than K3ZRI5 and K3XFW4, respectively (Table 3.5). Using a standard MS approach without enriching for phosphopeptides, 21 phosphorylation sites in NADP-malic enzyme were identified. Five putative phosphorylation sites were identified in K3XFH6 during the light time-points, of which three were significant (Xcorr > 2.15). The phosphorylation at Ser-429 (Figure 3.18, residues 417–430, VWLVDSKGLIVSSR) corresponded to the phosphorylation at Ser-380 in K3XFW4 and Ser-363 in K3XG11 (Figure 3.17). Although, the phosphorylations at Ser-373, Ser-379 and Ser-380 in K3XFW4 were identified in separate experiments, the phosphopeptides and phosphorylation sites were not significant. Furthermore, the triply phosphorylated peptide was not detected in the light samples.

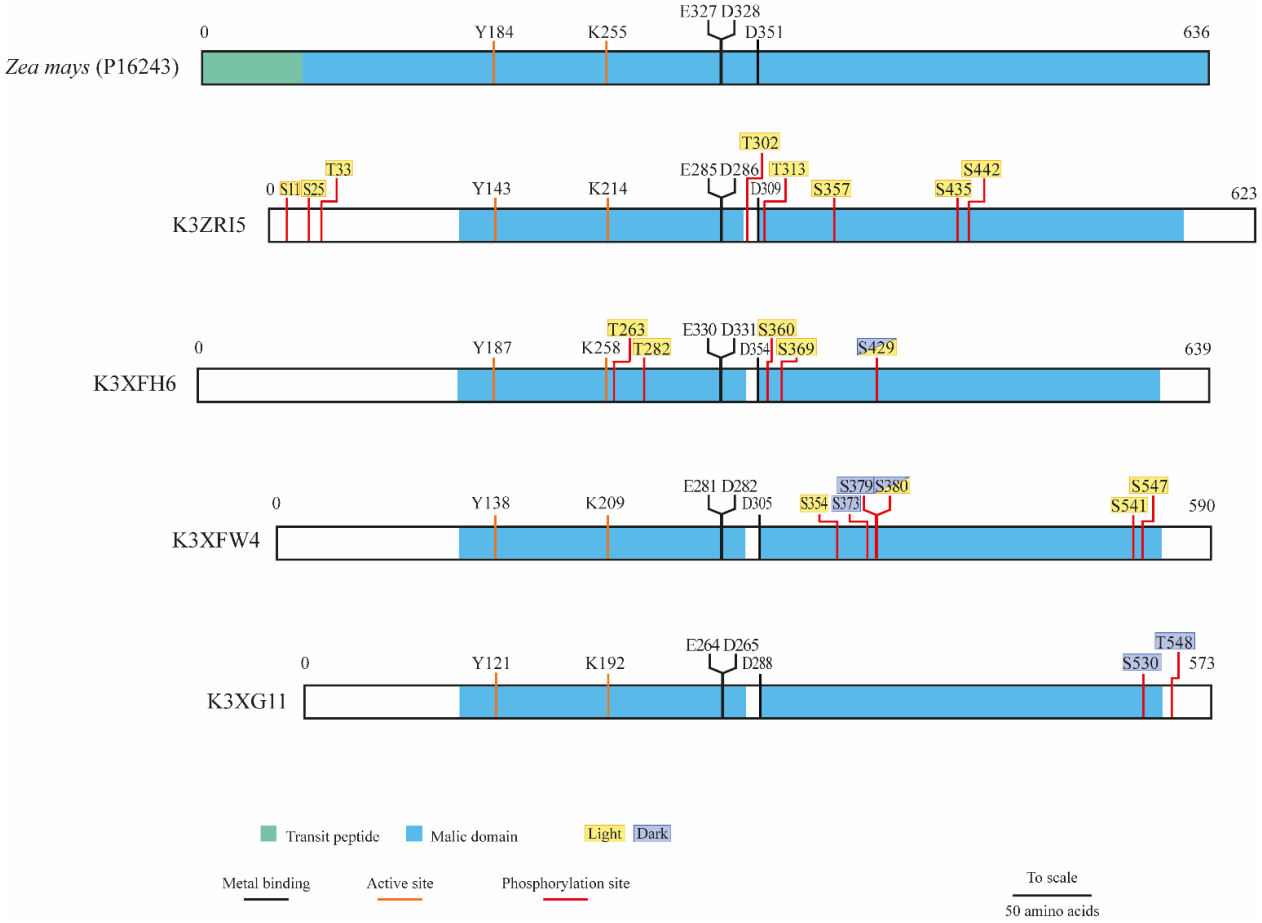

Fig. 3.17. NADP-malic enzyme isoforms identified in *Setaria viridis* leaf extracts compared to NADP-malic enzyme from *Zea mays* (top). Protein sequences (rectangles) were obtained from UniProtKB. Light or dark occurring phosphorylation sites are highlighted in yellow or blue, respectively. Phosphosites present in light and dark highlighted in blue and yellow. Proteins are aligned at the metal binding sites.

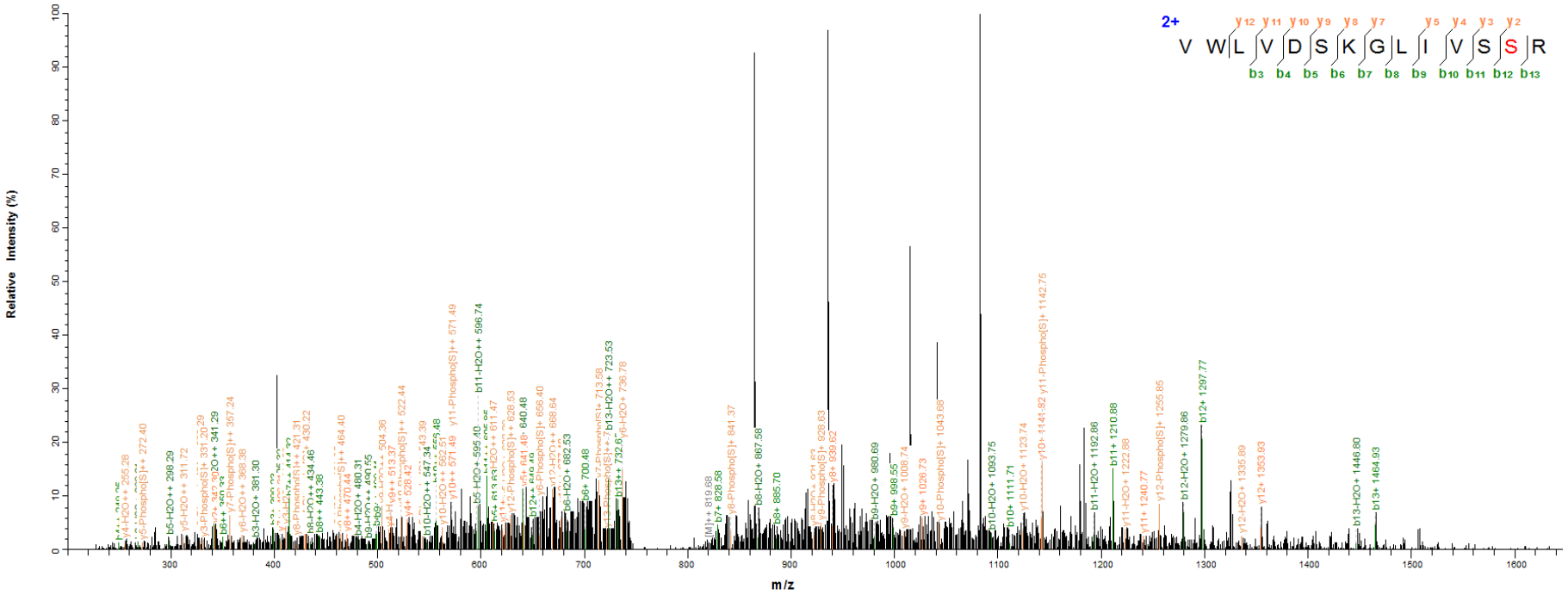

Fig. 3.18. Peptide spectrum showing novel NADP-malic enzyme phosphorylation at Ser-429 in *Setaria viridis*. NADP-malic enzyme peptide spectrum showing the ion fragmentation pattern of residues 417–430 (above spectrum) along the mass-to-charge (*m*/*z*) ratio. Charge of the peptide is indicated by the blue number above the peptide sequence. The detected b- and y-ions (including loss of H_2O, 18 Da and loss of $(PO_4)^{3-}$, 80 Da) are indicated in green and yellow, respectively. Putative phosphorylation sites highlighted in red.

3.2.5 Alanine and aspartate aminotransferase phosphorylation

Seven phosphopeptides were identified in alanine aminotransferase, of which six were significant (Xcorr > 2.15). In total, 12 phosphorylation sites were identified in alanine aminotransferase (Figure 3.20). Reoccurring phosphorylations occurred at Thr-167 and Ser-189 (Figure 3.19, residues 166–190, ATGAYSHSQGIKGLRDAIAAGIASR) in 7.5 h into dark and 4 h after the onset of light and remained phosphorylated until 30 min before the dark period. The phosphorylations at Thr-57, Ser-62, Thr-203, Ser-207, Thr-288, Ser-290, Ser-322 and Ser-326 occurred in illuminated leaves, whereas the phosphorylations at Thr-167, Ser-189 and Ser-206 occurred in darkened and illuminated leaves. Only one putative phosphorylation site, at Ser-285, was present in darkened leaves. Conversely, aspartate aminotransferase was phosphorylated at more residues during the dark period. Seven phosphopeptides, of the nine identified in aspartate aminotransferase, were significant (Xcorr > 2.15). The phosphorylations at Ser-10, Ser-11, Ser-99, Ser-266, Ser-273, Ser-341 and Ser-391, were only found in darkened leaves, whereas the phosphorylations of Ser-300, Thr-394 and Thr-397 were only present after illumination (Figure 3.21).

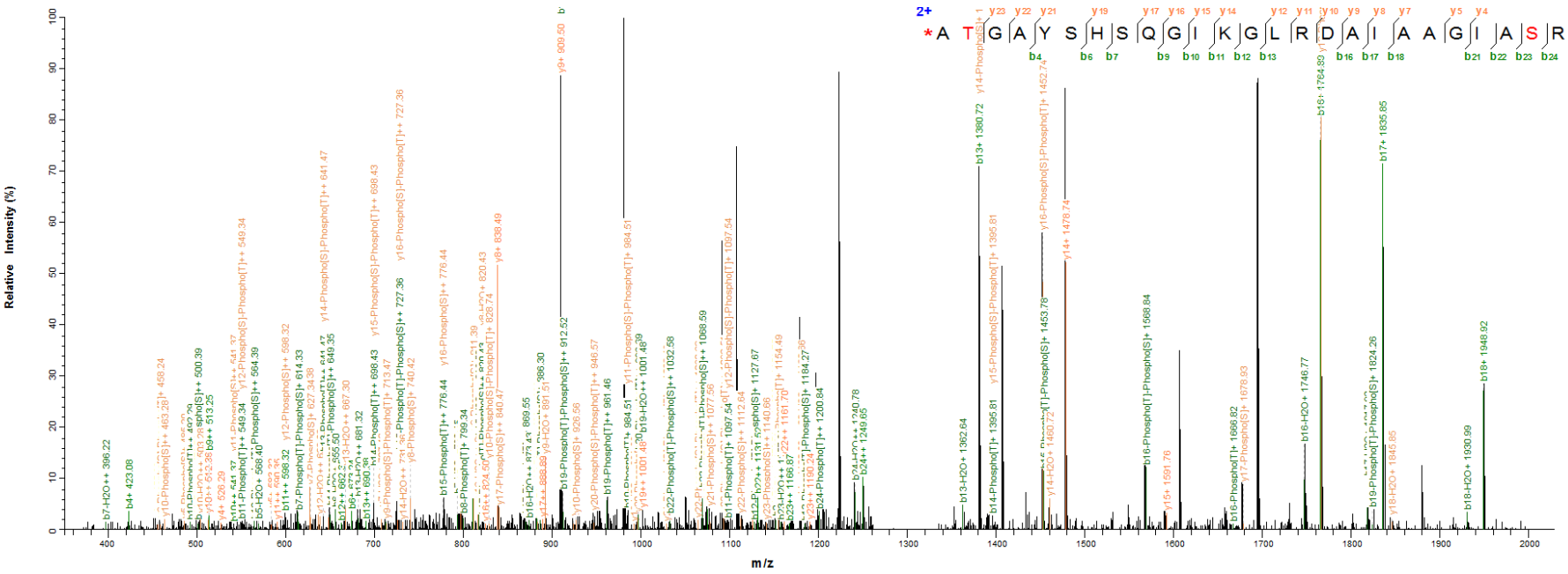

Fig. 3.19. **Peptide spectrum showing alanine aminotransferase phosphorylations at Thr-167 and Ser-189**. Alanine aminotransferase peptide spectrum showing the ion fragmentation pattern of residues 166–190 (above spectrum) along its mass-to-charge (*m*/*z*) ratio. Charge of the peptide is indicated by the blue number above the peptide sequence. The detected b- and y-ions (including loss of H_2O, 18 Da and loss of $(PO_4)^{3-}$, 80 Da) are indicated in green and yellow, respectively. Putative phosphorylation sites highlighted in red. * *N*-acetylation.

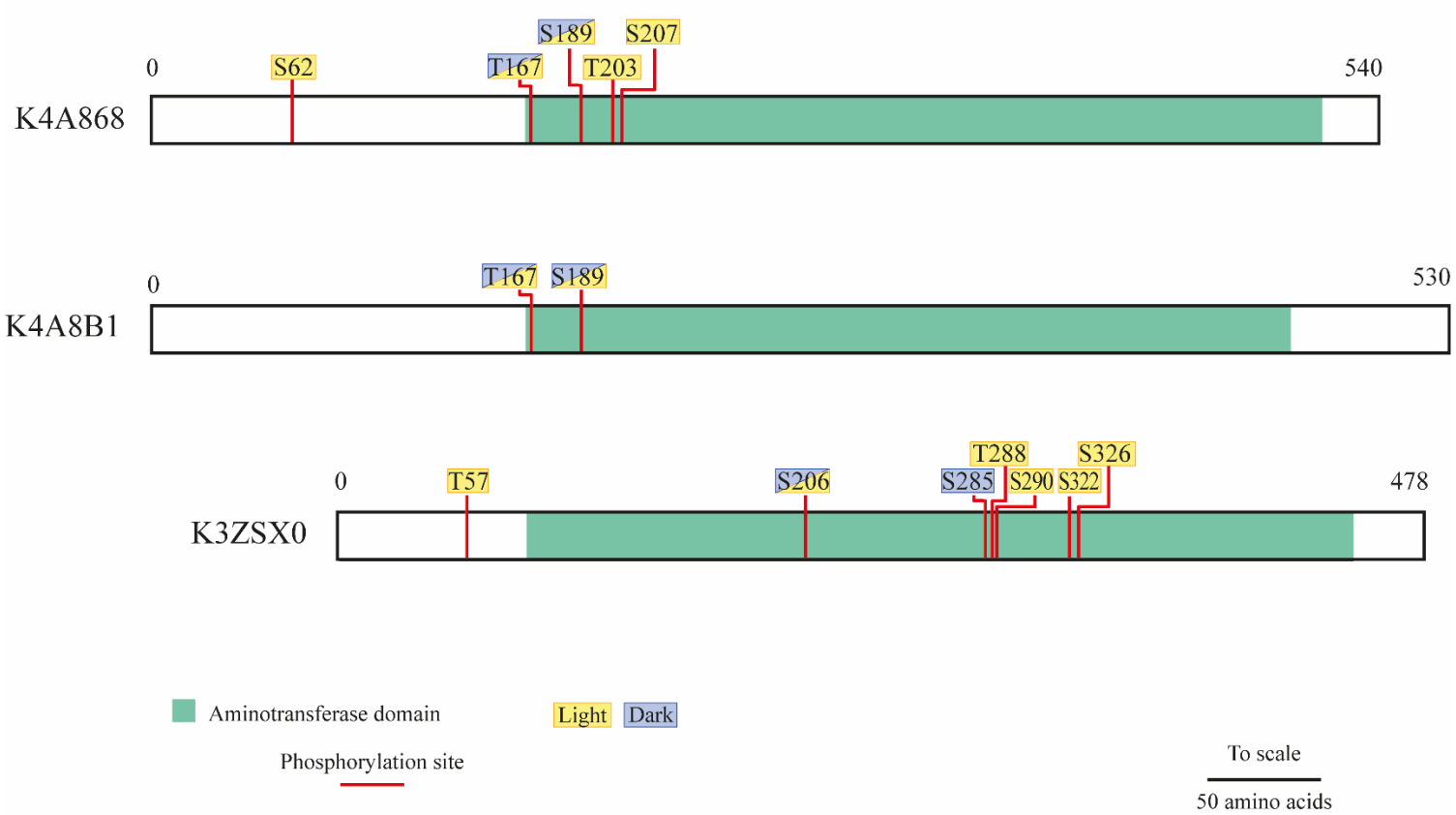

Fig. 3.20. The phosphorylation of alanine aminotransferase in *Setaria viridis* occurred predominantly after illumination. Protein sequences (rectangles) were obtained from the UniProtKB database and aligned using Clustal Omega. Key amino acids are indicated by the coloured lines and residue number. Novel sites of phosphorylation are indicated in red. Light or dark occurring phosphorylation sites are highlighted in yellow or blue, respectively. Phosphorylations occurring in light and dark are highlighted in yellow and blue boxes.

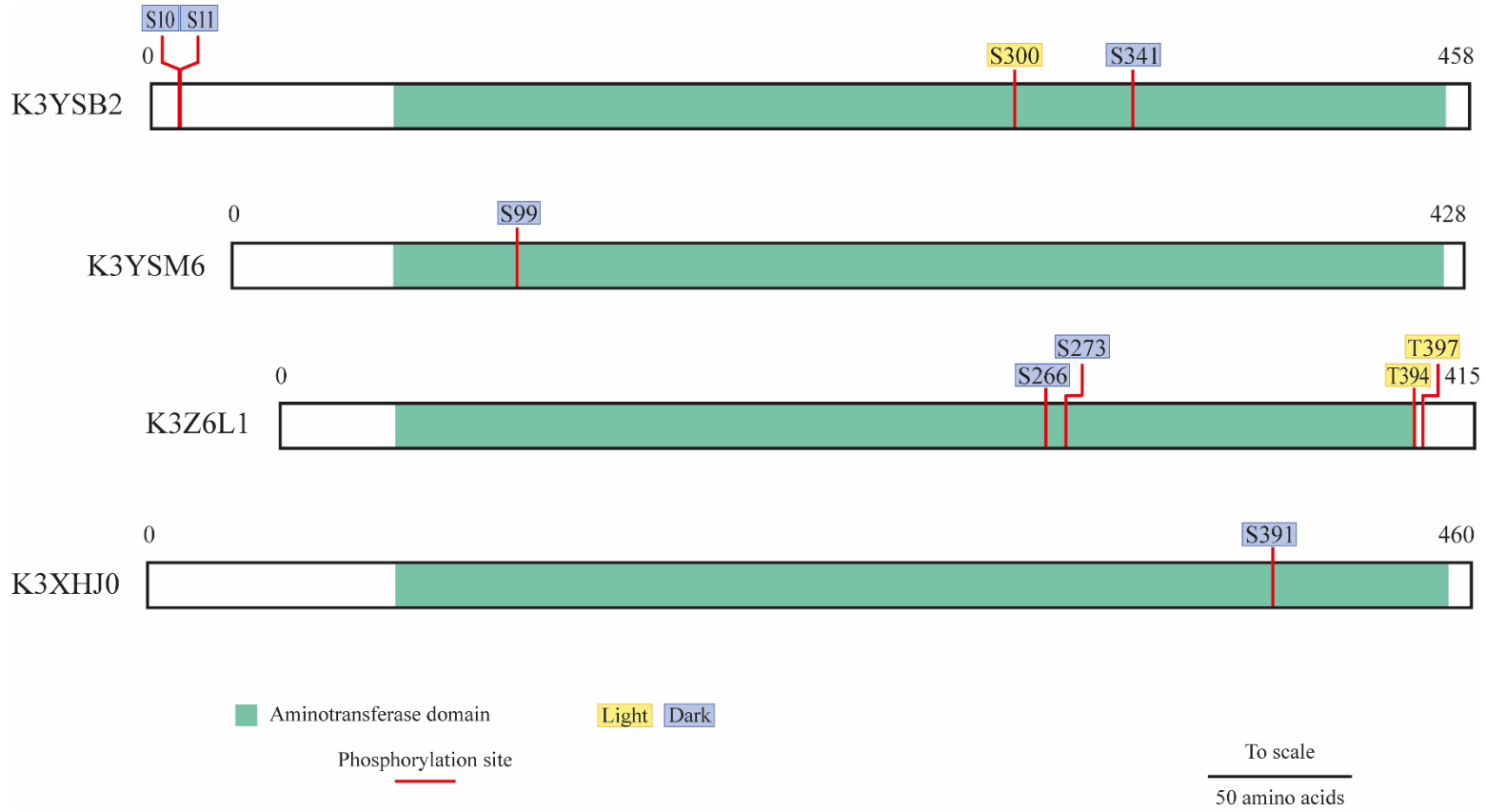

Fig. 3.21. The phosphorylation of aspartate aminotransferase in *Setaria viridis* occurred predominantly in darkened leaves. Protein sequences (rectangles) were obtained from the UniProtKB database and aligned using Clustal Omega. Key amino acids are indicated by the coloured lines and residue number. Novel sites of phosphorylation are indicated in red. Light or dark occurring phosphorylation sites are highlighted in yellow or blue, respectively.

3.2.6 Phosphoglycerate mutase and enolase phosphorylation

Three phosphopeptides were identified in phosphoglycerate mutase (K3XFX0), one of which was detected in the phosphopeptide enrichment experiments (Table 3.4B). The phosphorylation at Ser-109 (Figure 3.22A, residues 93–120, AHGTAVGLPSDDDMGN-SEVGHNALGAGR) occurred in 4 h and 15.5 h illuminated leaves of *Setaria viridis*, and during phosphopeptide validation experiments, the phosphorylation was detected in three replicates of 7.5 h darkened *Setaria viridis* and *Sorghum bicolor* leaves (Table 3.6 and Table 3.7). The phosphopeptide was not detected in darkened leaves in previous experiments. Additionally, the phosphorylations at Ser-520, Thr-527 (Figure 3.22B, residues 520–549, SGGIQILTSHTLQPVPVAIGGPGLHPGVKFR) occurred at 7.5 h into the dark period and 15.5 h into the photoperiod, but were absent 4 h after illumination. Either Ser-528 or Thr-530 could be phosphorylated in 7.5 h darkened and 15.5 h illuminated leaves, but the identified sites were not significant ($P < 0.75$). However, based on a 240.9 Da mass shift between the identified phosphopeptide and the unmodified counterpart, the peptide (residues 520–549) could be triply phosphorylated in darkened and illuminated leaves.

Two enolase proteins with 90% sequence similarity (K3XWW9 and K3Z681), represented as Figure 3.23, were identified in *Setaria viridis*. The 7.5 h into dark and 4 h into light phosphorylation at Ser-121 (K3XWW9, residues 112–132, LGANAILAVSLAVCKAGAMVK) corresponded to the phosphorylation at Ser-120 (K3Z681, residues 112–133, LGANAILAVSLAVCKAGASIKK) in an almost identical phosphopeptide. The phosphorylation of Ser-129 was only present in protein K3Z681, while the phosphorylations at Thr-334 and Thr-337 only occurred in K3XWW9.

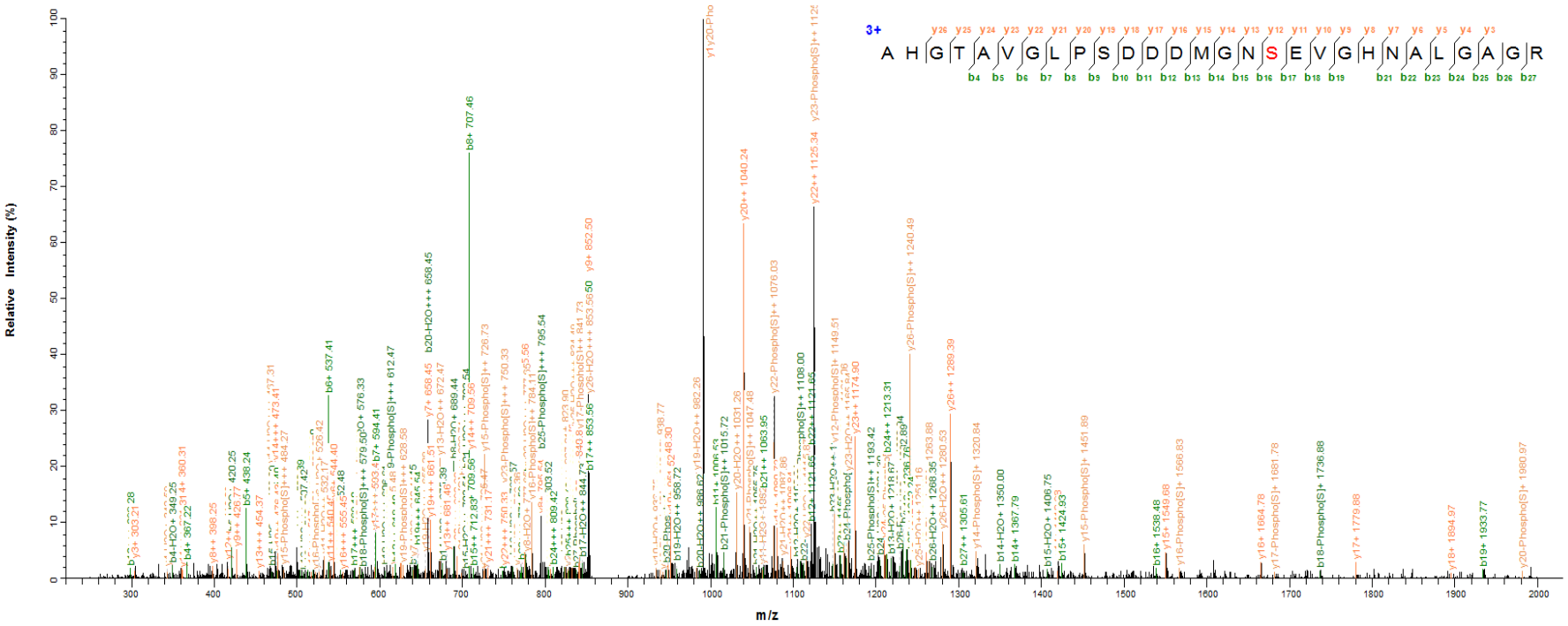

Fig. 3.22A. Peptide spectra showing the phosphorylation at Ser-109 (residues 93–120) on phosphoglycerate mutase in *Setaria viridis*.

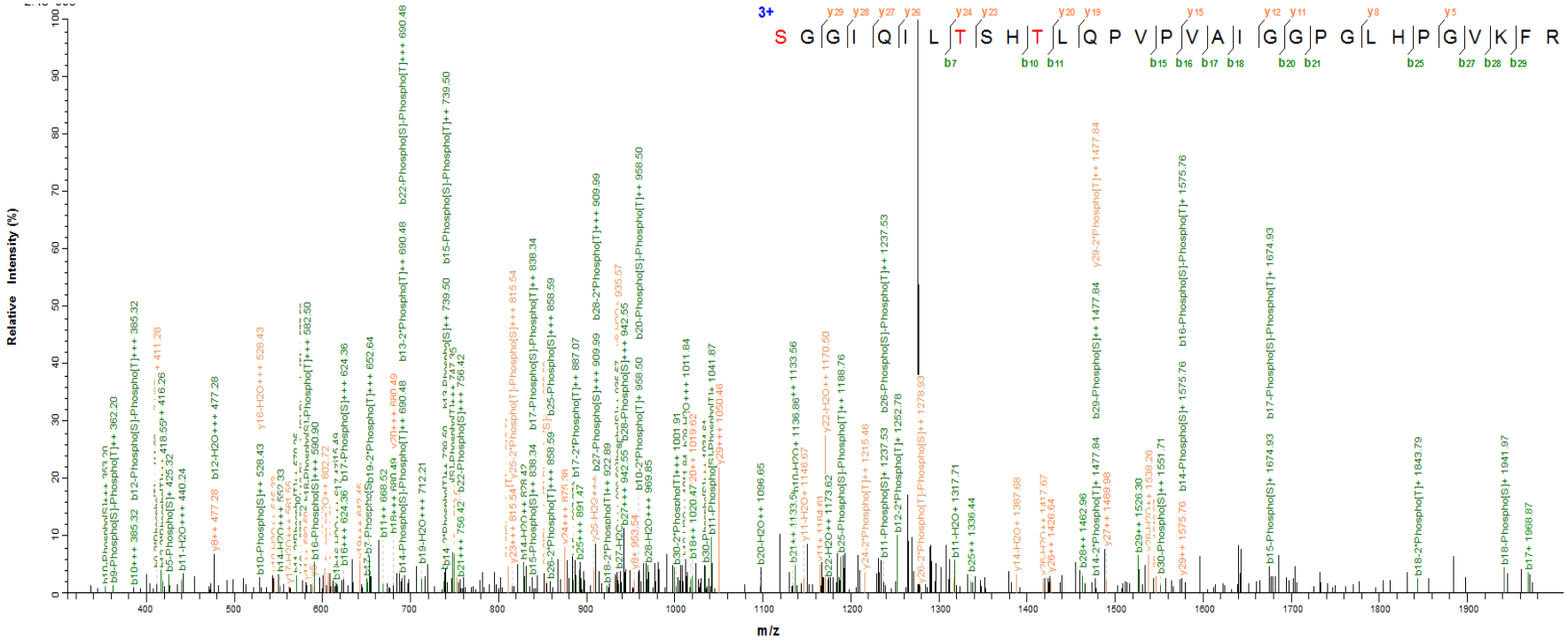

Fig. 3.22B. Peptide spectra showing the phosphorylations at Ser-520, Thr-527 and Thr-530 on phosphoglycerate mutase in *Setaria viridis*. Phosphoglycerate mutase peptide spectra showing the ion fragmentation pattern of residues 520–549 (above spectrum) along its mass-to-charge (*m*/*z*) ratio. Charge of the peptide is indicated by the blue number above the peptide sequence. The detected b- and y-ions (including loss of H_2O, 18 Da and loss of $(PO_4)^{3-}$, 80 Da) are indicated in green and yellow, respectively. Putative phosphorylation sites highlighted in red.

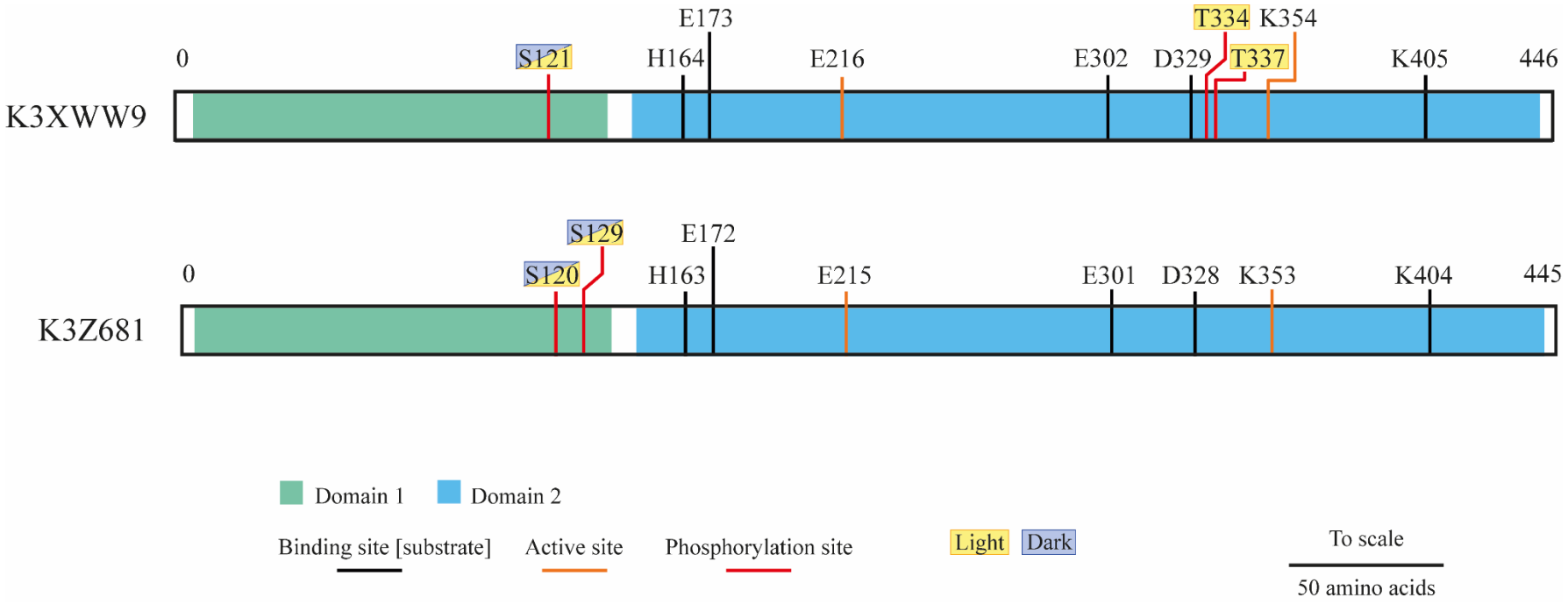

Fig. 3.23. Schematic showing the alignment of enolase K3XWW9 and K3Z681 from *Setaria viridis*. Protein sequences are represented by the rectangles. Putatively identified phosphorylation sites occurring in illuminated leaves or darkened leaves are highlighted in yellow or blue, respectively. Phosphorylation sites occurring in illuminated and darkened leaves are highlighted in blue and yellow.

3.2.7 Phosphopeptide validation

To validate the phosphopeptides that may be under light-dependent regulation, proteins between 110 kDa and 50 kDa from dark-grown *Setaria viridis* plants were analysed using a modified mass spectrometry protocol. Gradient lengths were optimised for the analyte and the resulting peptide spectra were searched against *Setaria italica* protein sequences using MaxQuant. Stringent tolerances were set for the classification of class I phosphopeptides and the FDR was set at 1%. Additional validations were carried out in two other C_4 species: *Sorghum bicolor* (Table 3.7) and *Megathyrsus maximus* (Table 3.8). The degree of reproducibility of putative phosphorylation sites was determined by the total number of times each phosphorylation site was observed across four biological replicates. Eight phosphorylation sites were validated in 7.5 h darkened *Setaria viridis* leaves (Table 3.7). Phosphoglycerate mutase was phosphorylated at Ser-17 in *Megathyrsus maximus* (Table 3.8), Ser-81 in *Sorghum bicolor* (searched against *Zea mays* protein sequences) and Ser-109 in *Setaria viridis* (searched against *Setaria italica* protein sequences). This phosphorylation was detected in several experiments (Table 3.4B; Table 3.6; Table 3.7; Table 3.8).

Table 3.6. **Phosphopeptide validation for 7.5 h darkened *Setaria viridis* leaves**. Class I phosphopeptides are given by localisation probabilities ($P \geq 0.75$ is significant) and score difference values (score diff. ≥ 5 is significant) across four replicates (R1–R4). Candidate phosphorylation sites are underlined. Phosphopeptides identified in *Sorghum bicolor* are in Table 3.7.

Protein	Accession	Phosphopeptide	Residue	Times observed	Localisation probability				Score difference			
					R1	R2	R3	R4	R1	R2	R3	R4
PGM	K3XFX0	AHGTAVGLPSDDDMGNS(1)EVGHNALGAGR	S109	3 of 4	0.99	0.99	-	0.99	62.81	48.10	-	48.91
PEPC	K3XV32	ASKPVEKHHS(1)IDAQLR	S11	4 of 4	0.99	0.99	0.99	0.99	24.72	28.15	49.86	25.56
PPDK	K3Z3Q6	GGMTS(0.78)HAAVVAR	S463	4 of 4	0.74	0.50	0.60	0.78	4.75	0.07	1.86	5.49

Table 3.7. **Phosphopeptide validation for 7.5 h darkened *Sorghum bicolor* leaves**.

Protein	Accession	Phosphopeptide	Residue	Times observed	Localisation probability				Score difference			
					R1	R2	R3	R4	R1	R2	R3	R4
PGM	P30792	AHGTAVGLPSDDDMGNS(1)EVGHNALGAGR	S81	3 of 4	0.99	-	0.99	0.99	30.9	-	56.1	32.7
PEPC	P04711	FTAATLEHGMHPPVS(0.97)PK	S708	1 of 4	0.98	-	-	-	16.5	-	-	-
		FS(0.68)SWMGGDRDGNPR	S286	1 of 4	-	-	-	0.69	-	-	-	3.4

Table 3.8. **Phosphorylation sites identified in 7.5 h darkened and 4 h illuminated leaves of *Megathyrsus maximus***. Novel phosphorylation sites identified in *Megathyrsus maximus* (Guinea grass). Experimental peptide spectra were searched against UniProtKB and NCBI *Zea mays* and *Megathyrsus maximus* protein sequences using MASCOT and phosphorylations were determined using PhosphoRS. Protein sequence coverage (out of 100%) is indicated for each protein. Phosphorylation sites are annotated by the position of the modified residue in the phosphopeptide sequence. Phosphorylation site localisation probabilities (*P*) are indicated in parentheses to the right of the modified amino acid, where $P \geq 0.75$ is significant. The calculated mass of the protonated precursor ion (MH^+) and the monoisotopic mass (Da) of the unmodified peptide are shown. Statistical confidence is given by the *E*-value, where an *E*-value ≤ 0.05 is significant. Reoccurring phosphorylation sites are indicated by [§].

Protein	Accession	Coverage (%)	Phosphopeptide	Position in peptide	MH^+ (Da)	Monoisotopic mass (Da)	*E*-value	Time point
PGM	P30792	24.33	AHGTAVGLPSDDDMGNS(1)EVG HNALGAGR	Ser-17	2801.20	2704.21	0.00389	TP3
PEPCK	Q9SLZ0	20.87	S(1)APTTPIK	Ser-1	894.43	813.45	0.0248	TP2
PEPCK	Q9SLZ0	20.87	S(1)APTTPIK	Ser-1	894.43	813.45	0.0382	TP3
PEPCK	33329363	70.72	S(0.98)APT(0.51)TPIKDGATSAF AAAISEEDR	Ser-1, Thr-4[§]	2566.11	2405.16	0.00486	TP3
PEPCK	33329363	70.72	S(0.03)APT(0.49)T(0.49)PIKDGAA STFAAALSEEER	Thr-4 or Thr-5	2500.17	2419.18	0.0433	TP3
PEPC	P04711	15.26	HHS(1)IDAQLR	Ser-3[§]	1156.53	1075.54	0.00324	TP3
PPDK	P11155	23.31	GGMT(1)SHAAVVAR	Thr-4[§]	1236.56	1155.57	0.00367	TP2
PPDK	P11155	24.24	GGMT(0.5)S(0.5)HAAVVAR	Thr-4, Ser-5	1236.56	1155.57	0.0546	TP3

3.3 Discussion

3.3.1 Overcoming the challenges of phosphoproteomics

Phosphorylated proteins account for approximately 0.1% of the proteome and phosphorylated peptides are difficult to detect because of their lower abundance relative to unmodified peptides (Seo and Lee, 2004; Tichy *et al.*, 2011). To increase the recovery of phosphopeptides in *Setaria viridis*, protein extracts were first subjected to phosphopeptide enrichment using TiO_2. TiO_2 enrichment was specifically chosen due to its low-cost, high specificity for phosphorylation sites and tolerance towards a range of detergents and buffers readily used during protein extractions (Tichy *et al.*, 2011). However, phosphopeptide enrichment in *Setaria viridis* was not successful, possibly due to low protein concentrations in plant cell lysates, which led to sub-optimal phosphopeptide binding. Future approaches may need pre-fractionation using strong cation exchange chromatography and multi-step enrichment techniques to gradually reduce proteome complexity (Zhao and Jensen, 2009; Fíla and Honys, 2012). Low quality spectra and high background noise indicate that there may have been contamination from unspecific binding during the enrichment (Figure 3.24). While TiO_2 is highly selective towards phosphopeptides, acidic residues or negatively charged contaminants may have bound to the resin instead, co-eluting with phosphopeptides. Phosphopeptide signal suppression was evident with most of the phosphorylation profiles in *Setaria viridis*, including the PEPC *N*-terminal phosphopeptide (Figure 3.24). The majority of phosphopeptides identified by TiO_2 phosphopeptide enrichment were singly phosphorylated (Table 3.4, 3.6), while containing several serine and threonine residues that were not mistaken as putative phosphorylation sites, which is likely to occur when site-determining ions are absent (Taus *et al.*, 2011). The presented data suggests that phosphorylation sites were correctly assigned despite loss of phosphopeptide resolution. The use of phosphopeptide enrichment, however, for this analytical approach was not efficient mainly due to low peptide recovery, resulting in approximately 80–90% of protein sequences being absent.

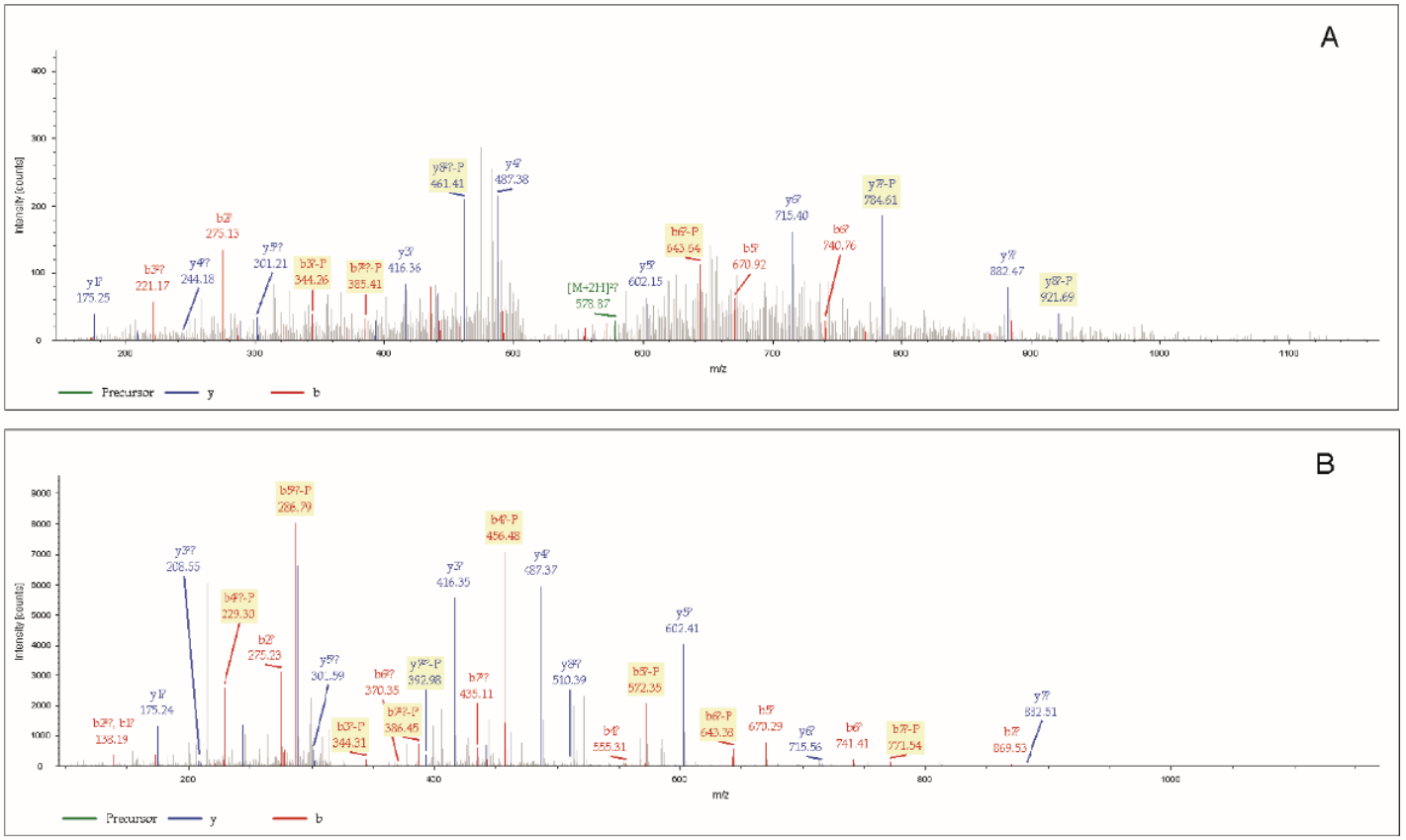

Fig. 3.24. PEPC MS/MS spectra after A) TiO_2 phosphopeptide enrichment and B) no phosphopeptide enrichment. Phosphopeptide (residues 9–17, HHSIDAQLR, *m/z* 578.77, *z* = 2+) shows increased background signals after phosphopeptide enrichment **(A)** when compared to the phosphopeptide (residues 9–17, HHSIDAQLR, *m/z* 386.18, *z* = 3+) from non-enriched samples **(B)**.

Insufficient fragment ion information from mass spectra hindered phosphorylation site assignment in *Setaria viridis*. While the observation was more notable after phosphopeptide enrichment, less abundant ions in the analyte showed diminished peptide resolution across all experiments, which not only affected PTM assignment but also made it difficult to properly infer proteins or distinguish protein isoforms. PTM assignment was also hindered by a low abundance of phosphopeptides in sample mixtures. It is not known at which stage the loss of phosphopeptides occurred, but addition of protease and phosphatase inhibitors in subsequent protein extracts contributed to increased phosphopeptide recovery. In phosphopeptide enrichments, strong binding affinities between multiply phosphorylated peptides and the enrichment resin may have made it difficult to elute several phosphopeptides. Phosphopeptide elution can be increased in future studies by optimising the pH of the peptide elution buffer, since phosphate groups contribute to the solution charge, affecting the elution efficiencies of phosphorylated peptides (Villen and Gygi, 2008). While subsequent analyses did not include a phosphopeptide enrichment step, it remains clear that to counter the effects of sub-stoichiometric phosphorylation, plant cell lysates should undergo several steps to reduce sample complexity and reduce dephosphorylated peptides, which can supress signals from the modified counterparts.

Singly and multiply phosphorylated peptides in the mixture can also affect the overall elution of phosphopeptides. In these experiments, proteins were digested with trypsin to guarantee the presence of either lysine or arginine, generating peptides of basic nature, which aid the elution of singly phosphorylated peptides after their dephosphorylated counterparts, reducing the loss of phosphopeptides during the early stages of the flow gradient (Steen *et al.*, 2006). The effects are reversed in the presence of multiply phosphorylated peptides, and may be lost due to the predominantly negative charge. In multiply phosphorylated peptides, the rate of peptide hydrolysis by trypsin may decrease if phosphorylation sites are in proximity to the cleavage site (Figure 3.25), increasing peptide lengths, thereby increasing the number basic residues, which may counter the effects of multiply phosphorylated peptides (Schlosser *et al.*, 2001; Steen *et al.*, 2006). Phosphopeptides could also be lost due to lower ionisation efficiencies, but in a similar approach using ESI-LC-MS/MS, phosphopeptides showed better ionisation and detection efficiencies than dephosphorylated peptides (Steen *et al.*, 2006).

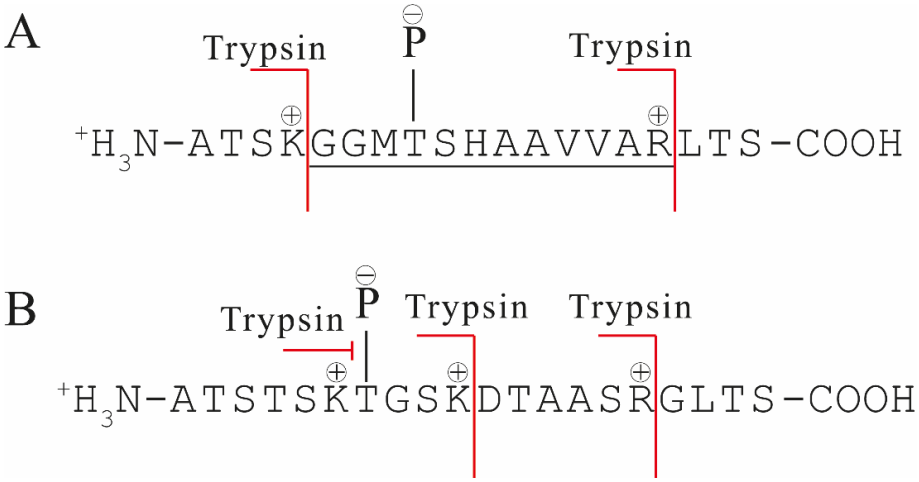

Fig. 3.25. Schematic showing trypsin inaction due to a phosphorylation site along a peptide. **A**) Tryptic digestion of a phosphopeptide (underlined) showing cleavage sites (red lines) at lysine (K) and arginine (R). The phosphorylation site is indicated by P. **B**) Hypothetical protein peptide digestion affected by phosphorylation next to cleavage site (K). Red lines crossing peptide sequence represent a successful cleavage. Negative charge (–); positive charge (+).

The light intensity for these experiments was maintained at 350 µmol m^{-2} s^{-1}, which was approximately six-fold lower than the intensity of full sunlight (Peri *et al.*, 2009). Although this may have had minimal effect on proteins that undergo light-dependent phosphorylation, enzymes that are regulated by more complex light-intensity mechanisms, like PPDK (Chen *et al.*, 2014), may have been less phosphorylated at key regulatory sites after the dark to light transition or visa-versa. Therefore, these phosphorylations may have been more difficult to detect because of their low abundance in the analyte. In addition to this, given that the rate of photosynthesis and activity of key enzymes could be affected by lower light intensities (Figure 3.26), subsequent enzyme kinetic experiments described in Chapter 4 and Chapter 5 were conducted using plants grown at 900 µmol m^{-2} s^{-1}.

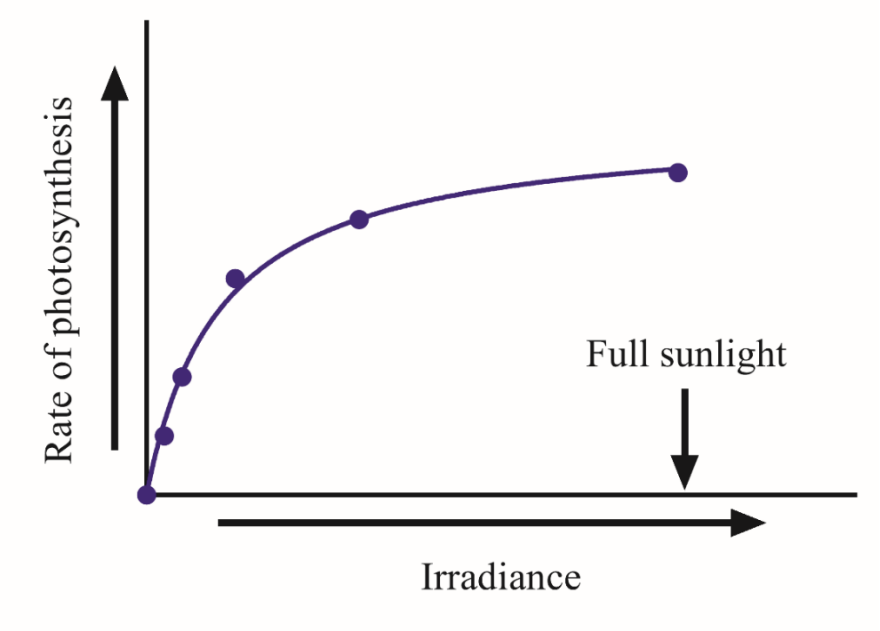

Fig. 3.26. Model relationship between irradiance and rates of photosynthesis in C_4 plants. Low rates of photosynthesis are observed when light-intensity is low. Rates of photosynthesis increase with increasing light intensities. Schematic is adapted from experimental data collected by Milner and Hiesey (1964) and Bräutigam *et al.* (2014).

Aside from experimental difficulties for PTM assignment in plants, incomplete or poorly annotated databases affect protein identification (van Wijk, 2001; Abdallah *et al.*, 2012). In UniProtKB, there are currently 267 unreviewed protein entries and 17 reviewed entries for *Setaria viridis*, compared to 40,779 and 27 entries, respectively, in the *Setaria italica* database. Choosing *Setaria italica* protein sequences as the target database for this study was essential for the identification of proteins from MS/MS peptide spectra. Although peptide spectra from *Setaria viridis* could be searched against the well-annotated and larger *Zea mays* protein sequences, *Setaria italica* is more comparable due to high genome similarity (Bennetzen *et al.*, 2012). Initial experimental data was searched using MASCOT and NCBI green plant protein sequences. While the advantage of using a larger database and filtering peptides using a narrow mass window may assist in increasing protein identification, database search times were substantially longer and did not yield significant results, as the probability of peptide spectra mismatches increased (Hsieh *et al.*, 2010). There were similar issues with the *Sorghum bicolor* database in UniProtKB and resulting MS/MS peptide spectra were searched against the *Zea mays* protein database, which aided the identification of *Sorghum bicolor* proteins and subsequent phosphorylation site assignment.

3.3.2 Phosphorylation of phospho*enol*pyruvate carboxylase

In *Zea mays* and *Sorghum bicolor*, the regulatory phosphorylation of PEPC occurs at Ser-15 and Ser-8 respectively (Jiao and Chollet, 1990; Jiao *et al.*, 1991; Chollet *et al.*, 1996; Vidal and Chollet, 1997). However, regulatory phosphorylation of PEPC at additional serine or threonine residues has not been described. Using a non-targeted approach in *Setaria viridis*, seven novel phosphorylation sites were identified (Figure 3.27). PEPC phosphorylation in *Setaria viridis* increased after illumination (Figure 3.10), but this may be due to increased content of PEPC through the photoperiod, since PEPC content in leaves can vary in response light intensity (Slack *et al.*, 1969; Hatch, 1987). Also, increased PEPC content was only discernible from 2D gels using 80 µg of total protein (Figure 3.10) and not 1D gels using 10 µg of total protein (Figure 3.9) and phosphorylated PEPCs in darkened leaves may be in very low content to be detected by phosphoprotein staining.

```
                   20                  40                  60                  80
            S11             S25
MASKPVEKHHSIDAQLRLLA PGKVSEDDKLVEYDALLIDR FLDIFQDLHGPNIREFVQEC YEVAAEYERDRDAAKLSELG
            *               *
                  100                 120                 140                 160
SRLTKLSPNDAIVVASSFSN MLNLTNLAEEVQLAHLRRNK LKRGDFADEGFAATESDIEE TLKRLVTELGKSKEEVFDAL
                  180                 200                 220                 240
           Active state
             S180
KNQTVDLVFTAHPTQSVRRS LLQKHARIRNCLTQLYAKDI TEDDKQELDEALQREIQACF RTDEIRRAQPTPQDEMRYGM
            ^       *
                  260                 280                 300                 320
SYFHETIWKGVPKFLRRVDT ALKNIGIDERLPYNAPLIQF SSWMGGDRDGNPRVTPEVTR DVCLLARMMASNLYFSQIEE
                  340                 360                 380                 400
                                                       S378
                                                        T379
LMFELSMWRCNDELRARAEE LHASSQKISKHYIEFWRQLP ANEPYRVVLGYVRDKLYSTR ERSRHLLTSGFSDIPEDSAF
                                                       **
                  420                 440                 460                 480
KNVEEFLEPLELCYKSLCDC GDKTIADGSLLDFMRQVSTF GLSMVKLDIRQESERHTDVI DAITTHLGIGSYREWSEEKR
                  500                 520                 540                 560
QEWLLSELRGKRPLLSKDMP QTEEIADVLGCFHVLAELPR DSFGPYIISMATAPSDVLAV ELLQRECHVKQPLPVVPLFE
                  580                 600                 620                 640
                                   Active site
KLADLQSAPASIERLFSLDW YMNRIGGKQQVMVGYSDSGK DAGRLSAAWHLYKAQEAMAK VAKRYGVKLTMFHGRGGTVG
                                      ^
                  660                 680                 700                 720
                                                                 S702
RGGGPTHLAILSQPPDTING SLRVTVQGEVIETSFGEEHL CFRTLQRFTAATLEHGMHPP VSPKPEWRALMDEIAAVATD
                                                                 *
                  740                 760                 780                 800
                            S752
EYRSVVMREPRFVEYFRSAT PETEYGRLNIGSRPAKRKPK GGIESLRAIPWIFSWTQTRF HLPVWLGFGAAFKHAMKKDI
                            *
```

Fig. 3.27. Phosphorylation of PEPC from *Setaria viridis*. Cleavage sites at lysine (K) and arginine (R) are highlighted in red. Phosphorylation sites indicated by asterixis. Active sites are indicated. Sequence annotated with *FASTA*nnotate.

The phosphorylation at Ser-11 (residues 9–17, HHSIDAQLR) in *Setaria viridis*, which corresponds to Ser-15 in *Zea mays*, occurred after illumination (Jiao and Chollet, 1988; Bailey *et al.*, 2007). The phosphorylation of Ser-11 in darkened leaves was only detected in a larger peptide (residues 2–17, ASKPVEKHHSIDAQLR), suggesting that a missed cleavage at Lys-8 could be affecting the retention of this larger phosphorylated peptide, as depicted in Figure 3.25. Furthermore, the identification of phosphorylation sites at Ser-25, Ser-180, Ser-378, Thr-379, and Ser-752 could be affected by the proximity of cleavage sites (Figure 3.27). In fact, all these phosphorylation sites were detected in phosphopeptides with two missed cleavages and it is possible that small phosphopeptides were lost during analysis.

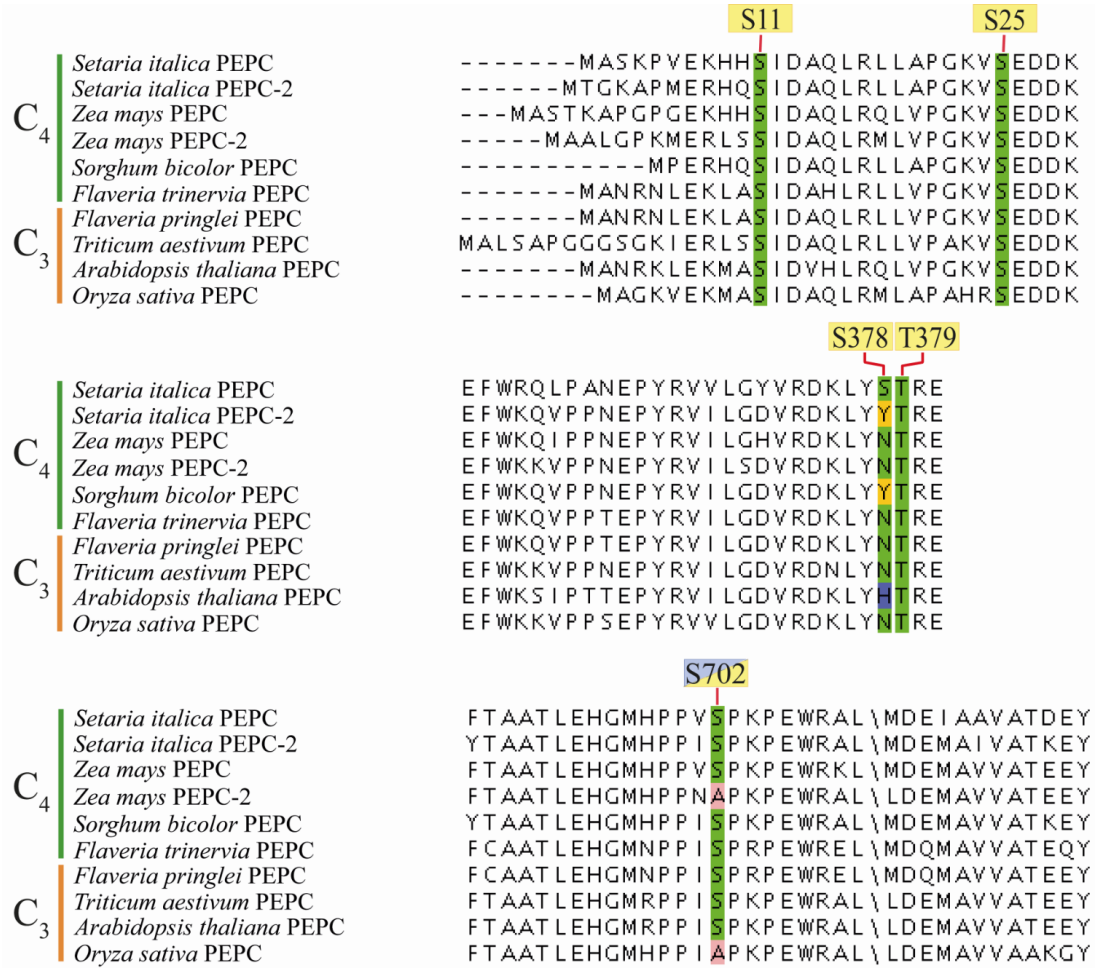

Fig. 3.28. Alignment of PEPCs from C4 and C3 plants. PEPC and PEPC-2 (housekeeping enzyme) are aligned and the phosphorylation sites identified in *Setaria viridis* are shown. Phosphorylations identified in illuminated leaves highlighted yellow and phosphorylations found in both light and dark highlighted in blue and yellow. Similar residues highlighted green.

Ser-11 is conserved in major C_4 and C_3 plants (Figure 3.28) and it may have similar regulatory properties in *Setaria viridis* as it does in closely related C_4 plants. In addition, Ser-11 may be a substrate for PEPC kinase. The non-photosynthetic PEPC in C_3 plants undergoes regulatory phosphorylation *in vitro* and *in vivo* by the light- and Ca^{2+}-dependent PEPC kinase at the invariant *N*-terminal serine (Wang and Chollet, 1993; Duff and Chollet, 1995; Li *et al.*, 1996; Zhang and Chollet, 1997), which suggests that these regulatory mechanisms are conserved in plant species, but whether these regulatory mechanisms extend to other highly conserved residues like Ser-25 or Thr-379 is unknown. The position of conserved positively charged lysine and arginine residues around putative phosphorylation sites could also act as recognition binding sites for PEPC kinase (Ueno *et al.*, 1997).

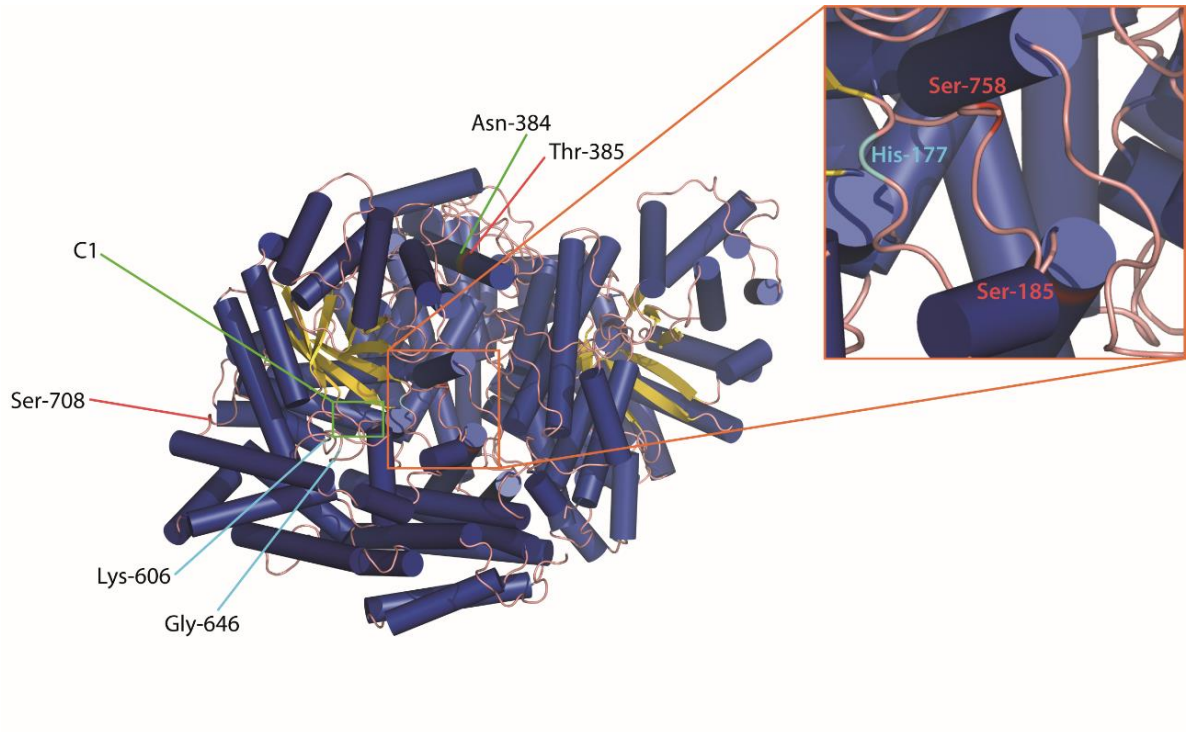

Fig. 3.29. *Zea mays* PEPC annotated with phosphorylation identified in *Setaria viridis*. Annotated residues (red markings) correspond to the phosphorylated sites identified in *Setaria viridis*. C1 indicates the region important for catalysis and PEP binding. Cyan lines and markers indicate active sites. Green line indicates the phosphorylated Ser-378 residue in *Setaria viridis*, which corresponds to Asn-384 in *Zea mays*. Blue tubes are alpha helices and yellow arrows show beta sheets. Protein structure taken from Matsumura *et al.* (2002).

Using the PEPC structure from *Zea mays*, the positions of the identified phosphorylated residues were determined (Figure 3.29). Using this model, residues Asn-384, Thr-385 and Ser-708 (corresponding to Ser-378, Thr-379 and Ser-702 in *Setaria viridis*), are exposed and could be readily phosphorylated by kinases, whereas residues Ser-185 and Ser-758 (corresponding to Ser-180 and Ser-752 in *Setaria viridis*) are less accessible. In *Arabidopsis thaliana*, phosphorylation of the C_3-form PEPC occurs at Ser-704 (de la Fuente van Bentem *et al.*, 2008), which corresponds to Ser-702 in *Setaria viridis*, but this residue is not known to be phosphorylated in C_4 species, and could be a determinant for C_4-specific PEPC function as previously found for Ser-774 in *Flaveria species* (Bläsing *et al.*, 2000; Jacobs *et al.*, 2008).

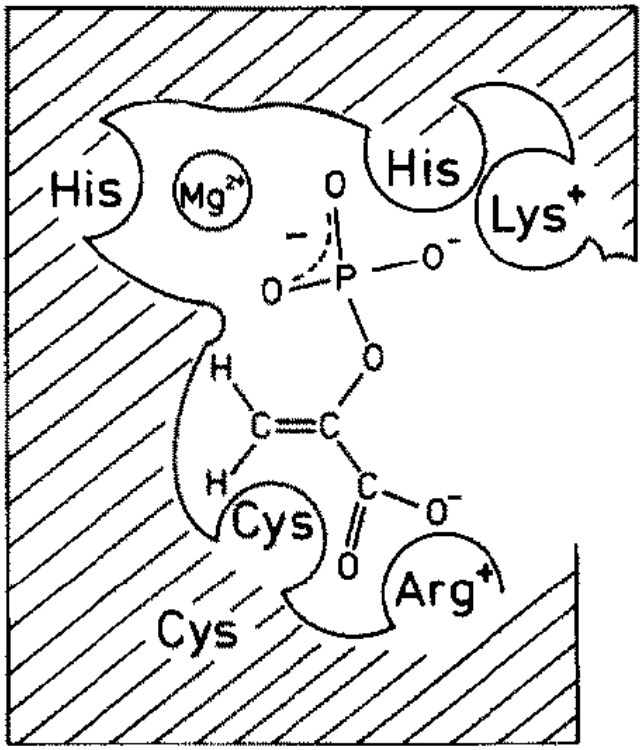

Fig. 3.30. Schematic model showing the active site of PEPC in higher plants. The phosphate and carboxylate of PEP interacts with positively charged lysine (Lys) and arginine (Arg) residues. Active site in *Setaria viridis* at His-172. Figure taken from Andreo *et al.* (1987).

More importantly, Ser-752 is conserved in all PEPCs and is near the active site at His-177 in *Zea mays* or His-172 in *Setaria viridis*, suggesting phosphorylation could have direct interaction with the carboxylation reaction (Kai *et al.*, 2003). Furthermore, the cavity between His-177 and Arg-647, shown as C1 in Figure 3.29, allows for movement of PEP during catalysis (Andreo *et al.*, 1987; Matsumura *et al.*, 2002). It is therefore possible that the negative charge from a nearby phosphorylated residue (Ser-752) may counteract the positive charge of Arg-647 or Lys-606 (Andreo *et al.*, 1987; Scheeff *et al.*, 2009). Moreover, the phosphorylation of Ser-752 was only identified in darkened leaves. Phosphorylation at Ser-752 could influence the way that PEP interacts with the catalytic site. A phosphate interacting with the positively charged lysine and arginine residues at the catalytic site might also alter the shape of the catalytic pocket and hinder the entrance of Mg^{2+} and PEP into the active site or disrupt the interaction with histidine and cysteine residues, as shown in Figure 3.30. This, together with the identification solely in the dark period, suggests that phosphorylation at Ser-752 might correlate with PEPC inactivation in darkened leaves and regulate PEP binding during the dark period. This region of PEPC may also contribute to C_4-specific function and contain regulatory properties (Bläsing *et al.*, 2000).

Additionally, the side chain of Ser-185 in *Zea mays* (Ser-180 in *Setaria viridis*) may interact with the side chains of Arg-182, Arg-183, Arg-231 and Arg-372 during the allosteric binding of glucose-6-phosphate (Bläsing *et al.*, 2000; Matsumura *et al.*, 2002; Kai *et al.*, 2003). If Ser-185 (*Zea mays* numbering) is phosphorylated, the negative charge of the phosphate group could repel the phosphate from glucose-6-phosphate, thus affecting its binding to PEPC. Ser-180 is also conserved in all C_3 and C_4 PEPCs and in *Setaria viridis*, Ser-180 was phosphorylated in darkened and illuminated leaves. It is therefore possible that phosphorylation at Ser-180 is a necessary structural component to regulate activator binding, rather than prevent or promote binding at one specific time-point.

3.3.3 Phosphorylation of pyruvate, phosphate dikinase

Unlike PEPC, the regulatory phosphorylation of PPDK at Thr-462 in *Setaria viridis* occurred in both darkened and illuminated leaves, as evident from phosphoprotein stained gels (Figure 3.9 and Figure 3.10). In the phosphoprotein stained 1D gel (Figure 3.9), the PPDK band intensity from darkened leaves appeared to be greater than PPDK from illuminated leaves. This was confirmed by relative quantitation of Thr-462, which showed that the phosphopeptide was in higher amounts in darkened leaves. Unlike PEPC, there is little indication whether the content of PPDK varied between darkened and illuminated conditions, but 2D gels (Figure 3.10) suggest that there was a higher PPDK content per 80 µg of total protein in darkened leaves than in illuminated leaves. The phosphorylation of Thr-462 in darkened leaves is consistent with the regulatory site previously identified in *Zea mays* (Ashton and Hatch, 1983; Chastain *et al.*, 2000; Chastain and Chollet, 2003; Chen *et al.*, 2014). Moreover, the higher degree of phosphorylation at Thr-462 in darkened leaves is consistent with the inactivation mechanism by phosphorylation (Budde *et al.*, 1985).

The phosphorylation of Ser-463 was also identified in darkened leaves of *Setaria viridis* (Figure 3.6), but with a lower localisation probability ($P = 0.78$) when compared to the phosphorylation at Thr-462 ($P = 0.99$). Additionally, the phosphorylation at Ser-463 was also identified in *Megathyrsus maximus* ($P = 0.50$) in illuminated leaves. However, despite Ser-463 being less accessible for phosphorylation, it is possible that Ser-463 in *Setaria viridis*, like in leaves of *Zea mays*, might be a substrate for PPDK-RP (Chen *et al.*, 2014). In a previous study, the phosphoserine was identified in both active and inactive preparations of PPDK, while the phosphothreonine was only present in the inactive PPDK and although Chen *et al.* (2014) identified Ser-528 as a substrate for PPDK-RP, the phosphorylation at Ser-463 in *Setaria viridis* may be the result of a non-enzymatic, nitrogen to oxygen phosphoryl migration (Plapinger and Wagner-Jauregg, 1953; Rathlev and Rosenberg, 1956; Budde *et al.*, 1985).

Fig. 3.31. Alignment of PPDKs from C_4 and C_3 plants. Phosphorylation sites identified in *Setaria viridis* are indicated. Phosphorylations identified in illuminated leaves highlighted yellow and those found in darkened leaves highlighted blue. Phosphorylations found in both light and dark highlighted in blue and yellow. Similar residues highlighted green. Substrate binding sites highlighted in purple. His-364 (*Setaria italica* numbering) is the active site. Green triangle represents phosphorylation of Ser-528 identified in *Zea mays*.

Thr-704, Thr-721 and Thr-753 are conserved across C_4 and C_3 plants (Figure 3.31), however there is no indication that these residues are phosphorylated. Moreover, the proximity of Thr-753 to the metal binding site (Glu-756) could affect binding mechanisms. Of the phosphorylation sites identified, Thr-462, Thr-557 and Thr-753 are close to the catalytic site of PPDK and may influence catalytic properties (Figure 3.32). Thr-593, Thr-721, Thr-704 and possibly Ser-394 are exposed to the surface of the protein and may be targets for phosphorylation. However, whether any of these putative sites are regulated cannot be determined from these data.

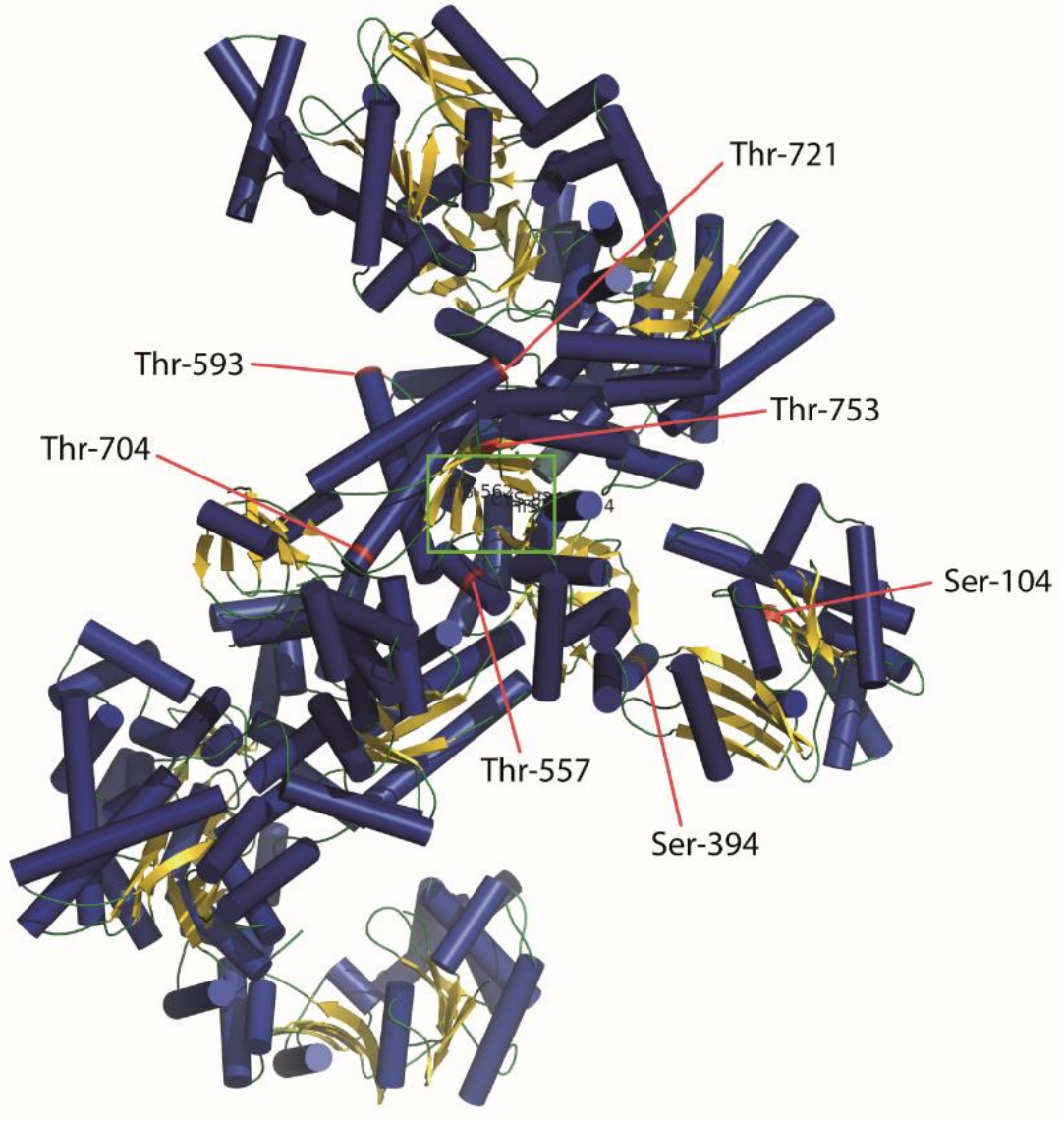

Fig. 3.32. Structure of PPDK from *Flaveria trinervia* reveals the position of phosphorylation sites (in red) identified in *Setaria viridis*. Green rectangle indicates the main catalytic domain of PPDK, including the position of the catalytic site at His-464 and Cys-842 (not labelled). Blue tubes are alpha helices and yellow arrows show beta sheets. PPDK structure taken from Minges *et al.* (2017).

In the crystal structure of the C_4 PPDK, the phosphorylation at Thr-753 may directly affect catalysis by interacting with the PEP binding site, which is indicated by the green rectangle on Figure 3.32. In addition, the phosphorylation at Thr-753 was only detected in illuminated leaves and might hinder PEP binding, thus limiting the reverse reaction towards the formation of pyruvate. This could regulate selectivity towards pyruvate binding and not PEP binding during illumination, when PPDK is needed to regenerate PEP. Furthermore, in *Zea mays*, binding of PEP during phosphate transfer results in a swivelling-domain motion at the *C*-terminal active site (Nakanishi *et al.*, 2005). During

this motion, PEP interacts with surrounding residues and may be easily be influenced by proximal negatively charged moieties (Minges *et al.*, 2017). The phosphorylation at Thr-557 could also influence the binding interaction between PEP and PPDK, but Thr-557 is not as close to the catalytic site as Thr-753.

3.3.4 Phosphorylation of NADP-malic enzyme

The regulatory phosphorylation of NADP-malic enzyme has not been described in plants, but phosphorylation has been described in mice (*Mus musculus*) (Huttlin *et al.*, 2010). In this study, 20 putative phosphorylation sites were identified. Although four isoforms were identified, protein K3XG11 was 53-times more abundant in darkened leaves than protein K3XFW4 and six-times more abundant than K3ZRI5 (Table 3.5). However, only two phosphorylation sites were identified on the most abundant protein isoform (Figure 3.17). The phosphorylation at Ser-373 had been previously identified in *Zea mays* using a similar proteomic approach (I. Abreu, personal communication). Ser-343 is conserved in three isoforms in *Setaria viridis* (Figure 3.33). Aside from NAD-malic enzyme from *Zea mays* and *Arabidopsis thaliana*, this serine residue is conserved in both NAD- and NADP-malic enzyme of C_3 and C_4 origin (Figure 3.33). Not all the phosphorylation sites were identified on every protein isoform detected in *Setaria viridis* leaf lysates (Figure 3.34). However, because of high sequence homology, it is possible that some phosphopeptides were inferred from different isoforms when in fact they were only from a single isoform. Based on sequence similarity to the main NADP-malic enzyme isoform from *Zea mays* and molecular masses, proteins K3XFH6 and K3XG11 might be the primary NADP-malic enzyme isoforms in *Setaria viridis* and correspond to the two major C_4-specific isoforms previously identified in *Zea mays* (Maurino *et al.*, 1996).

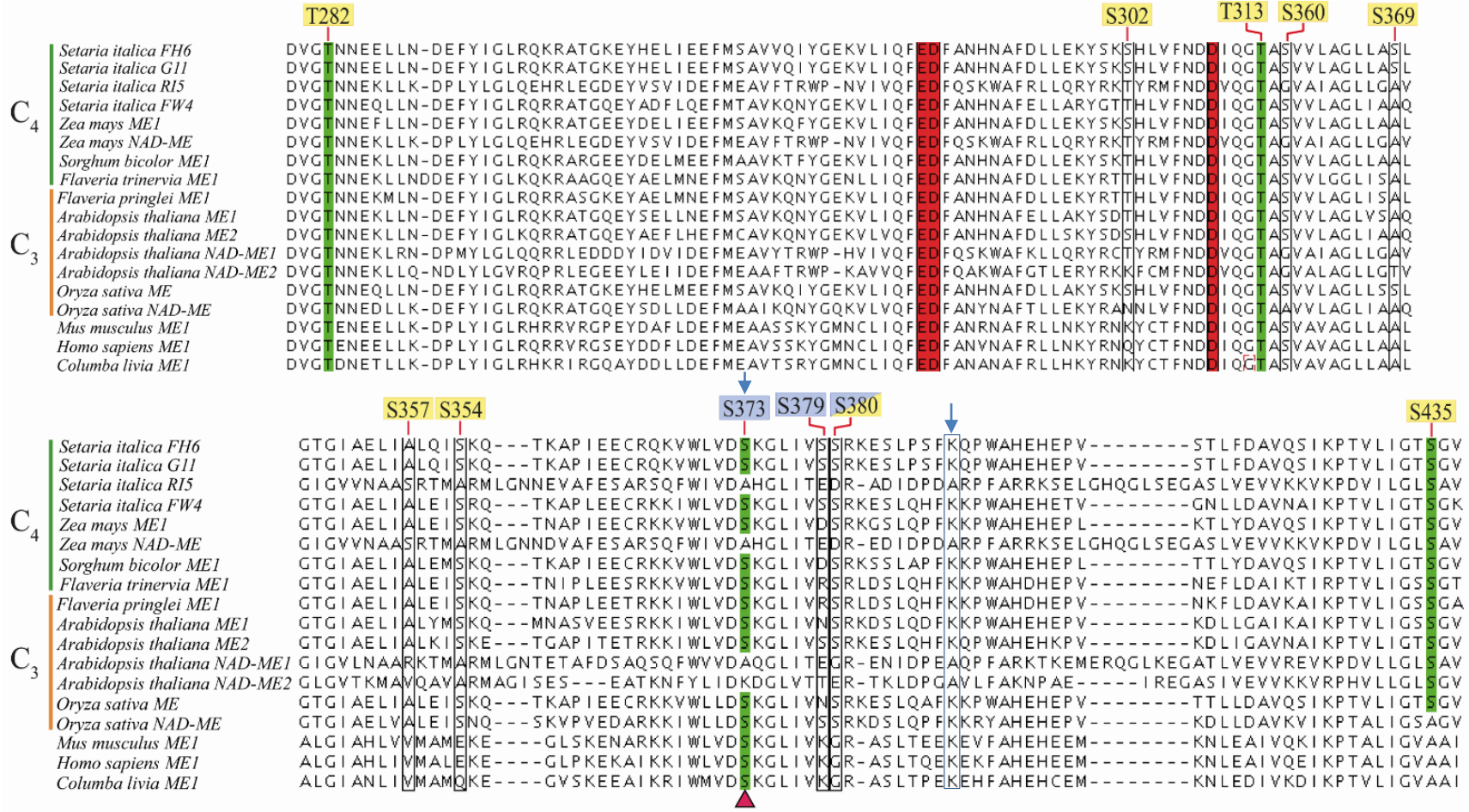

Fig. 3.33. Alignment of NAD- and NADP-malic enzymes across plant (C_4 and C_3), mammalian and avian origins. Putative phosphorylation sites identified in illuminated leaves highlighted yellow and those found in darkened leaves highlighted blue. Phosphorylations found in both light and dark highlighted in blue and yellow. Highly conserved residues highlighted green. Metal binding sites highlighted in red. Red triangle indicates phosphoserine-336 identified in *Mus musculus* and Ser-346 in *Columba livia* (discussed below). Blue arrows indicate $NADP^+$ interaction sites.

In mice (*Mus musculus*), NADP-malic enzyme is phosphorylated at Ser-336 (Ser-373 in *Setaria italica* numbering), though its phosphoregulatory properties have not been described (Huttlin *et al.*, 2010). In addition, studies have suggested that Asp-335 is selective towards NAD^+ co-factor binding rather than $NADP^+$, because the negative charge of aspartate repels the negative charge of 2′-phosphate of $NADP^+$ (Wierenga *et al.*, 1986; Scrutton *et al.*, 1990; Yang *et al.*, 2002). Although it was shown that this interaction may not occur since Asp-335 interacts with Arg-354, the presence of phosphate groups from nearby phosphorylated residues may confer some disadvantages to $NADP^+$ binding. Therefore, the phosphorylation at Ser-373 might conflict with $NADP^+$ binding since the 2′-phosphate might interact with the phosphoserine-373 as has been shown in the cytosolic-form of NADP-malic enzyme from pigeon (*Columba livia*) (Yang *et al.*, 2002). The phosphorylation at Ser-373, which only occurred in darkened leaves, may be part of a mechanism to reduce the activity of NADP-malic enzyme during the dark period when CO_2 fixation is not required. The phosphorylation of Ser-379 and Ser-380 on the same phosphopeptide from protein K3XFW4 may cause additional charge differences and disrupt $NADP^+$ binding (Figure 3.34). In addition to this, one protein isoform identified in *Setaria viridis* (K3ZRI5) and NAD-malic enzyme from *Zea* mays and *Arabidopsis thaliana* have an alanine residue instead of serine in position 373, which cannot undergo phosphorylation. This substitution might also indicate preference towards NAD^+ binding in the NAD-malic enzyme from *Zea mays* and *Arabidopsis thaliana*. This assumption would also indicate that the identified malic enzyme in *Setaria viridis* (K3ZRI5) might be NAD- rather than NADP-dependent, but despite inferred to be NAD^+-dependent on the UniProt protein database, there is no other evidence to verify this. In addition to Ser-346 (pigeon numbering), $NADP^+$ interaction with the side-chain ammonium group of Lys-362 is essential for NADP-dependent enzymatic activity (Yang *et al.*, 2002). It was previously shown that the pigeon NADP-malic enzyme with a lysine to alanine substitution at position 362 (K362A) drastically decreased the affinity for $NADP^+$ (Kuo *et al.*, 2000). All the proteins that do not have a serine at the first $NADP^+$ binding site, indicated above Ser-373 by the blue arrow on Figure 3.33, have an alanine at the second $NADP^+$ binding site. Since Lys-362 serves an important role in determining $NADP^+$ selectivity in NADP-malic enzyme from pigeon (Yang *et al.*, 2002), plant proteins lacking the lysine residue at this position may have preference for NAD^+ binding instead. Both residues at these positions may be determinants for NAD-specific malic enzyme activity.

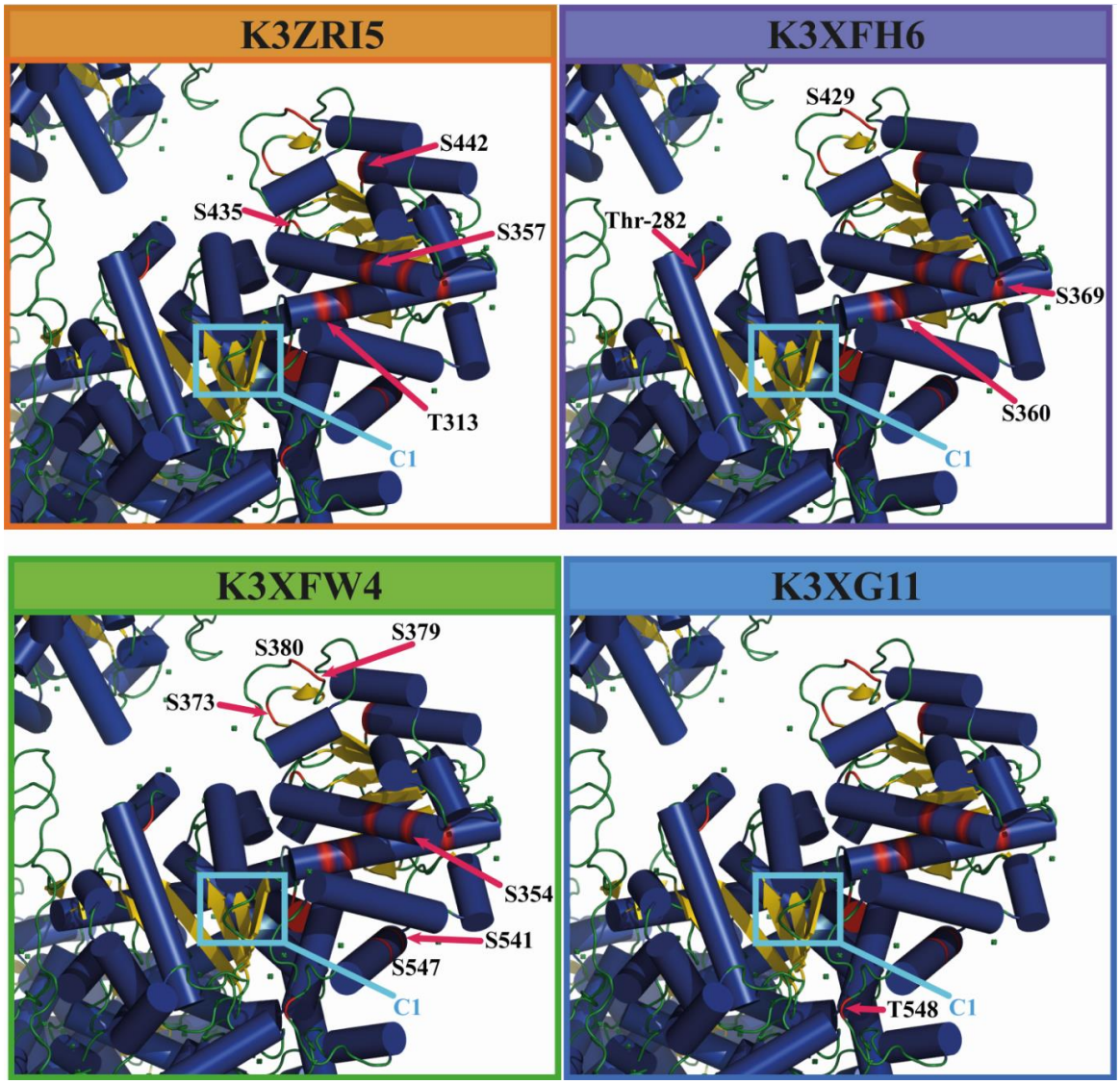

Fig. 3.34. Position of phosphorylation sites identified in *Setaria viridis*. Cyan rectangle (C1) indicates the catalytic centre of NADP-malic enzyme. Blue tubes are alpha helices and yellow arrows show beta sheets. Phosphorylation sites (*Setaria italica* numbering) are highlighted red on the protein. The labelled residues are the phosphorylation sites identified on each protein isoform. Only Ser-429 (K3XFH6) and Ser-380 (K3XFW4) occur on both proteins. Protein model based on the pigeon cytosolic NADP-malic enzyme taken from Yang *et al.* (2002).

The position of Ser-373, Ser-379 and Ser-380, shown in Figure 3.34, further demonstrates show this cluster of phosphorylations could be affecting $NADP^+$ binding during the dark period. The phosphorylation at Ser-379 and Ser-380 could potential cause a charge repulsion with $NADP^+$ as it interacts with Ser-373 during catalysis. Although not shown in Figure 3.34, the phosphorylations at Ser-302, Thr-313 and Ser-360 might disrupt binding of the metal ion at the aspartate binding site (Figure 3.33). These

phosphorylation sites are the first indication of a phosphoregulatory mechanism of the C_4-specific NADP-malic enzyme from *Setaria viridis*. Recent research using a recombinant NADP-malic enzyme from *Zea mays*, suggests that NADP-malic enzyme is inactivated by phosphorylation in the dark period (V.G. Maurino, personal communication). In *Setaria viridis*, Ser-373, which corresponds to Ser-419 in *Zea mays*, is possibly the most likely target for regulatory phosphorylation because of its role in the $NADP^+$ binding mechanism (Kuo *et al.*, 2000; Yang *et al.*, 2002) and previous identification in mice (Huttlin *et al.*, 2010). However, validation of this phosphorylation in *Setaria viridis* or identification in *Sorghum bicolor* has been unsuccessful. The recovery of the NADP-malic enzyme containing the phosphorylation at Ser-373 was very low, relative to the other isoforms identified (Table 3.5). However, the relative abundance coefficient (iBAQ) does not accurately quantify all isoforms expressed *in vivo* and is rather an approximation. Increasing the recovery of phosphopeptides of protein K3XFW4 may be the first step in future studies for validating the phosphorylation at Ser-373 in *Setaria viridis*.

3.3.5 Phosphorylation of aspartate and alanine aminotransferase

Three phosphorylation sites were solely identified in aspartate aminotransferase from illuminated leaves of *Setaria viridis* (Figure 3.35A), which could be regulating activity during the photoperiod. Aspartate aminotransferase is phosphorylated at Ser-49 and Ser-149 in rat (*Rattus norvegicus*) (Lundby *et al.*, 2012), though these serine residues are not completely conserved in plant species. *Setaria italica* aspartate aminotransferase (K3YSB2) could potentially be phosphorylated at Ser-73 (corresponding to Ser-149 in rat), but there is no evidence of this phosphorylation. Ser-300 and Ser-341 from protein K3YSB2 are highly conserved in both C_3 and C_4 species and could be potential targets for regulatory phosphorylation, while amino acid substitutions at these positions could indicate specific isoform activity (Figure 3.35A). In C_4 plants there are at least two major aspartate aminotransferase isoforms, compared to three that were identified in *Arabidopsis thaliana* (Numazawa *et al.*, 1989; Wilkie and Warren, 1998). Having identified four isoforms in *Setaria viridis*, it is difficult to ascertain which ones have C_4-specific function. In addition, there could be differences in the regulatory properties

between the aspartate aminotransferase isoform localised in the chloroplasts and mitochondria (Hatch and Mau, 1973; Meister *et al.*, 1996), which cannot be ascertained using whole leaf protein extracts.

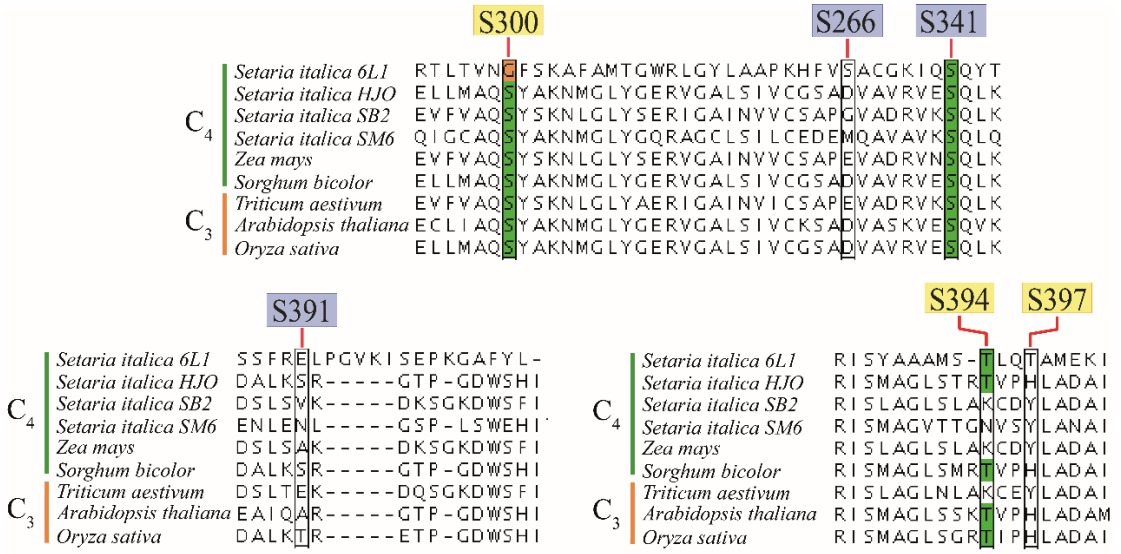

Fig. 3.35A. Alignment of aspartate aminotransferases from C4 and C3 plants. Putative phosphorylation sites identified in illuminated leaves highlighted yellow and those found in darkened leaves highlighted blue. Highly conserved residues highlighted green.

Conversely, alanine aminotransferase was predominantly phosphorylated after illumination Figure 3.35B). If the degree of phosphorylation (total number of phosphorylation sites identified) were important for enzyme activity, then it would suggest that the phosphorylation mechanisms are different for alanine and aspartate aminotransferase. While it appeared that Thr-167, Ser-189 and Ser-206 are not light-dependent, because they were present in both darkened and illuminated leaves, phosphorylation at these residues could contribute to enzymatic activity or stability. Unlike that phosphorylation sites identified in aspartate aminotransferase, those identified in alanine aminotransferase are highly conserved in *Zea mays* and C_3 species, except for Ser-326 (Figure 3.35B). Whether the cysteine residue in position 326 (K3ZSX0 numbering) contributes to additional regulatory mechanisms, such as redox regulation, is unknown. Despite catalysing the amino transfer in two similar reactions, protein sequences between the aspartate and alanine aminotransferase are very dissimilar, probably due to high specificity for either aspartate or alanine, respectively (Ashton *et al.*, 1990; Duff *et al.*, 2012). Moreover, the optimal activity of aspartate and alanine aminotransferase might directly be associated with upstream enzymes like PEPC

or NADP-malic enzyme, respectively (Andrews *et al.*, 1971; Hatch and Mau, 1973). In addition to this, alanine aminotransferase is not associated with chloroplasts (Meister *et al.*, 1996) and the regulatory properties of the identified isoforms might be more similar as opposed to the aspartate aminotransferase isoforms, which may be differently compartmentalised.

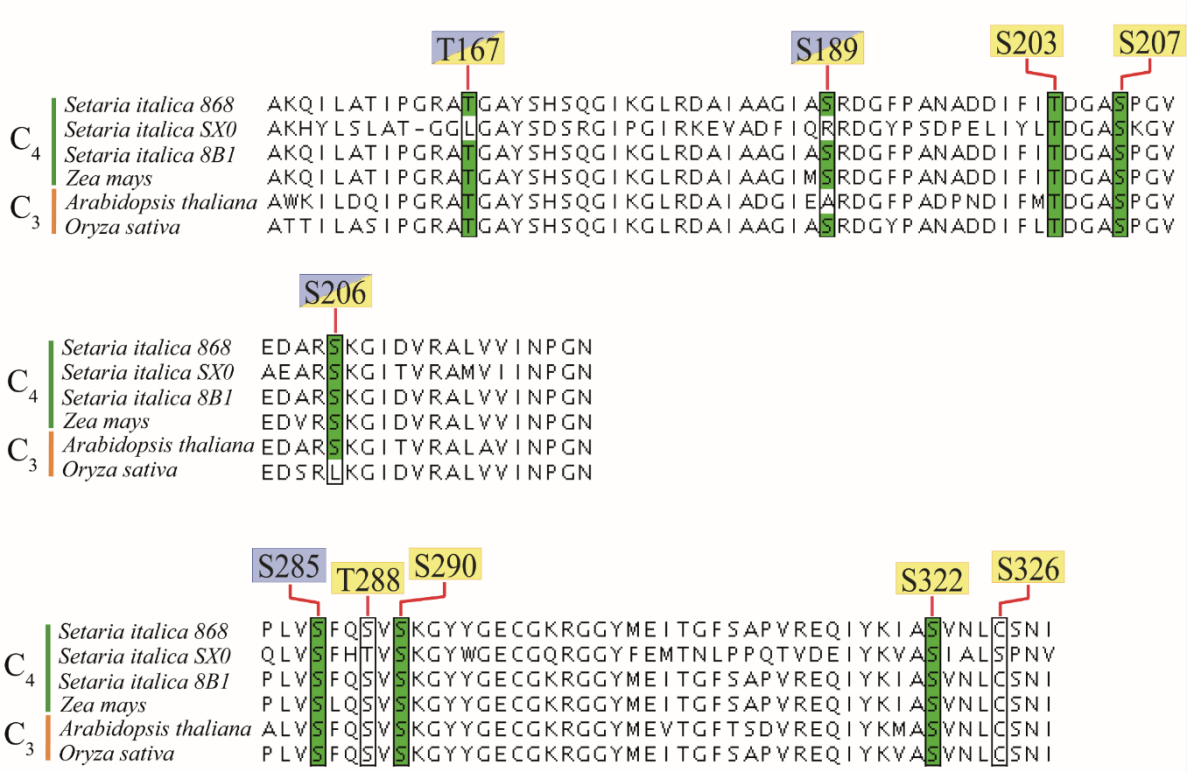

Fig. 3.35B. Alignment of alanine aminotransferases from C_4 and C_3 plants. Putative phosphorylation sites identified in illuminated leaves highlighted yellow and those found in darkened leaves highlighted blue. Phosphorylations found in both light and dark highlighted in blue and yellow. Highly conserved residues highlighted green.

The activities of major aspartate and alanine aminotransferase isoforms in C_4 plants are higher in dark-grown plants, while minor isoforms differ very little in activity between darkened and illuminated conditions (Hatch and Mau, 1973). However, from the phosphorylation data, it is not possible to ascertain whether the changes to the degree of phosphorylation in darkened and illuminated conditions might be regulating the activity of aspartate or alanine aminotransferase. In an early study on the activity of aspartate and aminotransferase in C_4 plants, Hatch and Mau (1973) suggest that the aminotransferases evolved C_4-specific function, possibly after the C_4 cycle was fully established. Also, the activity of these enzymes is linked to decarboxylation by PEPCK in bundle sheath cells or NAD-malic enzyme in mitochondria in bundle sheath cells, and not with C_4 subtypes

that predominantly use NADP-malic enzyme (Andrews *et al.*, 1971; Huber and Edwards, 1975; Chapman and Hatch, 1981; Meister *et al.*, 1996). Therefore, it is possible that aspartate aminotransferase activity evolved together with downstream PEPCK activity and the phosphoregulatory mechanisms that evolved with PEPCK could have been adapted to regulate the activity of aspartate aminotransferase (Gowik and Westhoff, 2011). PEPCK, unlike PEPC, is inactivated by the degree of phosphorylation in dark-grown plants (Bailey *et al.*, 2007). Alternatively, regulatory elements could have evolved along with the regulatory phosphorylation of PEPC activation, as aspartate aminotransferase could have evolved C_4-specific activity in order to increase the options for carbon flux during high rates of carboxylation by PEPC (Bräutigam *et al.*, 2014; Wang *et al.*, 2014).

3.3.6 Phosphorylation of enolase and phosphoglycerate mutase

Although not directly associated with the C_4 pathway, the activity of phosphoglycerate mutase and enolase in leaves of C_4 plants, particularly in *Zea mays*, has been considered to contribute for the supply of 3-PGA and PEP (Huber and Edwards, 1975; Furbank and Leegood, 1984). However, the rate at which this interconversion occurs and how it may be regulated is unknown (Arrivault *et al.*, 2016). In this study, novel light-dependent phosphorylation sites identified in enolase and phosphoglycerate mutase from *Setaria viridis* suggest that the formation of PEP through enolase and phosphoglycerate mutase is regulated. In yeast (*Saccharomyces cerevisiae*), enolase undergoes phosphorylation at Ser-10 (Pearlman *et al.*, 2011), but this residue is not conserved in plants (Figure 3.36).

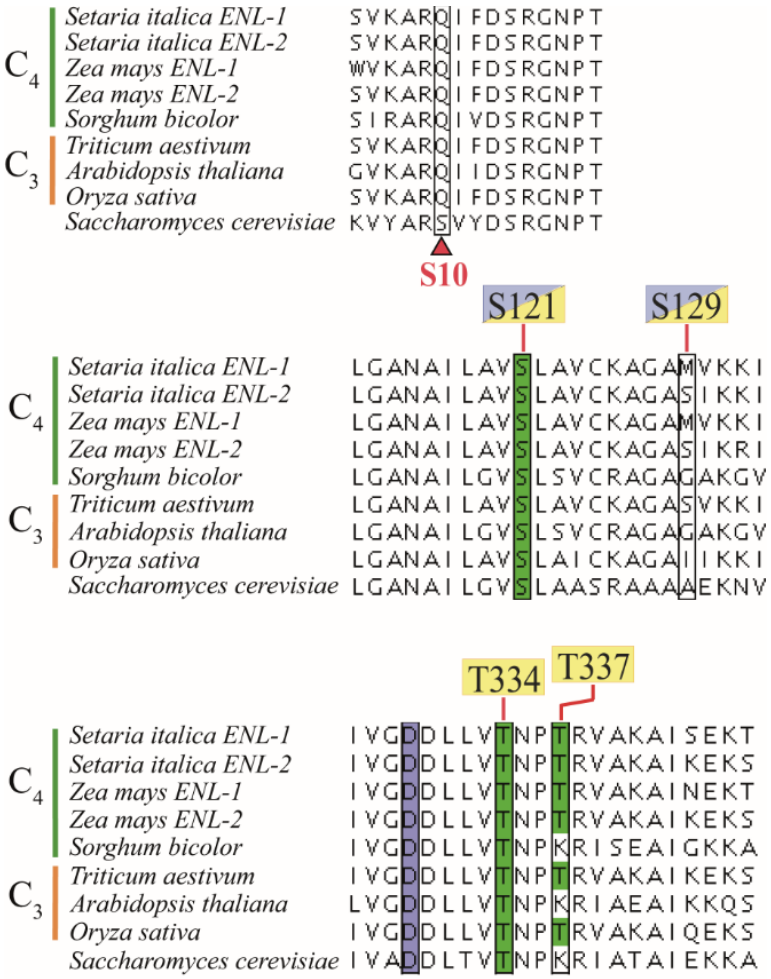

Fig. 3.36. Alignment of enolase (ENL) protein sequences. Novel phosphorylation sites indicated in yellow (occurring in light) and yellow and blue (occurring in light and dark). Substrate binding site in purple. Red triangle shows phosphoserine in yeast.

Enolase catalyses the interconversion of 2-PGA and PEP (Zhang *et al.*, 1997) and its activity might provide an alternative route for the formation of PEP. The phosphorylation at Ser-129 occurred only in enolase-2 in *Setaria viridis*, though enolase-2 from *Zea mays* and *Triticum aestivum* could potentially be phosphorylated (Figure 3.36). This might be indicative of a specific mechanism regulating the activity of enolase-2 in *Setaria viridis*. In addition, despite Thr-334 and Thr-337 being conserved in enolase-1 and enolase-2, only enolase-1 underwent phosphorylation in illuminated leaves in *Setaria viridis*. Because of the proximity to the binding site (Asp-329) and active site (Lys-354), phosphorylation at these two residues might hinder substrate binding by charge repulsion with the phosphate of 2-PG or PEP.

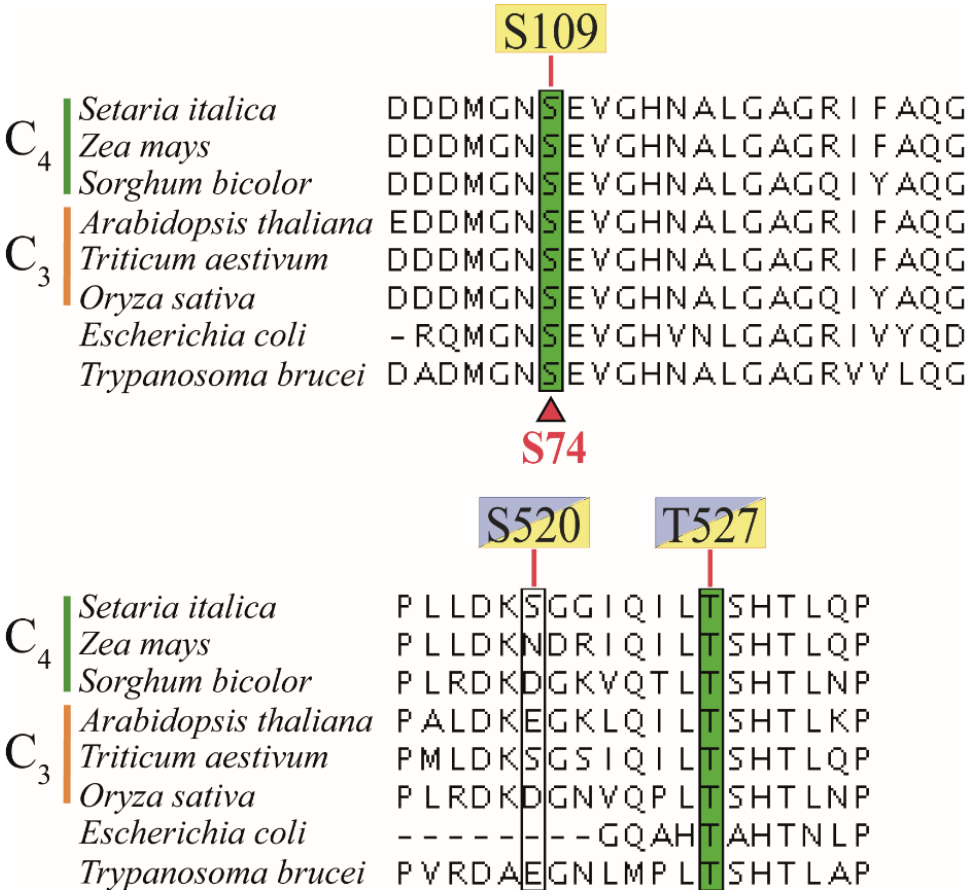

Fig. 3.37. Alignment of phosphoglycerate mutase protein sequences. Novel phosphorylation sites indicated in yellow (occurring in light) and yellow and blue (occurring in light and dark). Red triangle shows phosphoserine-74 in *Trypanosoma brucei*.

Phosphoglycerate mutase catalyses the interconversion of 2-PGA and 3-PGA and might serve as a direct link with the activity of enolase and formation of PEP (Huber and Edwards, 1975). While Ser-520 and Thr-527 were only identified in *Setaria viridis*, the phosphorylation at Ser-109 was detected in illuminated and darkened leaves of *Setaria viridis* (Table 3.4B, 3.6), *Sorghum bicolor* (Table 3.7) and *Megathyrsus maximus* (Table 3.8), suggesting that it serves an important role in the catalytic mechanism. In fact, this residue is important for catalysis and exists as a phosphointermediate in several non-plant species (Collet *et al.*, 2001; Jedrzejas and Setlow, 2001; Potters *et al.*, 2003; Rigden *et al.*, 2003). Based on sequence homology, it is possible that the phosphorylation site identified in this study might be part of the reaction mechanism rather than a phosphoregulatory site.

In *Trypanosoma brucei*, phosphoglycerate mutase undergoes phosphorylation at Ser-74 and because of the low rates of formation and disappearance during the reaction, the phosphoserine is produced as an intermediate of the phosphatase reaction when phosphate is removed from either 2-PGA or 3-PGA (Jedrzejas *et al.*, 2000; Collet *et al.*, 2001). Despite being distant to plants, it has been suggested that trypanosomes retain several plant-like genes, most of which are involved in central metabolism and at some point, in their evolutionary past, trypanosomes contained chloroplasts (Hannaert *et al.*, 2003; Martin and Borst, 2003). However, sequence similarity between plant and *Trypanosoma brucei* phosphoglycerate mutase (Figure 3.37) does not necessarily imply that the phosphoregulatory elements in the protozoa are retained in plant species. Due to the high reproducibility of Ser-109 across three of the investigated C_4 plants, the phosphorylation at Ser-109 might be a phosphointermediate or at least an important residue essential for catalysis. It would be interesting to investigate whether the replacement of serine to alanine would affect the catalytic properties of phosphoglycerate mutase in plants, as previously investigated in *Bacillus stearothermophilus*, which drastically reduced enzyme activity (Jedrzejas *et al.*, 2000; Jedrzejas and Setlow, 2001).

3.3.7 Quantitative proteomics and future study

In this study, several novel phosphorylation sites were identified on key C_4-related proteins, suggesting that multiple sites, in addition to those already identified, might regulate enzymatic activity. However, it is unlikely that all phosphorylation sites identified are under regulation. To ascertain the sites that are under regulation, the degree of phosphorylation and how it changes during dark to light transitions requires further investigation. This can be done by either quantifying the signal intensity of phosphoprotein stained gels or using quantitative proteomics. One method commonly used to quantify peptides by mass spectrometry is using stable isotope labelling by amino acids in cell culture (SILAC) in conjunction with immunoprecipitation (Zhang and Neubert, 2009; Matthes *et al.*, 2014), however, the incorporation of heavy amino acids into proteins has only recently been optimised for *Arabidopsis thaliana* seeds and may not be compatible with seeds of other plant species (Lewandowska *et al.*, 2013). An alternative to metabolic labelling is using isobaric tags for relative and absolute

quantitation (iTRAQ), whereby peptides are chemically tagged *in vitro* (Wiese *et al.*, 2007), however is not as reproducible as SILAC (Zhang and Neubert, 2009).

Having identified putative phosphopeptides, selected reaction monitoring (SRM) is more applicable for quantifying phosphorylation than using metabolic labelling. In complex mixtures, particularly in untargeted approaches, the analysis of proteins of interest can be overwhelmed by more abundant proteins, resulting in poor consistency in fragmentation spectra and detection of the associated peptides of interest (Lange *et al.*, 2008). In SRM, the peptide of interest can be selected by defining a search range given its corresponding *m*/*z* value, thus the elution of ions can be monitored in the run and interfering ions, which are out of the pre-defined monitoring range, can be filtered out (Lange *et al.*, 2008). These analyses are performed using triple quadrupole mass spectrometers, which can monitor the precursor ion and fragment ion of a given peptide over time (Williamson *et al.*, 2006), however, unlike tandem mass spectrometers, SRM-capable mass spectrometers utilise a non-scanning approach, which by not recording all fragmentation spectra detected, the targeted peptide can be preferentially observed (Lange *et al.*, 2008). This allows for the selection of ions of interest in a complex mixture, which can then be accurately quantified. However, for SRM to be effective for PTM identification and quantification, the *m*/*z* value of the peptide must be known.

It is possible that there are additional phosphorylation sites that have not been identified in this study due to the loss of peptides of interest during analysis or low amount of phosphopeptides due to suboptimal concentration of proteins from the leaf lysate. One method to increase the concentration of phosphopeptides is by preparing peptides using a gel-free approach. However, the heterogeneity of the protein suspension and nature of globular proteins in their native three-dimensional state makes it difficult to guarantee that the trypsin-mediated proteolysis has been equally applied to every protein in the sample (Zhang *et al.*, 2013). Also, despite trypsin is widely used, the dynamic mechanism of proteolytic digestion does not guarantee complete coverage of the protein sequence and peptides are readily lost during analysis (McLachlin and Chait, 2001), making it difficult to map all modifications on the protein of interest. To overcome this, intact proteins can be analysed, thereby reducing the loss of peptides of interest. However, fragmentation efficiencies of intact proteins are lower than that of peptides, compromising on the fragment ion spectra needed for subsequent mass spectrometry analysis and determination of site-specific modifications (Moradian *et al.*, 2014). In

addition to this, fractionating intact proteins by SDS-PAGE is hindered by reduced compatibility with non-volatile buffers required for the extraction from the polyacrylamide matrix (Garcia, 2010; Zhang *et al.*, 2013). Intact proteins can also be enriched using phosphoprotein enrichment, however, the binding interaction between an intact, folded phosphoprotein and resin particle in the enrichment column is difficult to predict, thus making phosphoprotein enrichment less reliable than phosphopeptide enrichment (Fíla and Honys, 2012). Alternatively, larger polypeptides, instead of intact proteins, can be analysed using size-dependent peptide fractionation. In this method, proteins are partially digested to form large polypeptide fragments, which are then selectively fractionated by size (Garcia, 2010). However, this approach is not optimised for large-scale phosphoproteomic studies (Zhang *et al.*, 2013). Despite being several methods to overcome the difficulties of phosphoproteomics, contaminant peptides from human proteins, co-migrating proteins or from the autolysis of trypsin can still pose challenges (Seo and Lee, 2004).

3.3.8 Conclusion

It was hypothesised that C_4-related proteins in *Setaria viridis* undergo light-dependent phosphorylation similar to the mechanisms elucidated for PEPC and PPDK in *Zea mays*. The findings in this chapter verified that the PEPC and PPDK undergo light-dependent phosphorylation at the conversed residues as in *Zea mays*, and that the degree for phosphorylation of PPDK increased after the transition into darkness, as previously observed (Chao *et al.*, 2014). In addition, several other C_4-related enzymes such as NADP-malic enzyme, were phosphorylated, supporting the hypothesis that phosphoregulatory mechanisms might regulate the activity of other key C_4-related proteins. While the exact effect of these modifications cannot be ascertained from this data alone, structural evidence has shown that the phosphorylation of NADP-malic enzyme at Ser-373, along with Ser-379 and Ser-380 in darkened leaves might regulate $NADP^+$ co-factor binding when there is no requirement for NADP-malic enzyme activity. This region of NADP-malic enzyme in C_4 plants might contain selective factors for either NAD^- or $NADP^+$ co-factor binding, and therefore could be a prime region for post-translational regulation.

Chapter 4 – The kinetics of C_4-acid decarboxylation by NADP-malic enzyme in response to pH and illumination in C_4 grasses

4.1 Introduction

4.1.1 Regulation of NADP-malic enzyme in plants

NADP-malic enzyme (EC 1.1.1.40) is one of the three decarboxylases in C_4 plants, along with NAD-malic enzyme and PEPCK. It is widespread in higher plants, including Crassulacean acid metabolism (CAM) plants, and present in various tissues including leaves, seeds and roots (Edwards and Andreo, 1992; Drincovich *et al.*, 2001). NADP-malic enzyme is found in bundle sheath chloroplasts of C_4 plants and catalyses the oxidative decarboxylation of L-malate (Figure 4.1), forming pyruvate and releasing CO_2 at the site of Rubisco (Slack *et al.*, 1969; Hatch, 1987; Maurino *et al.*, 1997; Drincovich *et al.*, 2001).

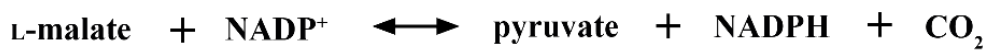

Fig. 4.1. Oxidative decarboxylation of L-malate via NADP-malic enzyme.

Aside from its essential role in C_4 photosynthesis, cytosolic, non-photosynthetic NADP-malic enzyme isoforms in C_4 plants are involved in cellular defence mechanisms, nitrogen assimilation and supplying reducing equivalents for use in central metabolism, much like their counterparts present in C_3 plants (Drincovich *et al.*, 2001; Tausta *et al.*, 2002; Maier *et al.*, 2011; Badia *et al.*, 2015; Ludwig, 2016). The C_4-specific function of NADP-malic enzyme, with regards to its subcellular compartmentalisation in bundle sheath chloroplasts and activation by illumination (Lai *et al.*, 2002), was acquired from an ancestral, chloroplastic NADP-malic enzyme following a gene duplication event (Monson, 1999; Tausta *et al.*, 2002). In the *Flaveria* species, which has C_3 and C_4 plant variants, NADP-malic enzyme belongs to a small gene family, which encodes its expression in the cytosol and chloroplasts (Rajeevan *et al.*, 1991). Genes encoding the chloroplastic NADP-malic enzyme protein found in *Flaveria trinervia* (C_4) and *Flaveria*

pringlei (C_3) were shown to have high similarity and likely to have evolved from a common ancestor (Lipka *et al.*, 1994; Marshall *et al.*, 1996). The C_3-specific NADP-malic enzyme, the likely ancestor to the C_4-specific form, is also present in chloroplasts of C_3 plants, but is expressed in low amounts (Maurino *et al.*, 1997; Drincovich *et al.*, 1998).

Despite having multiple functions, photosynthetic NADP-malic enzyme isoforms in bundle sheath chloroplasts of C_4 plants evolved a specialised role in decarboxylase activity to suit the demands of malate metabolism in C_4 photosynthesis (Maurino *et al.*, 1996; Maurino *et al.*, 1997; Drincovich *et al.*, 2001; Tsuchida *et al.*, 2001). In *Zea mays*, NADP-malic enzyme isoforms found in the cytosol and chloroplasts show distinct kinetic properties and are regulated differently by pH and malate (Johnson and Hatch, 1970; Nishikido and Wada, 1974; Asami *et al.*, 1979; Edwards and Andreo, 1992; Maurino *et al.*, 1996; Tausta *et al.*, 2002). When compared to C_3 relatives, NADP-malic enzyme in C_4 plants has a higher affinity for L-malate and operates at a higher pH optimum (Nishikido and Wada, 1974). Furthermore, in *Zea mays*, the activity of NADP-malic enzyme is dependent on pH, which alters its sensitivity to inhibition by L-malate (Asami *et al.*, 1979). At pH 8.0, NADP-malic enzyme is in its active homotetramer form consisting of identical 62 to 68 kDa subunits, and has a high V_{max} and a high affinity for $NADP^+$ during illumination (Edwards and Andreo, 1992; Kanai and Edwards, 1999). The active form dissociates into homodimers at pH 7.0 (Iglesias and Andreo, 1990), which decreases its affinity for L-malate and $NADP^+$ and becomes more sensitive to allosteric inhibition by high malate concentrations (Asami *et al.*, 1979; Edwards and Andreo, 1992; Kanai and Edwards, 1999; Detarsio *et al.*, 2007). While NADP-malic enzyme remains active in all oligomeric forms, it is most active at pH 8.0 (Edwards and Andreo, 1992). Holaday and Lowder (1989) suggest that the weak acidity of the malate binding site promotes catalysis *in vivo* at the high optimal pH, but Michaelis-Menten kinetics are lost at pH 9.0, where some degree of cooperative interaction is observed (Holaday and Lowder, 1989; Edwards and Andreo, 1992).

4.1.2 Regulation by pH and illumination

The relationship between pH and illumination may be part of a more complex mechanism for the regulation of NADP-malic enzyme-dependent decarboxylation in C_4 plants. The C_4-specific NADP-malic enzyme has a lower affinity for L-malate at an alkaline pH, albeit activity increases with increasing pH (Edwards and Andreo, 1992). In addition, the effect of pH on the activity of NADP-malic enzyme varies with the L-malate concentration (Johnson and Hatch, 1970). It is also evident that pH and Mg^{2+}, both of which are factors that regulate the activity of NADP-malic enzyme (Johnson and Hatch, 1970; Asami *et al.*, 1979), increase in the chloroplast stroma when illuminated (Edwards and Andreo, 1992). During illumination, the pH in the thylakoid space decreases and increases in the stroma, due to the proton flux into the former (Neumann and Jagendorf, 1964; Heldt *et al.*, 1973; Werdan *et al.*, 1975). In darkened conditions, pH in the stroma decreases, which consequently inhibits CO_2 fixation, and is considerably a necessary mechanism to make sure carbohydrate oxidation occurs exclusively in illuminated conditions (Werdan *et al.*, 1975). This oscillation of pH in darkened and illuminated conditions may be playing a much greater role in the activation of NADP-malic enzyme in C_4 plants; and being chloroplastic (Slack *et al.*, 1969), it is conceivable that the activity is regulated by light-dependent changes in the stromal pH (Asami *et al.*, 1979; Edwards and Andreo, 1992).

Apart from its regulation by pH, the activity of NADP-malic enzyme is regulated by changes in thiol-disulphide bonds in *Zea mays* leaves (Drincovich and Andreo, 1994; Alvarez *et al.*, 2012; Saigo *et al.*, 2013). The *in vitro* activity of NADP-malic enzyme from dark-grown plants can be stimulated in the presence of DTT (reducing agent), and under such conditions, the activity in darkened leaves is close to the activity of the light-form (Drincovich and Andreo, 1994). However, apart from the light-dependent regulation by pH or redox regulation, more extensive post-translational mechanisms that modulate enzyme activity, like those described for other C_4-related proteins, have not been described of NADP-malic enzyme in C_4 grasses. For instance, the phosphoregulatory properties of PEPCK and its involvement in C_4-acid decarboxylation have been extensively studied in C_4 plants (Walker and Leegood, 1996; Walker *et al.*, 1997; Walker *et al.*, 2002; Bailey *et al.*, 2007; Chao *et al.*, 2014). This poses an issue with regards to engineering C_4 photosynthesis into target C_3 crops, and there is growing

advocacy for PEPCK subtypes, with both PEPCK and NAD-malic enzyme activity, to be used as an engineering blueprint rather than plants which predominantly use NADP-malic enzyme (Bräutigam *et al.*, 2014; Wang *et al.*, 2014). Furthermore, PEPCK may be subjected to different regulatory mechanisms than NADP-malic enzyme, simply based on its location in the cytosol, rather than in plastids.

4.1.3 Identifying species specific NADP-malic enzyme properties

It is important to ascertain if the catalytic properties of NADP-malic enzyme from closely related C_4 plants are similar or if distinct differences in the molecular design of NADP-malic enzyme from each of the C_4 grasses may be contributing to species-specific C_4-function and regulation. Putatively identified light-dependent phosphorylation sites presented in Chapter 3 are the first evidence of the post-translational regulation of NADP-malic enzyme in *Setaria viridis*, but whether these sites confer any biological significance, is unknown. Furthermore, phosphorylation at the identified residues may alter the physiochemical properties of NADP-malic enzyme, which could possibly alter sensitivity to pH and induce changes in the catalytic properties for its reaction with L-malate. This investigation was aimed to understand the significance of chloroplastic NADP-malic enzyme activity and its regulation in response to illumination and pH, and aid our attempts in engineering the C_4-specific NADP-malic enzyme into target C_3 crops. This Chapter will show that the activity and kinetics of NADP-malic enzyme from three NADP-malic enzyme type C_4 grasses varies in response to pH, illumination and reducing conditions with DTT (reducing agent). Data presented in this study will also demonstrate that the NADP-malic enzyme regulatory mechanism by light activation applies differently to NADP-malic enzyme subtypes.

4.2 Results

4.2.1 Kinetics of phospho*enol*pyruvate carboxylase and NADP-malic enzyme

The dark and light regulation of PEPC and NADP-malic enzyme was determined by comparing their *in vitro* activities. The activity of these enzymes was monitored in continuous assays for approximately 20 min using a 96-well plate format, consisting of 150 µL reaction volumes and a small volume of crude enzyme extract normalised against the lowest concentration. Testing the design of this approach, the *in vitro* activities of PEPC showed a decrease in affinity for PEP at 7.5 h into dark (Figure 4.2) consistent with the activation mechanism by light-dependent phosphorylation demonstrated by Bailey *et al.* (2007). The K_M for PEP decreased approximately 0.45-fold after illumination and remained relatively low until the end of the photoperiod. There was no significant difference in K_M between 4 h and 15.5 h into light and 2 h into dark time-points.

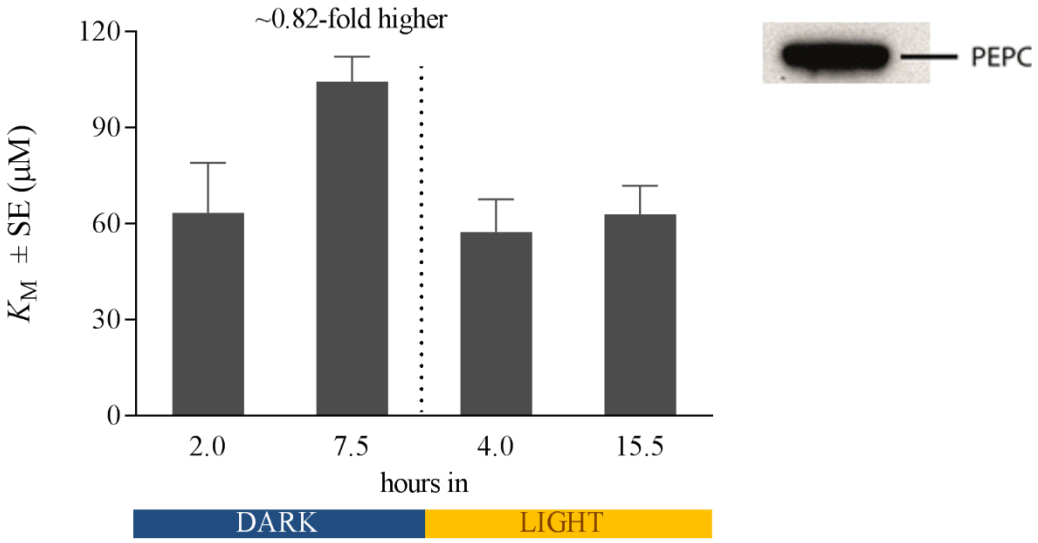

Fig. 4.2. The activity of PEPC in *Setaria viridis* corresponds to shifts in K_M during the photoperiod. The kinetic properties of PEPC from darkened (2 and 7.5 h into dark period) and illuminated (4 and 15.5 h into light) leaves were determined by enzyme assays. Immunoblot indicating PEPC content in 2 µL of leaf lysate is shown to the right. Data are based on six biological replicates and error bars show the standard error (SE).

This approach was also used to assay the activity of NADP-malic enzyme in *Setaria viridis*. The K_M for L-malate was higher at 7.5 h into the dark and 4 h into the light, when compared to 2 h into the dark and 15.5 h into the light (Figure 4.3). However, despite that the K_M for L-malate increased by 1.3-fold from 2 h into the dark and 4 h into the light, NADP-malic enzyme maintained high activity. There was no significant difference in K_M for L-malate in 15.5 h illuminated and 2 h darkened leaves. Considering light availability at these two transition points, it is possible that the light-dependent mechanism for enzyme activation occurs or is in operation at least 4 h after the onset of light.

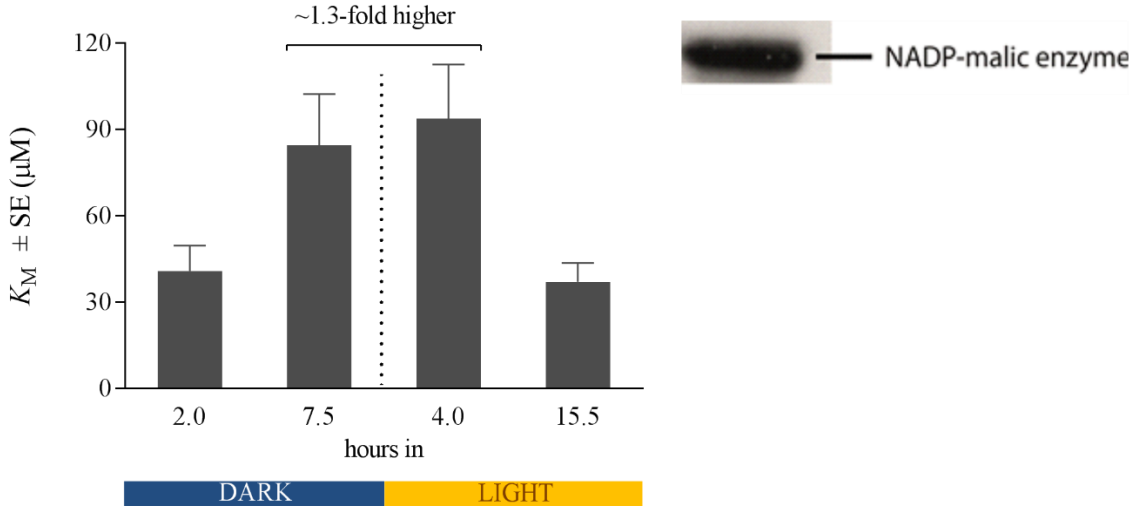

Fig. 4.3. NADP-malic enzyme K_M for L-malate was highest during the dark to light transition in *Setaria viridis*. The kinetic properties of NADP-malic enzyme from darkened (2 and 7.5 h into dark period) and illuminated (4 and 15.5 h into light) leaves were determined by enzyme assays. Immunoblot indicating NADP-malic enzyme content in 2 µL leaf lysate shown to the right. Data are based on six biological replicates and error bars show the standard error (SE).

The initial results suggest that malate metabolism by NADP-malic enzyme occurred predominantly towards the end of the photoperiod in *Setaria viridis*. These observations may warrant further investigation into the how NADP-malic enzyme responds to during the photoperiod and dark period in other C_4 grasses.

4.2.2 NADP-malic enzyme is regulated by pH

In the initial test assays the optimal conditions for assaying malic enzyme were obtained from Ashton *et al.* (1990). To further investigate the light-dependent regulation of NADP-malic enzyme, the optimal assay conditions in *Setaria viridis*, *Sorghum bicolor* and *Zea mays* were determined. NADP-malic enzyme from *Sorghum bicolor* displayed two distinct pH optima. One at pH 7.4 in illuminated leaves and another at pH 8.2 in darkened leaves (Figure 4.4). At a low pH, the activity of NADP-malic enzyme was highest in illuminated leaves, but lowest in darkened leaves. Conversely, at a high pH, the activity of NADP-malic enzyme was highest in darkened leaves and lowest in illuminated leaves. The differences in NADP-malic enzyme activity between 2 and 7.5 h darkened or 4 and 15.5 h illuminated leaves was not significant.

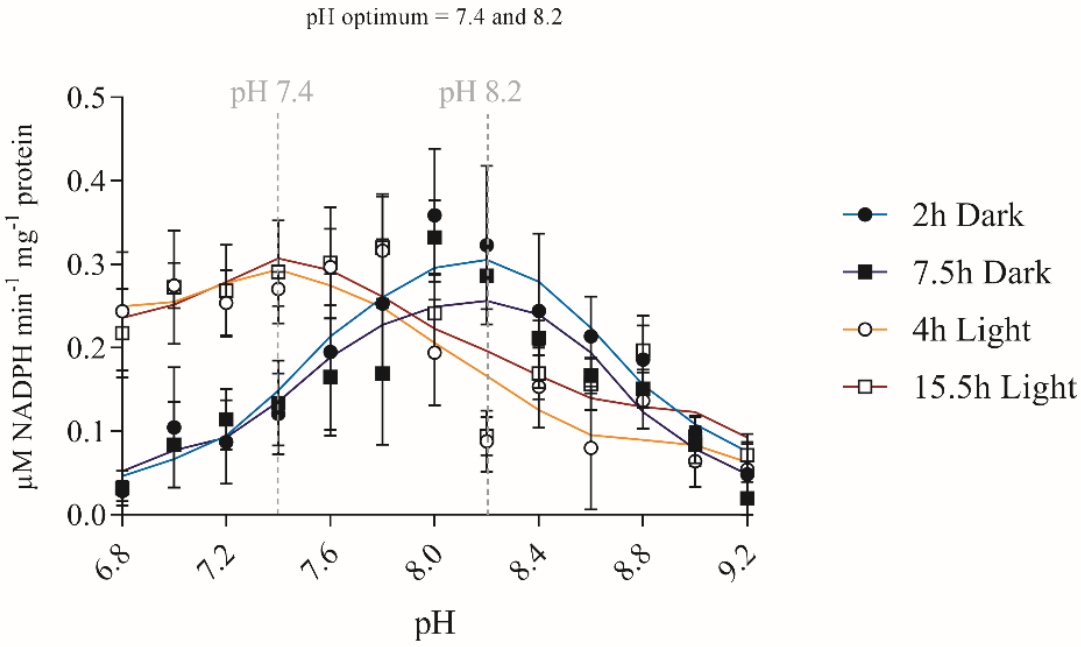

Fig. 4.4. The pH optimum of NADP-malic enzyme activity in *Sorghum bicolor* shifted after illumination. The optimum activity of NADP-malic enzyme, in terms of NADPH produced over time, was determined using a pH range from 6.8 to 9.2. NADP-malic enzyme from *Sorghum bicolor* displayed two distinct pH optima in light and dark (indicated by dashed lines). pH optima were determined at four time-points: 2 and 7.5 h into dark (blue lines, black markers) and 4 and 15.5 h into the light (orange lines, clear markers). Curve fitting was performed in GraphPad Prism 7, considering the standard deviation error bars.

Unlike *Sorghum bicolor*, NADP-malic enzyme in *Setaria viridis* from darkened and illuminated leaves remained active across a broader pH range (Figure 4.5). Furthermore, NADP-malic enzyme activity in darkened leaves decreased after pH 8.2, whereas enzyme activity in illuminated leaves decreased after pH 9.2. Also, unlike S*orghum bicolor*, the pH response of NADP-malic enzyme from *Setaria viridis* illuminated leaves was broader and peaked at pH 8.6, while the activity in darkened leaves peaked around pH 8.2, which was similar to the activity observed in darkened leaves of *Sorghum bicolor* (Figure 4.4).

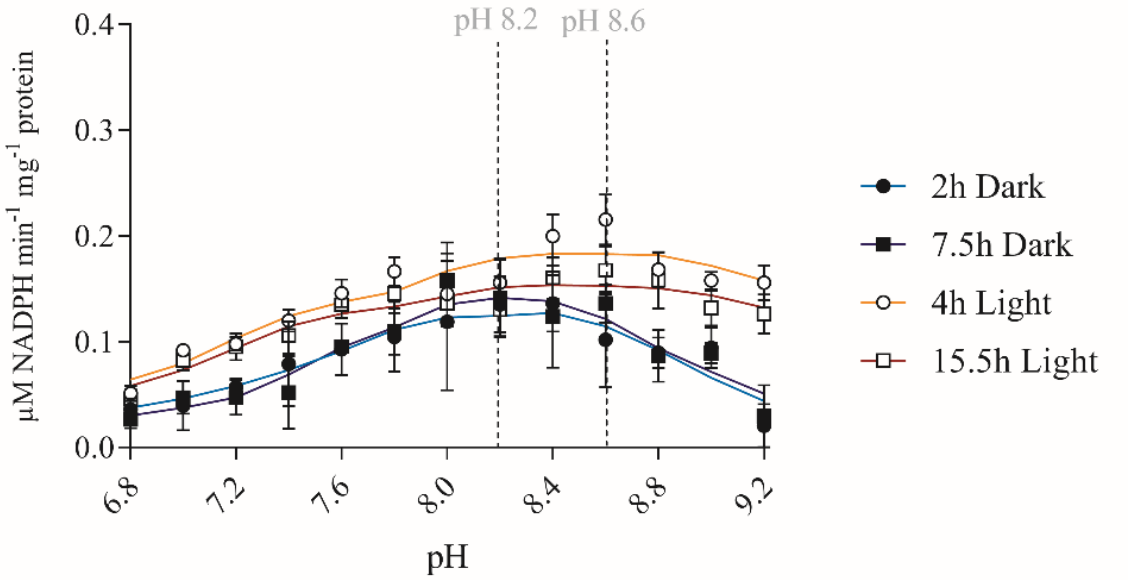

Fig. 4.5. NADP-malic enzyme from illuminated *Setaria viridis* leaves remained active across a broader pH range. The optimum activity of NADP-malic enzyme was determined using a pH range from 6.8 to 9.2. NADP-malic enzyme from *Setaria viridis* displayed higher tolerance to increasing pH, peaking at pH 8.2 and pH 8.6 (indicated by dashed lines), in darkened and illuminated leaves, respectively. The differences in optimum activity between light and dark were not significant. pH optima were determined at four time-points: 2 and 7.5 h into dark (blue lines) and 4 and 15.5 h into the light (orange lines). Curve fitting was performed in GraphPad Prism 7, considering the standard deviation error bars.

In *Zea mays*, the NADP-malic enzyme pH curve (Figure 4.6) was similar to that of *Sorghum bicolor* and like *Sorghum bicolor*, the activity of NADP-malic enzyme in *Zea mays* displayed a distinct peak at pH 8.2, but there was no difference in the pH optimum between 7.5 h darkened and 15.5 h illuminated leaves.

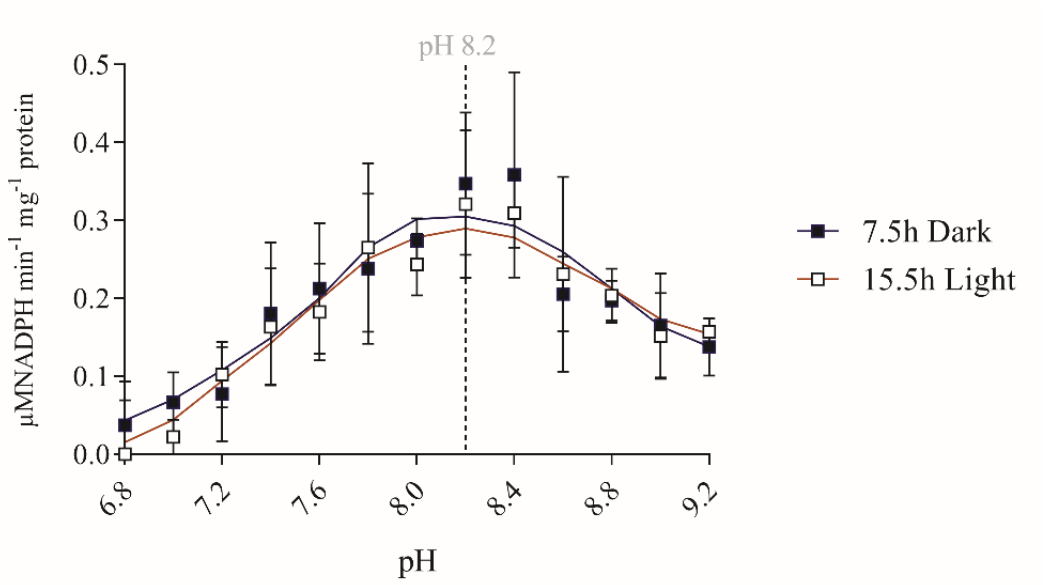

Fig. 4.6. There was no change in the pH optimum of NADP-malic enzyme activity in *Zea mays* leaves. The optimum activity of NADP-malic enzyme was determined using a pH range from 6.8 to 9.2. Activity at pH 8.2 (dashed line). pH optima were determined at two time-points: 7.5 h into dark (black squares) and 15.5 h into the light (clear squares). Curve fitting was performed in GraphPad Prism 7, considering the standard deviation error bars.

NADP-malic enzyme activity in illuminated *Zea mays* leaves exhibited low activity at a lower pH, which was similar to the activity of NADP-malic enzyme from illuminated *Setaria viridis* leaves at pH 7.0 (Figure 4.5). Additionally, the activity of NADP-malic enzyme from illuminated leaves of *Zea mays* dropped substantially at pH 6.8. This was not observed in *Sorghum bicolor* or *Setaria viridis*. The activity of NADP-malic enzyme from darkened leaves in response to pH was similar in *Sorghum bicolor* (Figure 4.4) and *Zea mays* (Figure 4.6). In *Setaria viridis*, NADP-malic enzyme displayed a flatter peak at the pH optimum (Figure 4.5) and the maximum activity was approximately three times lower compared to *Sorghum bicolor* and *Zea mays* (Figure 4.7). The differences of NADP-malic enzyme activity across all three C_4 grasses, in response to increasing pH, were mostly observed in illuminated leaves.

In *Zea mays*, there was no significant difference in the NADP-malic enzyme activity between illuminated and darkened leaves. Similarly, the dark and light activities of NADP-malic enzyme in *Setaria viridis* were not significant around the pH optimum, but were distinguishable below and above the pH optimum. In *Sorghum bicolor*, NADP-malic enzyme from illuminated leaves remained active at a lower pH (Figure 4.4), unlike NADP-malic enzyme activity from *Setaria viridis* or *Zea mays*, which was much lower

at pH 6.8. Additionally, the activity of NADP-malic enzyme in *Sorghum bicolor* in illuminated leaves, unlike that of *Setaria viridis* (Figure 4.5) was not restored with increasing pH, and declined about 0.5-fold lower than the optimum activity at pH 7.4.

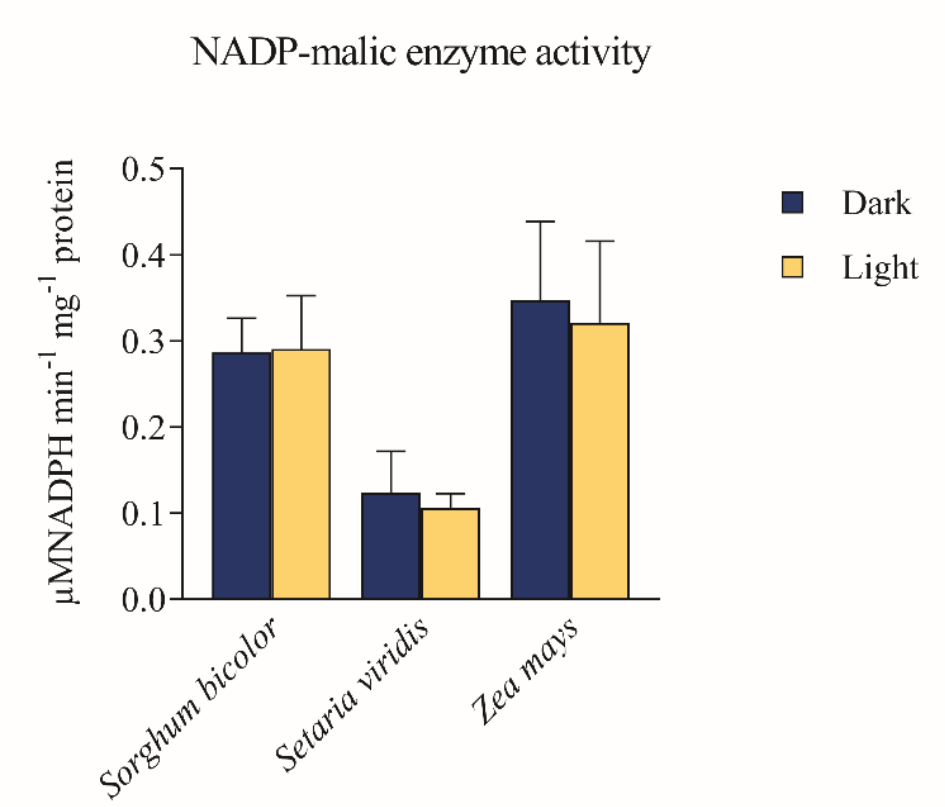

Fig. 4.7. Dark and light NADP-malic enzyme activity in leaves of *Sorghum bicolor*, *Setaria viridis* and *Zea mays* at the optimum pH. Activity of NADP-malic enzyme in leaf lysates normalised against the lowest concentration. Data are based on six biological replicates and the error bars show the standard deviation.

4.2.3 Optimal NADP-malic enzyme activity at low a Mg^{2+} concentration

The optimum activity of NADP-malic enzyme was determined in the presence of Mg^{2+}, its preferred divalent metal co-factor as previously reported by Johnson and Hatch (1970). For both *Setaria viridis* and *Sorghum bicolor*, there was no NADP-malic enzyme activity in the absence of Mg^{2+}. NADP-malic enzyme from *Setaria viridis* (Figure 4.8), was active in the presence of 1–15 mM at the optimum pH. Activity declined in the presence of 20 and 30 mM. In addition, there was no difference in Mg^{2+} dependence between darkened and illuminated leaves.

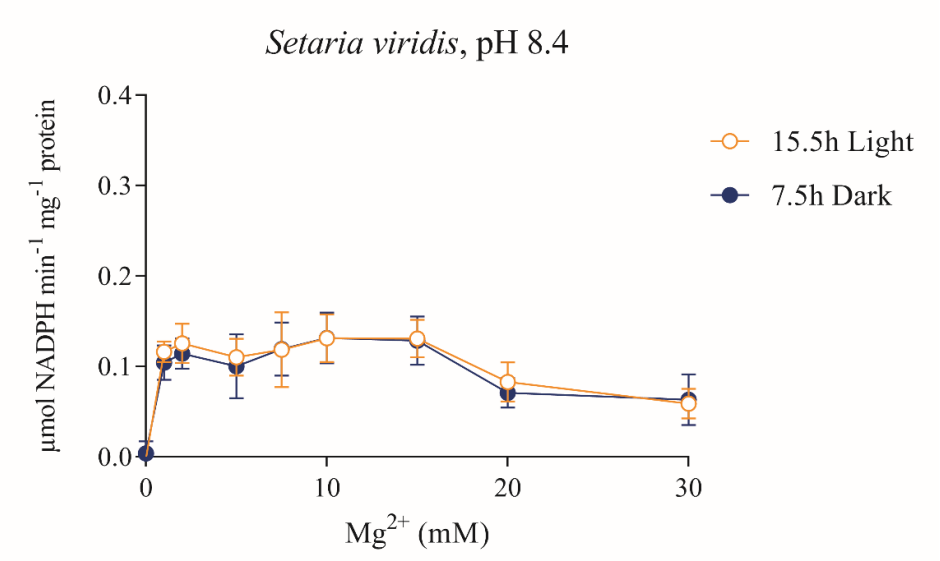

Fig. 4.8. No difference in NADP-malic enzyme activity from darkened and illuminated leaves of *Setaria viridis* in the presence of Mg^{2+}. NADP-malic enzyme was assayed in the decarboxylation direction, towards the formation of pyruvate, in the presence of $MgCl_2$ (0–30 mM), at pH 8.4. Data are based on six biological replicates and error bars show the standard deviation.

At the light pH optimum (pH 7.4), the activity of NADP-malic enzyme from *Sorghum bicolor* (Figure 4.9) did not significantly change in the presence of 1 and 30 mM $MgCl_2$. NADP-malic enzyme activity was less stable at the dark pH optimum (pH 8.2). Unlike *Setaria viridis*, the activity of *Sorghum bicolor* NADP-malic enzyme was light-dependent. In addition, the activity of NADP-malic enzyme from darkened leaves was lower than illuminated leaves in both optimal and suboptimal pH.

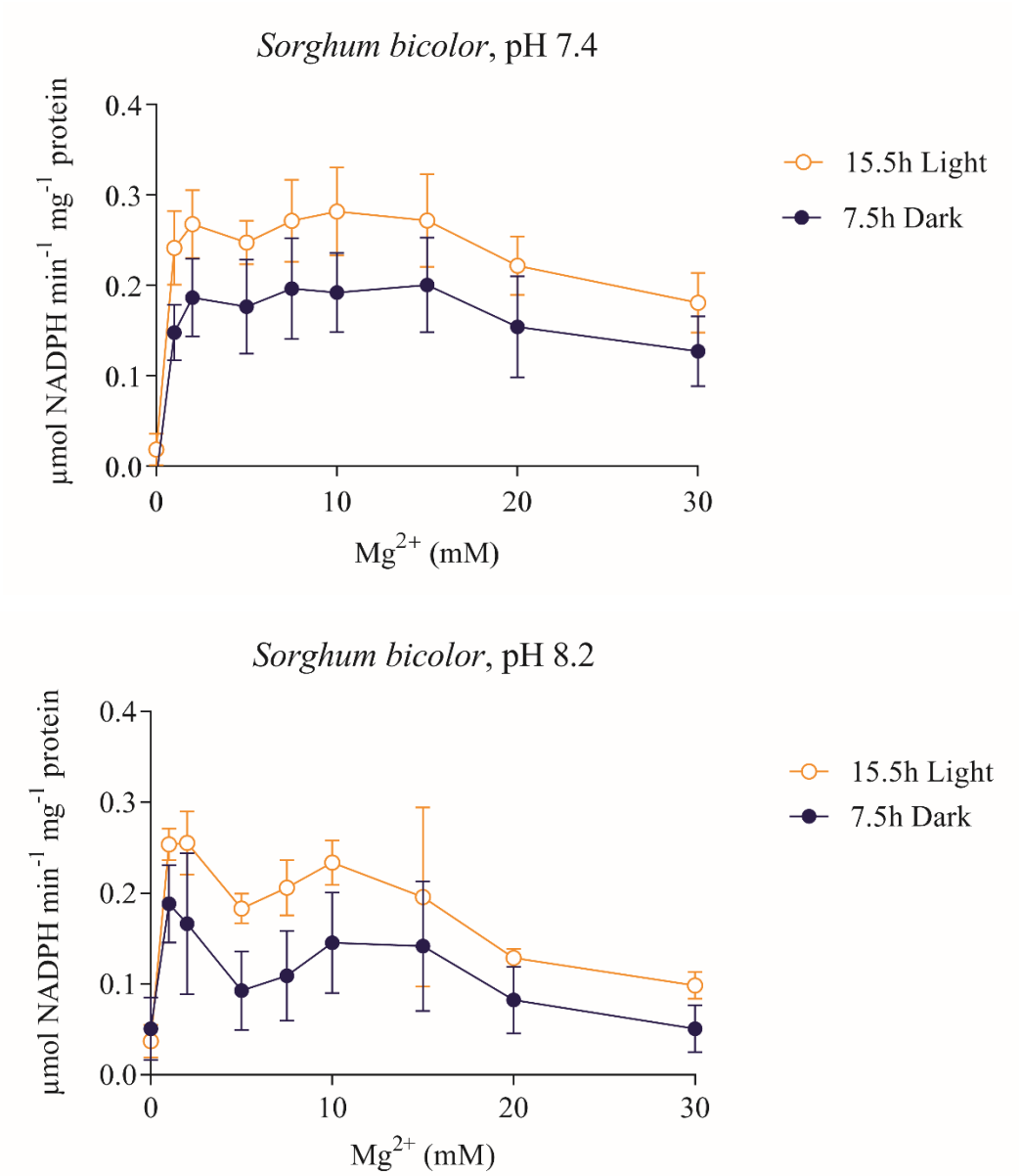

Fig. 4.9. Activity of NADP-malic enzyme in response to Mg^{2+} may be pH- and light-dependent in *Sorghum bicolor*. NADP-malic enzyme assayed in the decarboxylation direction, towards the formation of pyruvate, in the presence of $MgCl_2$ (0–30 mM), at pH 7.4 (light optimum) and pH 8.2 (dark optimum). Data are based on six biological replicates and error bars show the standard deviation.

The optimal Mg^{2+} concentration for *Setaria viridis* and *Sorghum bicolor* NADP-malic enzyme was determined at 2 mM. Dependence on Mg^{2+} may be pH-dependent in *Sorghum bicolor*. The optimal concentration of Mg^{2+} was not determined for *Zea mays*.

4.2.4 Michaelis-Menten kinetics of NADP-malic from three C_4 grasses

To further analyse the effects of illumination and pH, the dark and light Michaelis-Menten kinetics of NADP-malic enzyme, at the identified pH and Mg^{2+} optima, were investigated. In addition, to test the effect of reducing conditions, the activity of NADP-malic enzyme was measured by adding 10 mM DTT (reducing agent) into the reaction assay. In *Sorghum bicolor*, the previous results showing that NADP-malic enzyme had two distinct pH optima under illuminated or darkened conditions were further substantiated by shifts in K_M for L-malate under optimal and suboptimal conditions (Figure 4.10). There was no change in the K_M for L-malate under optimal and suboptimal pH in 15.5 h illuminated leaves. At pH 7.4 and pH 8.2, NADP-malic enzyme K_M for L-malate in darkened *Sorghum bicolor* leaves decreased in the presence of DTT. In darkened leaves, the K_M for L-malate was nearly 1.8-fold higher than the K_M in illuminated leaves in optimal pH and about 0.66-fold higher in the suboptimal pH (Figure 4.10), suggesting that the affinity for L-malate increases after the dark to light transition, regardless of pH. This observation concurred with previous findings in *Setaria viridis* (Figure 4.3), in which the K_M for L-malate was about 1.3-fold higher at 7.5 h into dark and remained high after 4 h of illumination, until lowering after 15.5 h of illumination. However, the K_M for L-malate decreased in response to suboptimal pH, regardless the light condition.

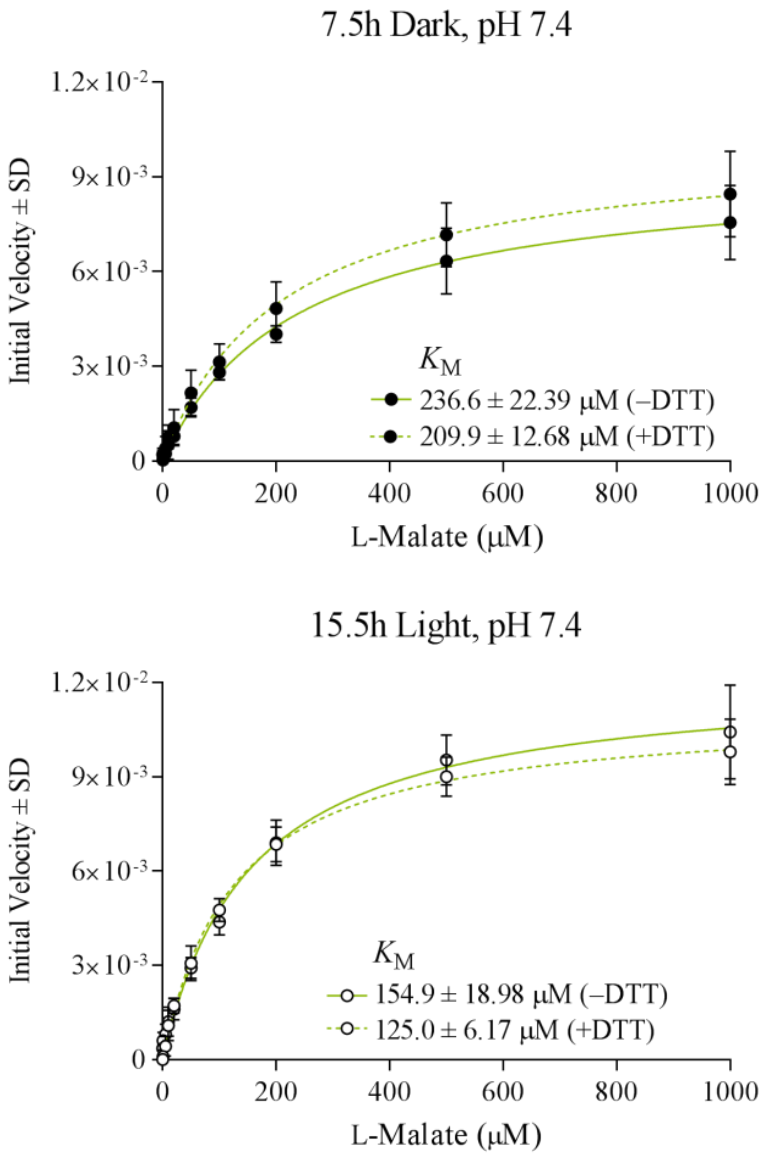

pH 7.4 (K_M ± SE µM)		pH 7.4 + DTT (K_M ± SE µM)	
Dark	Light	Dark	Light
236.6 ± 22.39	154.9 ± 18.98	209.9 ± 12.68	125.0 ± 6.17

Fig. 4.10.

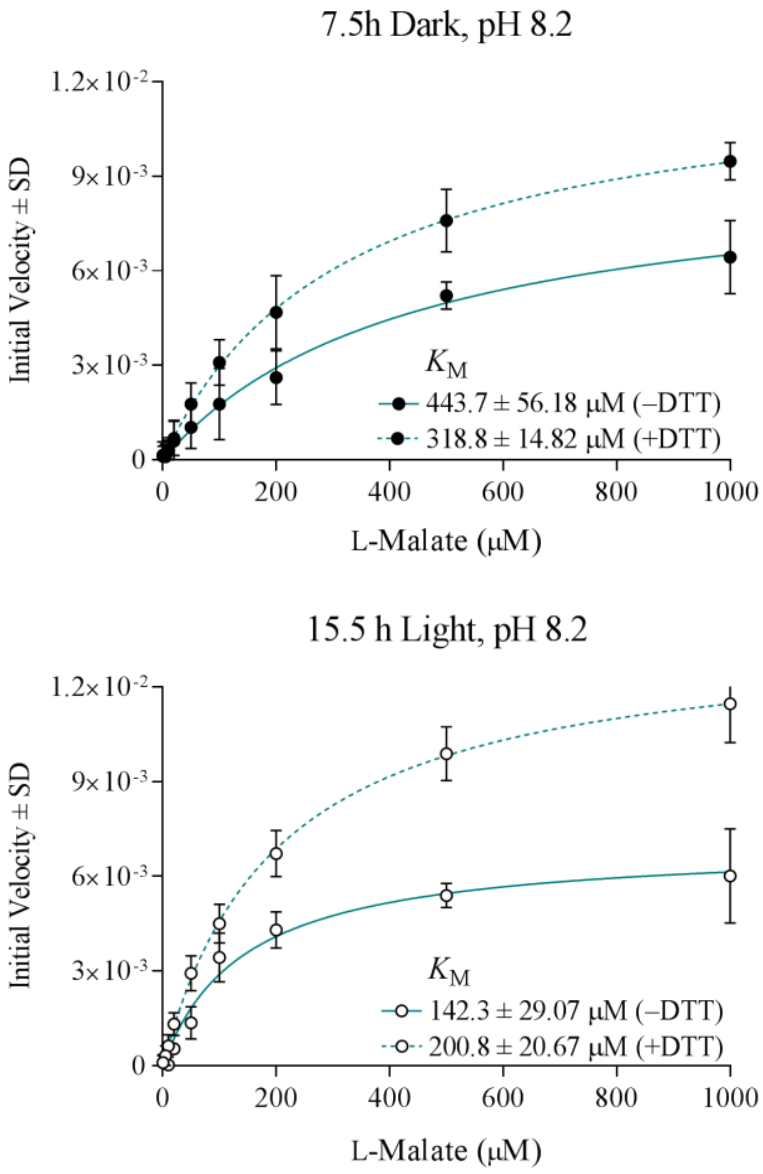

pH 8.2 (K_M ± SE µM)		pH 8.2 + DTT (K_M ± SE µM)	
Dark	Light	Dark	Light
443.7 ± 56.18	142.3 ± 29.07	318.8 ± 14.82	200.8 ± 20.67

Fig. 4.10. The differences in light and dark activities of *Sorghum bicolor* NADP-malic enzyme in response to pH linked to shifts in K_M. Michaelis-Menten curves for the NADP-malic reaction in darkened (black dots) and illuminated (clear dots) *Sorghum bicolor* leaves in response to increasing L-malate concentrations. K_M was determined at two pH optima (pH 7.4 in green and pH 8.2 in blue) and in response to DTT (+) and no added DTT (–). Data are based on six biological replicates and error bars show the standard deviation (SD). SE, standard error. Units for initial velocity are Abs/min.

The relationship between optimal and suboptimal pH and NADP-malic enzyme activity was not conclusive in *Setaria viridis*. At the optimal pH (pH 8.4), NADP-malic enzyme did not display Michaelis-Menten kinetics and the K_M for L-malate was ambiguous without the addition of DTT (Figure 4.11). However, Michaelis-Menten kinetics were restored at the suboptimal (pH 7.4) in both darkened and illuminated leaves. In addition, at a higher pH, the activity of NADP-malic enzyme in *Setaria viridis* was higher, but the affinity for L-malate was low. Conversely, enzyme activity was low at a lower pH, but the affinity for L-malate was higher.

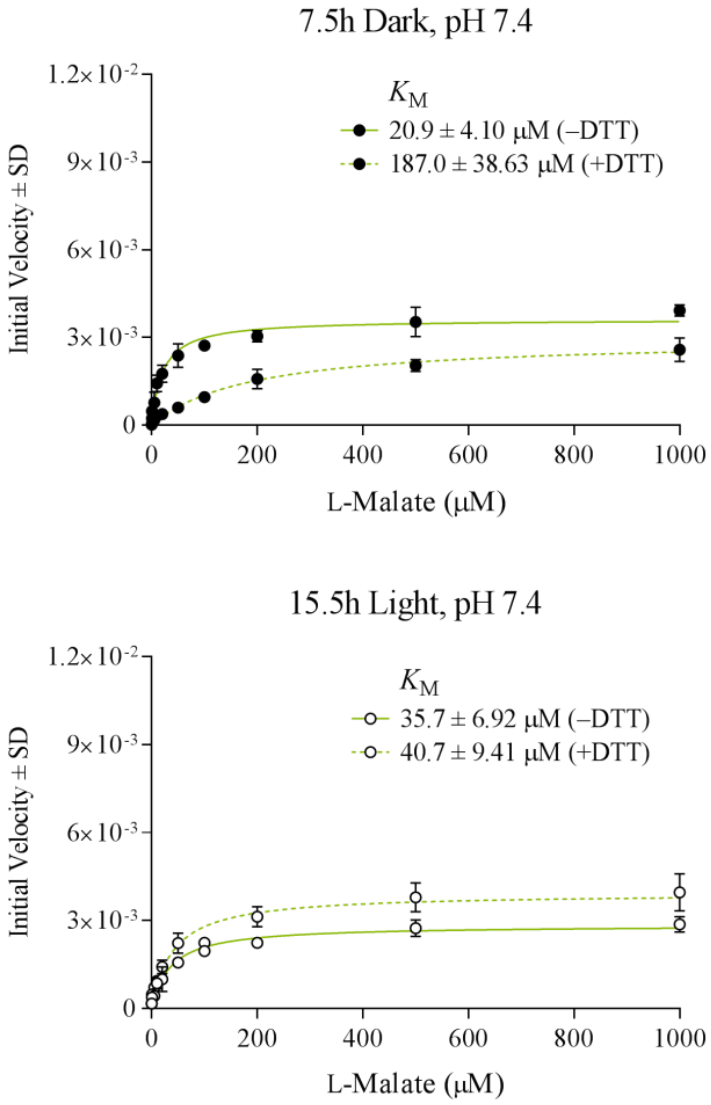

pH 7.4 (K_M ± SE µM)		pH 7.4 + DTT (K_M ± SE µM)	
Dark	Light	Dark	Light
20.9 ± 4.10	35.7 ± 6.92	187.0 ± 38.63	40.7 ± 9.41

Fig. 4.11.

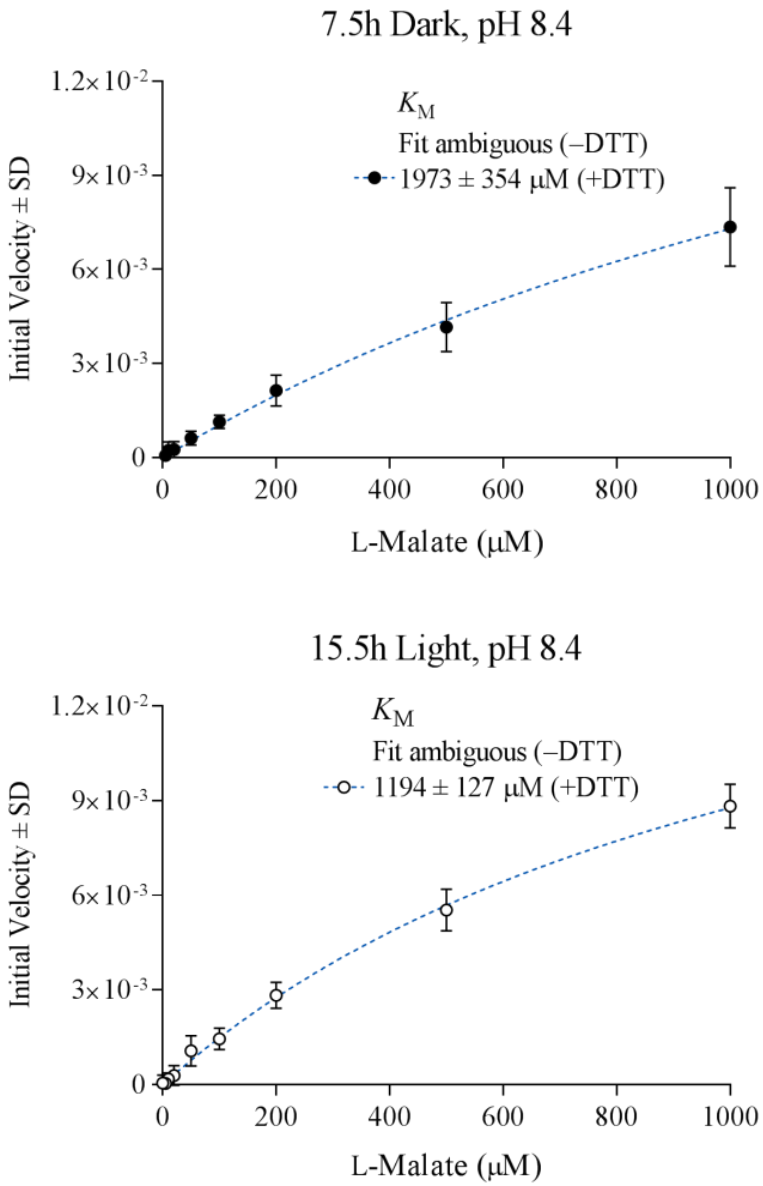

pH 8.4 (K_M ± SE µM)		pH 8.4 + DTT (K_M ± SE µM)	
Dark	Light	Dark	Light
Ambiguous	Ambiguous	1973 ± 354	1194 ± 127

Fig. 4.11. Link between pH and light/dark activity of NADP-malic enzyme in *Setaria viridis*. Michaelis-Menten curves for the NADP-malic reaction in darkened (black dots) and illuminated (clear dots) *Setaria viridis* leaves in response to increasing L-malate concentrations. K_M was determined at the optimal pH 8.4 (blue) and suboptimal pH 7.4 (green), in response to DTT (+) and no added DTT (–). Data are based on six biological replicates and error bars show the standard deviation (SD). SE, standard error. Units for initial velocity are Abs/min.

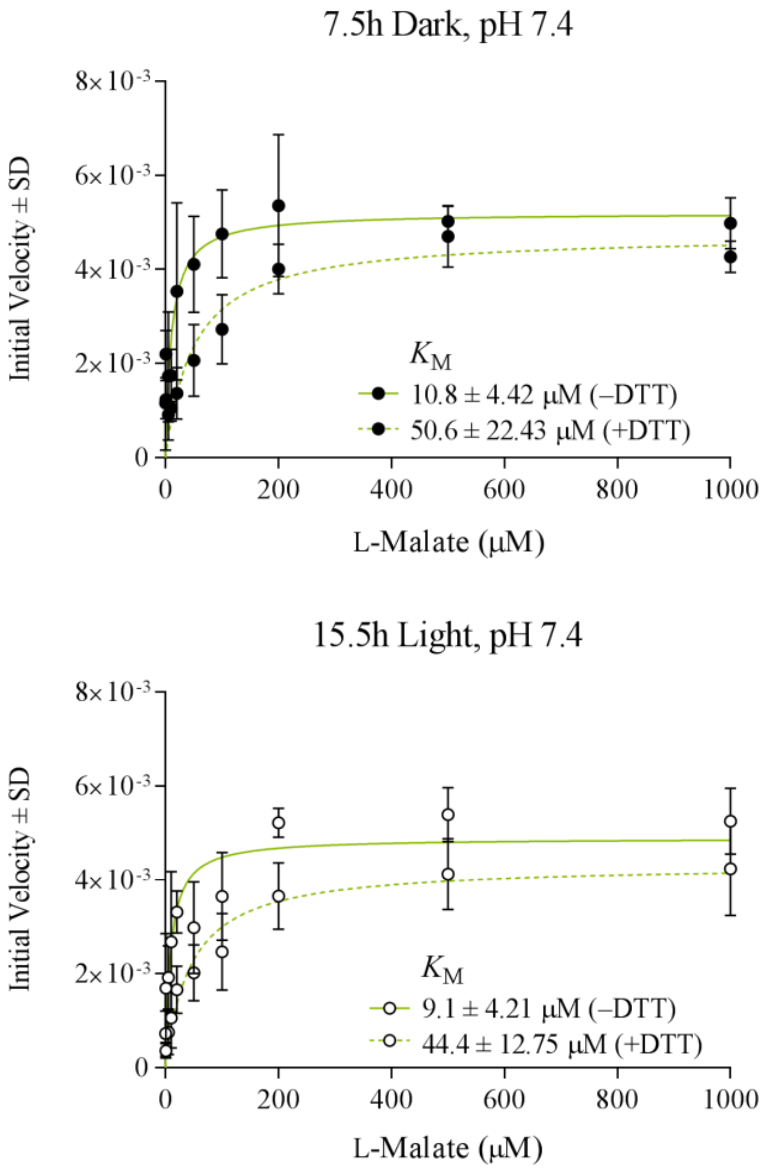

pH 7.4 (K_M ± SE µM)		pH 7.4 + DTT (K_M ± SE µM)	
Dark	Light	Dark	Light
10.8 ± 4.42	9.1 ± 4.21	50.6 ± 22.43	44.4 ± 12.75

Fig. 4.12.

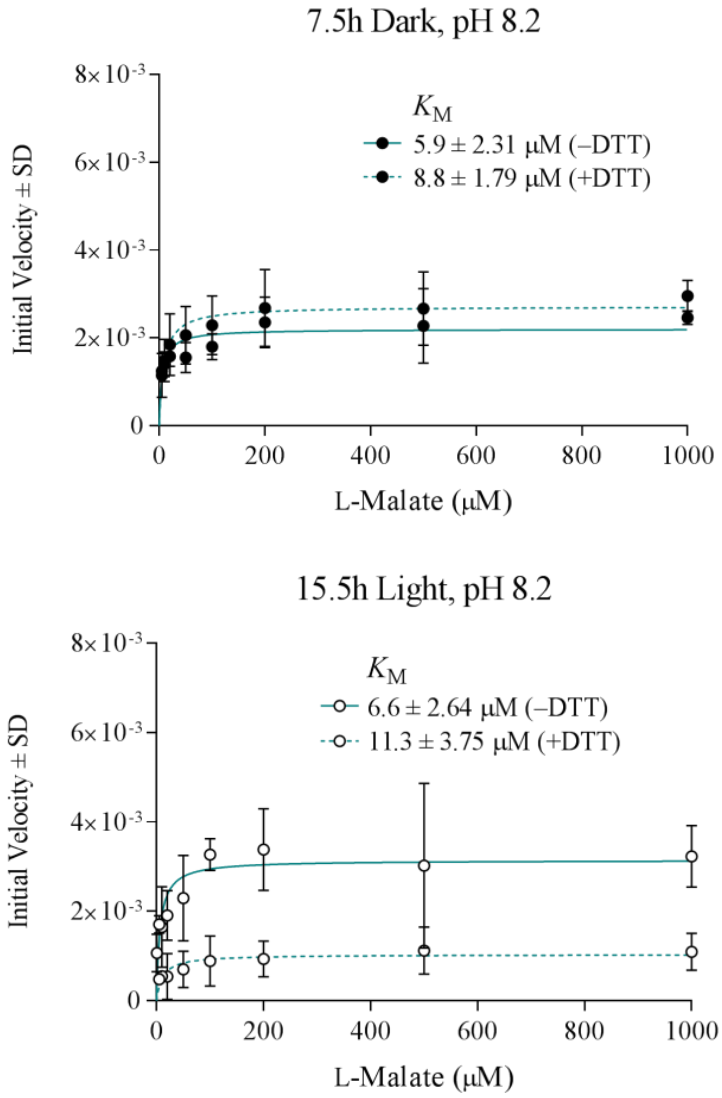

pH 8.2 (K_M ± SE µM)		pH 8.2 + DTT (K_M ± SE µM)	
Dark	Light	Dark	Light
5.9 ± 2.31	6.6 ± 2.64	8.8 ± 1.79	11.3 ± 3.75

Fig. 4.12. NADP-malic enzyme in *Zea mays* maintained high substrate affinity in response to pH. Michaelis-Menten curves for the NADP-malic reaction in darkened (black dots) and illuminated (clear dots) *Zea mays* leaves in response to increasing L-malate concentrations. K_M was determined at a single pH optimum (pH 8.2 in blue) and a suboptimal pH (pH 7.4 in green), in response to DTT (+) and no added DTT (–). Affinity for L-malate remained consistently high (low K_M) in darkened and illuminated leaves in high and low pH. Presence of DTT had a marginal effect on NADP-malic enzyme affinity for L-malate. Data are based on six biological replicates and error bars show the standard deviation (SD). SE, standard error. Units for initial velocity are Abs/min.

In *Zea mays*, NADP-malic enzyme maintained a higher substrate affinity across all time-points (Figure 4.12), unlike *Sorghum bicolor* or *Setaria viridis*. In the presence of DTT, there was a significant change in K_M in darkened and illuminated leaves in suboptimal pH (pH 7.4). These differences were greater than those observed in *Sorghum bicolor* and *Setaria viridis* leaves in response to DTT. However, at the pH optimum (pH 8.2), a marginal increase in K_M was observed, but was not significant. In *Zea mays*, *Sorghum bicolor* and *Setaria viridis*, the effect of DTT on the activity and K_M for L-malate was not discernible in these assays. Furthermore, there were no distinct patterns in the change of K_M at the optimal and suboptimal pH in response to DTT across the three C_4 grasses, and therefore the effect of DTT on the activity of NADP-malic enzyme was inconclusive.

Table 4.1. **Changes to NADP-malic enzyme affinity for L-malate in response to illumination**. Summary of the change in NADP-malic enzyme affinities for L-malate in response the light transition, under optimal and suboptimal pH. Up-arrows indicate increase in affinity, while down-arrows indicate decrease in affinity. *Fold change calculated in the presence of DTT.

	Optimal pH	Suboptimal pH
	Affinity (fold change)	
Sorghum bicolor	0.65 ↑	0.40 ↑
Setaria viridis	0.40* ↑	0.71 ↓
Zea mays	0.12 ↓	0.16 ↑

It was evident that under optimal conditions, the NADP-malic enzyme affinity range for L-malate was very high in *Zea mays*, moderate in *Sorghum bicolor*, but much lower in *Setaria viridis*. In illuminated leaves, NADP-malic enzyme affinity for L-malate increased by almost 0.65-fold in *Sorghum bicolor*, 0.40-fold in *Setaria viridis*, but decreased about 0.12-fold in *Zea mays* after the dark to light transition at the pH optimum (Table 4.1). Furthermore, under optimal and suboptimal conditions, NADP-malic enzyme affinity for L-malate in *Zea mays* leaves remained higher than in *Sorghum bicolor* and *Setaria viridis*. However, since NADP-malic enzyme in *Setaria viridis* did not display Michaelis-Menten kinetics under optimal conditions and K_M was ambiguous, the true relationship between affinity for L-malate and pH cannot be determined.

4.3 Discussion

4.3.1 Low pH optimum ensures NADP-malic enzyme activity at the onset of light

The C_4-specific NADP-malic enzyme is generally assayed at pH 8.0 (Ashton *et al.*, 1990; Edwards and Andreo, 1992), which correlates to the physiological pH in the chloroplast stroma during illumination, when NADP-malic enzyme is active in C_4 plants (Neumann and Jagendorf, 1964; Heldt *et al.*, 1973; Kanai and Edwards, 1999). In this study, NADP-malic enzyme activity was determined in low and high pH and varying concentrations of Mg^{2+}. These results show that the activity of NADP-malic enzyme from darkened and illuminated leaves of *Setaria viridis* (Figure 4.5) and *Zea mays* (Figure 4.6) was at its optimum at a high pH (pH 8.0), which is consistent with previous findings (Johnson and Hatch, 1970; Nishikido and Wada, 1974; Edwards and Andreo, 1992). However, the activity of the enzyme from illuminated leaves of *Sorghum bicolor* was at its optimum at a lower pH (Figure 4.4), and activity declined as the pH increased. In fact, NADP-malic enzyme from *Sorghum bicolor* exhibited two distinct pH optima (Figure 4.13). These results indicate that there are interspecies differences in the regulation of NADP-malic enzyme activity in closely related C_4 grasses. Also, while *in vitro* enzyme assays have been performed using 5 mM Mg^{2+} (Ashton *et al.*, 1990), maximal activity was achieved using 2 mM Mg^{2+} (Figure 4.8, 4.9). This correlates to the physiological concentration of Mg^{2+} in the chloroplast stroma, which rises from about 0.5 mM to 2 mM upon illumination (Portis and Heldt, 1976; Heldt, 1979; Ishijima *et al.*, 2003). Apart from serving as a co-factor in the reaction, Mg^{2+} protects NADP-malic enzyme from becoming oxidised (Drincovich and Andreo, 1994). Whether 2 mM Mg^{2+} can grant the same protection as 10 mM used in previous experiments, is unclear. It was clear however, that the activity of NADP-malic enzyme decreased when using Mg^{2+} concentrations over 10 mM. This suggests that a high concentration of Mg^{2+} can lead to the blockage of substrate binding sites in the C_4-specific NADP-malic enzyme, and should be taken into consideration for future *in vitro* assays. This has been previously speculated to occur in the NADP-malic enzyme from *Escherichia coli*, whereby concentrations of 4 mM Mg^{2+} and above inhibited enzyme activity (Bologna *et al.*, 2007). Loss of NADP-malic enzyme activity could have been due to the oxidised form of the enzyme present in the reaction assay. However, these effects were kept to a minimum, because NADP-malic enzyme

was extracted in reducing conditions with 5 mM DTT to prevent the formation of disulphide bonds.

NADP-malic enzyme from illuminated *Sorghum bicolor* leaves displayed maximal activity at pH 7.4, but there was no change in affinity for L-malate between pH 7.4 and pH 8.2. This suggests that NADP-malic enzyme from *Sorghum bicolor* is maximally active at the onset of light, when the pH in the stroma is close to pH 7.0 (Werdan *et al.*, 1975). Optimal NADP-malic enzyme activity from dark-grown *Sorghum bicolor* plants was achieved at pH 8.2, which is close to the pH optimum generally used to assay NADP-malic enzyme activity (Ashton *et al.*, 1990).

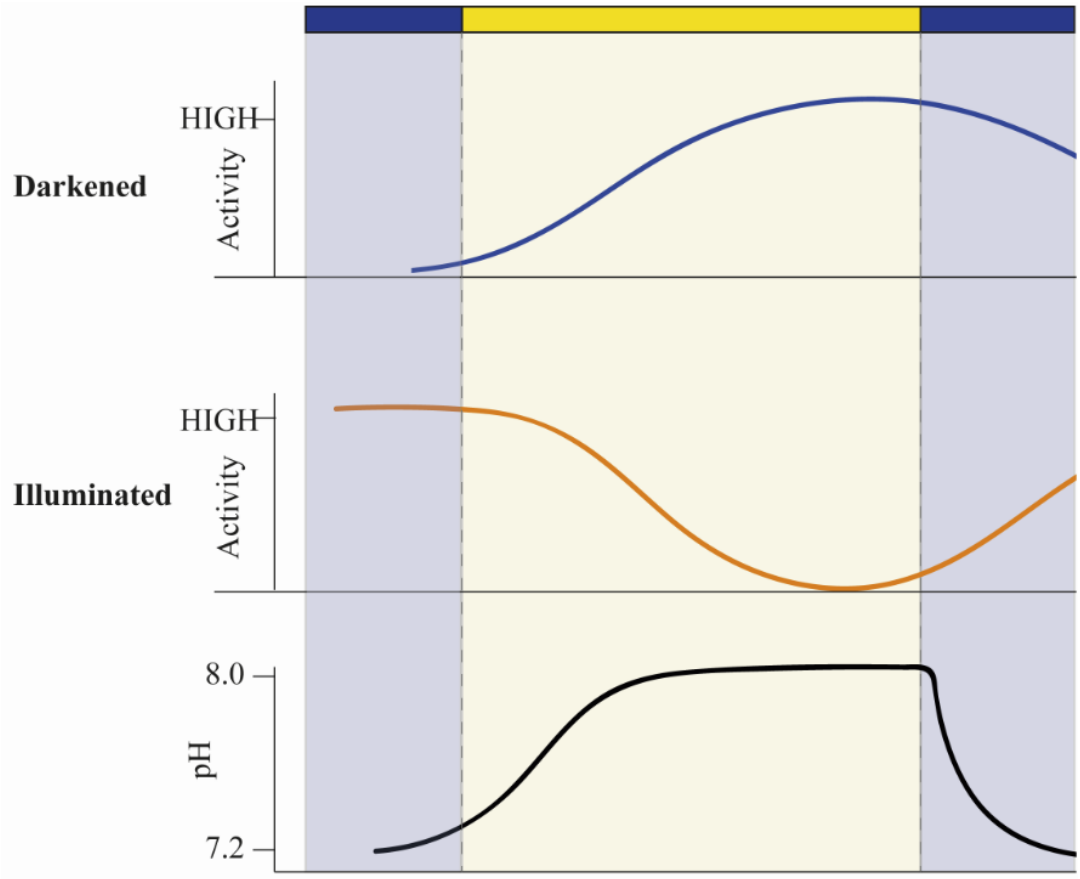

Fig. 4.13. Simple model showing two distinct activities of NADP-malic enzyme from darkened (blue line) and illuminated (orange line) leaves of *Sorghum bicolor*. Activity of NADP-malic enzyme is shown as high and low, which is modelled from the changes in activity shown in Figure 4.4. Dark and light periods are shown in light blue and light yellow shaded regions, respectively. A simple model shows the changes in pH in the stroma during light transitions (bottom).

A simple model of NADP-malic enzyme activity in *Sorghum bicolor*, Figure 4.13, shows that when the activity of NADP-malic enzyme from illuminated leaves is high, the activity of the NADP-malic enzyme from darkened leaves is low. These inverse changes in dark and light NADP-malic enzyme activity align with the diurnal change of the pH in the stroma, which rises after illumination (Heldt *et al.*, 1973; Werdan *et al.*, 1975). The pH in the stroma declines at the beginning of the dark period and inhibits carbon fixation (Werdan *et al.*, 1975), and it is unlikely that NADP-malic enzyme maintains high *in vivo* activity at a high pH after the light to dark transition. The difference in the pH optimum between light-grown and dark-grown *Sorghum bicolor* plants suggests that NADP-malic enzyme exists as two separate isoforms during light transitions. Previous studies have shown that the photosynthetic NADP-malic enzyme in *Zea mays* and *Flaveria floridana* has a high pH optimum, while the non-photosynthetic form, which is present in both C_3 and C_4 species, has a low pH optimum (Drincovich *et al.*, 1991; Marshall *et al.*, 1996; Maurino *et al.*, 1996; Casati *et al.*, 1997; Casati *et al.*, 1999). This suggests that the distinct differences in the pH optimum observed in these assays may have been due to non-photosynthetic NADP-malic enzyme activity in crude leaf extracts.

However, it is unclear whether the formation of NADPH at a low pH was due to activity from the non-photosynthetic form of NADP-malic enzyme in the crude leaf lysates. While this may be the case, it is uncertain why NADP-malic enzyme activity was relatively lower at the pH optimum of the C_4-form (Edwards and Andreo, 1992). Also, if NADP-dependent activity came from the non-photosynthetic isoform, then the two distinct pH optima would have been evident in assays conducted in *Setaria viridis* and *Zea mays*, which may contain appreciable amounts of non-photosynthetic NADP-malic enzyme (Drincovich *et al.*, 2001), and thus could have contributed to the formation of NADPH. A model of NADP-malic enzyme activity from illuminated and darkened leaves of *Setaria viridis* (Figure 4.14) shows that NADP-malic enzyme from illuminated leaves had a broader pH dependency and it did not exhibit two distinct pH optima, like *Sorghum bicolor*. Instead, the activity of NADP-malic enzyme rose as pH increased after illumination, and the pH optimum was determined at pH 8.4, irrespective of the light condition, aligning to the pH optimum of NADP-malic enzyme in C_4 plants (Ashton *et al.*, 1990) and light-dependent activity of NADP-malic enzyme *in vivo* (Asami *et al.*, 1979; Edwards and Andreo, 1992).

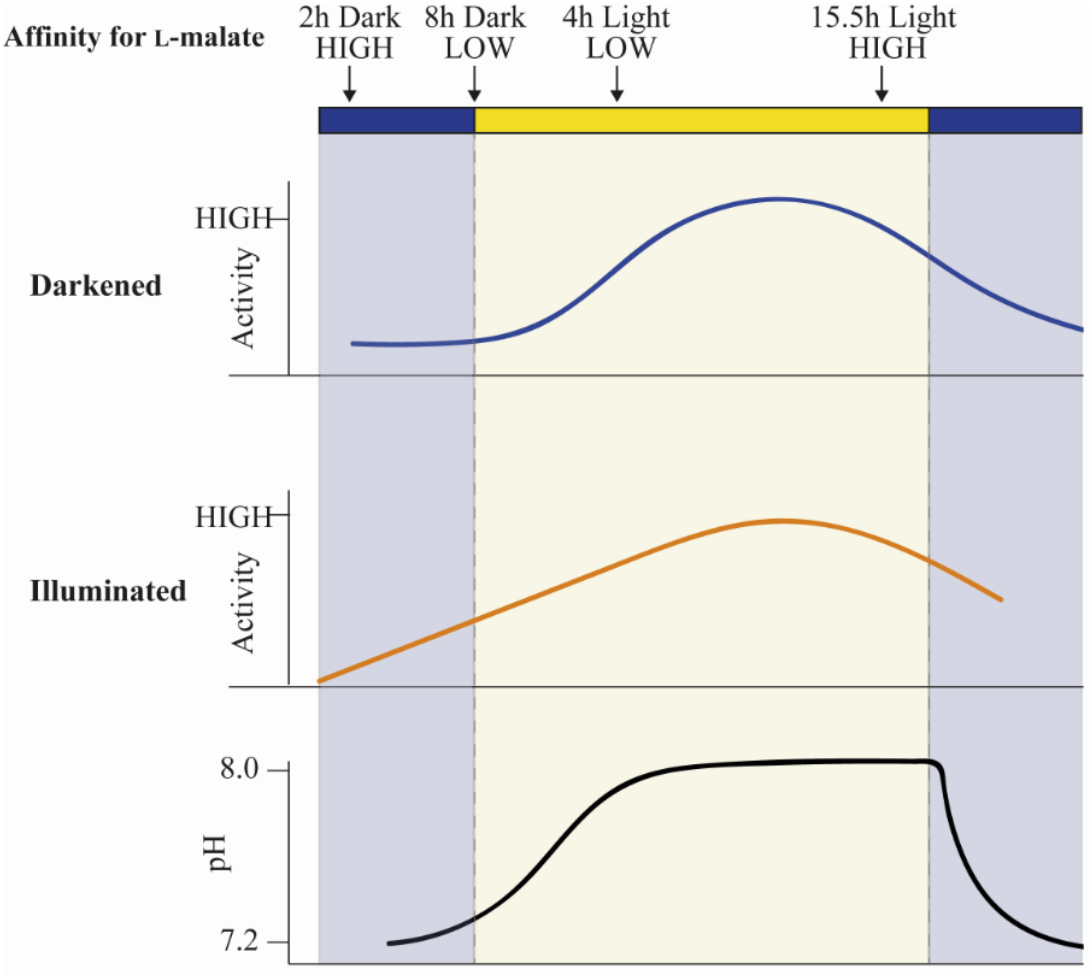

Fig. 4.14. Simple model showing NADP-malic enzyme activity from darkened (blue line) and illuminated (orange line) leaves of *Setaria viridis*. Activity of NADP-malic enzyme is shown as high and low, which is modelled from the changes in activity shown in Figure 4.5. Dark and light periods are shown in light blue and light yellow shaded regions, respectively. A simple model shows the changes in pH in the stroma during light transitions (bottom).

When compared to the modelled activity of NADP-malic enzyme from darkened and illuminated leaves of *Zea mays* (Figure 4.15) it is unlikely that activity from the non-photosynthetic NADP-malic enzyme was observed. NADP-malic enzyme activity was lower at pH 7.4 in *Zea mays* and *Setaria viridis*, while high activity was observed in high pH, suggesting that NADP-dependent activity came from the C_4-specific malic enzyme, which has a high pH optimum. Had there been non-photosynthetic NADP-malic enzyme activity, such activity would have been distinctly higher at a lower pH, as observed in *Sorghum bicolor*. Another possibility is that *Zea mays* and *Setaria viridis* may have a relatively lower amount of the non-photosynthetic NADP-malic enzyme. However, this is unlikely since the non-photosynthetic form is the second major isoform of NADP-

malic enzyme present in chloroplasts of *Zea mays* (Maurino *et al.*, 1996; Maurino *et al.*, 1997; Drincovich *et al.*, 2001).

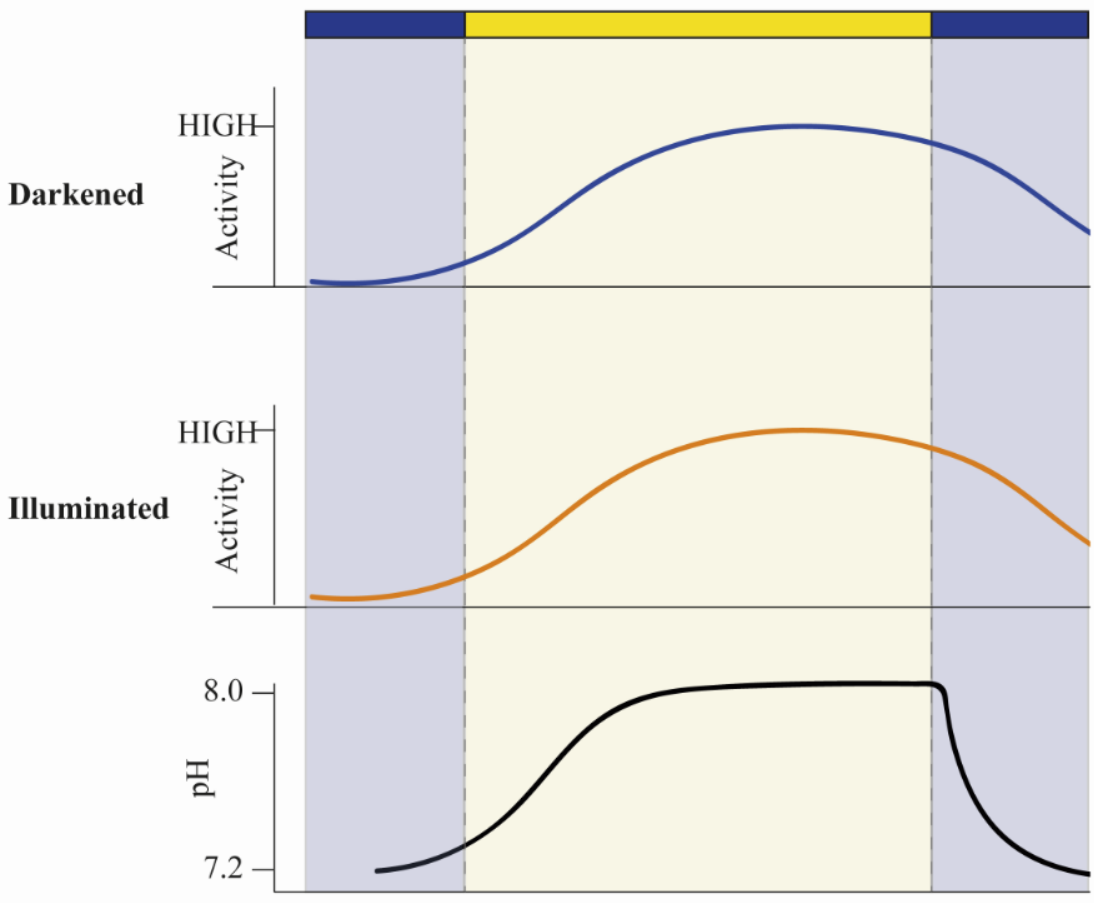

Fig. 4.15. Simple model showing NADP-malic enzyme activity from darkened (blue line) and illuminated (orange line) leaves of *Zea mays*. Activity of NADP-malic enzyme is shown as high and low, which is modelled from the changes in activity shown in Figure 4.6. Dark and light periods are shown in light blue and light yellow shaded regions, respectively. A simple model shows the changes in pH in the stroma during light transitions (bottom).

Since the activity of NADP-malic enzyme was not as high at a low pH in neither *Setaria viridis* or *Zea mays*, there may be other factors regulating activity of NADP-malic enzyme in *Sorghum bicolor*. Light-dependent differences at the pH optimum may be due to post-translational regulation mechanisms occurring at least 30 min before the onset of light and 30 min before the dark period. The latter would correlate with the previous finding in *Setaria viridis*, in which NADP-malic enzyme displayed a higher affinity for L-malate 30 min before dark period, while the affinity for L-malate was about 1.3-fold lower 4 h after the onset of light (Figure 4.3, 4.14). Furthermore, in *Sorghum bicolor*, the affinity for L-malate was about 0.46-fold higher at pH 7.4 than at pH 8.2, 30 min before

the onset of light, which does not concur with previous findings that showed that the C_4-form has a lower affinity for L-malate at pH 7.0 when the tetrameter dissociates (Asami *et al.*, 1979; Detarsio *et al.*, 2007). However, before the onset of light, a high affinity for L-malate might be required to achieve and maintain a high reaction rate since malate has not accumulated in the chloroplast. Therefore, the overlap in activity of NADP-malic enzyme between darkened and illuminated leaves may contribute to achieving a seamless transition in activity between light conditions, and may also correlate to the time it takes for metabolites to accumulate in C_4 plants. In this case, it is unlikely that NADP-malic enzyme in *Sorghum bicolor* is regulated by diurnal changes in the pH of the stroma, but pH serves more as fine-control of enzyme isoforms. An additional time-point, around 4.5 h into the dark period would ascertain whether this mechanism occurs solely at dark to light transitions.

NADP-malic enzyme may alternatively be regulated by redox mechanisms, which can exert more control over the activation and inactivation of chloroplastic enzymes, than through diurnal changes in the pH of the stroma (Jacquot *et al.*, 1981; Leegood and Walker, 1983; Drincovich and Andreo, 1994; Schürmann and Buchanan, 2008). Addition of 10 mM DTT to lysates from illuminated leaves containing NADP-malic enzyme from *Sorghum bicolor* increased the affinity for L-malate when assayed at pH 7.4 (Figure 4.10), but had no effect on the activity of NADP-malic enzyme. Conversely, addition of DTT to illuminated leaf lysates increased the maximal activity of NADP-malic enzyme at pH 8.2 and decreased affinity for L-malate (Figure 4.10). This might indicate that at pH 8.2 the oxidised-form of the enzyme, from *Sorghum bicolor*, might have a higher sensitivity to allosteric inhibition (non-competitive), possibly by malate, than the reduced-form, which displayed a higher maximal activity. However, this does not align with the catalytic properties of NADP-malic enzyme, whereby sensitivity to allosteric inhibition by malate increases at a lower pH (Asami *et al.*, 1979). A previous study has shown that NADP-malic enzyme from the intermediate C_3–C_4 species *Flaveria floridana* is not inhibited by malate at pH 7.0 (Casati *et al.*, 1999), suggesting that the enzyme assayed in illuminated leaves of *Sorghum bicolor* may be distinctly different than the C_4-form found in leaves of *Zea mays*. The calculated pI for NADP-malic enzyme from these C_4 grasses ranges from 5.8 to 6.7 (isoform K3XG11 has pI 7.15) and under the range of pH used in these assays (pH 6.8 to 9.2), the enzymes should exist as net-negatively charged species. Any differences to their activities or affinities for L-malate

might be due to the action of the reducing agent (DTT) on cysteine-cysteine disulphide bonds, which confers stability to the protein. There are ten cysteine residues in *Sorghum bicolor*, nine residues in *Zea mays* and seven residues in *Setaria viridis*, which could theoretically be affected. However, since these assays were performed using enzyme in crude leaf extracts, kinetic constants like V_{max}, K_{cat} or K_i cannot be calculated, and the exact effects of DTT on the activity of NADP-malic enzyme cannot be determined.

The NADP-malic enzyme *in vivo* activity in illuminated leaves of *Sorghum bicolor* may increase because malate is at high concentrations (Leegood and von Caemmerer, 1989) and therefore, a high affinity for malate might not be required. Also, despite that the lower affinity for L-malate at pH 8.2 in illuminated leaves of *Sorghum bicolor*, the maximal activity of NADP-malic enzyme increased (Figure 4.10), which aligns with the *in vivo* NADP-malic enzyme activity, which is activated by a light-induced thiol-disulphide interchange (Drincovich and Andreo, 1994). The effect of DTT on the activity of NADP-malic enzyme is also consistent with that of other chloroplastic enzymes, which are regulated by light-dependent redox mechanisms (Jacquot *et al.*, 1981; Ashton and Hatch, 1983; Leegood and Walker, 1983; Drincovich and Andreo, 1994; Raines *et al.*, 2000; Schürmann and Buchanan, 2008; Gütle *et al.*, 2016).

Addition of 10 mM DTT to darkened and illuminated leaf lysates from *Zea mays* lowered the affinity for L-malate by fourfold at pH 7.4. A lower affinity at pH 7.4 may affect the rate of malate decarboxylation at the onset of light, because malate has not accumulated in the stroma. Conversely, the changes in affinity for L-malate were negligible between the oxidised- and reduced-form of the enzyme at pH 8.2. This is significant as it ensures that NADP-malic enzyme reaches maximal activity, with no major changes to its affinity for L-malate at a high pH in the light, regardless whether the enzyme is reduced or not. This mechanism may grant some protection since the redox state of disulphide bonds of NADP-malic enzyme may depend greatly on cellular stimuli or can be blocked under certain conditions such as immune responses (Drincovich and Andreo, 1994; Michelet *et al.*, 2013; Bhattacharjee *et al.*, 2015; Friso and van Wijk, 2015).

4.3.2 PEPCK dependence may influence NADP-malic enzyme activity

NADP-malic enzyme from illuminated leaves of *Setaria viridis* had a broader pH-dependence and exhibited a higher affinity for L-malate at light transitions (Figure 4.14). This suggests that the *in vivo* NADP-malic enzyme activity might be required at the onset of light, in a mechanism similar to that of NADP-malic enzyme from *Sorghum bicolor*. Transcriptomic analyses performed in leaves of *Sorghum bicolor*, *Setaria italica*, which is genetically similar to *Setaria viridis* (Bennetzen *et al.*, 2012) and *Zea mays* (Figure 4.16B and 4.16C) show the relative expression of NADP-malic enzyme and PEPCK in these C_4 grasses. Therefore, it is conceivable that the activity of NADP-malic enzyme might be needed at the onset of light in *Setaria viridis* and *Sorghum bicolor*, because these two grasses have lower expression of PEPCK, whereas *Zea mays* has an appreciable amount of PEPCK (Figure 4.16). In addition to this, since NADP-malic enzyme is localised in the chloroplast, the activity of NADP-malic enzyme would depend more on fine-control by pH than PEPCK (Edwards and Andreo, 1992). Despite being closely related, the pH-dependency of NADP-malic enzyme from *Sorghum bicolor* was drastically different than that of *Zea mays*. Unlike NADP-malic enzyme from illuminated leaves of *Sorghum bicolor*, the activity of NADP-malic enzyme from *Zea mays* was relatively lower at pH 7.4 (Figure 4.6, 4.15). This suggests that decarboxylation by NADP-malic enzyme is not required in the same degree in *Zea mays* at the onset of light, as it seems for NADP-malic enzyme from *Sorghum bicolor* and *Setaria viridis*. One possibility might be that at the onset of light, the C_4-transfer acid in *Zea mays* is preferentially decarboxylated by PEPCK, instead of NADP-malic enzyme. This might also indicate that NADP-malic enzyme from *Zea mays* is differently regulated during light transitions, than the enzyme from *Sorghum bicolor* and *Setaria viridis*. Furthermore, the flux through aspartate and decarboxylation by PEPCK might be more energetically favoured than the flux through malate after the onset of light, since PEP does not need to be regenerated via PPDK using an extra ATP (Wang *et al.*, 2014).

In addition, the conversion of oxaloacetate to malate in the chloroplast of mesophyll cells depends on the MDH, which must also undergo activation by light (Johnson and Hatch, 1970; Jacquot *et al.*, 1981; Ashton and Hatch, 1983; Leegood and Walker, 1983). It is unlikely that the supply of NADPH, which is needed for the conversion of oxaloacetate to malate by reduction, is limiting the rate of malate formation at the onset of light, since

large amounts of NADPH are produced within milliseconds of illumination or supplied from metabolite exchanges (Huber and Edwards, 1975; Furbank and Leegood, 1984; Stitt and Zhu, 2014). Instead, it is conceivable that decarboxylation by PEPCK might not be equally as accessible in *Sorghum bicolor* and *Setaria viridis*, simply because expression of PEPCK is lower in these two grasses (Figure 4.16C). This is also supported by the inability to detect PEPCK in leaves of *Sorghum bicolor* or *Setaria viridis* by mass spectrometry and suggests that the abundance of PEPCK is lower than that of NADP-malic enzyme, which was readily detected in leaves of *Sorghum bicolor* and *Setaria viridis*. Although there may be supplementary PEPCK activity, this shows how much lower the amount of PEPCK is relative to the primary decarboxylase. This is further supported by the inability to detect NADP-malic enzyme in *Megathyrsus maximus* using a similar approach, while PEPCK, its primary decarboxylase (Bräutigam *et al.*, 2014), was readily detected. Comparatively, the expression of PEPCK in *Megathyrsus maximus* is about 88-fold higher than in *Setaria italica* and *Sorghum bicolor* and about 10-fold higher than in *Zea mays*.

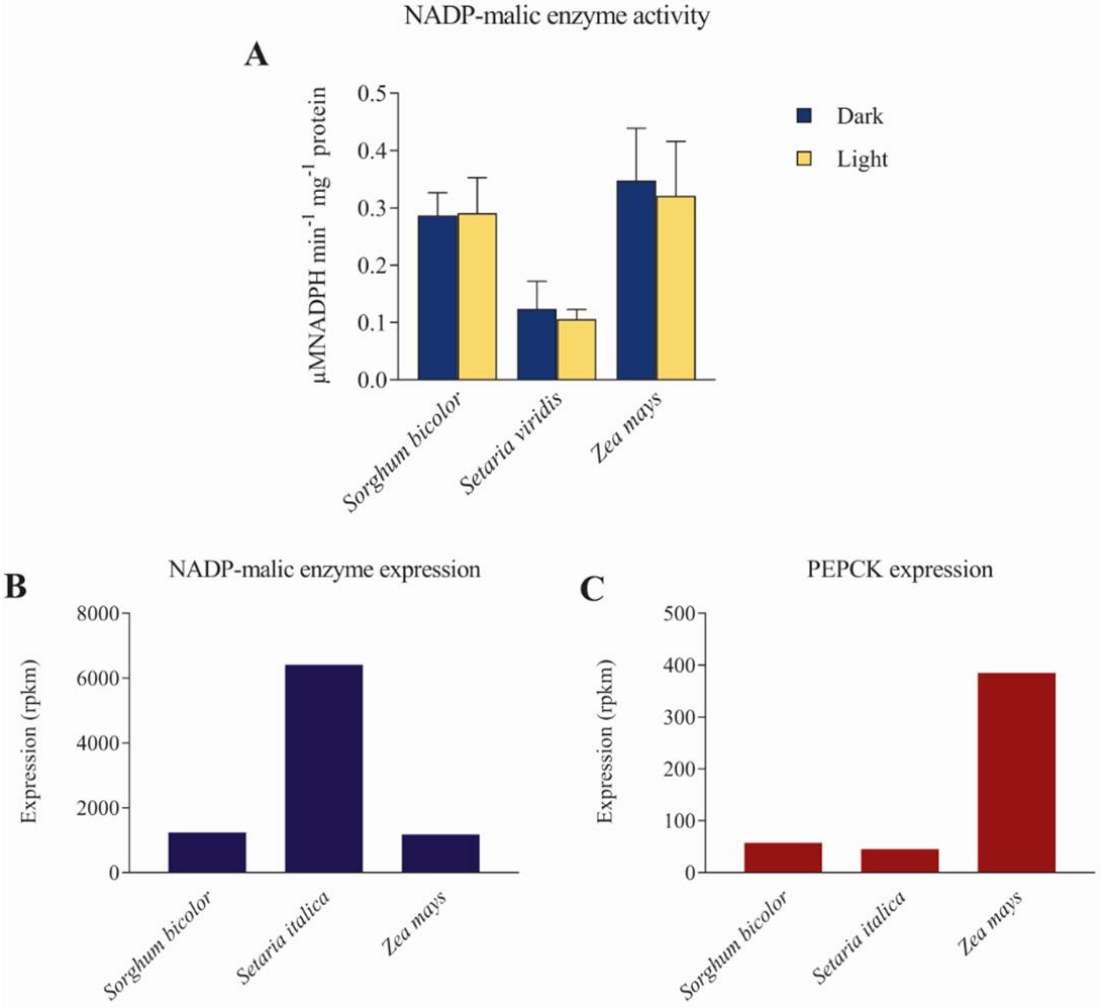

Fig. 4.16. Relative expression of NADP-malic enzyme (B) and PEPCK (C) in C_4 grasses. Activity of NADP-malic enzyme also shown (A). Expression in reads per kilobase million (rpkm). Expression data obtained from PA Christin (unpublished).

In addition, compared to the maximal activity of *Sorghum bicolor* and *Zea mays*, the activity of *Setaria viridis* was substantially lower (Figure 4.16A), while transcriptomic evidence shows that NADP-malic enzyme is highly expressed in *Setaria italica* (Figure 4.16B). K_M plots showed that NADP-malic enzyme at that pH optimum (pH 8.4) did not saturate with 1 mM L-malate (Figure 4.11). This suggests that the activity of NADP-malic enzyme from *Setaria viridis* might have been lower because the concentration of L-malate was limiting the rate of the *in vitro* reaction, rather than containing less NADP-malic enzyme than *Sorghum bicolor* or *Zea mays*. Alternatively, there could have been active inhibitors in the *Setaria viridis* leaf lysates that affected the activity of NADP-malic enzyme. A comparative assessment between the maximal activities of NADP-malic enzyme can be further ascertained by mixing *Zea mays* and *Sorghum bicolor* leaf

lysates with *Setaria viridis* leaf lysates and determine whether activity in the mixed assays is inhibited.

4.3.3 New insights on NADP-malic enzyme regulation in C_4 plants

These results indicate that the pH optimum of NADP-malic enzyme activity varies in C_4 grasses. However, the regulatory mechanisms that promote high activity of NADP-malic enzyme at a lower pH in *Sorghum bicolor*, but not *Setaria viridis* and *Zea mays* are unknown. One major limitation of this investigation is that NADP-malic enzyme was assayed in crude leaf extracts. Firstly, the exact concentration of NADP-malic enzyme cannot be determined because several isoforms of the enzyme are present in the leaf lysate and can, if not equally, contribute to NADP-dependent activity. In addition, kinetic coefficients like V_{max} and K_{cat} cannot be calculated and precise changes in NADP-malic enzyme activity in response to illuminate cannot be ascertained. Secondly, the formation of NADPH may have come from mitochondrial NAD-malic enzyme activity, because it can utilise $NADP^+$ as a co-factor and contribute to NADP-dependent activity (Edwards and Andreo, 1992).

The K_M determined for L-malate in illuminated leaves of *Sorghum bicolor* was close to the K_M previously reported in crude leaf extracts (Table 4.2). The results in this Chapter show that affinity for L-malate decreases during the dark period in *Sorghum bicolor*, which is consistent with the light-dependent activation mechanism. More importantly, these results indicate that the affinity for L-malate does not change *in Zea mays*, and is significantly lower than that found in purified NADP-malic enzyme (Drincovich *et al.*, 2001). This further suggests that there were different isoforms of NADP-malic enzyme in the crude leaf lysate that may have contributed to the reaction. In this case, K_M values reported may be the cumulative kinetic properties of all NADP-malic enzyme isoforms present in the leaf lysate. In addition to the two major isoforms of NADP-malic enzyme in C_4 grasses, evidence in the *Flaveria* species suggests that there are three or four NADP-malic genes in total, one of which encodes a cytosolic enzyme (Marshall *et al.*, 1996; Lai *et al.*, 2002). If the cytosolic enzyme were present in crude leaf lysates, then it is conceivable that its pH optimum is different than that of the chloroplastic form.

Table 4.2. Comparing the K_M for L-malate from previous studies.

Plant species	K_M for L-malate (mM)	K_M for L-malate (mM) (this study)		References
		Dark	Light	
Zea mays	0.19	0.006	0.007	(Drincovich *et al.*, 2001)
Sorghum bicolor	0.10	0.44	0.15	(Nishikido and Wada, 1974)
Setaria viridis	0.25	–	–	(Nishikido and Wada, 1974)

The reason for using crude leaf extracts in this study was to maximise the recovery of NADP-malic enzyme in its phosphorylated state. It is likely that during extraction some enzymes may have been dephosphorylated, thereby losing the chemical modifications that may confer some biochemical change. In addition to this, it is not known to what degree NADP-malic enzyme remained phosphorylated during the reaction assays. Unless the phosphorylated form of NADP-malic enzyme is purified, it is not possible to ascertain whether the phosphorylation state is affecting enzymatic activity. The kinetic properties of NADP-malic enzyme determined in this study may represent both the phosphorylated and dephosphorylated forms of NADP-malic enzyme.

4.3.4 Conclusion

It was shown that the NADP-malic enzyme from *Sorghum bicolor* leaves was distinctly different from the enzyme in *Setaria viridis* and *Zea mays*, supporting the hypothesis that interspecies variation may account for different NADP-malic enzyme requirements. With regards to regulation, pH may modulate the activities of dark and light forms, thus ensuring a seamless transition of chloroplastic activity between light conditions. This aligns with the initial hypothesis and previous speculation (Asami *et al.*, 1979; Edwards and Andreo, 1992). In addition to this, the affinity for L-malate decreased in the light in *Sorghum bicolor*, whereas there was no change in the affinity for L-malate in *Zea mays*. These responses might be particularly important in *Sorghum bicolor*, because of higher requirements for malate decarboxylation than *Zea mays*, which may operate a dual-decarboxylation system, whereby decarboxylation is partitioned between PEPCK and NADP-malic enzyme (Gutierrez *et al.*, 1974; Wang *et al.*, 2014).

Chapter 5 – The regulation of transamination and its involvement in controlling carbon trafficking in C_4 photosynthesis

5.1 Introduction

5.1.1 The dual-decarboxylation system of C_4 photosynthesis

C_4 photosynthesis is a highly complex, but efficient process, which involves the movement of carbon between specialised mesophyll and bundle sheath cells, which partition carboxylation and decarboxylation pathways and compartmentalises cell-specific enzymes such as PEPC and Rubisco (Leegood, 2002; von Caemmerer and Furbank, 2003). To achieve the efficient movement of organic carbon, mesophyll cells surround bundle sheath cells and vascular tissue (Figure 5.1), creating a densely packed, wreath-like arrangement of cells that establishes an intimate relationship between the two cell types.

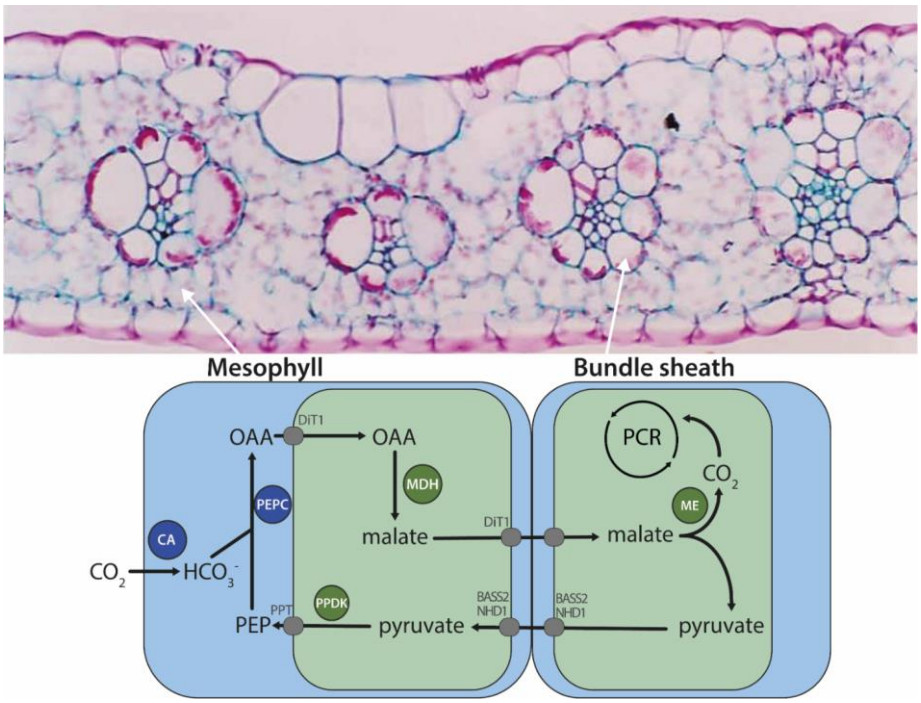

Fig. 5.1. Kranz anatomy in C_4 plants. C_4 leave cross-section (top) shows structure of Kranz anatomy in *Zea mays* made up of concentric tubes of vascular tissue bundle sheath cells and mesophyll cells. Biochemical specialisation of these tissues indicated (bottom).

This arrangement also promotes the rapid diffusion of organic carbon along concentration gradients via plasmodesmata, ensuring the movement of intermediate metabolites that drive the C_4 cycle and contribute to the carbon pool (Osmond, 1971; Hatch and Osmond, 1976; Leegood, 1985; Stitt and Heldt, 1985; Stitt and Zhu, 2014). In their elucidation of C_4 photosynthesis, Hatch and Slack (1966) showed that radioactively labelled CO_2 in sugarcane was rapidly incorporated into oxaloacetate, malate and aspartate, but not initially into metabolites produced in the PCR cycle as previously shown (Benson, 1954; Bassham and Kirk, 1960; Bassham and Calvin, 1962). Further dissection of the C_4 trait revealed that there were distinct biochemical variations in the mechanism used for photosynthetic carbon fixation, thus creating NADP-malic enzyme, PEPCK and NAD-malic enzyme subtypes of the C_4 pathway (Hatch *et al.*, 1975; Furbank, 2011; Furbank, 2016). In NADP-malic enzyme subtype grasses, malate is the predominant C_4-acid utilised during C_4 photosynthesis (Ku *et al.*, 1996), though aspartate also contributes, if not equally, to the CO_2 pool in bundle sheath cells (Andrews *et al.*, 1971; Hatch, 1971; Meister *et al.*, 1996; Bräutigam *et al.*, 2014; Arrivault *et al.*, 2016; Furbank, 2016; Ludwig, 2016). Recent radioactive CO_2 labelling experiments conducted in *Zea mays*, a NADP-malic enzyme subtype, demonstrated that gradients of aspartate, as well as alanine and phospho*enol*pyruvate (PEP), contribute to the transfer of carbon via the PEPCK decarboxylation pathway (Arrivault *et al.*, 2016).

It is apparent that NADP-malic enzyme subtype C_4 plants operate a dual-decarboxylation system (Figure 5.2), whereby C_4-acid decarboxylation, through the conversion of oxaloacetate to aspartate by transamination or to malate by reduction, is divided between PEPCK and NADP-malic enzyme, respectively (Wingler *et al.*, 1999; Furbank, 2011; Pick *et al.*, 2011; Bellasio and Griffiths, 2014; Bräutigam *et al.*, 2014; Furbank, 2016). Also, PEPCK activity in bundle sheath cells may be linked to NAD-malic enzyme decarboxylation in the mitochondria in NAD-malic enzyme type C_4 plants (Bräutigam *et al.*, 2014). One proposed advantage of utilising multiple decarboxylase pathways is that they increase the flexibility of carbon trafficking mechanisms, thus creating pools of intermediate metabolites that are used as a source of carbon in the absence of CO_2 fixation or during intervals of low-light (Leegood and von Caemmerer, 1989; Stitt and Zhu, 2014).

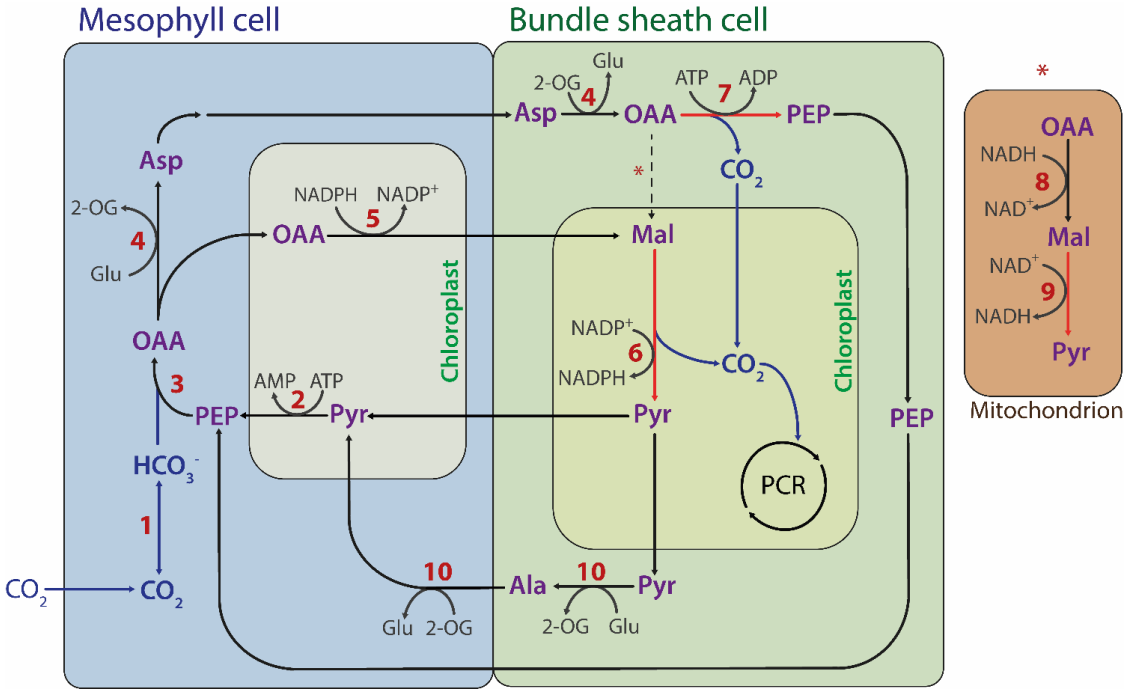

Fig. 5.2. C_4 pathway showing a theoretical dual-decarboxylation system using NADP-malic enzyme (6), PEPCK (7) and NAD-malic enzyme (9). Metabolites (purple/grey): PEP, phospho*enol*pyruvate; OAA, oxaloacetate; Asp, aspartate; Glu, glutamate; 2-OG, 2-oxoglutarate; Mal, malate; Pyr, pyruvate; Ala, alanine. Enzymes: **1**, carbonic anhydrase; **2**, pyruvate, phosphate dikinase; **3**, PEP carboxylase; **4**, aspartate aminotransferase; **5**, NADPH-malate dehydrogenase; **6**, NADP-malic enzyme; **7**, PEP carboxykinase; **8**, NAD-malate dehydrogenase; **9**, NAD-malic enzyme; **10**, alanine aminotransferase. PCR, photosynthetic carbon reduction cycle. Blue arrows indicate movement of assimilated CO_2; red arrows show decarboxylation reactions. Adapted from Wang *et al.* (2014).

It is also plausible that the use of multiple decarboxylases was favoured during the evolution of C_4 photosynthesis, increasing the options for carbon flux, decreasing the concentration of malate required to operate the C_4 cycle, and alleviating the burden on a single transport mechanism (Furbank and Leegood, 1984; Bräutigam *et al.*, 2014; Wang *et al.*, 2014). In fact, several shuttle mechanisms are present in leaves of C_4 plants that aid in the efficiency of net carbon assimilation. In all C_4 plants, a large proportion of 3-phosphoglycerate (3-PGA) produced in bundle sheath cell chloroplasts is transported to mesophyll chloroplasts via the 3-PGA/triose-phosphate shuttle, where it is reduced to triose-phosphates, which are transported back to the bundle sheath, and subsequently used for the regeneration of ribulose-1,5-bisphosphate (RuBP) (Hatch, 1987). Similarly, the interconversion of 3-PGA and PEP is proposed to serve in the flux of carbon from bundle sheath to mesophyll cells and increase the amounts of C_4 metabolites, though its

regulation is not known (Furbank and Leegood, 1984; Leegood and von Caemmerer, 1989; Bräutigam *et al.*, 2014; Arrivault *et al.*, 2016). The regulation of carbon movement through the relative flux of aspartate and malate in plants operating a dual-decarboxylation system is not entirely understood. Furthermore, there has been some debate as to how much the secondary decarboxylation by PEPCK contributes to photosynthetic efficiency of C_4 plants and whether flux through aspartate is necessary for maintaining biochemical stability in plants operating a NADP-malic enzyme system (Bräutigam *et al.*, 2014; Wang *et al.*, 2014). Additionally, there is no evidence in C_4 grasses that the interconversion between aspartate and oxaloacetate via aspartate aminotransferase or pyruvate and alanine via alanine aminotransferase is regulated at the protein level. The formation of aspartate and alanine is linked to PEPCK and NAD-malic enzyme decarboxylation (Wang *et al.*, 2014) (Figure 5.2, reactions 4 and 10) and alanine might control the flux of carbon through this decarboxylation pathway by regulating the activity aspartate aminotransferase. To address whether alanine can stimulate the activity of aspartate aminotransferase and understand the regulation of carbon movement, through shuttle mechanisms associated with decarboxylation by PEPCK and NADP-malic enzyme, the kinetics of aspartate and alanine aminotransferase were studied in three NADP-malic enzyme C_4 grasses: *Setaria viridis*, *Sorghum bicolor* and *Zea mays.*

5.1.2 Regulation of aspartate and alanine aminotransferase

Fig. 5.3. Interconversion of aspartate and oxaloacetate by aspartate aminotransferase.

Aspartate aminotransferase (EC 2.6.1.1) catalyses the interconversion of L-aspartate (Asp) and 2-oxoglutarate (2-OG) to L-glutamate (Glu) and oxaloacetate (OAA) (Figure 5.3), by coupling to pyridoxal 5-phosphate (PLP), via a ping-pong kinetic mechanism (Toney, 2014) in mesophyll and bundle sheath cells of C_4 plants typically using the NAD-malic enzyme or PEPCK decarboxylation pathway (Hatch, 1987). In the first reaction, aspartate aminotransferase coupled with PLP reacts with L-aspartate forming pyridoxamine 5-phosphate (PMP) enzyme and oxaloacetate, then aspartate

aminotransferase coupled with PMP reacts with 2-oxoglutarate forming L-glutamate and regenerates PLP (Toney, 2014). In NAD-malic enzyme subtypes, there are three aspartate aminotransferase isoforms, two of which are specific to C_4 photosynthesis and present either in the mesophyll cytosol or in mitochondria of bundle sheath cells (Kanai and Edwards, 1999). The third isoform does not contribute to C_4-specific activity and resembles the C_3-form localised in chloroplasts (Taniguchi and Sugiyama, 1990). In *Panicum miliaceum* (NAD-malic enzyme subtype) there are three major alanine aminotransferase isoforms (Kanai and Edwards, 1999). In plants alanine aminotransferase (EC 2.6.1.2) catalyses the interconversion between L-alanine and 2-oxoglutarate to L-glutamate and pyruvate (Figure 5.4) and besides its essential role in C_4 photosynthesis, it is involved in gluconeogenesis, glycolysis and amino acid metabolism (McAllister and Good, 2015).

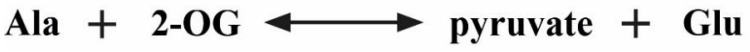

Fig. 5.4. Interconversion of aspartate and oxaloacetate by aspartate aminotransferase.

Aspartate and alanine aminotransferase serve a central role in C_4 photosynthesis (Andrews *et al.*, 1971; Hatch and Mau, 1973; Pick *et al.*, 2011; Toney, 2014; Wang *et al.*, 2014), however their underlying regulatory mechanisms and catalytic properties for the transamination of oxaloacetate and L-aspartate by aspartate aminotransferase or pyruvate and L-alanine by alanine aminotransferase, along with their involvement in the flux of carbon with regards to the partitioning control of PEPCK and NADP-malic enzyme decarboxylation, are yet to be elucidated in C_4 grasses. Large pools of metabolites are required to drive the C_4 cycle (Leegood and Furbank, 1984; Leegood and von Caemmerer, 1989; Stitt and Zhu, 2014), however the effect of feedback inhibition or activation by transfer acids such as malate and alanine on the activity of aspartate aminotransferase has not been explored in NADP-malic enzyme subtypes. Since aspartate aminotransferase acts as a bridge for the PEPCK pathway, activation by alanine or malate might be a requirement in C_4 grasses that can switch between NADP-malic enzyme and PEPCK decarboxylation. It is therefore hypothesised that C_4 grasses with the ability to use both decarboxylation pathways, such as *Zea mays*, might be conditioned to maintain high aspartate aminotransferase activity in the presence of malate and alanine. The results in this Chapter will show that the kinetic properties of aspartate

aminotransferase are sensitive to dark and light changes and that the response to effector metabolites may contribute to a much greater role in regulating the movement of carbon through the PEPCK and NADP-malic enzyme decarboxylation pathways. These novel findings indicate that the efficiency and flexibility of C_4 photosynthesis depends on the proper regulation of aspartate and alanine aminotransferase in NADP-malic enzyme subtypes.

5.2 Results

5.2.1 The role and regulation of aspartate aminotransferase in C_4 photosynthesis

The kinetic properties of aspartate aminotransferase were determined in the forward direction, following the conversion of L-aspartate to oxaloacetate and glutamate utilising 2-oxoglutarate (Wilkie and Warren, 1998; Toney, 2014). Novel phosphoproteomic data presented in Chapter 3 showed that aspartate aminotransferase isoforms undergo phosphorylation predominantly in darkened conditions. To further investigate the regulation of aspartate aminotransferase in response to illumination, changes in Michaelis-Menten kinetics were determined for its primary substrate, L-aspartate, and secondary substrate, 2-oxoglutarate, in *Setaria viridis*, *Sorghum bicolor* and *Zea mays*.

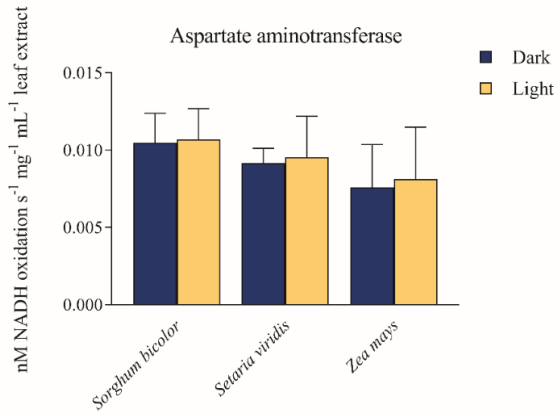

Fig. 5.5. Activity of aspartate aminotransferase in *Sorghum bicolor*, *Setaria viridis* and *Zea mays*. The activity of aspartate aminotransferase was determined towards the formation of oxaloacetate using 2.5 mM L-aspartate and 2-oxoglutarate. Data are based on six biological replicates and the error bars show the standard deviation.

There was no difference in the activity of aspartate aminotransferase in the presence of 2.5 mM L-aspartate, in leaf lysates of *Sorghum bicolor*, *Setaria viridis* and *Zea mays* (Figure 5.5). In addition, aspartate aminotransferase was not active in the presence of L-alanine. To determine the concentration of L-aspartate and 2-oxoglutarate required to reach saturation, the activity of aspartate aminotransferase was assayed in response to increasing substrate concentrations. The initial activity of aspartate aminotransferase was high in *Setaria viridis* and *Sorghum bicolor* darkened and illuminated leaves, but low in *Zea mays*. In *Setaria viridis* (Figure 5.6), the aspartate aminotransferase K_M for L-aspartate increased from 1624 ± 233.8 µM to 2334 ± 392.8 µM after the dark to light transition, equivalent to approximately a 0.44-fold decrease in affinity for L-aspartate. Similarly, the K_M for 2-oxoglutarate increased 0.20-fold in response to illumination.

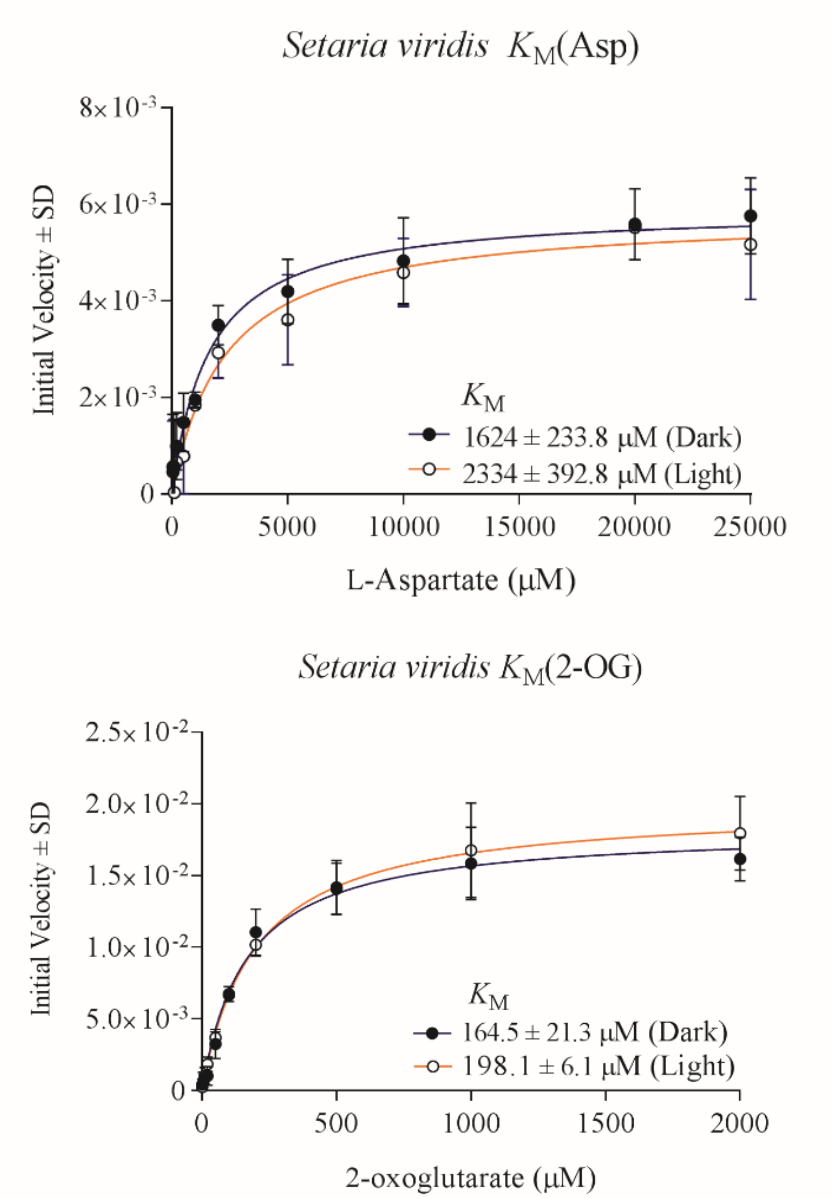

L-Aspartate (K_M ± SE µM)		2-oxoglutarate (K_M ± SE µM)	
Dark	Light	Dark	Light
1624 ± 233.8	2334 ± 392.8	164.5 ± 21.3	198.1 ± 6.1

Fig. 5.6. Aspartate aminotransferase affinity for L-aspartate and 2-oxoglutarate declines in response to light in *Setaria viridis*. Michaelis-Menten curves for the aspartate aminotransferase reaction in darkened (black lines, black dots) and illuminated (yellow lines, clear dots) *Setaria viridis* leaves in response to increasing L-aspartate (Asp) or 2-oxoglutarate (2-OG) concentrations. K_M was determined at pH 8.0. Data are based on six biological replicates and error bars show the standard deviation (SD). SE, standard error. Units for initial velocity are Abs/min.

The Michaelis-Menten curve of *Sorghum bicolor* (Figure 5.7) was similar to that of *Setaria viridis* (5.6). However, the change in the aspartate aminotransferase K_M for L-aspartate was more substantial in response to the dark to light transition in *Sorghum bicolor* (Figure 5.7). In *Sorghum bicolor*, the K_M for L-aspartate increased from 1782 ± 256.2 µM to 5185 ± 1378.0 µM after illumination, which was about twice as high as the K_M for L-aspartate in *Setaria viridis*. Conversely, the K_M for 2-oxoglutarate declined in response to light in *Sorghum bicolor* leaves. In *Setaria viridis* and *Zea mays*, the K_M for 2-oxoglurate increased after illumination.

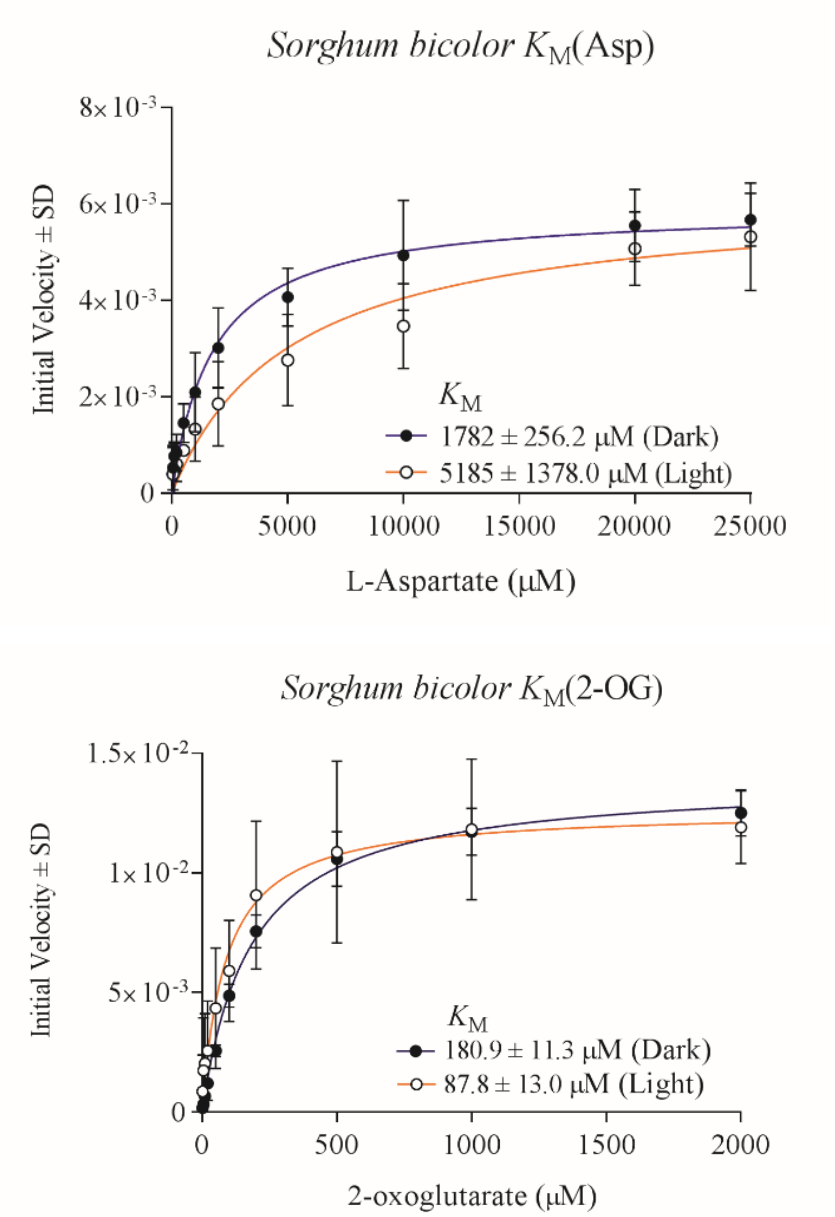

L-Aspartate (K_M ± SE µM)		2-oxoglutarate (K_M ± SE µM)	
Dark	Light	Dark	Light
1782 ± 256.2	5185 ± 1378.0	180.9 ± 11.3	87.8 ± 13.0

Fig. 5.7. Light-induced changes to aspartate aminotransferase affinity for L-Asp and 2-oxoglutarate in *Sorghum bicolor*. Michaelis-Menten curves for the aspartate aminotransferase reaction in darkened (black lines, black dots) and illuminated (yellow lines, clear dots) *Sorghum bicolor* leaves in response to increasing L-aspartate or 2-oxoglutarate (2-OG) concentrations. K_M was determined at pH 8.0. Data are based on six biological replicates and error bars show the standard deviation (SD). SE, standard error. Units for initial velocity are Abs/min.

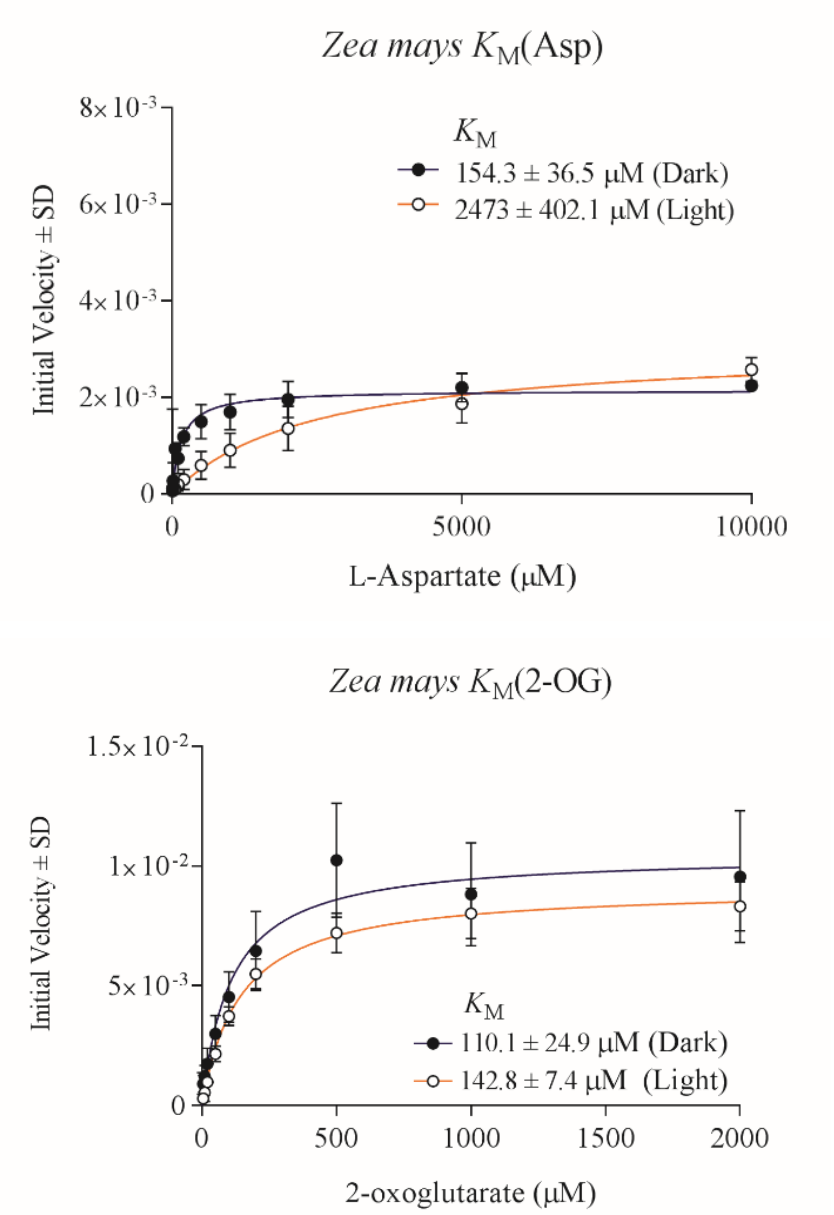

L-Aspartate (K_M ± SE µM)		2-oxoglutarate (K_M ± SE µM)	
Dark	Light	Dark	Light
154.3 ± 36.5	2473 ± 402.1	110.1 ± 24.9	142.8 ± 7.4

Fig. 5.8. Aspartate aminotransferase affinity for L-aspartate declines after the onset of light in *Zea mays*. Michaelis-Menten curves for the aspartate aminotransferase reaction in darkened (black dots) and illuminated (clear dots) *Zea mays* leaves in response to increasing L-aspartate or 2-oxoglutarate (2-OG) concentrations. Data are based on six biological replicates and error bars show the standard deviation (SD). SE, standard error. Units for initial velocity are Abs/min.

While the changes in K_M for L-aspartate and 2-oxoglutarate were significantly different in *Setaria viridis* and *Sorghum bicolor*, aspartate aminotransferase displayed similar rates of activity. In contrast, the activity of aspartate aminotransferase in *Zea mays* decreased by approximately 0.7-fold in saturating conditions with 10 mM L-aspartate (Figure 5.8). Aspartate aminotransferase from darkened leaves reached saturation in the presence of at least 2.5 mM L-aspartate, while the aspartate aminotransferase in illuminated leaves did not saturate until 10 mM L-aspartate. Additionally, the K_M for L-aspartate increased from 154.3 ± 36.5 µM to 2473 ± 402.1 µM after the dark to light transition in *Zea mays*, which was higher than the observed changes to the affinity for L-aspartate in *Setaria viridis* and *Sorghum bicolor* in response to light. The affinity for L-aspartate and 2-oxoglutarate decreased in the dark to light transition in the three C_4 grasses, but the dark and light affinity differences for L-aspartate were most evident in *Zea mays*, followed by *Sorghum bicolor* and *Setaria viridis* (Table 5.1).

Table 5.1. **Aspartate aminotransferase affinity for primary and secondary substrates after 15.5 h illumination**. Summary of the change in aspartate aminotransferase affinities for L-aspartate and 2-oxoglutarate in response to light. In 15.5 h illuminated leaves, the decrease in affinity for L-aspartate was highest in *Zea mays*, moderate in *Sorghum bicolor* and smallest in *Setaria viridis*. The affinity for 2-oxoglutarate increased in *Sorghum bicolor* after the transition to light, but decreased in both *Setaria viridis* and *Zea mays*. Up-arrows indicate increase in affinity (a negative fold change, decrease in K_M), while down-arrows indicate decrease in affinity (a positive fold change, increase in K_M).

	L-Aspartate	2-oxoglutarate
	Affinity (fold change)	
Sorghum bicolor	1.9 ↓	0.51 ↑
Setaria viridis	0.44 ↓	0.20 ↓
Zea mays	15.0 ↓	0.30 ↓

Aspartate aminotransferase affinity for dimethyl-2-oxoglutarate, an analogue of 2-oxoglutarate produced during glucose metabolism (Odegaard *et al.*, 2010), was also tested. The changes in K_M for 2-oxoglutarate and dimethyl-2-oxoglutarate were larger in *Zea mays* followed equally by *Sorghum bicolor* and *Setaria viridis* (Figure 5.9). Aspartate aminotransferase activity was reduced across all three C_4 species, but was relatively higher in *Setaria viridis*. Moreover, the response to dimethyl-2-oxoglutarate was more consistent in darkened and illuminated *Setaria viridis* leaves, unlike *Sorghum bicolor* and *Zea mays*. The activity of aspartate aminotransferase in *Sorghum bicolor* and *Zea mays* declined in the presence of dimethyl-2-oxoglutarate and less consistent than in *Setaria viridis*.

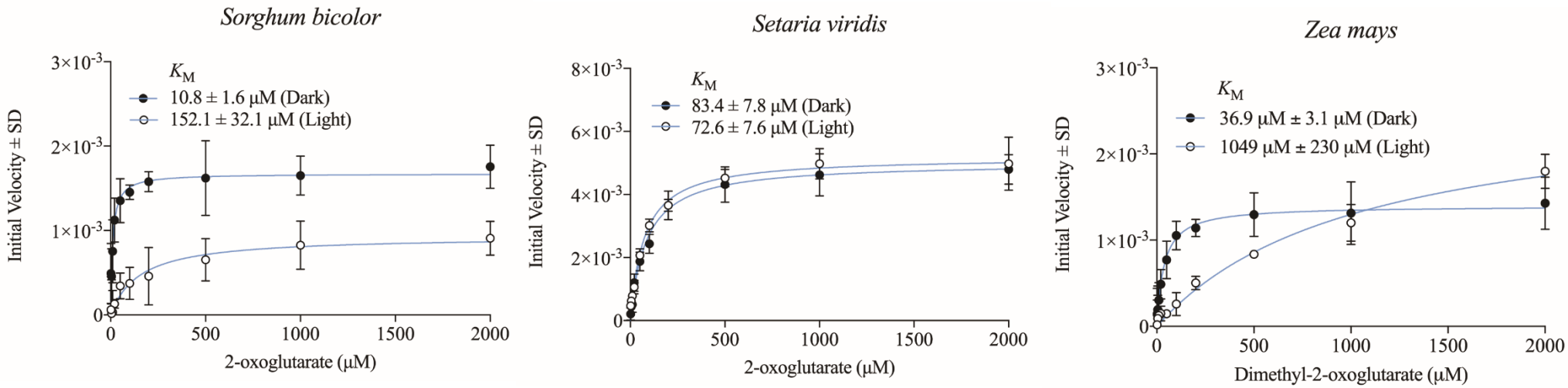

Species	Dimethyl-2-oxoglutarate (K_M ± SE µM)	
	Dark	Light
Sorghum bicolor	10.8 ± 1.6	152.1 ± 32.1
Setaria viridis	83.4 ± 7.8	72.6 ± 7.6
Zea mays	36.9 ± 3.1	1049 ± 230

Fig. 5.9. Dark and light *Setaria viridis* aspartate aminotransferase responds better to dimethyl-2-oxoglutarate. Michaelis-Menten curves for the aspartate aminotransferase reaction in darkened (black dots) and illuminated (white dots) leaves in response to increasing dimethyl-2-oxoglutarate concentrations. Data are based on six biological replicates and error bars show the standard deviation (SD). SE, standard error. Units for initial velocity are Abs/min.

5.2.2 The effect of metabolites on the activity of aspartate aminotransferase

The sensitivity of aspartate aminotransferase activity was tested in response to metabolites produced during C_4 photosynthesis. In *Setaria viridis*, *Sorghum bicolor* and *Zea mays*, increasing concentrations of L-malate reduced activity in darkened and illuminated leaves (Figure 5.10). However, the magnitude of the inhibitory effect of L-malate was different across the three C_4 species. In Figure 5.10B, aspartate aminotransferase from *Sorghum bicolor* illuminated leaves showed the highest decrease in activity in the presence of 20 and 50 mM L-malate when compared to the controls (paired *t*-test: df=5, $P < 0.001$). This trend was closely followed by *Setaria viridis* (Figure 5.10A), in which the changes of enzyme activity between controls and 10, 20 and 50 mM L-malate was also significant (paired *t*-test: df=5, $P < 0.001$). Conversely, the activity in darkened and illuminated *Zea mays* leaves was the least affected by increasing L-malate concentrations (Figure 5.10C) when compared to aspartate aminotransferase activity in *Setaria viridis* and *Sorghum bicolor*. In darkened leaves of *Sorghum bicolor*, the inhibitory effect of L-malate was evident in the presence of 10 mM (Figure 5.10B), whereas the activity of aspartate aminotransferase in illuminated leaves was unaffected, suggesting that in the light, the enzyme was less responsive to increasing L-malate concentrations. Additionally, the activity of aspartate aminotransferase from darkened leaves was not further reduced in the presence of 20 or 50 mM L-malate, while activity decreased in illuminated leaves. This effect was also observed in *Setaria viridis* leaves (Figure 5.10A), however aspartate aminotransferase activity in *Setaria viridis* was lower in the presence of 10 mM L-malate. Although the differences in activity between control reaction assays and treatment with L-malate were significant, the changes in activity between the different concentrations of L-malate were not significant.

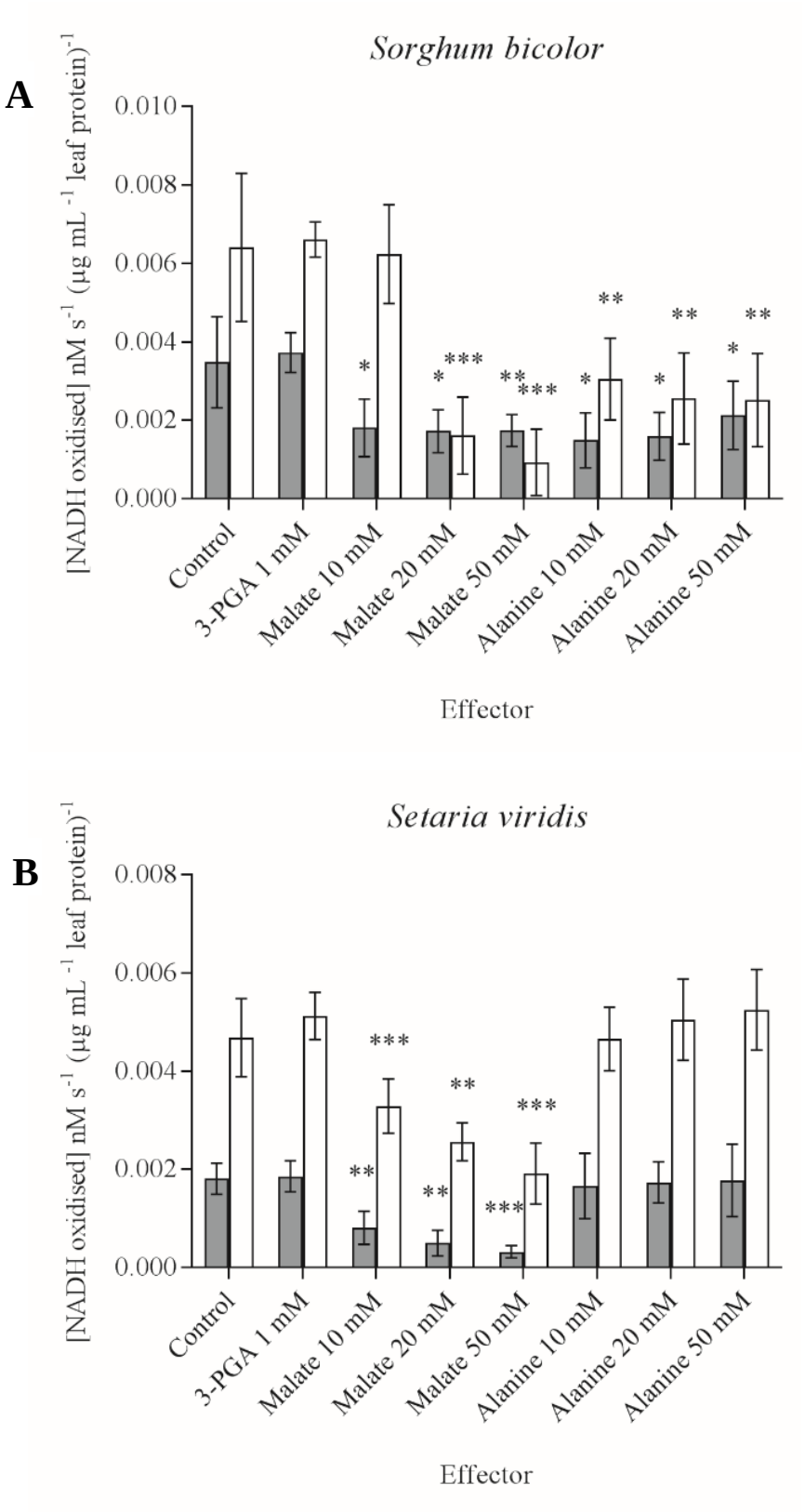
A
Sorghum bicolor
[NADH oxidised] nM s-1 (µg mL -1 leaf protein)-1
0.010
0.008
0.006
0.004
0.002
0.000
Control
3-PGA 1 mM
Malate 10 mM
Malate 20 mM
Malate 50 mM
Alanine 10 mM
Alanine 20 mM
Alanine 50 mM
Effector
B
Setaria viridis
[NADH oxidised] nM s-1 (µg mL -1 leaf protein)-1
0.008
0.006
0.004
0.002
0.000
Control
3-PGA 1 mM
Malate 10 mM
Malate 20 mM
Malate 50 mM
Alanine 10 mM
Alanine 20 mM
Alanine 50 mM
Effector

Fig. 5.10.

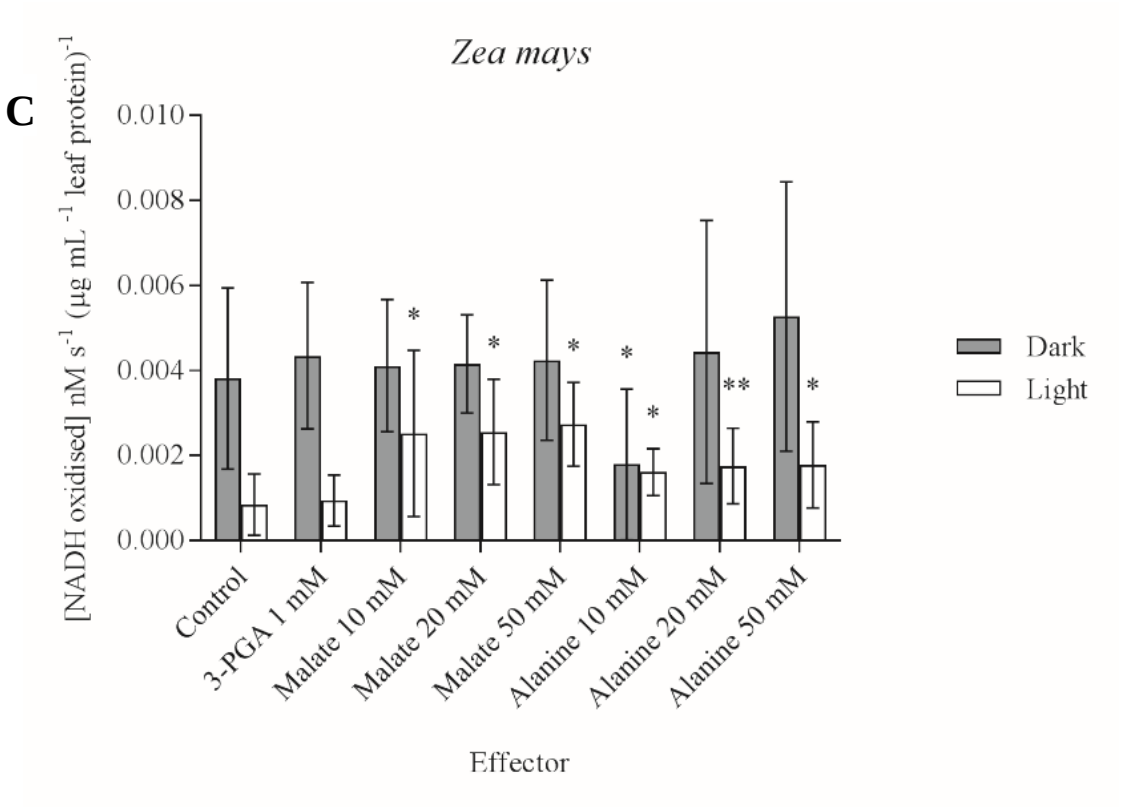

Fig. 5.10. 3-PGA, L-alanine and L-malate affect aspartate aminotransferase activity differently in three C_4 species. Activity bar graphs show the rate of aspartate aminotransferase activity from darkened (grey bars) and illuminated (white bars) *Setaria viridis* (**A**), *Sorghum bicolor* (**B**) and *Zea mays* (**C**) leaves in response of 10, 20 and 50 mM L-malate and L-alanine, and 1 mM 3-PGA. An inhibitory effect is observed by bars lowering relatively to controls, whereas an activation effect is observed by bars increasing relatively to controls. The changes to aspartate aminotransferase activity in the presence of L-malate and L-alanine were most significant in *Sorghum bicolor* and least significant in *Zea mays*. In *Setaria viridis*, activity lowered in response to L-malate, but not L-alanine. 1 mM 3-PGA had no effect on the activity of aspartate aminotransferase across all species. 3-PGA, phosphoglycerate. The significance between the average activity between control and metabolite concentrations were determined by paired *t*-tests, where * = $P < 0.05$, ** = $P < 0.005$, *** = $P < 0.0005$. Error bars show the standard deviation.

Unlike *Sorghum bicolor* and *Zea mays*, the activity of aspartate aminotransferase from darkened and illuminated *Setaria viridis* leaves was not inhibited by increasing concentrations of L-alanine (Figure 5.10A–C). However, despite that the activity of aspartate aminotransferase was lower in response to L-alanine in *Sorghum bicolor*, enzyme activity in *Zea mays* in response to L-alanine was enhanced across all concentrations (Figure 5.10C), though not significantly in darkened leaves.

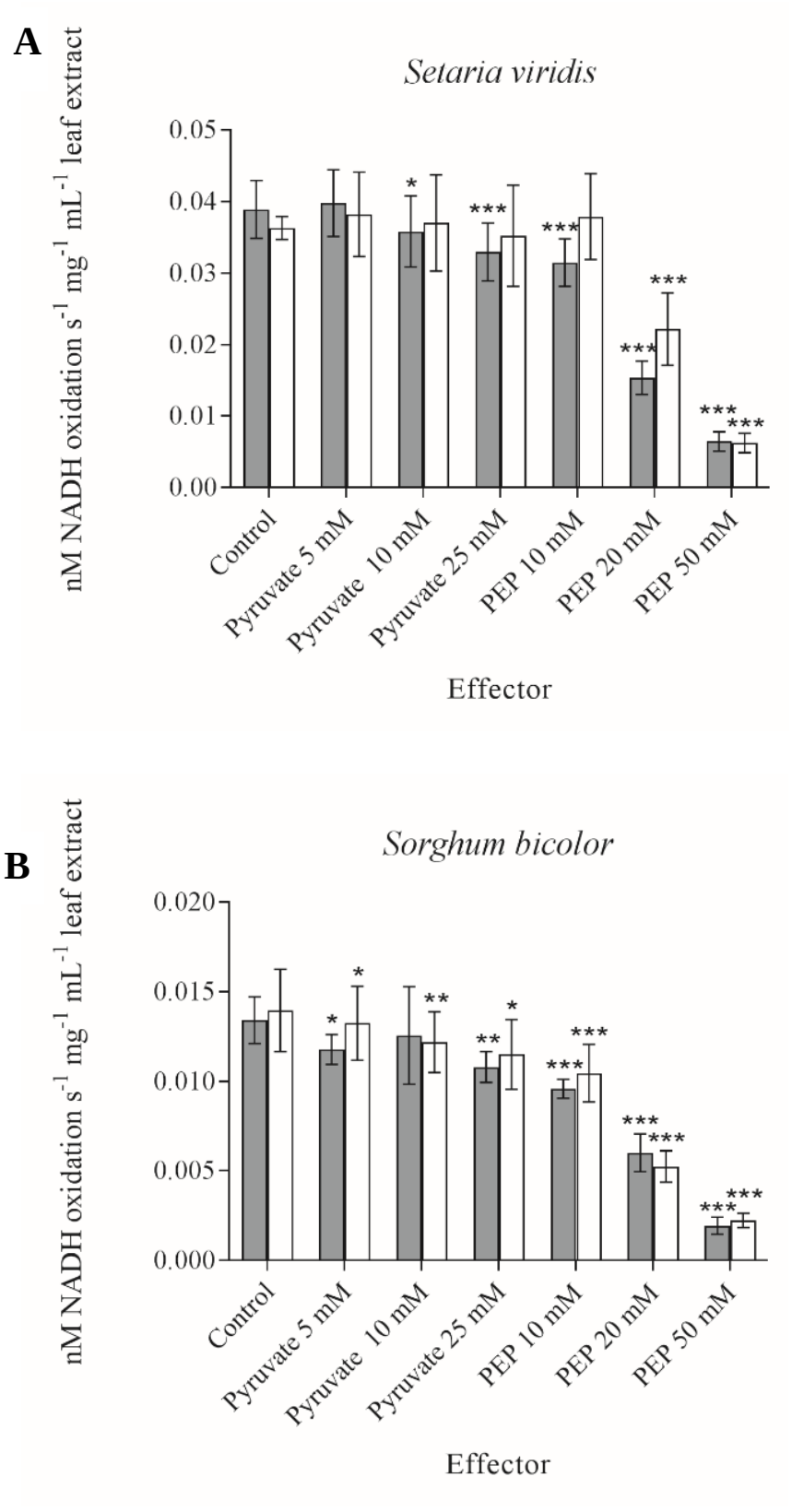
A
Setaria viridis
nM NADH oxidation s-1 mg-1 mL-1 leaf extract
0.05
0.04
0.03
0.02
0.01
0.00
Control
Pyruvate 5 mM
Pyruvate 10 mM
Pyruvate 25 mM
PEP 10 mM
PEP 20 mM
PEP 50 mM
Effector
B
Sorghum bicolor
nM NADH oxidation s-1 mg-1 mL-1 leaf extract
0.020
0.015
0.010
0.005
0.000
Control
Pyruvate 5 mM
Pyruvate 10 mM
Pyruvate 25 mM
PEP 10 mM
PEP 20 mM
PEP 50 mM
Effector

Fig. 5.11.

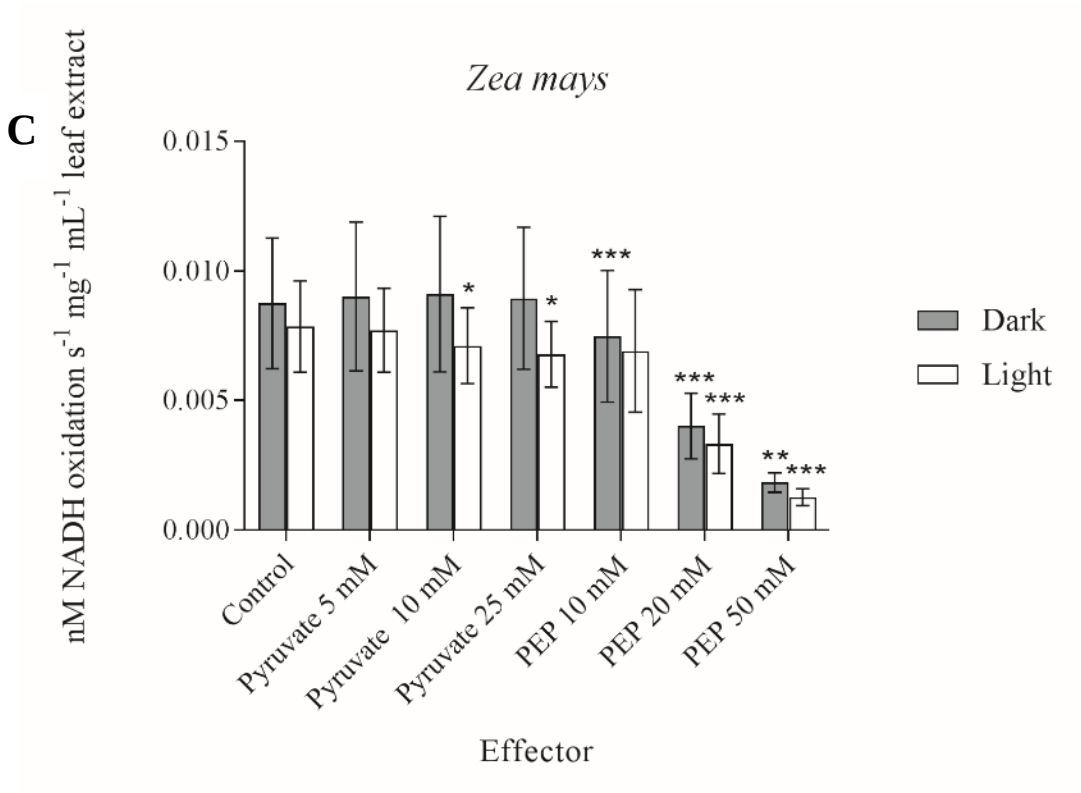

Fig. **5**.**11**. **Aspartate aminotransferase activity in response to PEP and pyruvate**. Activity bar graphs show the rate of aspartate aminotransferase activity from darkened (grey bars) and illuminated (white bars) *Setaria viridis* (**A**), *Sorghum bicolor* (**B**) and *Zea mays* (**C**) leaves in response of 5, 10 and 25 mM pyruvate and 10, 20 and 50 mM phospho*enol*pyruvate (PEP). PEP reduces aspartate aminotransferase activity equally across C_4 species, while pyruvate has no effect on activity. The significance between the average activity between control and metabolite concentrations were determined by paired *t*-tests, where * = $P < 0.05$, ** = $P < 0.005$, *** = $P < 0.0005$. Error bars show the standard deviation.

The activity of aspartate aminotransferase in *Setaria viridis, Sorghum bicolor* and *Zea mays* was differently affected by L-malate and L-alanine and it was evident that the sensitivity to L-malate and L-alanine of light and dark activities were most significant in *Sorghum bicolor* (Figure 5.10B). Activity in *Setaria viridis* was most affected by L-malate, but not by L-alanine (Figure 5.10A), whereas increasing concentrations of L-malate and L-alanine had the least inhibitory effects on aspartate aminotransferase activity in *Zea mays* (Figure 5.10C). There was no effect on the activity of 1 mM 3-PGA on aspartate aminotransferase across all C_4 species.

Aspartate aminotransferase activity was unaffected by 5 mM pyruvate (Figure 5.11A–C). Changes to mean activities between controls and 25 mM pyruvate were most significant in darkened *Setaria viridis* leaves (paired *t*-test; df = 5, $P < 0.001$) as shown in Figure 5.11A, although, the standard deviation showed a large degree of variation in enzyme activity across the six biological replicates. Furthermore, the inhibitory effect of pyruvate was more evident in illuminated *Sorghum bicolor* leaves in the presence of 10 mM pyruvate (paired *t*-test; df = 5, $P = 0.0037$) (Figure 5.11B) than in the presence of 25 mM pyruvate (paired *t*-test; df = 5, $P = 0.0359$). The activity of aspartate aminotransferase in *Zea mays* leaves was the least affected by pyruvate (Figure 5.11C), although changes in activity in illuminated leaves in the presence of 10 mM and 25 mM were significant (paired *t*-test; df = 5, $P < 0.05$). Conversely, all C_4 plants were equally affected by increasing concentrations of PEP. Aspartate aminotransferase remained active in darkened and illuminated leaves in up to 50 mM PEP, but activity decreased 0.81-fold in *Zea mays*, 0.84-fold in *Sorghum bicolor* and 0.83-fold in *Setaria viridis*, when compared to controls (Figure 5.11A–C).

5.2.3 Specific activity of alanine aminotransferase

Alanine aminotransferase from *Sorghum bicolor*, *Setaria viridis* and *Zea mays* was assayed *in vitro* in the reverse direction towards the formation of pyruvate by coupling to lactate dehydrogenase (LDH). No enzyme activity was observed in reaction mixtures containing 20 mM L-alanine. Based on alanine aminotransferase assays in *Arabidopsis thaliana* (Miyashita *et al*., 2007), the concentration of L-alanine was increased to 25, 50 and 75 mM. However, after 20 min, there was no activity. In the negative control, there was no activity observed in the presence of L-aspartate.

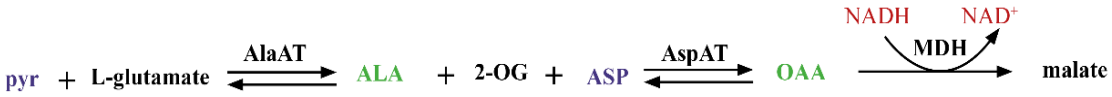

Fig. 5.12. Alanine aminotransferase (AlaAT) reaction mechanism towards the formation of malate. Metabolites in purple were added to the reaction mixture and metabolites in green were produced during the reaction. Assay measures the formation of malate through the oxidation of NADH (in red). Pyr, pyruvate; 2-OG, 2-oxoglutarate; OAA, oxaloacetate. Aspartate aminotransferase (AspAT) and malate dehydrogenase (MDH).

Alanine aminotransferase was also assayed in the forward direction towards the formation of malate, coupling to aspartate aminotransferase and malate dehydrogenase (MDH) (Figure 5.12). Activity was measured 10 min after priming the reaction assay with leaf protein. Preliminary measurements showed that the activity of alanine aminotransferase was highest in *Setaria viridis*, when compared to *Sorghum bicolor* and *Zea mays* (Figure 5.13).

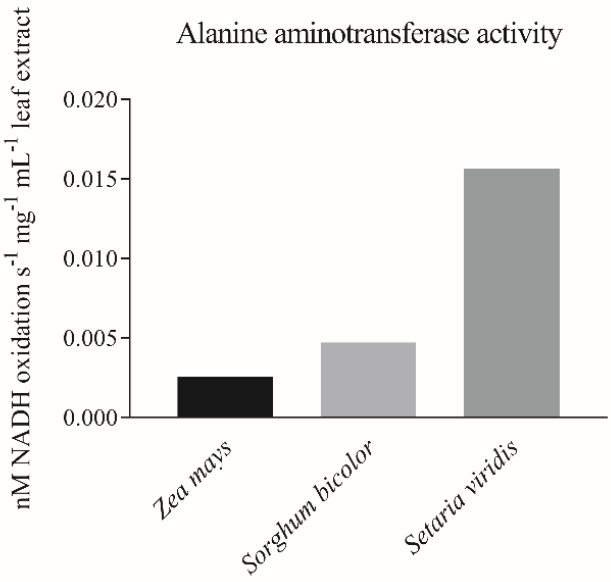

Fig. 5.13. Alanine aminotransferase activity in illuminated *Zea mays*, *Sorghum bicolor* and *Setaria viridis* leaf lysates. Alanine aminotransferase was assayed in the forward direction towards the formation of alanine in leaf lysates normalised against the lowest total protein concentration. Preliminary data are based on one biological replicate from 15.5 h illuminated leaves.

The assay was repeated with four biological replicates, normalised against the lowest total protein concentration. The second assay showed that the activity of alanine aminotransferase was highest in *Setaria viridis* (Figure 5.14), consistent with preliminary data in Figure 5.13. There was no significant difference in the activity of alanine aminotransferase in *Zea mays* and *Sorghum bicolor*. Also, there was no change in activity between darkened and illuminated leaf protein.

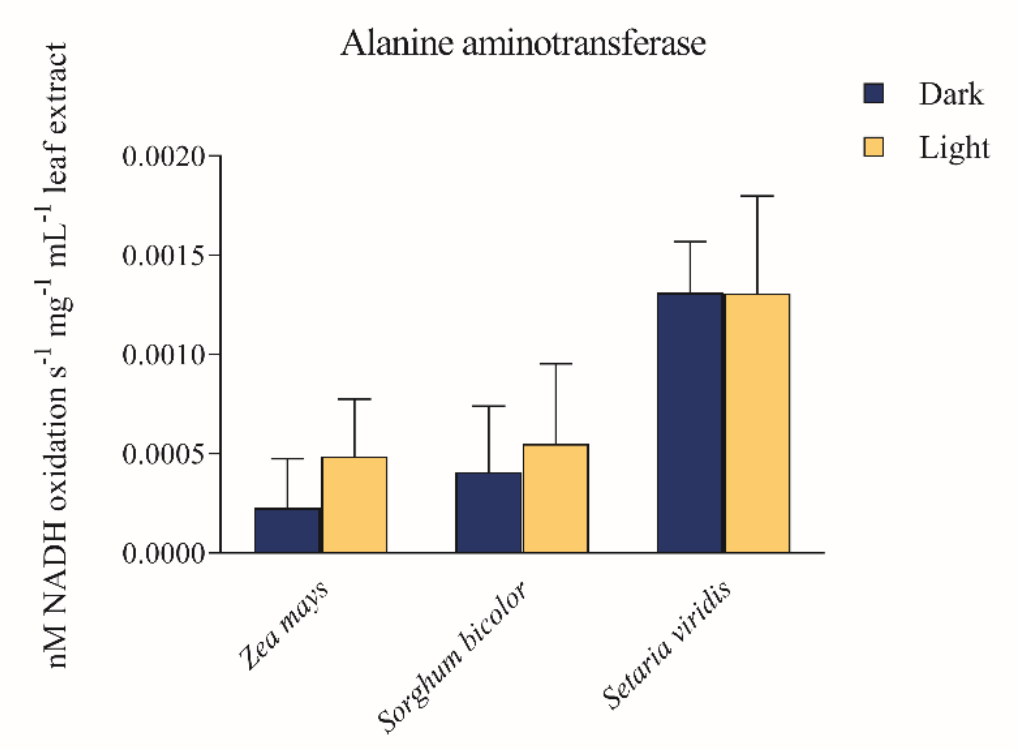

Fig. 5.14. Alanine aminotransferase activity in *Setaria viridis* leaf lysates is higher than in *Zea mays* and *Sorghum bicolor*. Alanine aminotransferase was assayed in the forward direction towards the formation of alanine in leaf lysates normalised against the lowest total protein concentration. Data are based on four biological replicates and error bars show the standard deviation.

5.3 Discussion

5.3.1 Aspartate aminotransferase affinity aspartate is sensitive to dark–light transitions

C_4 plants that use NADP-malic enzyme as the primary decarboxylase may also use a supplementary decarboxylation pathway via PEPCK through the conversion of oxaloacetate to aspartate and then back to oxaloacetate (Pick *et al.*, 2011; Bräutigam *et al.*, 2014; Wang *et al.*, 2014) (Figure 5.2). Previous studies have noted that the C_4-acid transfer via aspartate aminotransferase is essential in plants with low NADP-malic enzyme activity (Andrews *et al.*, 1971; Hatch and Mau, 1973; Meister *et al.*, 1996). However, the regulation of carbon flux through aspartate in C_4 grasses that predominantly use NADP-malic enzyme remains unclear. The results in this Chapter show that the catalytic properties of aspartate aminotransferase from three NADP-malic enzyme subtypes are sensitive to dark to light transitions and there may be interspecies differences, particularly with regards to regulation by transfer acids. In the three C_4 species studied, the affinity for L-aspartate declined in illuminated leaves, which suggests that the conversion of aspartate to oxaloacetate may be regulated in illuminated conditions, but could correlate to the initial increase of aspartate in illuminated leaves (Leegood and von Caemmerer, 1989). Increased affinity for L-aspartate in darkened conditions is consistent with previous findings that showed that major aspartate aminotransferase isoforms have increased activity in dark-grown plants (Hatch and Mau, 1973). In activity assays (Figure 5.5), there was no change in aspartate aminotransferase activity in darkened and illuminated leaves, which is not characteristic of major isoforms as previously shown (Hatch and Mau, 1973). It is possible that activity from minor isoforms was observed and could have masked changes in dark and light activity of major isoforms.

In *Megathyrsus maximus* (PEPCK subtype), the K_M for L-aspartate is 2.3 mM (Numazawa *et al.*, 1989), which is close to the K_M for L-aspartate in illuminated leaves of *Setaria viridis* (2.3 mM) and *Zea may* (2.5 mM), but not *Sorghum bicolor* (5.2 mM), which may require relatively less PEPCK activity (Gutierrez *et al.*, 1974). In addition, the K_M for oxaloacetate in *Megathyrsus maximus* is 0.049 mM (Numazawa *et al.*, 1989) and although not determined in this study, the K_M for oxaloacetate may be lower than

that of L-aspartate in the NADP-malic enzyme subtypes. Large fluxes of oxaloacetate are generated by PEPC in the light, but oxaloacetate does not accumulate to high concentrations in the cell, because it is quickly converted to malate by reduction via MDH in NADP-malic enzyme subtypes (Hatch, 1987). In species like *Zea mays* that can use PEPCK as a supplementary decarboxylation pathway, a relatively higher affinity for oxaloacetate may be needed to maintain high rates of aspartate aminotransferase activity towards the formation of aspartate. In *Sorghum bicolor*, the K_M for L-aspartate in illuminated leaves was substantially higher than the K_M for L-aspartate in *Setaria viridis* and *Zea mays*. Unlike *Zea mays*, *Sorghum bicolor* almost exclusively uses NADP-malic enzyme (Gutierrez *et al.*, 1974), whereas *Zea mays* can use both NADP-malic enzyme and PEPCK (Hatch, 1987). Thus, a relatively lower affinity for L-aspartate may correlate to both the lower activity of PEPCK in *Sorghum bicolor* leaves and relatively lower expression of PEPCK than in *Zea mays* (Figure 4.16).

Differences in the decarboxylation chemistry of these C_4 grasses may have also contributed to the decrease in affinity for 2-oxoglutarate in *Sorghum bicolor*, while in both *Setaria viridis* and *Zea mays*, the affinity for 2-oxoglutarate increased after the dark to light transition. Unlike oxaloacetate, the amount of aspartate available in the *Zea mays* leaf can vary in response to light intensity or dark to light transitions, and the concentration increases upon illumination and then rapidly declines, but remains between 25 to 60 mM in the whole cell (Hatch and Osmond, 1976; Leegood and Furbank, 1984; Hatch, 1987; Leegood and von Caemmerer, 1989). Therefore, it is unlikely that the activity of aspartate aminotransferase towards the formation of oxaloacetate will be limited by the amount of aspartate when the K_M for aspartate is high, but if the K_M for oxaloacetate were high, then the reverse reaction (towards the formation of aspartate) may be limited by the availability of oxaloacetate. Alternatively, if the affinity for L-aspartate were higher, then aspartate aminotransferase would readily catalyse the conversion of aspartate to oxaloacetate, decreasing the amount of substrate for PEPCK.

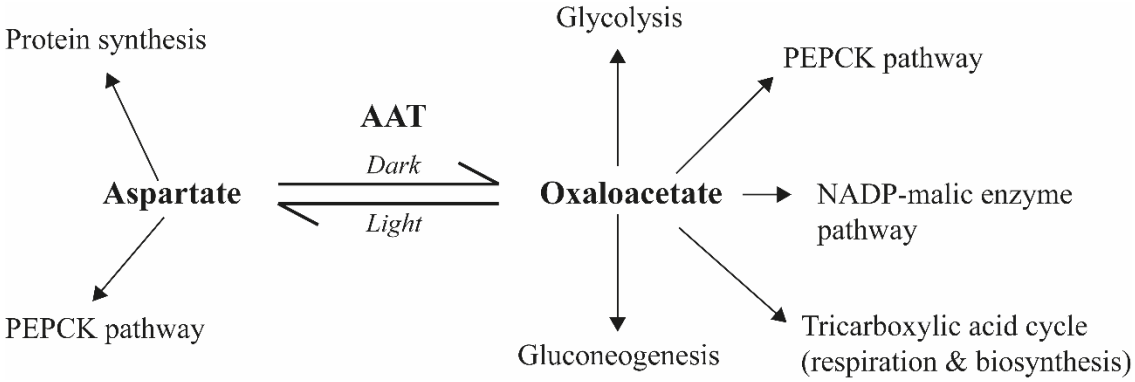

Fig. 5.15. Interchange between aspartate and oxaloacetate by aspartate aminotransferase (AAT).

In illuminated leaves, there was a 15-fold decrease in affinity for L-aspartate in *Zea mays*, which correlates to the increase in aspartate after the onset of light. This suggests that there may be additional need for aspartate aminotransferase activity towards the formation of oxaloacetate in darkened conditions. This activity might not be associated with C_4 photosynthesis, and instead aspartate aminotransferase in darkened leaves may be catalysing the formation of oxaloacetate from aspartate for cellular respiration or for biosynthesis. In fact, oxaloacetate serves a central role in metabolism (Buchanan *et al.*, 2015) and requirements may differ between dark and light conditions (Figure 5.15). There may also be a link between the phosphorylation sites identified solely in darkened leaves of *Setaria viridis* and the relatively higher affinity for L-aspartate in darkened conditions. From these observations, it is probable that the activity of aspartate aminotransferase is partitioned between photosynthesis in illuminated conditions and other cellular processes in darkened conditions, somewhat similar to the regulation of photosynthetic PEPC in leaves and anaplerotic activity in non-photosynthetic tissues (O'Leary *et al.*, 2011; Shane *et al.*, 2013; Ruiz-Ballesta *et al.*, 2014). These results also suggest that the regulation of aspartate aminotransferase may be an additional control for downstream PEPCK activity. This is supported by the fact that the amount of PEPCK protein and PEPCK activity in C_4 plants changes very little in darkened and illuminated conditions and PEPCK needs to be regulated to prevent depletion of ATP (Carnal *et al.*, 1993; Walker *et al.*, 2002). Although PEPCK is regulated by reversible phosphorylation, this occurs in darkened leaves of *Megathyrsus maximus* (Walker and Leegood, 1995; Walker *et al.*, 1997; Bailey *et al.*, 2007). In *Zea mays*, PEPCK appears to be phosphorylated in illuminated leaves (Chao *et al.*, 2014) and its regulation might be distinctly different than in PEPCK subtypes. Therefore, the regulation of aspartate

aminotransferase in illuminated conditions may serve to regulate PEPCK activity by controlling the supply of oxaloacetate.

In addition to this, there may be some aspartate aminotransferase activity associated with chloroplasts or mitochondria (Hatch and Mau, 1973; Hatch, 1987; Meister *et al.*, 1996). This may contribute to additional regulation by pH, as observed for NADP-malic enzyme. Moreover, the stability of aspartate aminotransferase and its interaction with competitive inhibitors can be influenced by pH (Bonsib *et al.*, 1975). When assayed at pH 8.0 in the presence of dimethyl-2-oxoglutarate, an analogue of 2-oxoglutarate (Odegaard *et al.*, 2010), aspartate aminotransferase still followed Michaelis-Menten kinetics. However, the affinity for dimethyl-2-oxoglutarate was higher than the affinity for 2-oxoglutarate in darkened leaves of *Sorghum bicolor*, *Setaria viridis* and *Zea mays* (Table 5.2), suggesting that in the absence of 2-oxoglutarate, dimethyl-2-oxoglutarate could be an effective replacement.

Table 5.2. **Aspartate aminotransferase affinity for 2-oxoglutarate and dimethyl-2-oxoglutarate**. Up-arrows indicate an increase in affinity against the original K_M value for 2-oxoglutarate (a negative fold change, decrease in K_M), while down-arrows indicate a decrease in affinity (a positive fold change, increase in K_M).

	Dark	Light
	Affinity (fold change)	
Sorghum bicolor	0.9 ↑	0.7 ↓
Setaria viridis	0.5 ↑	0.6 ↑
Zea mays	0.66 ↑	6.3 ↓

In the presence of 2 mM dimethyl-2-oxoglutarate, aspartate aminotransferase from illuminated *Zea mays* leaves did not saturate and in *Sorghum bicolor*, the activity of aspartate aminotransferase in the presence of dimethyl-2-oxoglutarate declined. This indicates that the properties of aspartate aminotransferase from illuminated leaves of *Zea mays* and *Sorghum bicolor* may be distinctly different than that of aspartate aminotransferase from *Setaria viridis*, which remained equally active in darkened and illuminate leaf lysates in the presence of dimethyl-2-oxoglutarate. This may modulate C_4-specific function after the onset of light. Furthermore, computer analyses have predicted that dimethyl-2-oxoglutarate is a weak inhibitor of aspartate aminotransferase

(Bonsib *et al.*, 1975), which is consistent with the minimal effect of dimethyl-2-oxoglutarate on the activity of the transaminase (Figure 5.9). However, these effects may be more pronounced in the presence of stronger dicarboxylic inhibitors and may conflict with native substrate binding and affect the role of aspartate aminotransferase in C_4 photosynthesis. To assess the stability of the enzyme, it would be useful to determine if the activity of aspartate aminotransferase and affinity for L-aspartate and 2-oxoglutarate changes in low and high pH.

5.3.2 C_4 metabolites may regulate the activity of aspartate aminotransferase

C_4 photosynthesis involves the efficient movement of carbon between mesophyll and bundle sheath cells by the transfer acids malate, aspartate, alanine, pyruvate and PEP (Hatch, 1987; Bräutigam *et al.*, 2014). Previous studies have shown that these transfer acids are crucial for the coordination of carboxylation and decarboxylation pathways (Chapman and Hatch, 1981; Furbank and Leegood, 1984; Leegood, 1985; Stitt and Heldt, 1985; Leegood and von Caemmerer, 1989; Bräutigam *et al.*, 2014; Arrivault *et al.*, 2016). Results presented in this Chapter have shown that the activity of aspartate aminotransferase was activated or inhibited in the presence of C_4 transfer acids. This suggests that similar to the coordination of C_3 and C_4 cycles afforded by the exchange of transfer acids, there could be additional mechanisms that regulate decarboxylation by either NADP-malic enzyme or PEPCK/NAD-malic enzyme in C_4 species that operate the dual-decarboxylation system (Figure 5.2) (Chapman and Hatch, 1979).

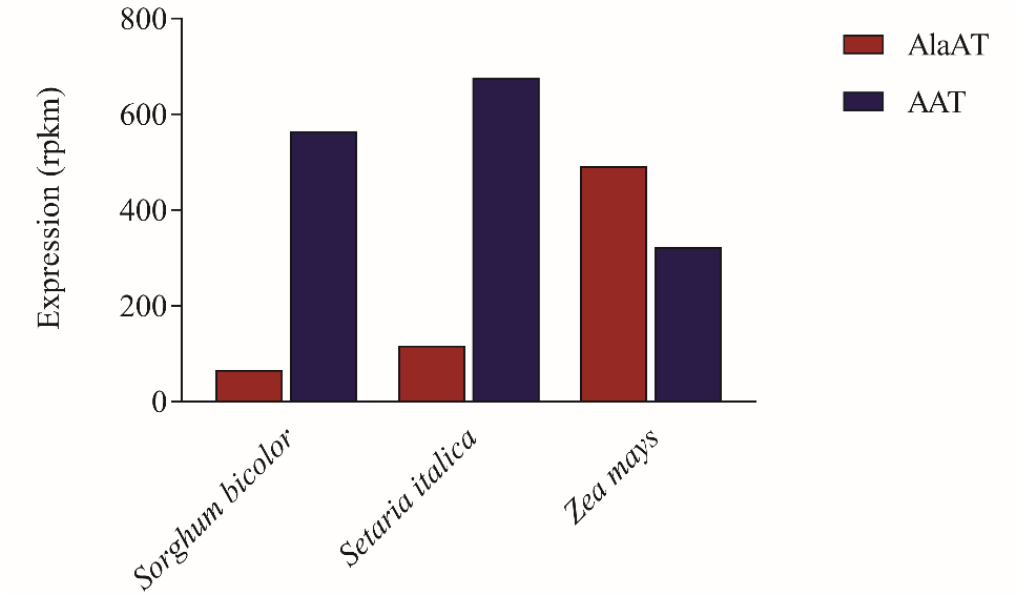

Fig. 5.16. Relative expression of aspartate aminotransferase (AAT) and alanine aminotransferase (AlaAT). Expression in reads per kilobase million (rpkm). Transcriptomic data obtained from PA Christin (unpublished).

This is supported by the inhibition of aspartate aminotransferase activity from *Sorghum bicolor* in the presence of L-alanine (Figure 5.10A), while aspartate aminotransferase from *Setaria viridis* was not inhibited (Figure 5.10B) and in *Zea mays*, the transaminase was activated (Figure 5.10C). This suggests that aspartate aminotransferase from *Sorghum bicolor* might lack regulatory controls that would otherwise maintain high *in vivo* activity in an excess of alanine. This may also reflect the decarboxylation pathway in *Sorghum bicolor*, which unlike *Setaria viridis* or *Zea mays*, *Sorghum bicolor* uses NADP-malic enzyme and may not have high *in vivo* activities of aspartate aminotransferase or alanine aminotransferase (Andrews *et al.*, 1971; Gutierrez *et al.*, 1974). Conversely, aspartate aminotransferase from *Zea mays* contains more aspartate aminotransferase activity (Andrews *et al.*, 1971), albeit has a lower expression of aspartate aminotransferase than *Sorghum bicolor* and *Setaria viridis* (Figure 5.16). More importantly, transcriptomic data shows that the expression of alanine aminotransferase in *Zea mays* is substantially higher than that of *Setaria viridis* and *Sorghum bicolor*. This may indicate that aspartate aminotransferase in *Zea mays* is adapted to maintain activity in a high concentration of L-alanine, because of the relative dependence on alanine aminotransferase activity. Moreover, increasing the concentration of L-alanine stimulated the activity of aspartate aminotransferase from illuminated *Zea mays* leaf lysates. This suggests that aspartate aminotransferase may be linked to alanine

aminotransferase activity, and is consistent with decarboxylation via PEPCK/NAD-malic enzyme pathways, which require both aspartate aminotransferase and alanine aminotransferase activity (Andrews *et al.*, 1971; Bräutigam *et al.*, 2014; Wang *et al.*, 2014).

Aspartate aminotransferase from darkened leaves of *Zea mays* was not activated by L-alanine (Figure 5.10C), suggesting that the dark-form of the transaminase may not be preconditioned for C_4-specific activity. In the absence of L-alanine, the formation of oxaloacetate seemed to be favoured in darkened conditions (Figure 5.8), but as noted, may not be associated with C_4-specific activity. Also, since aspartate aminotransferase from *Zea mays* appeared to be stimulated by the C_4 metabolite solely in illuminated leaf lysates, this might correspond to an activation mechanism for C_4-specific function and could signal the formation of oxaloacetate in illuminated leaves and stimulate PEPCK activity. Conversely, aspartate aminotransferase from *Setaria viridis* was not affected by L-alanine, which may reflect that *Setaria viridis* depends more on the flux of L-alanine than *Sorghum bicolor*, but may not utilise a secondary decarboxylation pathway via PEPCK/NAD-malic enzyme as readily as *Zea mays*. This is partially supported by the relatively higher alanine aminotransferase activity in *Setaria viridis* (Figure 5.14) and higher alanine aminotransferase expression when compared to alanine aminotransferase from *Sorghum bicolor*, but substantially lower expression of alanine aminotransferase when compared to *Zea mays* (Figure 5.16).

In addition to this, L-malate stimulated the activity of aspartate aminotransferase in illuminated *Zea mays* leaf lysates, whereas in darkened and illuminated *Setaria viridis* leaf lysates, the activity of aspartate aminotransferase was inhibited by an excess of L-malate, which is consistent with previous findings (Chapman and Hatch, 1979). Furthermore, the activation of aspartate aminotransferase towards the formation of oxaloacetate in the presence of L-malate may link malate metabolism via NADP-malic enzyme and oxaloacetate decarboxylation via PEPCK (Figure 5.17).

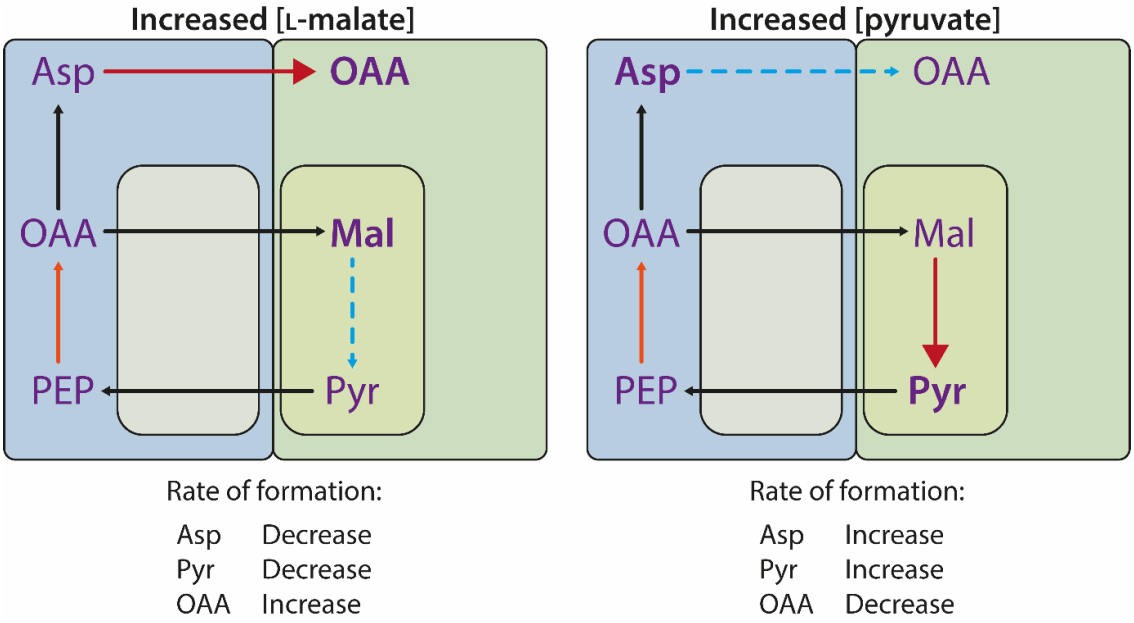

Fig. 5.17. Simple schematic depicting a mechanism that could regulate the relative flux through malate or aspartate in a dual-decarboxylation system in *Zea mays*. Red arrows indicate increase rate of formation (in the indicated direction; metabolite in bold), blue arrows (dashed lines) indicate reduced rate of formation and orange arrows indicate PEPC inhibition by aspartate or malate. For simplicity, other feedback inhibition mechanisms are not shown. Figure based on experimental data shown in Figures 5.10 and 5.11 and data from Chapman and Hatch (1979). Asp, aspartate; Pyr, pyruvate; Mal, malate; OAA, oxaloacetate.

This link was previously shown when the formation of pyruvate via malate metabolism was stimulated in the presence of aspartate (Chapman and Hatch, 1979). This implies that NADP-malic enzyme activity towards the formation of pyruvate is favoured when aspartate is formed, but this may affect PEPCK activity, because the formation of oxaloacetate may not be favoured. Alternatively, if the formation of oxaloacetate is favoured and aspartate declines, then the formation of pyruvate via NADP-malic enzyme may decline, implying that malate would be more readily available since the rate at which is it decarboxylated may decrease. Conversely, if there were more aspartate and pyruvate, it would imply that the rate at which malate is decarboxylated increases. The link between aspartate, pyruvate and malate (Figure 5.17), as part of an extended aspartate–malate shuttle, is further supported by the decrease in the rate at which aspartate is converted to oxaloacetate in an excess of pyruvate (Figure 5.11C).

Therefore, in the same way that aspartate can induce the formation of pyruvate and stimulate the activity of NADP-malic enzyme (Müller *et al.*, 2008), then malate might induce the formation of oxaloacetate and stimulate PEPCK activity. This activation effect, which was solely evident in aspartate aminotransferase from *Zea mays*, may reflect the fine control of PEPCK and NADP-malic enzyme decarboxylation, particularly when the activity of either decarboxylase is reduced or not favoured. In rats (*Rattus norvegicus*), aspartate aminotransferase activation by L-malate may contribute to the fine control and reversibility of the transaminase, and most importantly, may regulate the relative flux through aspartate or malate (McKenna *et al.*, 2006). Whether the oxaloacetate formed in this mechanism contributes to malate metabolism or PEPCK decarboxylation is not clear. The inhibitory effect of L-malate observed in *Sorghum bicolor* and *Setaria viridis* may suggest the relatively lower dependence on PEPCK-dependent decarboxylation compared to *Zea mays*, as previously shown in transcriptomic analyses (Figure 4.16).

10 mM PEP had no effect on the activity of aspartate aminotransferase from illuminated leaves of *Setaria viridis* (Figure 5.11A) and *Zea mays* (Figure 5.11C), while 20 mM and 50 mM PEP affected the activity of aspartate aminotransferase from the three C_4 grasses equally. This suggests that the activity of aspartate aminotransferase may be linked to the activity of PEPC, but may not be as significant as control by L-malate or L-alanine, since the concentration of PEP used in the experiments was well above the physiological amounts (Leegood and von Caemmerer, 1989). The amount of PEP increases upon illumination, but is rapidly assimilated into oxaloacetate by PEPC during photosynthesis (Leegood and von Caemmerer, 1988; Leegood and von Caemmerer, 1989) and PEP can serve as an activator for PEPC activity (Tovar-Méndez and Muñoz-Clares, 2001). Aspartate can inhibit PEPC activity (Mareš *et al.*, 1979), and therefore a inhibitory mechanism regulated by PEP or aspartate may link aspartate aminotransferase and PEPC activities, respectively, and might regulate the formation of oxaloacetate when the rate of PEP carboxylation is reduced or in darkened conditions, when photosynthesis is not occurring. This may lead to higher aspartate aminotransferase activity in darkened leaves and contribute to the fine control of PEPC activity during light transitions, in addition to regulation by phosphorylation or other C_4 metabolites (Budde and Chollet, 1986; Doncaster and Leegood, 1987; Hatch, 1987; Leegood and von Caemmerer, 1988).

5.3.3 Alanine aminotransferase may be differently regulated in C_4 species

Alanine aminotransferase activity measured towards the formation of pyruvate was negligible when assayed in the presence of 20, 50 and 75 mM L-alanine. Previous studies have shown that alanine aminotransferase has a high K_M for L-alanine (K_M 3.03 mM in *Zea mays* compared to K_M 10.4 mM in *Arabidopsis thaliana*) and the reaction assays require a high concentration of the substrate (Miyashita *et al.*, 2007; Duff *et al.*, 2012; Kendziorek *et al.*, 2012; McAllister *et al.*, 2013). In *Zea mays*, the K_M for pyruvate is lower than the K_M for L-alanine (Duff *et al.*, 2012), which suggests some selectivity towards pyruvate binding. This may also be part of the mechanism to preferentially bind pyruvate in illuminated conditions, since the amount of pyruvate decreases with increasing light intensity, and while the amount of alanine declines after the onset of light, it remains between 30 to 70 mM in darkened or illuminated conditions (Leegood and Furbank, 1984; Leegood and von Caemmerer, 1989).

Preference for pyruvate might be significant for the formation alanine in C_4 plants, particularly in PEPCK/NAD-malic enzyme subtypes, where the balance of amino acids between mesophyll and bundle sheath cells must be kept by transferring alanine from bundle sheath to mesophyll cells after aspartate is transferred from mesophyll to bundle sheath cells (Hatch, 1987; Weber and Bräutigam, 2013). Furthermore, a concentration gradient for the movement of pyruvate from bundle sheath cells to mesophyll cells is not required (Arrivault *et al.*, 2016). In addition to this, theoretical models used to model the energy costs of C_4 photosynthesis have also shown that in PEPCK subtypes, the transport of alanine, presumably after the conversion from pyruvate via alanine aminotransferase, and PEP via PEPCK compensates the reduction of malate metabolism and pyruvate transport to regenerate PEP via PPDK (Wang *et al.*, 2014). This suggests that activity of alanine aminotransferase may be preferential for the pyruvate reaction, towards the formation of alanine, since a concentration gradient of alanine is required to operate the C_4 cycle (Arrivault *et al.*, 2016).

The relative activity of alanine aminotransferase in the three C_4 grasses did not correlate to transcriptomic analyses (Figure 5.16). High expression of alanine aminotransferase and aspartate aminotransferase expression in *Zea mays* correlates to aspartate–oxaloacetate and pyruvate–alanine interconversion pathways in species that use PEPCK

and NADP-malic enzyme (Hatch, 1987; Wang *et al.*, 2014). However, changes to alanine aminotransferase activity as seen on Figure 5.14 may not correlate to requirements of PEPCK, but rather to the relative activity of NADP-malic enzyme. This is supported by the activity of alanine aminotransferase being lower in *Zea mays* than in *Setaria viridis*, when *Zea mays* contains relatively more PEPCK than either *Sorghum bicolor* or *Setaria viridis* (Gutierrez *et al.*, 1974).

Considering these results, the alanine aminotransferase reaction towards the formation of alanine requires further optimisation and investigation in these C_4 species. One major problem was that the reaction took more than 20 min to have detectable changes in NADH oxidation, compared to only a few minutes to see a decline in the concentration of NADH in the aspartate aminotransferase reaction. Also, whether the reaction towards the formation of alanine is being masked by catalysis in the reverse direction, is unclear, but may be unlikely since activity was not previously observed in high concentrations of L-alanine. Improvements to the assay of the activity of alanine aminotransferase and determining its kinetic properties in darkened and illuminated leaves may provide some indication to its regulation and role in NADP-malic enzyme subtype C_4 grasses.

5.3.4 Conclusion

The results in this chapter showed that solely the aspartate aminotransferase from illuminated *Zea mays* leaf lysates was activated by an excess of L-malate and L-alanine, whereas aspartate aminotransferase activity in *Sorghum bicolor* was inhibited by both L-malate and L-alanine. In *Setaria viridis*, the inhibitory effect was only observed in the presence of L-malate. These results support the role of aspartate aminotransferase as a link between PEPCK and NADP-malic enzyme decarboxylation, as well as align with the hypothesis that different NADP-malic enzyme C_4 subtypes might have differing demands for aspartate aminotransferase activity and PEPCK-dependent decarboxylation. In addition, these effects were more predominant in illuminated leaf lysates and might correspond to a C_4-specific aspartate aminotransferase isoform in NADP-malic enzyme subtypes. Effector metabolites, rather than light conditions, might assert more control over the activation of the transaminase, which appeared to have a lower affinity for L-aspartate after transition into the light period.

Chapter 6 – General Discussion

6.1 Regulating the relative flux through malate and aspartate

In C_4 photosynthesis, assimilated carbon is delivered at the site of Rubisco via two main pathways through fluxes of malate or aspartate (Bellasio and Griffiths, 2014). Historically, C_4 plants exist as three distinct subtypes, NAD- and NADP-malic enzyme and PEPCK, and are classified by their primary decarboxylase (Hatch, 1987). It has become apparent, however, that certain NADP-malic enzyme C_4 grass species can partition between NADP-malic enzyme and PEPCK decarboxylation using malate and aspartate as C_4 transfer acids. Furthermore, in PEPCK subtypes, NAD-malic enzyme contributes to malate metabolism in mitochondria of bundle sheath (Hatch, 1987; Bräutigam *et al.*, 2014). Recent evidence suggests that the decarboxylation pathways of C_4 grasses are flexible, and multiple decarboxylases may have been selected for during evolution (Furbank, 2011; Wang *et al.*, 2014). Moreover, the relative amounts of PEPCK, NADP-malic enzyme or NAD-malic enzyme vary among subtypes. For instance, certain NADP-malic enzyme subtypes, such as *Zea mays*, have appreciable amounts of PEPCK activity, while others, such as *Sorghum bicolor* or *Setaria viridis* have extremely low PEPCK activity (Gutierrez et al., 1974). Similarly, certain NAD-malic enzyme species, such as *Panicum decompositum* contain substantial amounts of PEPCK activity, while other NAD-malic enzyme species within the *Panicum* genus do not (Gutierrez *et al.*, 1974). Interestingly, the decarboxylation chemistry of the dicot NAD-malic enzyme C_4 plant, *Cleome gynandra*, can be developmentally regulated and mid-aged leaves are able to use both NAD-malic enzyme and PEPCK decarboxylase pathways, with enhanced aspartate aminotransferase and alanine aminotransferase activity in bundle sheath mitochondria (Sommer *et al.*, 2012). However, the regulation of carbon flux through malate or aspartate has not been properly understood in NADP-malic enzyme monocot grasses.

The findings presented in this thesis show that NADP-malic enzyme and aspartate aminotransferase may be differently regulated in NADP-malic enzyme subtype grasses and that the regulation of aspartate aminotransferase by C_4 transfer acids may reflect the relative flux through malate or aspartate and coordination of NADP-malic enzyme and

PEPCK decarboxylation in *Zea mays*. However, these mechanisms may not be present in C_4 grasses with lower expression of PEPCK, such as *Setaria viridis* and *Sorghum bicolor*, which may be less dependent on the flux through aspartate (Gutierrez *et al.*, 1974). These results describe three distinct regulatory properties of NADP-malic enzyme and aspartate aminotransferase that could control the flux of carbon between mesophyll and bundle sheath cells of NADP-malic enzyme subtypes. These results also show that the classification of C_4 plants as distinct subtypes may be an oversimplification and may not accurately reflect the regulation of carbon flux, as the interspecies differences in the catalytic properties of NADP-malic enzyme and activation of aspartate aminotransferase in response to C_4 metabolites have shown.

There is also doubt to how much the malate–pyruvate pathway for NADP-malic enzyme and the aspartate–alanine pathway for PEPCK/NAD-malic enzyme overlap. Plants using a dual-decarboxylation system may operate an oxaloacetate–aspartate pathway via aspartate aminotransferase and a pyruvate–alanine pathway via alanine aminotransferase. Although alanine aminotransferase is primarily used for converting pyruvate to alanine from the decarboxylation of malate via NAD-malic enzyme in mitochondria of NAD-malic enzyme subtypes (Bräutigam *et al.*, 2014), alanine aminotransferase could catalyse the interconversion of pyruvate and alanine downstream of malate decarboxylation by NADP-malic enzyme. Enhanced alanine aminotransferase activity was observed in leaves of *Cleome gynandra* in mid-development, while older leaves had reduced alanine aminotransferase activity (Sommer *et al.*, 2012).

While Leegood (1985), Stitt and Heldt (1985) and Arrivault *et al.* (2016) have identified the metabolites and their respective concentration gradients that contribute to the flux of carbon, this rate of diffusion must be balanced with the rate of metabolism (von Caemmerer and Furbank, 2003). Based on modelling analysis (Wang *et al.*, 2014), it is likely that the conversion of oxaloacetate to aspartate in mesophyll cells reduces carbon trafficking through malate, thus alleviating chloroplast transport mechanisms. However, converting too much aspartate may reduce the ratio of oxaloacetate to malate in mesophyll cells, hindering the uptake of oxaloacetate into chloroplasts for reduction to malate (Leegood, 2002). Also, movement of carbon through aspartate may reduce pools of malate necessary for downstream metabolism and decarboxylation by NADP-malic enzyme. This indicates that the diurnal regulation of the relative flux through aspartate or malate might be essential in plants that operate a dual-decarboxylation system.

Contribution of aspartate, along with malate, to the carbon pool was the subject of speculation since the elucidation of the carbon concentrating mechanism of C_4 photosynthesis (Hatch and Slack, 1966; Slack *et al.*, 1969). Recent evidence suggests that the utilisation of aspartate and malate in certain C_4 plants may improve assimilation efficiencies and reduce energy requirements (Wang *et al.*, 2014) and such flexibility in decarboxylation chemistry can allow C_4 plants to adapt better to environmental changes such as fluctuating light intensities (Furbank, 2011; Stitt and Zhu, 2014).

There has also been concern on which decarboxylation mechanism is most efficient and there is growing advocacy for PEPCK subtypes, with both PEPCK and NAD-malic enzyme activity, to be used as an engineering template for engineering the C_4 trait into existing C_3 crops. Recent evidence has shown that the PEPCK decarboxylation pathway requires fewer ATP than the NADP-malic enzyme pathway because PEP does not need to be regenerated via PPDK (Wang *et al.*, 2014). However, decarboxylation via PEPCK does not generate reducing equivalents and these must be generated via NAD-malic enzyme or enhanced photosystem II activity in bundle sheath cells (Bräutigam *et al.*, 2014). Since NADP-malic enzyme species have reduced photosystem II activity, because NADP-malic enzyme can generate reducing equivalents, relying fully on PEPCK decarboxylation might not be selected for during the evolution of decarboxylation mechanisms (Furbank, 2011). However, photosystem II activity varies between C_4 species and certain NADP-malic enzyme species, such as *Zea mays*, have higher photosystem II activity than other NADP-malic enzyme grasses (Hardt and Kok, 1978; Walker and Izawa, 1979). Enhancement of bundle sheath cell photosystem II activities in species such as *Zea mays*, which use a dual-decarboxylation system may compensate the generation of reducing equivalents that are not formed via NADP-malic enzyme. Differences in the kinetics of NADP-malic enzyme and aspartate aminotransferase may correlate to the relative rates of O_2 evolution in bundle sheath cells of NADP-malic enzyme subtypes. For instance, in *Sorghum bicolor*, the activity of NADP-malic enzyme might be required at the onset of light, whereas in *Zea mays*, the activity of NADP-malic enzyme at the onset of light might not be equally necessary. This may correlate to the absence of photosystem II activity in bundle sheath cells of *Sorghum bicolor* (Hatch, 1978; Meierhoff and Westhoff, 1993), whereas *Zea mays* contains appreciable amount of photosystem II and PEPCK activity in bundle sheath cells. The degree of O_2 evolution in bundle sheath cells of C_4 plants, particularly of NADP-malic enzyme subtypes, may

be interwoven with the relative flux through aspartate, as previously speculated (Chapman and Hatch, 1981; Meister *et al.*, 1996). Furthermore, if the formation of reducing equivalents in the bundle sheath is not regulated, then it can influence the amount of 3-PGA that is translocated to mesophyll cells, via the triose phosphate porter, for reduction to triose phosphates, as well as alter the amount of triose phosphates that are translocated back to bundle sheath cells and used to regenerate RuBP under high photosynthetic loads (Hatch, 1987; Furbank, 2011). An early attempt in transforming C_3 plants with copies of the *Zea mays* NADP-malic enzyme caused bleaching of leaves in rice and reduced photosynthetic capacity probably by photoinhibition due to an increase in the supply of NADPH (Tsuchida *et al.*, 2001). Although overexpression of NADP-malic enzyme can be deteriorating for transgenic C_3 plants, reduced grana stacking in bundle sheath cells of C_4 plants protects against photoinhibition by preventing the accumulation of NADPH in chloroplasts. This study is an example of how overexpressing the C_4-specific NADP-malic enzyme can induce phenotypic changes. Therefore, the formation of reducing equivalents in C_4-augemented plants must be considered, such that engineered protein networks do not perturb other transport mechanisms, such as the 3-PGA/triose-phosphate shuttle via the triose phosphate porter, which is relatively less expressed in C_3 grasses (Weber and von Caemmerer, 2010; Bräutigam *et al.*, 2011). Compared to C_3 species, C_3–C_4 intermediates, such as *Flaveria floridana* and *Moricandia arvensis*, and C_4 species have considerably higher amounts of 3-PGA and triose phosphates (Badger *et al.*, 1984; Leegood and von Caemmerer, 1994).

In addition to this, since PEPCK is cytosolic, its regulation may be simpler than that of NADP-malic enzyme, which is chloroplastic and may depend on regulation by light-dependent changes in the stromal pH (Asami *et al.*, 1979; Edwards and Andreo, 1992; Bräutigam *et al.*, 2014). It is argued, however, that NADP-malic enzyme might be the simplest to engineer, despite having to consider the expression of additional transporters for oxaloacetate, malate, 3-PGA and triose phosphates (Bräutigam *et al.*, 2008; Weber and von Caemmerer, 2010; Bräutigam *et al.*, 2011; Leegood, 2013). There may also be some importance to the selection of decarboxylation by NADP-malic enzyme, which was acquired as the primary decarboxylase in over 50% of C_4 grasses (Sage *et al.*, 2011). Also, the catalytic properties of NADP-malic enzyme may not only differ between C_4 subtypes, but also between species using the same primary decarboxylation pathway. For instance, NADP-malic enzyme from *Sorghum bicolor* exhibited two distinct pH optima,

one of which contributed to maximal activity at pH 7.4. This may ensure high *in vivo* activity at the onset of light when the pH of the stroma is low (Werdan *et al.*, 1975). In *Setaria viridis*, also a NADP-malic enzyme subtype, NADP-malic enzyme activity in illuminated leaf lysates had a broader pH dependence, and despite that maximal activity was not observed at a low pH, like in *Sorghum bicolor*, the differences in activity between low and high pH were negligible (Figure 4.5). These changes were not as distinct as the changes in NADP-malic enzyme activity in *Zea mays* between pH 7.0 and pH 8.4 (Figure 4.6). Unlike *Sorghum bicolor* and *Setaria viridis*, *Zea mays* has appreciable amounts of PEPCK expression and activity (Walker *et al.*, 1997; Furumoto *et al.*, 1999; Wingler *et al.*, 1999). These results also indicate that in NADP-malic enzyme subtypes, the activity and regulation of NADP-malic enzyme activity may be influenced by a gradient of PEPCK-dependent decarboxylation. The dependence on PEPCK decarboxylation is higher in *Zea mays* and lower in *Sorghum bicolor* (Gutierrez *et al*., 1974) and PEPCK activity in *Setaria viridis* may be somewhere between that of *Zea mays* and *Sorghum bicolor* (Figure 6.1) (Gutierrez *et al.*, 1974).

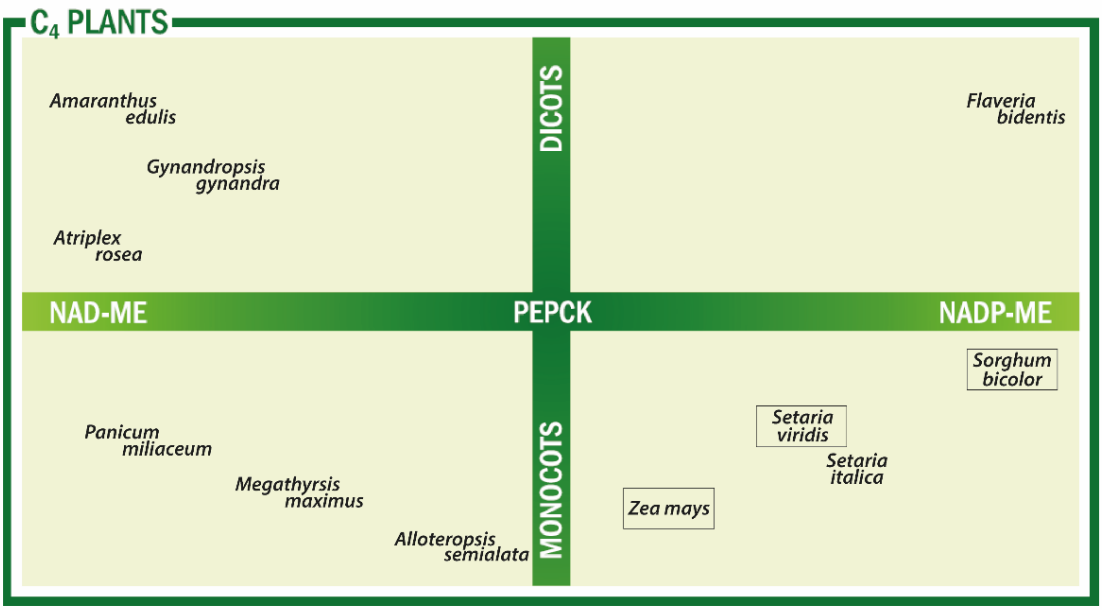

Fig. 6.1. C_4 plants grouped by their primary decarboxylase. C_4 species are grouped by their primary decarboxylase. Positioning depends on the relative expression of NADP-malic enzyme (far right), NAD-malic enzyme (far left) and PEPCK (towards the centre of the cross). NADP-malic enzyme subtypes used in this study are indicated by the boxes. Figure from APM Weber (unpublished).

While the kinetics of NADP-malic enzyme may dependent on PEPCK, the regulation and activity of aspartate aminotransferase may depend on diurnal PEPC activity and correlate to changes in the affinity of PEP between dark and light transitions. Figure 4.2 shows that the affinity for PEP was lowest in 7.5 h darkened leaves. This is consistent with the downregulation of PEPC in darkened conditions to prevent PEP carboxylation (Jiao and Chollet, 1988; Jiao and Chollet, 1991; Chollet *et al.*, 1996; O'Leary *et al.*, 2011). Additionally, the amounts of PEP may be higher in the absence of carbon fixation and PEP content may not decrease as rapidly when PEPC is not active (Leegood and von Caemmerer, 1989). Conversely, in darkened leaves, aspartate aminotransferase exhibited a higher affinity for aspartate and 2-oxoglutarate (Figure 5.6), albeit the activity in the dark period was lower than in illuminated leaves (Figure 5.10B). If the concentration of PEP were higher, possibly due to the reduced PEPC activity in darkened leaves, then the activity of aspartate aminotransferase might be downregulated as well. This is supported by the inhibition of aspartate aminotransferase activity in the presence of PEP (Figure 5.11). In addition to this, PEPC affinity for PEP increased after the dark to light transition, but aspartate aminotransferase affinity for aspartate and 2-oxoglutarate declined. This implies that when PEP is readily metabolised by PEPC, the activity of aspartate aminotransferase can be higher, and it may be less inhibited by PEP. In the absence of PEP, the activity of aspartate aminotransferase was higher in illuminated leaf lysates of *Setaria viridis* (Figure 5.10B).

In addition to this, the activity of alanine aminotransferase may depend on NADP-malic enzyme, rather than the relative PEPCK expression in NADP-malic enzyme subtypes. This is supported by the relative differences between NADP-malic enzyme activity and alanine aminotransferase activity in the C_4 grasses studied. Figure 4.7 showed that in *Setaria viridis* the activity of NADP-malic enzyme was substantially lower than that in *Sorghum bicolor* and *Zea mays*. However, the activity of alanine aminotransferase was relatively higher in *Setaria viridis*, compared to the activity in *Sorghum bicolor* and *Zea mays*. This observation is supported by the relative expression of alanine aminotransferase in Figure 5.16 and corresponds to the higher activity of alanine aminotransferase in C_4 species with reduced NADP-malic enzyme activity (Andrews *et al.*, 1971; Hatch, 1987). It is important to note however, that the rate of NADP-malic enzyme activity was substantially higher than that of alanine aminotransferase, and this observation is not a direct comparison between changes in specific activities.

Novel phosphorylation data presented in Chapter 3 showed that PEPC, aspartate and alanine aminotransferase and NADP-malic enzyme undergo light-dependent phosphorylation (Appendix A). Along with the *in vitro* activity assays, it appeared that there were changes in the dark and light *in vitro* activities of these enzymes. However, whether the phosphorylation sites identified serve a biological function remains unclear. These can be further investigated using phosphomimetic mutants expressed in *Escherichia coli*, similar to the approach used to study the effect of phosphorylation of PPDK (Chastain *et al.*, 1997; Chastain *et al.*, 2000). Using site-directed mutagenesis of *Setaria viridis* C_4-related proteins, such as PEPC and NADP-malic enzyme, the phosphorylation sites identified in this study can be further validated. Recombinant proteins can be purified and assayed *in vitro* and assessed whether the phosphorylations affect enzymatic activity. Furthermore, kinetic constants, like V_{max} and K_{cat} can be calculated and compared to the *in vitro* activities of the enzymes from crude leaf lysates. While this approach may prove useful, it might not be truly representative of *in vivo* phosphorylation. For instance, phosphorylations are dynamic and the degree of phosphorylation of a protein may change in response to intracellular stimuli or environmental cues, such as varying light intensities (Chen *et al.*, 2014; Friso and van Wijk, 2015). While phosphomimetic mutants can show whether a certain modification can alter enzyme activity, the genetically introduced modifications are static and cannot dynamically respond to stimulants *in vitro*. A supplementary approach would be to selectively purify phosphorylated proteins from the crude leaf lysate. Anti-phosphoprotein antibodies are commonly used for phosphoprotein identification by immunoblotting or mass spectrometry, but up to now their applications for immunoprecipitating phosphorylated proteins and determining physiological enzymatic activity are limited. This is partly due to reactions conducted in non-physiological conditions, which are likely to lead to loss of enzyme activity and because of low binding efficiencies of commercially available anti-phosphoprotein antibodies, namely the differences between anti-phosphotyrosine and anti-phosphoserine or anti-phosphothreonine, which consequently enrich phosphorylated tyrosine residues with higher efficiency than phosphoserines and phosphothreonines (Grønborg *et al.*, 2002). One method to overcome this might be to develop gel activity assays, whereby proteins are kept and assayed in their native conditions (Covian *et al.*, 2012). In addition, by selectively purifying proteins of interest using antibodies, proteins may be as close to their physiological phosphorylation state and the effects of phosphorylation on protein

activity can be determined. Also, certain issues such as ensuring phosphomimetic proteins are structurally comparable to the candidate wildtype proteins can be avoided.

6.2 Communication between C_3 and C_4 cycles and the formation of PEP

The efficient and rapid movement of C_4 metabolites depends on the coordinate regulation of C_3 and C_4 pathways (Furbank and Leegood, 1984; Leegood and Furbank, 1984). However, one interaction that has not been fully understood is the interchange of 3-PGA and PEP using phosphoglycerate mutase and enolase. This pathway was first elucidated by Huber and Edwards (1975), suggesting that PEP could be formed via phosphoglycerate mutase and enolase without using energy (Figure 6.2). This is significant because the two main pathways that form PEP in C_4 photosynthesis, via the reactions catalysed by PEPCK or PPDK, require energy. However, it is not known how rapidly the interconversion between 3-PGA to PEP occurs or whether it is regulated (Arrivault *et al.*, 2016), but an early study estimated that the interconversion between 3-PGA and PEP occurred at one-third the maximal rate of the reactions in the PCR cycle (Monson and Moore, 1989).

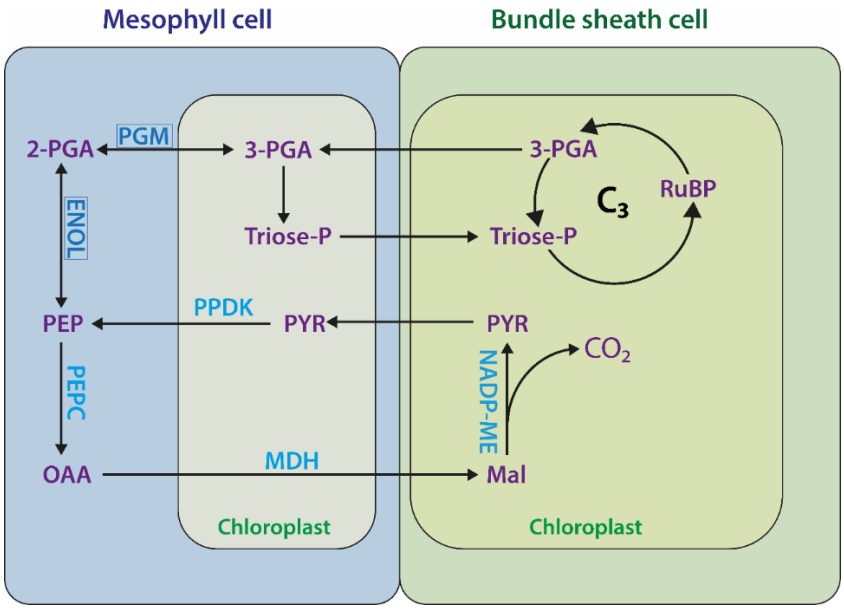

Fig. 6.2. Interconversion of 3-PGA and PEP via phosphoglycerate mutase and enolase in a NADP-malic enzyme system. The interconversion of 3-PGA and PEP in C_4 plants may link C_3 and C_4 cycles, thereby generating PEP in a sequential, non-energy requiring mechanism. Adapted from Huber and Edwards (1975).

Light-dependent phosphorylation sites identified in phosphoglycerate mutase and enolase are the first indication that this pathway is regulated in C_4 plants. However, since the interconversion of 3-PGA and PEP is not energy-dependent, like PEPCK or PPDK, its regulation might not be as critical as that of other key C_4 enzymes (M. Stitt, personal communication). The interconversion between 3-PGA and triose phosphates is crucial in C_4 plants and the 3-PGA that is translocated from bundle sheath to mesophyll cells needs to be reduced to triose phosphates and not necessarily used to form PEP. The conversion of 3-PGA to triose phosphates requires three steps and energy (Huber and Edwards, 1975) (Figure 1.2). First, 3-PGA is converted to 1,3 bisphosphoglycerate via phosphoglycerate kinase, which requires activation by ATP. Then, 1,3 bisphosphoglycerate is reduced to glyceraldehyde-3-phosphate via glyceraldehyde-3-phosphate dehydrogenase using NADPH. Finally, glyceraldehyde-3-phosphate is converted to dihydroxyacetone phosphate (triose phosphate) via triose phosphate isomerase (Anderson, 1971; Huber and Edwards, 1975).

Alternatively, the conversion of 3-PGA to PEP via phosphoglycerate mutase and enolase does not require energy, and therefore the flux of carbon through this pathway may offer less resistance than the energy-dependent reduction of 3-PGA to triose phosphates. Therefore, these two pathways could potentially compete for 3-PGA. The conversion between 3-PGA to triose phosphates via the reactions catalysed by phosphoglycerate kinase, glyceraldehyde-3-phosphate dehydrogenase and triose phosphate isomerase in mesophyll cells is crucial in C_4 plants and alleviates the burden of 3-PGA dependent O_2 evolution from bundle sheath cells especially in NADP-malic enzyme subtypes, which lack the capacity to generate reducing equivalents due to reduced photosystem II activity in bundle sheath cells (Chapman *et al.*, 1980; Leegood, 2013). Triose phosphates that are formed in mesophyll cells must be transported back to bundle sheath chloroplasts and are essential to regenerate RuBP in the PCR cycle (Hatch, 1987).

Formation of PEP through the conversion from 3-PGA might be a way of increasing C_4 metabolites by feeding in from the PCR cycle (Leegood and von Caemmerer, 1994) and may be advantageous in C_3–C_4 intermediate species or C_4 species such as *Sorghum bicolor* and *Setaria viridis*, which solely rely on one decarboxylation pathway (Gutierrez *et al.*, 1974). Furthermore, metabolites could effectively move between C_3 and C_4 cycles, thus contributing to the larger pool of metabolites in mesophyll or bundle sheath cells (Arrivault *et al.*, 2016). Communication between C_3 and C_4 pathways along with

mechanisms allowing to switch between using fluxes malate or aspartate, can increase the flexibility of the C_4 phenotype and maintain photosynthetic performance during intervals of low-light or reduced rates of carbon fixation (Huber and Edwards, 1975; Furbank and Leegood, 1984; Leegood and von Caemmerer, 1989; Bellasio and Griffiths, 2014; Stitt and Zhu, 2014). In addition to this, the interconversion of 3-PGA and PEP might have evolved when the C_4 pump was first established and PEPC activity was enhanced, but there might not have been sufficient PPDK activity in mesophyll cells to regenerate PEP since PPDK did not acquire C_4-specific function until much later (Sage, 2004). It has been suggested that reduced rates of PEP formation might have limited the progression of C_4-evolution in C_3–C_4 intermediates (Peisker, 1986) and certain C_3–C_4 *Flaveria* intermediates might have used the interconversion of 3-PGA and PEP to increase the amount of C_4 metabolites needed to operate the CO_2 pump (Monson and Moore, 1989). The importance of this interconversion in *Flaveria* C_3–C_4 intermediates is further supported by the higher activities of phosphoglycerate mutase and enolase when compared to the activities in *Flaveria cronquistii* (C_3), *Flaveria trinervia* (C_4) (Monson and Moore, 1989), *Zea mays* and *Spinacea oleracea* (C_3) (Furbank and Leegood, 1984). Although the non-energy requiring interconversion between 3-PGA and PEP could have been selected for during the early stages of C_4-evolution, it is speculated that its importance declined after PPDK acquired C_4-specific function and could regenerate PEP at higher rates (Monson and Moore, 1989).

Both phosphoglycerate mutase and enolase are present in appreciable amounts in mesophyll cells of C_4 plants (Ku and Edwards, 1975) and activity might be strictly dependent on illumination, which would correlate to the increase in the amount of PEP and 3-PGA available in the whole leaf (Furbank and Leegood, 1984; Leegood and von Caemmerer, 1989). While this pathway may not be the primary route for PEP formation in C_4 plants, its reversibility, together with requiring no energy, can be the only way that carbon is moved between C_3 and C_4 cycles. Such communication between C_3 and C_4 cycles might be necessary in C_4 plants and intermediate species, since they generate higher amounts of 3-PGA and triose phosphates during photosynthesis than C_3 plants (Badger *et al.*, 1984; Leegood and von Caemmerer, 1994; Arrivault *et al.*, 2016). It would be interesting to determine if there are any changes in the kinetic properties of phosphoglycerate mutase and enolase in response to the dark to light transition in both the forward and reverse reactions. It might also be important to understand how the

phosphorylation of phosphoglycerate mutase and enolase might affect enzymatic activity. In addition to this, it might be beneficial to consider this pathway when engineering C_4 photosynthesis into C_3 crops, since it might have served an important role during the early stages of C_4 photosynthesis and may have confer some biochemical stability for the CO_2 pump (Monson and Moore, 1989). Moreover, this pathway might maintain high photosynthetic efficiency during light fluctuations by supplying metabolites when the rate of CO_2 assimilation declines (Furbank and Leegood, 1984; Leegood and von Caemmerer, 1989; Stitt and Zhu, 2014).

With regards to C_3–C_4 intermediate species, there is some concern as to how PEP is regenerated in C_3–C_4 intermediates and C_4 variants of *Alloteropsis semialata* populations. Transcriptomic analyses have shown that the relative expression of PPDK in the C_4 variant of *Alloteropsis semialata* is about 0.5-fold lower than the expression in *Setaria italica* (unpublished), raising concern whether there is significant PPDK activity in mesophyll cells. Comparatively, PEPCK expression in *Alloteropsis semialata* is approximately 122-fold higher than the expression in *Setaria italica*, whereas the relative expression of NADP-malic enzyme in *Setaria italica* is approximately 12-fold higher than in *Alloteropsis semialata* (unpublished). Furthermore, evidence suggests that there is no substantial formation of pyruvate in *Alloteropsis semialata* via NADP-malic enzyme, suggesting the *Alloteropsis semialata* might be a true PEPCK subtype, and therefore PEP cannot be efficiently regenerated via PPDK (P.A. Christin, personal communication). It was also found that C_4 *Alloteropsis semialata* have high PEP phosphatase activity and this might serve as an alternative pathway for the formation of PEP (P.A. Christin, personal communication).

6.3 Conclusion

In summary, it was shown that NADP-malic enzyme, aspartate aminotransferase and alanine aminotransferase undergo light-dependent phosphorylation. This study also showed that PEPC and PPDK were phosphorylated at the previously described residues in *Zea mays* and *Sorghum bicolor*, but there are additional phosphorylation sites that have not been described in other C_4 plants. It is possible that some of these phosphorylated amino acids affect enzymatic activity. Aside from the phosphorylation of key C_4-related

proteins, the light-dependent phosphorylation of phosphoglycerate mutase and enolase was shown. This might be important for regulating the flux of carbon through C_3 and C_4 cycles and if there are phosphoregulatory controls, it might be an indication to the importance of this pathway and formation of C_4 metabolites.

In addition, this study showed that the properties of NADP-malic enzyme and aspartate aminotransferase are species-specific. It is apparent that the flexibility of NADP-malic enzyme and aspartate or alanine aminotransferase activity might be important for maintaining high photosynthetic performance. Certain NADP-malic enzyme plants, like *Zea mays*, may have the ability to switch between NADP-malic enzyme and PEPCK decarboxylation. This is shown by the differences in catalytic properties of NADP-malic enzyme and aspartate aminotransferase between *Zea mays* and *Sorghum bicolor*. This study further supports the fact that the classification of C_4 plants as distinct subtypes might not be truly representative of the interspecies differences that exist.

With regards to engineering the C_4 trait into existing C_3 crops, efforts should consider engineering multiple decarboxylase pathways, such that the metabolic robustness of the carbon concentrating mechanism of C_4 photosynthesis is maintained and responds to environmental changes such as fluctuating light intensities (Wang *et al.*, 2014). Furthermore, there may not be a single species that provides the best blueprint for engineering C_4 photosynthesis, as species-dependent changes in NADP-malic enzyme activity have been shown to exist. In addition to this, post-translational regulatory mechanisms must be validated such that C_4-related proteins expressed in target C_3 species maintain the expected photosynthetic capacity. This is particularly important since NADP-malic enzyme, aspartate aminotransferase and alanine aminotransferase exist in both C_3 and C_4 plants, but these may be regulated differently (Hibberd and Quick, 2002).

References

Abdallah C, Dumas-Gaudot E, Renaut J, Sergeant K (2012) Gel-based and gel-free quantitative proteomics approaches at a glance. *International Journal of Plant Genomics* **2012**: 494572.

Aebersold R and Mann M (2003) Mass spectrometry-based proteomics. *Nature* **422**: 198–207.

Agetsuma M, Furumoto T, Yanagisawa S, Izui K (2005) The ubiquitin-proteasome pathway is involved in rapid degradation of phospho*enol*pyruvate carboxylase kinase for C_4 photosynthesis. *Plant Cell Physiol* **46**: 389–398.

Agrawal GK and Thelen JJ (2009) A high-resolution two dimensional gel- and Pro-Q DPS-based proteomics workflow for phosphoprotein identification and quantitative profiling. *In* Graauw, MD, ed, *Phospho-Proteomics: Methods and Protocols*. Totowa, NJ, USA: Humana Press, 3–19.

Akyildiz M, Gowik U, Engelmann S, Koczor M, Streubel M, Westhoff P (2007) Evolution and function of a *cis*-regulatory module for mesophyll-specific gene expression in the C_4 dicot *Flaveria trinervia*. *The Plant Cell* **19**: 3391–3402.

Alvarez CE, Detarsio E, Moreno S, Andreo CS, Drincovich MF (2012) Functional characterization of residues involved in redox modulation of maize photosynthetic NADP-malic enzyme activity. *Plant Cell Physiol* **53**: 1144–1153.

Amthor JS (2001) Effects of atmospheric CO_2 concentration on wheat yield: review of results from experiments using various approaches to control CO_2 concentration. *Field Crops Res* **73**: 1–34.

Anderson LE (1971) Chloroplast and cytoplasmic enzymes II. Pea leaf triose phosphate isomerases. *Biochim Biophys Acta* **235**: 237–244.

Andersson I (2008) Catalysis and regulation in Rubisco. *J Exp Bot* **59**: 1555–1568.

Andreo CS, Gonzalez DH, Iglesias AA (1987) Higher plant phospho*enol*pyruvate carboxylase: structure and regulation. *FEBS Lett* **213**: 1–8.

Andrews TJ, Johnson HS, Slack CR, Hatch MD (1971) Malic enzyme and aminotransferases in relation to 3-phosphoglycerate formation in plants with the C_4-dicarboxylic acid pathway of photosynthesis. *Phytochemistry* **10**: 2005–2013.

Andrews TJ and Lorimer GH (1987) Rubisco: structure, mechanisms, and prospects for improvement. *In* Hatch, MD, Bordman, NK, eds, *The Biochemistry of Plants*. New York, NY, USA: Academic Press, 131–218.

Arnon DI (1949) Copper enzymes in isolated chloroplasts. Polyphenoloxidase in *Beta vulgaris*. *Plant Physiol* **24**: 1–15.

Arrivault S, Obata T, Szecowka M, Mengin V, Guenther M, Hoehne M, Fernie AR, Stitt M (2016) Metabolite pools and carbon flow during C_4 photosynthesis in maize: $^{13}CO_2$ labeling kinetics and cell type fractionation. *J Exp Bot* **68**: 283–298.

Asami S, Inoue K, Akazawa T (1979) NADP-malic enzyme from maize leaf: Regulatory properties. *Arch Biochem Biophys* **196**: 581–587.

Ashton AR, Burnell JN, Furbank RT, Jenkins CLD, Hatch MD (1990) Enzymes of C_4 photosynthesis. *In* Lea, PJ, ed, *Methods in plant biochemistry*. London, UK: Academic Press, 39–72.

Ashton AR and Hatch MD (1983) Regulation of C_4 photosynthesis: physical and kinetic properties of active (dithiol) and inactive (disulfide) NADP-malate dehydrogenase from *Zea mays*. *Arch Biochem Biophys* **227**: 406–415.

Ashton AR and Hatch MD (1983) Regulation of C_4 photosynthesis: regulation of pyruvate, Pi dikinase by ADP-dependent phosphorylation and dephosphorylation. *Biochem Biophys Res Commun* **115**: 53–60.

Atkin OK, Scheurwater I, Pons TL (2006) High thermal acclimation potential of both photosynthesis and respiration in two lowland *Plantago* species in contrast to an alpine congeneric. *Global Change Biol* **12**: 500–515.

Audagnotto M and Dal Peraro M (2017) Protein post-translational modifications: *in silico* prediction tools and molecular modeling. *Comput Struct Biotechnol J* **15**: 307–319.

Badger MR and Andrews TJ (1987) Co-evolution of Rubisco and CO_2 concentrating mechanisms. *In* Biggins, J, ed, *Progress in photosynthesis research*. Providence, RI, USA: Springer, 601–609.

Badger MR, Andrews TJ, Whitney SM, Ludwig M, Yellowlees DC, Leggat W, Price GD (1998) The diversity and coevolution of Rubisco, plastids, pyrenoids, and chloroplast-based CO_2-concentrating mechanisms in algae. *Can J Bot* **76**: 1052–1071.

Badger MR, Hanson D, Price GD (2002) Evolution and diversity of CO_2 concentrating mechanisms in cyanobacteria. *Funct Plant Biol* **29**: 161–173.

Badger MR, Sharkey TD, von Caemmerer S (1984) The relationship between steady-state gas exchange of bean leaves and the levels of carbon-reduction-cycle intermediates. *Planta* **160**: 305–313.

Badia MB, Arias CL, Tronconi MA, Maurino VG, Andreo CS, Drincovich MF, Wheeler MCG (2015) Enhanced cytosolic NADP-ME2 activity in *A. thaliana* affects plant development, stress tolerance and specific diurnal and nocturnal cellular processes. *Plant Sci* **240**: 193–203.

Bagag A, Jault JM, Sidahmed-Adrar N, Réfrégiers M, Giuliani A, Le Naour F (2013) Characterization of hydrophobic peptides in the presence of detergent by photoionization mass spectrometry. *PLoS One* **8**: e79033.

Bailey KJ, Gray JE, Walker RP, Leegood RC (2007) Coordinate regulation of phospho*enol*pyruvate carboxylase and phospho*enol*pyruvate carboxykinase by light and CO_2 during C_4 photosynthesis. *Plant Physiol* **144**: 479–486.

Bartsch O, Mikkat S, Hagemann M, Bauwe H (2010) An autoinhibitory domain confers redox regulation to maize glycerate kinase. *Plant Physiol* **153**: 832–840.

Bassham JA (2005) Mapping the carbon reduction cycle: a personal retrospective. *In* Govindjee, J, Beatty, T, Gest, H, Allen, JF, eds, *Discoveries in Photosynthesis*. The Netherlands: Springer, 817–832.

Bassham JA and Calvin M (1962) The way of CO_2 in plant photosynthesis. *Comp Biochem Physiol* **4**: 187–204.

Bassham JA and Kirk M (1960) Dynamics of the photosynthesis of carbon compounds I. Carboxylation reactions. *Biochim Biophys Acta* **43**: 447–464.

Bauwe H (1984) Photosynthetic enzyme activities and immunofluorescence studies on the localization of ribulose-1, 5-bisphosphate carboxylase/oxygenase in leaves of C_3, C_4, and C_3–C_4 intermediate species of *Flaveria* (Asteraceae). *Biochem Physiol Pflanz* **179**: 253–268.

Bauwe H (2011) Photorespiration: the bridge to C_4 photosynthesis. *In* Raghavendra, AS, Sage, RF, eds, *C_4 photosynthesis and related CO_2 concentrating mechanisms*. Dordrecht, The Netherlands: Springer, 81–108.

Bauwe H, Hagemann M, Fernie AR (2010) Photorespiration: players, partners and origin. *Trends Plant Sci* **15**: 330–336.

Bauwe H, Hagemann M, Kern R, Timm S (2012) Photorespiration has a dual origin and manifold links to central metabolism. *Curr Opin Plant Biol* **15**: 269–275.

Bellasio C and Griffiths H (2014) The operation of two decarboxylases (NADP-ME and PEPCK), transamination and partitioning of C_4 metabolic processes between mesophyll and bundle sheath cells allows light capture to be balanced for the maize C_4 pathway. *Plant Physiol* **164**: 466–480.

Bellasio C, Quirk J, Buckley TN, Beerling D (2017) A dynamic hydro-mechanical and biochemical model of stomatal conductance for C_4 photosynthesis. *Plant Physiol* **175**: 17.00666.

Bennetzen JL, Schmutz J, Wang H, Percifield R, Hawkins J, Pontaroli AC, Estep M, Feng L, Vaughn JN, Grimwood J, Jenkins J, Barry K, Lindquist E, Hellsten U, Deshpande S, Wang X, Wu X, Mitros T, Triplett J, Yang X, Ye CY, Mauro-Herrera M, Wang L, Li P, Sharma M, Sharma R, Ronald PC, Panaud O, Kellogg EA, Brutnell TP, Doust AN, Tuskan GA, Rokhsar D, Devos KM (2012) Reference genome sequence of the model plant *Setaria*. *Nat Biotech* **30**: 555–561.

Benson AA (1954) Photosynthesis: first reactions. *J chem Educ* **31**: 484.

Berghuijs HNC, Yin X, Ho QT, Driever SM, Retta MA, Nicolaï BM, Struik PC (2016) Mesophyll conductance and reaction-diffusion models for CO_2 transport in C_3 leaves; needs, opportunities and challenges. *Plant Sci* **252**: 62–75.

Berghuijs HNC, Yin X, Ho QT, van der Putten PEL, Verboven P, Retta MA, Nicolaï BM, Struik PC (2015) Modelling the relationship between CO_2 assimilation and leaf anatomical properties in tomato leaves. *Plant Sci* **238**: 297–311.

Bernacchi CJ, Portis AR, Nakano H, von Caemmerer S, Long SP (2002) Temperature response of mesophyll conductance. Implications for the determination of Rubisco enzyme kinetics and for limitations to photosynthesis *in vivo*. *Plant Physiol* **130**: 1992–1998.

Berry J and Bjorkman O (1980) Photosynthetic response and adaptation to temperature in higher plants. *Annu Rev Plant Physiol* **31**: 491–543.

Berry JO, Mure CM, Yerramsetty P (2016) Regulation of Rubisco gene expression in C_4 plants. *Curr Opin Plant Biol* **31**: 23–28.

Berry JO, Yerramsetty P, Zielinski AM, Mure CM (2013) Photosynthetic gene expression in higher plants. *Photosynth Res* **117**: 91–120.

Bhattacharjee S, Noor JJ, Gohain B, Gulabani H, Dnyaneshwar IK, Singla A (2015) Post-translational modifications in regulation of pathogen surveillance and signaling in plants: the inside- (and perturbations from) outside story. *IUBMB Life* **67**: 524–532.

Björkman O, Gauhl E, Hiesey WM, Nicholson F, Nobs MA (1969) Growth of *Mimulus*, *Marchantia*, and *Zea* under different oxygen and carbon dioxide levels. *Carnegie Inst Wash Year B* **67**: 477–478.

Blankenship RE (2010) Early evolution of photosynthesis. *Plant Physiol* **154**: 434–438.

Bläsing OE, Westhoff P, Svensson P (2000) Evolution of C_4 phospho*enol*pyruvate carboxylase in *Flaveria*, a conserved serine residue in the carboxyl-terminal part of the enzyme is a major determinant for C_4-specific characteristics. *J Biol Chem* **275**: 27917–27923.

Bloom AJ, Burger M, Asensio JSR, Cousins AB (2010) Carbon dioxide enrichment inhibits nitrate assimilation in wheat and *Arabidopsis*. *Science* **328**: 899–903.

Bloom AJ, Smart DR, Nguyen DT, Searles PS (2002) Nitrogen assimilation and growth of wheat under elevated carbon dioxide. *Proc Natl Acad Sci USA* **99**: 1730–1735.

Bologna FP, Andreo CS, Drincovich MF (2007) *Escherichia coli* malic enzymes: two isoforms with substantial differences in kinetic properties, metabolic regulation, and structure. *J Bacteriol* **189**: 5937–5946.

Bonsib SM, Harruff RC, Jenkins WT (1975) Factors contributing to the inhibition of aspartate aminotransferase by dicarboxylic acids. *J Biol Chem* **250**: 8635–8641.

Boxall SF, Dever LV, Knerova J, Gould PD, Hartwell J (2017) Phosphorylation of phospho*enol*pyruvate carboxylase is essential for maximal and sustained dark CO_2 fixation and core circadian clock operation in the obligate crassulacean acid metabolism species *Kalanchoë fedtschenkoi*. *The Plant Cell Online* **29**: tpc-00301.

Boyd RA, Gandin A, Cousins AB (2015) Temperature response of C_4 photosynthesis: biochemical analysis of Rubisco, phospho*enol*pyruvate carboxylase and carbonic anhydrase in *Setaria viridis*. *Plant Physiol* **169**: 1850–1861.

Bradford MM (1976) A rapid and sensitive method for the quantitation of microgram quantities of protein utilizing the principle of protein-dye binding. *Anal Biochem* **72**: 248–254.

Bräutigam A, Hoffmann-Benning S, Weber APM (2008) Comparative proteomics of chloroplast envelopes from C_3 and C_4 plants reveals specific adaptations of the plastid envelope to C_4 photosynthesis and candidate proteins required for maintaining C_4 metabolite fluxes. *Plant Physiol* **148**: 568–579.

Bräutigam A, Kajala K, Wullenweber J, Sommer M, Gagneul D, Weber KL, Carr KM, Gowik U, Maß J, Lercher MJ (2011) An mRNA blueprint for C_4 photosynthesis derived from comparative transcriptomics of closely related C_3 and C_4 species. *Plant Physiol* **155**: 142–156.

Bräutigam A, Schliesky S, Külahoglu C, Osborne CP, Weber AP (2014) Towards an integrative model of C_4 photosynthetic subtypes: insights from comparative transcriptome analysis of NAD-ME, NADP-ME, and PEP-CK C_4 species. *J Exp Bot* **65**: 3579–3593.

Brooks A and Farquhar GD (1985) Effect of temperature on the CO_2/O_2 specificity of ribulose-1, 5-bisphosphate carboxylase/oxygenase and the rate of respiration in the light. *Planta* **165**: 397–406.

Brown NJ, Newell CA, Stanley S, Chen JE, Perrin AJ, Kajala K, Hibberd JM (2011) Independent and parallel recruitment of preexisting mechanisms underlying C_4 photosynthesis. *Science* **331**: 1436–1439.

Brown RH (1978) A difference in N use efficiency in C_3 and C_4 plants and its implications in adaptation and evolution. *Crop Sci* **18**: 93–98.

Brown RH and Hattersley PW (1989) Leaf anatomy of C_3–C_4 species as related to evolution of C_4 photosynthesis. *Plant Physiol* **91**: 1543–1550.

Brutnell TP, Wang L, Swartwood K, Goldschmidt A, Jackson D, Zhu XG, Kellogg E, Van Eck J (2010) *Setaria viridis*: a model for C_4 photosynthesis. *The Plant Cell* **22**: 2537–2544.

Buchanan BB, Gruissem W, Jones RL (2015) Biochemistry and Molecular Biology of Plants, Ed 2. John Wiley & Sons, Wiley, Hoboken, NJ, USA.

Budde RJA and Chollet R (1986) *In vitro* phosphorylation of maize leaf phospho*enol*pyruvate carboxylase. *Plant Physiol* **82**: 1107–1114.

Budde RJA, Holbrook GP, Chollet R (1985) Studies on the dark/light regulation of maize leaf pyruvate, orthophosphate dikinase by reversible phosphorylation. *Arch Biochem Biophys* **242**: 283–290.

Burnell JN and Hatch MD (1988) Low bundle sheath carbonic anhydrase is apparently essential for effective C_4 pathway operation. *Plant Physiol* **86**: 1252–1256.

Burnell JN, Jenkins CLD, Hatch MD (1986) Regulation of C_4 photosynthesis a role for pyruvate in regulating pyruvate, Pi dikinase activity *in vivo*. *Funct Plant Biol* **13**: 203–210.

Busch FA, Sage TL, Cousins AB, Sage RF (2013) C_3 plants enhance rates of photosynthesis by reassimilating photorespired and respired CO_2. *Plant Cell Environ* **36**: 200–212.

Candau P, Manzano C, Losada M (1976) Bioconversion of light energy into chemical energy through reduction with water of nitrate to ammonia. *Nature* **262**: 715–717.

Carlson GM, Colombo G, Lardy HA (1978) A vicinal dithiol containing an essential cysteine in phospho*enol*pyruvate carboxykinase (guanosine triphosphate) from cytosol of rat liver. *Biochemistry* **17**: 5329–5338.

Carnal NW, Agostino A, Hatch MD (1993) Photosynthesis in phospho*enol*pyruvate carboxykinase-type C_4 plants: mechanism and regulation of C_4 acid decarboxylation in bundle sheath cells. *Arch Biochem Biophys* **306**: 360–367.

Carter PJ, Nimmo HG, Fewson CA, Wilkins MB (1990) *Bryophyllum fedtschenkoi* protein phosphatase type 2A can dephosphorylate phospho*enol*pyruvate carboxylase. *FEBS Lett* **263**: 233–236.

Carter PJ, Nimmo HG, Fewson CA, Wilkins MB (1991) Circadian rhythms in the activity of a plant protein kinase. *EMBO J* **10**: 2063–2068.

Casati P, Fresco AG, Andreo CS, Drincovich MF (1999) An intermediate form of NADP-malic enzyme from the C_3–C_4 intermediate species *Flaveria floridana*. *Plant Sci* **147**: 101–109.

Casati P, Spampinato CP, Andreo CS (1997) Characteristics and physiological function of NADP-malic enzyme from wheat. *Plant Cell Physiol* **38**: 928–934.

Chao Q, Liu XY, Mei YC, Gao ZF, Chen YB, Qian CR, Hao YB, Wang BC (2014) Light-regulated phosphorylation of maize phospho*enol*pyruvate carboxykinase plays a vital role in its activity. *Plant Mol Biol* **85**: 95–105.

Chapman KSR, Berry JA, Hatch MD (1980) Photosynthetic metabolism in bundle sheath cells of the C_4 species *Zea mays*: sources of ATP and NADPH and the contribution of photosystem II. *Arch Biochem Biophys* **202**: 330–341.

Chapman KSR and Hatch MD (1979) Aspartate stimulation of malate decarboxylation in *Zea mays* bundle sheath cells: possible role in regulation of C_4 photosynthesis. *Biochem Biophys Res Commun* **86**: 1274–1280.

Chapman KSR and Hatch MD (1981) Aspartate decarboxylation in bundle sheath cells of *Zea mays* and its possible contribution to C_4 photosynthesis. *Funct Plant Biol* **8**: 237–248.

Chastain CJ, Botschner M, Harrington GE, Thompson BJ, Mills SE, Sarath G, Chollet R (2000) Further analysis of maize C_4 pyruvate, orthophosphate dikinase phosphorylation by its bifunctional regulatory protein using selective substitutions of the regulatory Thr-456 and catalytic His-458 residues. *Arch Biochem Biophys* **375**: 165–170.

Chastain CJ and Chollet R (2003) Regulation of pyruvate, orthophosphate dikinase by ADP-/Pi-dependent reversible phosphorylation in C_3 and C_4 plants. *Plant Physiol Biochem* **41**: 523–532.

Chastain CJ, Failing CJ, Manandhar L, Zimmerman MA, Lakner MM, Nguyen TH (2011) Functional evolution of C_4 pyruvate, orthophosphate dikinase. *J Exp Bot* **62**: 3083–3091.

Chastain CJ, Lee ME, Moorman MA, Shameekumar P, Chollet R (1997) Site-directed mutagenesis of maize recombinant C_4-pyruvate, orthophosphate dikinase at the phosphorylatable target threonine residue. *FEBS Lett* **413**: 169–173.

Chen YB, Lu TC, Wang HX, Shen J, Bu TT, Chao Q, Gao ZF, Zhu XG, Wang YF, Wang BC (2014) Posttranslational modification of maize chloroplast pyruvate, orthophosphate dikinase reveals the precise regulatory mechanism of its enzymatic activity. *Plant Physiol* **165**: 534–549.

Chen Z and Spreitzer RJ (1992) How various factors influence the CO_2/O_2 specificity of ribulose-1, 5-bisphosphate carboxylase/oxygenase. *Photosynth Res* **31**: 157–164.

Chollet R and Ogren WL (1972) Oxygen inhibits maize bundle sheath photosynthesis. *Biochem Biophys Res Commun* **46**: 2062–2066.

Chollet R, Vidal J, O'Leary MH (1996) Phospho*enol*pyruvate carboxylase: a ubiquitous, highly regulated enzyme in plants. *Annu Rev Plant Physiol Plant Mol Biol* **47**: 273–298.

Christin PA, Edwards EJ, Besnard G, Boxall SF, Gregory R, Kellogg EA, Hartwell J, Osborne CP (2012) Adaptive evolution of C_4 photosynthesis through recurrent lateral gene transfer. *Curr Biol* **22**: 445–449.

Christin PA and Osborne CP (2013) The recurrent assembly of C_4 photosynthesis, an evolutionary tale. *Photosynth Res* **117**: 163–175.

Christin PA, Salamin N, Savolainen V, Duvall MR, Besnard G (2007) C_4 photosynthesis evolved in grasses via parallel adaptive genetic changes. *Curr Biol* **17**: 1241–1247.

Christin PA, Samaritani E, Petitpierre B, Salamin N, Besnard G (2009) Evolutionary insights on C_4 photosynthetic subtypes in grasses from genomics and phylogenetics. *Genome Biol Evol* **1**: 221–230.

Chung HS, Wang SB, Venkatraman V, Murray CI, van Eyk JE (2013) Cysteine oxidative post-translational modifications: emerging regulation in the cardiovascular system. *Circul Res* **112**: 382–392.

Collet JF, Stroobant V, Van Schaftingen E (2001) The 2,3-bisphosphoglycerate-independent phosphoglycerate mutase from *Trypanosoma brucei*: metal-ion dependency and phosphoenzyme formation. *FEMS Microbiol Lett* **204**: 39–46.

Cousins AB, Baroli I, Badger MR, Ivakov A, Lea PJ, Leegood RC, von Caemmerer S (2007) The role of phospho*enol*pyruvate carboxylase during C_4 photosynthetic isotope exchange and stomatal conductance. *Plant Physiol* **145**: 1006–1017.

Cousins AB, Ghannoum O, Von Caemmerer S, Badger MR (2010) Simultaneous determination of Rubisco carboxylase and oxygenase kinetic parameters in *Triticum aestivum* and *Zea mays* using membrane inlet mass spectrometry. *Plant Cell Environ* **33**: 444–452.

Covian R, Chess D, Balaban RS (2012) Continuous monitoring of enzymatic activity within native electrophoresis gels: application to mitochondrial oxidative phosphorylation complexes. *Anal Biochem* **431**: 30–39.

Covshoff S and Hibberd JM (2012) Integrating C_4 photosynthesis into C_3 crops to increase yield potential. *Curr Opin Biotechnol* **23**: 209–214.

Crafts-Brandner SJ and Salvucci ME (2000) Rubisco activase constrains the photosynthetic potential of leaves at high temperature and CO_2. *Proc Natl Acad Sci* **97**: 13430–13435.

Cui L, Yapici I, Borhan B, Reid GE (2014) Quantification of competing H_3PO_4 versus HPO_3 + H_2O neutral losses from regioselective ^{18}O-labeled phosphopeptides. *J Am Soc Mass Spectrom* **25**: 141–148.

Day DA and Hatch MD (1981) Dicarboxylate transport in maize mesophyll chloroplasts. *Arch Biochem Biophys* **211**: 738–742.

de la Fuente van Bentem S, Anrather D, Dohnal I, Roitinger E, Csaszar E, Joore J, Buijnink J, Carreri A, Forzani C, Lorkovic ZJ (2008) Site-specific phosphorylation profiling of *Arabidopsis* proteins by mass spectrometry and peptide chip analysis. *J Proteome Res* **7**: 2458–2470.

Decottignies P, Schmitter JM, Miginiac-Maslow M, Le Marechal P, Jacquot JP, Gadal P (1988) Primary structure of the light-dependent regulatory site of corn NADP-malate dehydrogenase. *J Biol Chem* **263**: 11780–11785.

Dephoure N, Gould KL, Gygi SP, Kellogg DR (2013) Mapping and analysis of phosphorylation sites: a quick guide for cell biologists. *Mol Biol Cell* **24**: 535–542.

Detarsio E, Alvarez CE, Saigo M, Andreo CS, Drincovich MF (2007) Identification of domains involved in tetramerization and malate inhibition of maize C_4-NADP-malic enzyme. *J Biol Chem* **282**: 6053–6060.

Doncaster HD and Leegood RC (1987) Regulation of phospho*enol*pyruvate carboxylase activity in maize leaves. *Plant Physiol* **84**: 82–87.

Dong L, Ermolova NV, Chollet R (2001) Partial purification and biochemical characterization of a heteromeric protein phosphatase 2A holoenzyme from maize (*Zea mays* L.) leaves that dephosphorylates C_4 phospho*enol*pyruvate carboxylase. *Planta* **213**: 379–389.

Dong LY, Masuda T, Kawamura T, Hata S, Izui K (1998) Cloning, expression, and characterization of a root-form phospho*enol*pyruvate carboxylase from *Zea mays*: comparison with the C_4-form enzyme. *Plant Cell Physiol* **39**: 865–873.

Drincovich MF and Andreo CS (1994) Redox regulation of maize NADP-malic enzyme by thiol-disulfide interchange: effect of reduced thioredoxin on activity. *Biochim Biophys Acta* **1206**: 10–16.

Drincovich MF, Casati P, Andreo CS (2001) NADP-malic enzyme from plants: a ubiquitous enzyme involved in different metabolic pathways. *FEBS Lett* **490**: 1–6.

Drincovich MF, Casati P, Andreo CS, Chessin SJ, Franceschi VR, Edwards GE, Ku MSB (1998) Evolution of C_4 photosynthesis in *Flaveria* species isoforms of NADP-malic enzyme. *Plant Physiol* **117**: 733–744.

Drincovich MF, Iglesias AA, Andreo CS (1991) Interaction of divalent metal ions with the $NADP^+$-malic enzyme from maize leaves. *Physiol Plant* **81**: 462–466.

Duff SMG and Chollet R (1995) *In vivo* regulation of wheat-leaf phospho*enol*pyruvate carboxylase by reversible phosphorylation. *Plant Physiol* **107**: 775–782.

Duff SMG, Giglioli-Guivarc'h N, Pierre JN, Vidal J, Condon SA, Chollet R (1996) *In-situ* evidence for the involvement of calcium and bundle-sheath-derived photosynthetic metabolites in the C_4 phospho*enol*pyruvate-carboxylase kinase signal-transduction chain. *Planta* **199**: 467–474.

Duff SMG, Lepiniec L, Crétin C, Andreo CS, Condon SA, Sarath G, Vidal J, Gadal P, Chollet R (1993) An engineered change in the L-malate sensitivity of a site-directed mutant of sorghum phospho*enol*pyruvate carboxylase: the effect of sequential mutagenesis and S-carboxymethylation at position 8. *Arch Biochem Biophys* **306**: 272–276.

Duff SMG, Rydel TJ, McClerren AL, Zhang W, Li JY, Sturman EJ, Halls C, Chen S, Zeng J, Peng J, Kretzler CN, Evdokimov A (2012) The enzymology of alanine aminotransferase (AlaAT) isoforms from *Hordeum vulgare* and other organisms, and the HvAlaAT crystal structure. *Arch Biochem Biophys* **528**: 90–101.

Dunning LT, Lundgren MR, Moreno-Villena JJ, Namaganda M, Edwards EJ, Nosil P, Osborne CP, Christin PA (2017) Introgression and repeated co-option facilitated the recurrent emergence of C_4 photosynthesis among close relatives. *Evolution* **71**: 1541–1555.

Echevarría C, Pacquit V, Bakrim N, Osuna L, Delgado B, Arriodupont M, Vidal J (1994) The effect of pH on the covalent and metabolic control of C_4 phospho*enol*pyruvate carboxylase from *Sorghum* leaf. *Arch Biochem Biophys* **315**: 425–430.

Echevarría C, Vidal J, Jiao JA, Chollet R (1990) Reversible light activation of the phospho*enol*pyruvate carboxylase protein-serine kinase in maize leaves. *FEBS Lett* **275**: 25–28.

Edwards EJ, Osborne CP, Strömberg CAE, Smith SA (2010) The origins of C_4 grasslands: integrating evolutionary and ecosystem science. *Science* **328**: 587–591.

Edwards G and Walker D (1983) C_3, C_4: mechanisms, and cellular and environmental regulation, of photosynthesis. Blackwell Scientific Publications, Oxford, UK.

Edwards GE and Andreo CS (1992) NADP-malic enzyme from plants. *Phytochemistry* **31**: 1845–1857.

Edwards GE, Franceschi VR, Ku MSB, Voznesenskaya EV, Pyankov VI, Andreo CS (2001) Compartmentation of photosynthesis in cells and tissues of C_4 plants. *J Exp Bot* **52**: 577–590.

Edwards GE, Franceschi VR, Voznesenskaya EV (2004) Single-cell C_4 photosynthesis versus the dual-cell (Kranz) paradigm. *Annu Rev Plant Biol* **55**: 173–196.

Ehleringer J and Björkman O (1977) Quantum yields for CO_2 uptake in C_3 and C_4 plants. *Plant Physiol* **59**: 86–90.

Ehleringer JR, Sage RF, Flanagan LB, Pearcy RW (1991) Climate change and the evolution of C_4 photosynthesis. *Trends Ecol Evol* **6**: 95–99.

Eisenhut M, Ruth W, Haimovich M, Bauwe H, Kaplan A, Hagemann M (2008) The photorespiratory glycolate metabolism is essential for cyanobacteria and might have been conveyed endosymbiontically to plants. *Proc Natl Acad Sci USA* **105**: 17199–17204.

Engelmann S, Bläsing OE, Gowik U, Svensson P, Westhoff P (2003) Molecular evolution of C_4 phospho*enol*pyruvate carboxylase in the genus *Flaveria*—a gradual increase from C_3 to C_4 characteristics. *Planta* **217**: 717–725.

Evans JR, Kaldenhoff R, Genty B, Terashima I (2009) Resistances along the CO_2 diffusion pathway inside leaves. *J Exp Bot* **60**: 2235–2248.

Evenson RE and Gollin D (2003) Assessing the impact of the Green Revolution, 1960 to 2000. *Science* **300**: 758–762.

Evert RF, Eschrich W, Heyser W (1977) Distribution and structure of the plasmodesmata in mesophyll and bundle-sheath cells of *Zea mays* L. *Planta* **136**: 77–89.

Fíla J and Honys D (2012) Enrichment techniques employed in phosphoproteomics. *Amino Acids* **43**: 1025–1047.

Friso G and van Wijk KJ (2015) Posttranslational protein modifications in plant metabolism. *Plant Physiol* **169**: 1469–1487.

Fu Y, Yang Q, Sun R, Li D, Zeng R, Ling CX, Gao W (2004) Exploiting the kernel trick to correlate fragment ions for peptide identification via tandem mass spectrometry. *Bioinformatics* **20**: 1948–1954.

Fujii JA and Kennedy RA (1985) Seasonal changes in the photosynthetic rate in apple trees a comparison between fruiting and nonfruiting trees. *Plant Physiol* **78**: 519–524.

Furbank RT (2011) Evolution of the C_4 photosynthetic mechanism: are there really three C_4 acid decarboxylation types? *J Exp Bot* **62**: 3103–3108.

Furbank RT (2016) Walking the C_4 pathway: past, present, and future. *J Exp Bot* **67**: 4057–4066.

Furbank RT and Leegood RC (1984) Carbon metabolism and gas exchange in leaves of *Zea mays* L.: interaction between the C_3 and C_4 pathways during photosynthetic induction. *Planta* **162**: 457–462.

Furbank RT and Taylor WC (1995) Regulation of photosynthesis in C_3 and C_4 plants: a molecular approach. *The Plant Cell* **7**: 797–807.

Furumoto T, Hata S, Izui K (1999) cDNA cloning and characterization of maize phospho*enol*pyruvate carboxykinase, a bundle sheath cell-specific enzyme. *Plant Mol Biol* **41**: 301–311.

Furumoto T, Izui K, Quinn V, Furbank RT, von Caemmerer S (2007) Phosphorylation of phospho*enol*pyruvate carboxylase is not essential for high photosynthetic rates in the C_4 species *Flaveria bidentis*. *Plant Physiol* **144**: 1936–1945.

Furumoto T, Yamaguchi T, Ohshima-Ichie Y, Nakamura M, Tsuchida-Iwata Y, Shimamura M, Ohnishi J, Hata S, Gowik U, Westhoff P (2011) A plastidial sodium-dependent pyruvate transporter. *Nature* **476**: 472–475.

Galmés J, Conesa MÀ, Díaz-Espejo A, Mir A, Perdomo JA, Niinemets Ü, Flexas J (2014) Rubisco catalytic properties optimized for present and future climatic conditions. *Plant Sci* **226**: 61–70.

Garcia BA (2010) What does the future hold for top down mass spectrometry? *J Am Soc Mass Spectrom* **21**: 193–202.

Ghosh SC, Asanuma KI, kusutani A, Toyota M (2000) Effects of temperature at different growth stages on nonstructural carbohydrate, nitrate reductase activity and yield of potato. *Environ Control Biol* **38**: 197–206.

Giglioli-Guivarc'h N, Pierre JN, Brown S, Chollet R, Vidal J, Gadal P (1996) The light-dependent transduction pathway controlling the regulatory phosphorylation of C_4 phospho*enol*pyruvate carboxylase in protoplasts from *Digitaria sanguinalis*. *The Plant Cell* **8**: 573–586.

Godfray HCJ, Beddington JR, Crute IR, Haddad L, Lawrence D, Muir JF, Pretty J, Robinson S, Thomas SM, Toulmin C (2010) Food security: the challenge of feeding 9 billion people. *Science* **327**: 812–818.

Gornall J, Betts R, Burke E, Clark R, Camp J, Willett K, Wiltshire A (2010) Implications of climate change for agricultural productivity in the early twenty-first century. *Philos Trans R Soc Lond, Ser B: Biol Sci* **365**: 2973–2989.

Gowik U, Burscheidt J, Akyildiz M, Schlue U, Koczor M, Streubel M, Westhoff P (2004) *cis*-Regulatory elements for mesophyll-specific gene expression in the C_4 plant *Flaveria trinervia*, the promoter of the C_4 phospho*enol*pyruvate carboxylase gene. *The Plant Cell* **16**: 1077–1090.

Gowik U and Westhoff P (2011) The path from C_3 to C_4 photosynthesis. *Plant Physiol* **155**: 56–63.

Graves PR and Haystead TAJ (2002) Molecular biologist's guide to proteomics. *Microbiol Mol Biol Rev* **66**: 39–63.

Griffin KL and Seemann JR (1996) Plants, CO_2 and photosynthesis in the 21st century. *Chem Biol* **3**: 245–254.

Grønborg M, Kristiansen TZ, Stensballe A, Andersen JS, Ohara O, Mann M, Jensen ON, Pandey A (2002) A mass spectrometry-based proteomic approach for identification of serine/threonine-phosphorylated proteins by enrichment with phospho-specific antibodies identification of a novel protein, Frigg, as a protein kinase A substrate. *Mol Cell Proteomics* **1**: 517–527.

Gutierrez M, Gracen VE, Edwards GE (1974) Biochemical and cytological relationships in C_4 plants. *Planta* **119**: 279–300.

Gütle DD, Roret T, Müller SJ, Couturier J, Lemaire SD, Hecker A, Dhalleine T, Buchanan BB, Reski R, Einsle O (2016) Chloroplast FBPase and SBPase are thioredoxin-linked enzymes with similar architecture but different evolutionary histories. *Proc Natl Acad Sci USA* **113**: 6779–6784.

Haberlandt G (1904) Physiologische Pflanzenanatomie. Engelmann, W., Leipzig, Germany.

Hagemann M and Bauwe H (2016) Photorespiration and the potential to improve photosynthesis. *Curr Opin Chem Biol* **35**: 109–116.

Hannaert V, Saavedra E, Duffieux F, Szikora JP, Rigden DJ, Michels PAM, Opperdoes FR (2003) Plant-like traits associated with metabolism of *Trypanosoma* parasites. *Proc Natl Acad Sci USA* **100**: 1067–1071.

Hansen JW (1996) Is agricultural sustainability a useful concept? *Agric Sys* **50**: 117–143.

Hardt H and Kok B (1978) Comparison of photosynthetic activities of spinach chloroplasts with those of corn mesophyll and corn bundle sheath tissue. *Plant Physiol* **62**: 59–63.

Hartwell J, Gill A, Nimmo GA, Wilkins MB, Jenkins GI, Nimmo HG (1999) Phospho*enol*pyruvate carboxylase kinase is a novel protein kinase regulated at the level of expression. *Plant J* **20**: 333–342.

Hashiguchi A and Komatsu S (2016) Impact of post-translational modifications of crop proteins under abiotic stress. *Proteomes* **4**:

Hatch MD (1971) The C_4-pathway of photosynthesis. Evidence for an intermediate pool of carbon dioxide and the identity of the donor C_4-dicarboxylic acid. *Biochem J* **125**: 425–432.

Hatch MD (1978) Regulation of enzymes in C_4 photosynthesis. *Curr Top Cell Regul* **14**: 1–27.

Hatch MD (1979) Regulation of C_4 photosynthesis: factors affecting cold-mediated inactivation and reactivation of pyruvate, Pi dikinase. *Funct Plant Biol* **6**: 607–619.

Hatch MD (1987) C_4 photosynthesis: a unique blend of modified biochemistry, anatomy and ultrastructure. *Biochim Biophys Acta* **895**: 81–106.

Hatch MD, Agostino A, Burnell JN (1988) Photosynthesis in phospho*enol*pyruvate carboxykinase-type C_4 plants: activity and role of mitochondria in bundle sheath cells. *Arch Biochem Biophys* **261**: 357–367.

Hatch MD and Burnell JN (1990) Carbonic anhydrase activity in leaves and its role in the first step of C_4 photosynthesis. *Plant Physiol* **93**: 825–828.

Hatch MD, Dröscher L, Flügge UI, Heldt HW (1984) A specific translocator for oxaloacetate transport in chloroplasts. *FEBS Lett* **178**: 15–19.

Hatch MD, Kagawa T, Craig S (1975) Subdivision of C_4-pathway species based on differing C_4 acid decarboxylating systems and ultrastructural features. *Funct Plant Biol* **2**: 111–128.

Hatch MD and Mau SL (1973) Activity, location, and role of asparate aminotransferase and alanine aminotransferase isoenzymes in leaves with C_4 pathway photosynthesis. *Arch Biochem Biophys* **156**: 195–206.

Hatch MD and Osmond CB (1976) Compartmentation and transport in C_4 photosynthesis. *In Transport in plants III*. Heidelberg: Springer Berlin, 144–184.

Hatch MD and Slack CR (1966) Photosynthesis by sugar-cane leaves. A new carboxylation reaction and the pathway of sugar formation. *Biochem J* **101**: 103–111.

Hatch MD and Slack CR (1968) A new enzyme for the interconversion of pyruvate and phosphopyruvate and its role in the C_4 dicarboxylic acid pathway of photosynthesis. *Biochem J* **106**: 141–146.

Hatfield JL, Boote KJ, Kimball BA, Ziska L, Izaurralde RC, Ort D, Thomson AM, Wolfe D (2011) Climate impacts on agriculture: implications for crop production. *Agron J* **103**: 351–370.

Hatfield JL and Prueger JH (2011) Agroecology: implications for plant response to climate change. *In* Yadav, SS, Redden, RJ, Hatfield, JL, Lotze-Campen, H, Hall, AE, eds, *Crop Adaptation to Climate Change*. West Sussex, UK: Wiley-Blackwell, 27–43.

Hatfield JL and Prueger JH (2015) Temperature extremes: effect on plant growth and development. *Weather Clim Extrem* **10**: 4–10.

Haynes PA and Roberts TH (2007) Subcellular shotgun proteomics in plants: looking beyond the usual suspects. *Proteomics* **7**: 2963–2975.

Heinricher E (1884) Ueber isolateralen Blattbau mit besonderer Berucksichtigung der europaischen, speciell der deutschen Flora. *Jb wiss Bot* **15**: 502–567.

Heldt HW (1979) Light-dependent changes of stromal H^+ and Mg^{2+} concentrations controlling CO_2 fixation. *In* Gibbs, M, Latzko, E, eds, *Photosynthesis II*. Berlin, Heidelberg: Springer, 202–207.

Heldt WH, Werdan K, Milovancev M, Geller G (1973) Alkalization of the chloroplast stroma caused by light-dependent proton flux into the thylakoid space. *Biochim Biophys Acta* **314**: 224–241.

Hermans J and Westhoff P (1990) Analysis of expression and evolutionary relationships of phospho*enol*-pyruvate carboxylase genes in *Flaveria trinervia* (C_4) and *F. pringlei* (C_3). *Mol Gen Genet* **224**: 459–468.

Hibberd JM and Quick WP (2002) Characteristics of C_4 photosynthesis in stems and petioles of C_3 flowering plants. *Nature* **415**: 451–454.

Hibberd JM, Sheehy JE, Langdale JA (2008) Using C_4 photosynthesis to increase the yield of rice-rationale and feasibility. *Curr Opin Plant Biol* **11**: 228–231.

Hodge AJ, McLean JD, Mercer FV (1955) Ultrastructure of the lamellae and grana in the chloroplasts of *Zea mays* L. *J Cell Biol* **1**: 605–614.

Hodges M, Jossier M, Boex-Fontvieille E, Tcherkez G (2013) Protein phosphorylation and photorespiration. *Plant Biol* **15**: 694–706.

Holaday AS and Lowder GW (1989) Effect of pH on the kinetic parameters of NADP-malic enzyme from a C_4 *Flaveria* (Asteraceae) species. *Plant Physiol* **90**: 401–405.

Houtz RL, Magnani R, Nayak NR, Dirk LM (2008) Co- and post-translational modifications in Rubisco: unanswered questions. *J Exp Bot* **59**: 1635–1645.

Hsieh EJ, Hoopmann MR, MacLean B, MacCoss MJ (2010) Comparison of database search strategies for high precursor mass accuracy MS/MS data. *J Proteome Res* **9**: 1138–1143.

Hu Q, Noll RJ, Li H, Makarov A, Hardman M, Graham Cooks R (2005) The Orbitrap: a new mass spectrometer. *J Mass Spectrom* **40**: 430–443.

Huber SC (2011) Grand challenges in plant physiology: the underpinning of translational research. *Front Plant Sci* **2**: 1–5.

Huber SC and Edwards GE (1975) Inhibition of phospho*enol*pyruvate carboxylase from C_4 plants by malate and aspartate. *Can J Bot* **53**: 1925–1933.

Huber SC and Edwards GE (1975) Regulation of oxaloacetate, aspartate, and malate formation in mesophyll protoplast extracts of three types of C_4 plants. *Plant Physiol* **56**: 324–331.

Huber SC and Huber JL (1996) Role and regulation of sucrose-phosphate synthase in higher plants. *Annu Rev Plant Physiol Plant Mol Biol* **47**: 431–444.

Hunter T (2007) The age of crosstalk: phosphorylation, ubiquitination, and beyond. *Mol Cell* **28**: 730–738.

Huttlin EL, Jedrychowski MP, Elias JE, Goswami T, Rad R, Beausoleil SA, Villen J, Haas W, Sowa ME, Gygi SP (2010) A tissue-specific atlas of mouse protein phosphorylation and expression. *Cell* **143**: 1174–1189.

Iglesias AA and Andreo CS (1990) Kinetic and structural properties of NADP-malic enzyme from sugarcane leaves. *Plant Physiol* **92**: 66–72.

Ishijima S, Uchibori A, Takagi H, Maki R, Ohnishi M (2003) Light-induced increase in free Mg^{2+} concentration in spinach chloroplasts: measurement of free Mg^{2+} by using a fluorescent probe and necessity of stromal alkalinization. *Arch Biochem Biophys* **412**: 126–132.

Jacobs B, Engelmann S, Westhoff P, Gowik U (2008) Evolution of C_4 phospho*enol*pyruvate carboxylase in *Flaveria*: determinants for high tolerance towards the inhibitor L-malate. *Plant Cell Environ* **31**: 793–803.

Jacquot JPP, Buchanan BB, Martin F, Vidal J (1981) Enzyme regulation in C_4 photosynthesis : purification and properties of thioredoxin-linked NADP-malate dehydrogenase from corn leaves. *Plant Physiol* **68**: 300–304.

Jedrzejas MJ, Chander M, Setlow P, Krishnasamy G (2000) Mechanism of catalysis of the cofactor-independent phosphoglycerate mutase from *Bacillus stearothermophilus* crystal structure of the complex with 2-phosphoglycerate. *J Biol Chem* **275**: 23146–23153.

Jedrzejas MJ, Chander M, Setlow P, Krishnasamy G (2000) Structure and mechanism of action of a novel phosphoglycerate mutase from *Bacillus stearothermophilus*. *EMBO J* **19**: 1419–1431.

Jedrzejas MJ and Setlow P (2001) Comparison of the binuclear metalloenzymes diphosphoglycerate-independent phosphoglycerate mutase and alkaline phosphatase: their mechanism of catalysis via a phosphoserine intermediate. *Chem Rev* **101**: 607–618.

Jiang H, Barbier H, Brutnell T (2013) Methods for performing crosses in *Setaria viridis*, a new model system for the grasses. *J Vis Exp* e50527.

Jiao JA and Chollet R (1988) Light/dark regulation of maize leaf phospho*enol*pyruvate carboxylase by *in vivo* phosphorylation. *Arch Biochem Biophys* **261**: 409–417.

Jiao JA and Chollet R (1990) Regulatory phosphorylation of serine-15 in maize phospho*enol*pyruvate carboxylase by a C_4-leaf protein-serine kinase. *Arch Biochem Biophys* **283**: 300–305.

Jiao JA and Chollet R (1991) Posttranslational regulation of phospho*enol*pyruvate carboxylase in C_4 and crassulacean acid metabolism plants. *Plant Physiol* **95**: 981–985.

Jiao JA and Chollet R (1992) Light activation of maize phospho*enol*pyruvate carboxylase protein-serine kinase activity is inhibited by mesophyll and bundle sheath-directed photosynthesis inhibitors. *Plant Physiol* **98**: 152–156.

Jiao JA, Echevarría C, Vidal J, Chollet R (1991) Protein turnover as a component in the light/dark regulation of phospho*enol*pyruvate carboxylase protein-serine kinase activity in C_4 plants. *Proc Natl Acad Sci USA* **88**: 2712–2715.

Jiao JA, Vidal J, Echevarría C, Chollet R (1991) *In vivo* regulatory phosphorylation site in C_4-leaf phospho*enol*pyruvate carboxylase from maize and sorghum. *Plant Physiol* **96**: 297–301.

Johnson HS and Hatch MD (1970) Properties and regulation of leaf nicotinamide-adenine dinucleotide phosphate-malate dehydrogenase and 'malic' enzyme in plants with the C_4-dicarboxylic acid pathway of photosynthesis. *Biochem J* **119**: 273–280.

Jordan DB and Ogren WL (1984) The CO_2/O_2 specificity of ribulose 1, 5-bisphosphate carboxylase/oxygenase. *Planta* **161**: 308–313.

Jorrín JV, Maldonado AM, Castillejo MA (2007) Plant proteome analysis: a 2006 update. *Proteomics* **7**: 2947–2962.

Kai Y, Matsumura H, Izui K (2003) Phospho*enol*pyruvate carboxylase: three-dimensional structure and molecular mechanisms. *Arch Biochem Biophys* **414**: 170–179.

Kanai R and Edwards GE (1999) The biochemistry of C_4 photosynthesis. *In* Sage, RF, Monson, RK, eds, *C_4 plant biology*. San Diego, California, USA: Academic Press, 49–87.

Karpilov YS (1960) The distribution of radioactive carbon 14 amongst the products of photosynthesis of maize. *Proc Kazan Agric Inst* **41**: 15–24.

Karve TM and Cheema AK (2011) Small changes huge impact: the role of protein posttranslational modifications in cellular homeostasis and disease. *J Amino Acids* **2011**: 207691–207691.

Kendziorek M, Paszkowski A, Zagdańska B (2012) Biochemical characterization and kinetic properties of alanine aminotransferase homologues partially purified from wheat (*Triticum aestivum* L.). *Phytochemistry* **82**: 7–14.

Kiesselbach TA (1916) Transpiration as a factor in crop production. *Nebr Exp Sta Res Bull* **6**: 1–214.

Kim HJ, Ha S, Lee HY, Lee KJ (2015) Rosics: chemistry and proteomics of cysteine modifications in redox biology. *Mass Spectrom Rev* **34**: 184–208.

Kimball BA, Mauney JR, Nakayama FS, Idso SB (1993) Effects of increasing atmospheric CO_2 on vegetation. *Vegetatio* **104**: 65–75.

Kocaçinar F and Sage RF (2004) Photosynthetic pathway alters hydraulic structure and function in woody plants. *Oecologia* **139**: 214–223.

Komatsu S, Mock HP, Yang P, Svensson B (2013) Application of proteomics for improving crop protection/artificial regulation. *Front Plant Sci* **4**:

Kortschak HP, Hartt CE, Burr GO (1965) Carbon dioxide fixation in sugarcane leaves. *Plant Physiol* **40**: 209–213.

Kozaki A and Takeba G (1996) Photorespiration protects C_3 plants from photooxidation. *Nature* **384**: 557–560.

Krautwurst H, Encinas MV, Marcus F, Latshaw SP, Kemp RG, Frey PA, Cardemil E (1995) *Saccharomyces cerevisiae* phospho*enol*pyruvate carboxykinase: revised amino acid sequence, site-directed mutagenesis, and microenvironment characteristics of cysteines 365 and 458. *Biochemistry* **34**: 6382–6388.

Ku MSB, Kano-Murakami Y, Matsuoka M (1996) Evolution and expression of C_4 photosynthesis genes. *Plant Physiol* **111**: 949–957.

Ku MSB, Monson RK, Littlejohn RO, Nakamoto H, Fisher DB, Edwards GE (1983) Photosynthetic characteristics of C_3–C_4 intermediate *Flaveria* species. *Plant Physiol* **71**: 944–948.

Ku MSB, Wu J, Dai Z, Scott RA, Chu C, Edwards GE (1991) Photosynthetic and photorespiratory characteristics of *Flaveria* species. *Plant Physiol* **96**: 518–528.

Ku SB and Edwards GE (1975) Photosynthesis in mesophyll protoplasts and bundle sheath cells of various types of C_4 plants. IV. Enzymes of kespiratory metabolism and energy utilizing enzymes of photosynthetic pathways. *Z Pflanzen-physiol* **77**: 16–32.

Ku SB and Edwards GE (1977) Oxygen inhibition of photosynthesis. *Plant Physiol* **59**: 991–999.

Kühlbrandt W and Wang DN (1991) Three-dimensional structure of plant light-harvesting complex determined by electron crystallography. *Nature* **350**: 130–134.

Kuo CC, Tsai LC, Chin TY, Chang GG, Chou WY (2000) Lysine residues 162 and 340 are involved in the catalysis and coenzyme binding of $NADP^+$-dependent malic enzyme from pigeon. *Biochem Biophys Res Commun* **270**: 821–825.

Kwon SJ, Choi EY, Choi YJ, Ahn JH, Park OK (2006) Proteomics studies of post-translational modifications in plants. *J Exp Bot* **57**: 1547–1551.

Laetsch WM (1968) Chloroplast specialization in dicotyledons possessing the C_4-dicarboxylic acid pathway of photosynthetic CO_2 fixation. *Am J Bot* **55**: 875–883.

Lai LB, Tausta SL, Nelson TM (2002) Differential regulation of transcripts encoding cytosolic NADP-malic enzyme in C_3 and C_4 *Flaveria* species. *Plant Physiol* **128**: 140–149.

Lai LB, Wang L, Nelson TM (2002) Distinct but conserved functions for two chloroplastic NADP-malic enzyme isoforms in C_3 and C_4 *Flaveria* species. *Plant Physiol* **128**: 125–139.

Langdale JA (2011) C_4 cycles: past, present, and future research on C_4 photosynthesis. *Plant Cell* **23**: 3879–3892.

Lange V, Picotti P, Domon B, Aebersold R (2008) Selected reaction monitoring for quantitative proteomics: a tutorial. *Mol Syst Biol* **4**: 1–14.

Lara MV and Andreo CS (2011) C_4 plants adaptation to high levels of CO_2 and to drought environments. *In* Shanker, A, ed, *Abiotic Stress in Plants-Mechanisms and Adaptations*. Hampshire, UK: InTech, 415–428.

Leegood RC (1985) The intercellular compartmentation of metabolites in leaves of *Zea mays* L. *Planta* **164**: 163–171.

Leegood RC (1993) Carbon metabolism. *In* Hall, DO, Scurlock, JMO, Bolhàr-Nordenkampf, HR, Leegood, RC, Long, SP, eds, *Photosynthesis and Production in a Changing Environment*. The Netherlands: Springer, 247–267.

Leegood RC (2002) C_4 photosynthesis: principles of CO_2 concentration and prospects for its introduction into C_3 plants. *J Exp Bot* **53**: 581–590.

Leegood RC (2008) Roles of the bundle sheath cells in leaves of C_3 plants. *J Exp Bot* **59**: 1663–1673.

Leegood RC (2013) Strategies for engineering C_4 photosynthesis. *J Plant Physiol* **170**: 378–388.

Leegood RC and Edwards GE (1996) Carbon metabolism and photorespiration: temperature dependence in relation to other environmental factors. *In* Backer, NR, ed, *Photosynthesis and the Environment*. Dordrecht, The Netherlands: Kluwer Academic, 191–221.

Leegood RC and Furbank RT (1984) Carbon metabolism and gas exchange in leaves of *Zea mays* L. *Planta* **162**: 450–456.

Leegood RC and von Caemmerer S (1988) The relationship between contents of photosynthetic metabolites and the rate of photosynthetic carbon assimilation in leaves of *Amaranthus edulis* L. *Planta* **174**: 253–262.

Leegood RC and von Caemmerer S (1989) Some relationships between contents of photosynthetic intermediates and the rate of photosynthetic carbon assimilation in leaves of *Zea mays* L. *Planta* **178**: 258–266.

Leegood RC and von Caemmerer S (1994) Regulation of photosynthetic carbon assimilation in leaves of C_3–C_4 intermediate species of *Moricandia* and *Flaveria*. *Planta* **192**: 232–238.

Leegood RC and Walker DA (1983) Modulation of NADP-malate dehydrogenase activity in maize mesophyll chloroplasts. *Plant Physiol* **71**: 513–518.

Leegood RC and Walker RP (1999) Regulation of the C_4 pathway. *In* Sage, RF, Monson, RK, eds, *C_4 plant biology*. San Diego, CA, USA: Academic Press, 89–131.

Lehtimäki N, Koskela MM, Mulo P (2015) Posttranslational modifications of chloroplast proteins: an emerging field. *Plant Physiol* **168**: 768–775.

Lewandowska D, ten Have S, Hodge K, Tillemans V, Lamond AI, Brown JW (2013) Plant SILAC: stable-isotope labelling with amino acids of *Arabidopsis* seedlings for quantitative proteomics. *PLoS One* **8**: e72207.

Li B and Chollet R (1993) Resolution and identification of C_4 phospho*enol*pyruvate-carboxylase protein-kinase polypeptides and their reversible light activation in maize leaves. *Arch Biochem Biophys* **307**: 416–419.

Li B, Zhang XQ, Chollet R (1996) Phospho*enol*pyruvate carboxylase kinase in tobacco leaves is activated by light in a similar but not identical way as in maize. *Plant Physiol* **111**: 497–505.

Li D, Fu Y, Sun R, Ling CX, Wei Y, Zhou H, Zeng R, Yang Q, He S, Gao W (2005) pFind: a novel database-searching software system for automated peptide and protein identification via tandem mass spectrometry. *Bioinformatics* **21**: 3049–3050.

Li P, Ponnala L, Gandotra N, Wang L, Si Y, Tausta SL, Kebrom TH, Provart N, Patel R, Myers CR (2010) The developmental dynamics of the maize leaf transcriptome. *Nat Genet* **42**: 1060–1067.

Linka M and Weber APM (2005) Shuffling ammonia between mitochondria and plastids during photorespiration. *Trends Plant Sci* **10**: 461–465.

Lipka B, Steinmüller K, Rosche E, Börsch D, Westhoff P (1994) The C_3 plant *Flaveria pringlei* contains a plastidic NADP-malic enzyme which is orthologous to the C_4 isoform of the C_4 plant *F. trinervia*. *Plant Mol Biol* **26**: 1775–1783.

Liu J, Ning D, Zhao G, Cheng Y, Wang B (2014) Large-scale analysis of protein phosphorylation in *Populus* leaves. *J Plant Biochem Biotechnol* **23**: 410–420.

Lobell DB, Schlenker W, Costa-Roberts J (2011) Climate trends and global crop production since 1980. *Science* **333**: 616–620.

Long JJ and Berry JO (1996) Tissue-specific and light-mediated expression of the C_4 photosynthetic NAD-dependent malic enzyme of amaranth mitochondria. *Plant Physiol* **112**: 473–482.

Long JJ, Wang JL, Berry JO (1994) Cloning and analysis of the C_4 photosynthetic NAD-dependent malic enzyme of amaranth mitochondria. *J Biol Chem* **269**: 2827–2833.

Long SP (1983) C_4 photosynthesis at low temperatures. *Plant Cell Environ* **6**: 345–363.

Long SP (1991) Modification of the response of photosynthetic productivity to rising temperature by atmospheric CO_2 concentrations: has its importance been underestimated? *Plant Cell Environ* **14**: 729–739.

Long SP (1999) Environmental responses. *In* Sage, RF, Monson, RK, eds, *C_4 Plant Biology*. San Diego, CA, USA: Academic Press, 215–249.

Long SP, Zhu XG, Naidu SL, Ort DR (2006) Can improvement in photosynthesis increase crop yields? *Plant Cell Environ* **29**: 315–330.

Lorimer GH, Chen YR, Hartman FC (1993) A role for the epsilon-amino group of lysine-334 of ribulose-1, 5-bisphosphate carboxylase in the addition of carbon dioxide to the 2, 3-enediol(ate) of ribulose 1, 5-bisphosphonate. *Biochemistry* **32**: 9018–9024.

Ludwig M (2012) Carbonic anhydrase and the molecular evolution of C_4 photosynthesis. *Plant Cell Environ* **35**: 22–37.

Ludwig M (2016) The roles of organic acids in C_4 photosynthesis. *Front Plant Sci* **7**:

Lundby A, Secher A, Lage K, Nordsborg NB, Dmytriyev A, Lundby C, Olsen JV (2012) Quantitative maps of protein phosphorylation sites across 14 different rat organs and tissues. *Nat Commun* **3**:

Lundgren MR, Besnard G, Ripley BS, Lehmann CER, Chatelet DS, Kynast RG, Namaganda M, Vorontsova MS, Hall RC, Elia J (2015) Photosynthetic innovation broadens the niche within a single species. *Ecol Lett* **18**: 1021–1029.

Lundgren MR, Christin PA, Gonzalez Escobar E, Ripley BS, Besnard G, Long CM, Hattersley PW, Ellis RP, Leegood RC, Osborne CP (2016) Evolutionary implications of C_3–C_4 intermediates in the grass *Alloteropsis semialata*. *Plant Cell Environ* **39**: 1874–1885.

Lv DW, Li X, Zhang M, Gu AQ, Zhen SM, Wang C, Li XH, Yan YM (2014) Large-scale phosphoproteome analysis in seedling leaves of *Brachypodium distachyon* L. *BMC Genomics* **15**: 375.

Ma B (2010) Challenges in computational analysis of mass spectrometry data for proteomics. *J Comput Sci Technol* **25**: 107–123.

Machová I, Hubálek M, Lepšík M, Bednárová L, Pazderková M, Kopecký Jr V, Snášel J, Dostál J, Pichová I (2017) The role of cysteine residues in catalysis of phospho*enol*pyruvate carboxykinase from *Mycobacterium tuberculosis*. *PloS One* **12**: e0170373.

Machová I, Snášel J, Zimmermann M, Laubitz D, Plocinski P, Oehlmann W, Singh M, Dostál J, Sauer U, Pichová I (2014) *Mycobacterium tuberculosis* phospho*enol*pyruvate carboxykinase is regulated by redox mechanisms and interaction with thioredoxin. *J Biol Chem* **289**: 13066–13078.

Mackinder LCM, Chen C, Leib RD, Patena W, Blum SR, Rodman M, Ramundo S, Adams CM, Jonikas MC (2017) A spatial interactome reveals the protein organization of the algal CO_2-concentrating mechanism. *Cell* **171**: 133–147.

Maier A, Zell MB, Maurino VG (2011) Malate decarboxylases: evolution and roles of NADP-ME isoforms in species performing C_4 and C_3 photosynthesis. *J Exp Bot* **62**: 3061–3069.

Majeran W and van Wijk KJ (2009) Cell-type-specific differentiation of chloroplasts in C_4 plants. *Trends Plant Sci* **14**: 100–109.

Mann M, Hendrickson RC, Pandey A (2001) Analysis of proteins and proteomes by mass spectrometry. *Annu Rev Biochem* **70**: 437–473.

Mann M, Ong SE, Grønborg M, Steen H, Jensen ON, Pandey A (2002) Analysis of protein phosphorylation using mass spectrometry: deciphering the phosphoproteome. *Trends Biotechnol* **20**: 261–268.

Marcotte EM (2007) How do shotgun proteomics algorithms identify proteins? *Nat Biotech* **25**: 755–757.

Mareš J, Barthová J, Leblová S (1979) Purification and properties of phospho*enol*pyruvate carboxylase from green leaves of maize. *Collect Czech Chem Commun* **44**: 1835–1840.

Marino SM and Gladyshev VN (2012) Analysis and functional prediction of reactive cysteine residues. *J Biol Chem* **287**: 4419–4425.

Marshall JS, Stubbs JD, Taylor WC (1996) Two genes encode highly similar chloroplastic NADP-malic enzymes in *Flaveria* (implications for the evolution of C_4 photosynthesis). *Plant Physiol* **111**: 1251–1261.

Martin W and Borst P (2003) Secondary loss of chloroplasts in trypanosomes. *Proc Natl Acad Sci USA* **100**: 765–767.

Masle J, Hudson GS, Badger MR (1993) Effects of ambient CO_2 concentration on growth and nitrogen use in tobacco (*Nicotiana tabacum*) plants transformed with an antisense gene to the small subunit of ribulose-1, 5-bisphosphate carboxylase/oxygenase. *Plant Physiol* **103**: 1075–1088.

Mathur S, Agrawal D, Jajoo A (2014) Photosynthesis: response to high temperature stress. *J Photochem Photobiol B: Biol* **137**: 116–126.

Matsumura H, Xie Y, Shirakata S, Inoue T, Yoshinaga T, Ueno Y, Izui K, Kai Y (2002) Crystal structures of C_4 form maize and quaternary complex of *E. coli* phospho*enol*pyruvate carboxylases. *Structure* **10**: 1721–1730.

Matthes A, Köhl K, Schulze WX (2014) SILAC and Alternatives in Studying Cellular Proteomes of Plants. *In* Warscheid, B, ed, *Stable Isotope Labeling by Amino Acids in Cell Culture (SILAC) (Methods and Protocols)*, Vol 1188. New York, NY, USA: Humana Press, 65–83.

Maurino VG, Drincovich MF, Andreo CS (1996) NADP-malic enzyme isoforms in maize leaves. *Biochem Mol Biol Int* **38**: 239–250.

Maurino VG, Drincovich MF, Casati P, Andreo CS, Edwards GE, Ku MSB, Gupta SK, Franceschi VR (1997) NADP-malic enzyme: immunolocalization in different tissues of the C_4 plant maize and the C_3 plant wheat. *J Exp Bot* **48**: 799–811.

Maurino VG and Peterhänsel C (2010) Photorespiration: current status and approaches for metabolic engineering. *Curr Opin Plant Biol* **13**: 249–256.

Mawson BT and Cummins WR (1989) Thermal acclimation of photosynthetic electron transport activity by thylakoids of *Saxifraga cernua*. *Plant Physiol* **89**: 325–332.

McAllister CH, Facette M, Holt A, Good AG (2013) Analysis of the enzymatic properties of a broad family of alanine aminotransferases. *PloS One* **8**: e55032.

McAllister CH and Good AG (2015) Alanine aminotransferase variants conferring diverse NUE phenotypes in *Arabidopsis thaliana*. *PloS One* **10**: e0121830.

McEvoy JP, Gascon JA, Batista VS, Brudvig GW (2005) The mechanism of photosynthetic water splitting. *Photochem Photobiol Sci* **4**: 940–949.

McKenna MC, Hopkins IB, Lindauer SL, Bamford P (2006) Aspartate aminotransferase in synaptic and nonsynaptic mitochondria: differential effect of compounds that influence transient hetero-enzyme complex (metabolon) formation. *Neurochem Int* **48**: 629–636.

McLachlin DT and Chait BT (2001) Analysis of phosphorylated proteins and peptides by mass spectrometry. *Curr Opin Chem Biol* **5**: 591–602.

McMichael AJ, Woodruff RE, Hales S (2006) Climate change and human health: present and future risks. *The Lancet* **367**: 859–869.

McNaughton GAL, MacKintosh C, Fewson CA, Wilkins MB, Nimmo HG (1991) Illumination increases the phosphorylation state of maize leaf phospho*enol*pyruvate carboxylase by causing an increase in the activity of a protein kinase. *Biochim Biophys Acta, Mol Cell Res* **1093**: 189–195.

Meierhoff K and Westhoff P (1993) Differential biogenesis of photosystem II in mesophyll and bundle-sheath cells of monocotyledonous NADP-malic enzyme-type C_4 plants: the non-stoichiometric abundance of the subunits of photosystem II in the bundle-sheath chloroplasts and the translational activity of the plastome-encoded genes. *Planta* **191**: 23–33.

Meister M, Agostino A, Hatch MD (1996) The roles of malate and aspartate in C_4 photosynthetic metabolism of *Flaveria bidentis* (L.). *Planta* **199**: 262–269.

Michelet L, Zaffagnini M, Morisse S, Sparla F, Perez-Perez ME, Francia F, Danon A, Marchand CH, Fermani S, Trost P, Lemaire SD (2013) Redox regulation of the Calvin-Benson cycle: something old, something new. *Front Plant Sci* **4**: 470.

Milner HW and Hiesey WM (1964) Photosynthesis in climatic races of *Mimulus*. I. Effect of light intensity and temperature on rate. *Plant Physiol* **39**: 208–213.

Minges A, Ciupka D, Winkler C, Höppner A, Gohlke H, Groth G (2017) Structural intermediates and directionality of the swiveling motion of pyruvate, phosphate dikinase. *Sci Rep* **7**: 45389.

Mitchell PL and Sheehy JE (2006) Supercharging rice photosynthesis to increase yield. *New Phytol* **171**: 688–693.

Miyashita Y, Dolferus R, Ismond KP, Good AG (2007) Alanine aminotransferase catalyses the breakdown of alanine after hypoxia in *Arabidopsis thaliana*. *Plant J* **49**: 1108–1121.

Mondal MH, Brun WA, Brenner ML (1978) Effects of sink removal on photosynthesis and senescence in leaves of soybean (*Glycine max* L.) plants. *Plant Physiol* **61**: 394–397.

Monson RK (1999) The origins of C_4 genes and evolutionary pattern in the C_4 metabolic phenotype. *In* Sage, RF, Monson, RK, eds, *C_4 Plant Biology*, Vol 1. San Diego, CA, USA: Academic Press, 377–410.

Monson RK (2003) Gene duplication, neofunctionalization, and the evolution of C_4 photosynthesis. *Int J Plant Sci* **164**: S43–S54.

Monson RK and Moore BD (1989) On the significance of C_3–C_4 intermediate photosynthesis to the evolution of C_4 photosynthesis. *Plant Cell Environ* **12**: 689–699.

Monson RK, Moore BD, Ku MSB, Edwards GE (1986) Co-function of C_3- and C_4-photosynthetic pathways in C_3, C_4 and C_3–C_4 intermediate *Flaveria* species. *Planta* **168**: 493–502.

Monson RK and Rawsthorne S (2000) CO_2 assimilation in C_3–C_4 intermediate plants. *In* Leegood, RC, Sharkey, TD, Von Caemmerer, S, eds, *Photosynthesis: Physiology and Metabolism*. Dordrecht, The Netherlands: Kluwer Academic, 533–550.

Monson RK, Teeri JA, Ku MSB, Gurevitch J, Mets LJ, Dudley S (1988) Carbon-isotope discrimination by leaves of *Flaveria* species exhibiting different amounts of C_3-and C_4-cycle co-function. *Planta* **174**: 145–151.

Monteith JL and Moss CJ (1977) Climate and the efficiency of crop production in Britain. *Philos Trans R Soc Lond, Ser B: Biol Sci* **281**: 277–294.

Moore B, Cheng SH, Sims D, Seemann JR (1999) The biochemical and molecular basis for photosynthetic acclimation to elevated atmospheric CO_2. *Plant Cell Environ* **22**: 567–582.

Moradian A, Kalli A, Sweredoski MJ, Hess S (2014) The top-down, middle-down, and bottom-up mass spectrometry approaches for characterization of histone variants and their post-translational modifications. *Proteomics* **14**: 489–497.

Morgan CL, Turner SR, Rawsthorne S (1993) Coordination of the cell-specific distribution of the four subunits of glycine decarboxylase and of serine hydroxymethyltransferase in leaves of C_3–C_4 intermediate species from different genera. *Planta* **190**: 468–473.

Muhaidat R, Sage TL, Frohlich MW, Dengler NG, Sage RF (2011) Characterization of C_3–C_4 intermediate species in the genus *Heliotropium* L. (Boraginaceae): anatomy, ultrastructure and enzyme activity. *Plant Cell Environ* **34**: 1723–1736.

Müller GL, Drincovich MF, Andreo CS, Lara MV (2008) *Nicotiana tabacum* NADP-malic enzyme: cloning, characterization and analysis of biological role. *Plant Cell Physiol* **49**: 469–480.

Naidu SL, Moose SP, Al-Shoaibi AK, Raines CA, Long SP (2003) Cold tolerance of C_4 photosynthesis in *Miscanthus* × *giganteus*: adaptation in amounts and sequence of C_4 photosynthetic enzymes. *Plant Physiol* **132**: 1688–1697.

Nakagami H, Sugiyama N, Mochida K, Daudi A, Yoshida Y, Toyoda T, Tomita M, Ishihama Y, Shirasu K (2010) Large-scale comparative phosphoproteomics identifies conserved phosphorylation sites in plants. *Plant Physiol* **153**: 1161–1174.

Nakanishi T, Nakatsu T, Matsuoka M, Sakata K, Kato H (2005) Crystal structures of pyruvate, phosphate dikinase from maize revealed an alternative conformation in the swiveling-domain motion. *Biochemistry* **44**: 1136–1144.

Nelson T and Dengler NG (1992) Photosynthetic tissue differentiation in C_4 plants. *Int J Plant Sci* **153**: S93–S105.

Neumann J and Jagendorf AT (1964) Light-induced pH changes related to phosphorylation by chloroplasts. *Arch Biochem Biophys* **107**: 109–119.

Nimmo GA, Nimmo HG, Fewson CA, Wilkins MB (1984) Diurnal changes in the properties of phospho*enol*pyruvate carboxylase in *Bryophyllum* leaves: a possible covalent modification. *FEBS Lett* **178**: 199–203.

Nimmo GA, Nimmo HG, Hamilton ID, Fewson CA, Wilkins MB (1986) Purification of the phosphorylated night form and dephosphorylated day form of phospho*enol*pyruvate carboxylase from *Bryophyllum fedtschenkoi*. *Biochem J* **239**: 213–220.

Nimmo HG (1998) Circadian regulation of a plant protein kinase. *Chronobiol Int* **15**: 109–118.

Nishikido T and Wada T (1974) Comparative studies of NADP-malic enzyme from C_4- and C_3-plants. *Biochem Biophys Res Commun* **61**: 243–249.

Numazawa T, Yamada S, Hase T, Sugiyama T (1989) Aspartate aminotransferase from *Panicum maximum* Jacq. var. *trichoglume* Eyles, a C_4 plant: purification, molecular properties, and preparation of antibody. *Arch Biochem Biophys* **270**: 313–319.

O'Farrell PH (1975) High resolution two-dimensional electrophoresis of proteins. *J Biol Chem* **250**: 4007–4021.

O'Leary B, Park J, Plaxton WC (2011) The remarkable diversity of plant PEPC (phospho*enol*pyruvate carboxylase): recent insights into the physiological functions and post-translational controls of non-photosynthetic PEPCs. *Biochem J* **436**: 15–34.

O'Leary MH, Rife JE, Slater JD (1981) Kinetic and isotope effect studies of maize phospho*enol*pyruvate carboxylase. *Biochemistry* **20**: 7308–7314.

Odegaard ML, Joseph JW, Jensen MV, Lu D, Ilkayeva O, Ronnebaum SM, Becker TC, Newgard CB (2010) The mitochondrial 2-oxoglutarate carrier is part of a metabolic pathway that mediates glucose- and glutamine-stimulated insulin secretion. *J Biol Chem* **285**: 16530–16537.

Ogle K (2003) Implications of interveinal distance for quantum yield in C_4 grasses: a modeling and meta-analysis. *Oecologia* **136**: 532–542.

Ogren WL (1984) Photorespiration: pathways, regulation, and modification. *Annu Rev Plant Physiol* **35**: 415–442.

Ohta S, Ishida Y, Usami S (2004) Expression of cold-tolerant pyruvate, orthophosphate dikinase cDNA, and heterotetramer formation in transgenic maize plants. *Transgenic Res* **13**: 475–485.

Osborne CP and Sack L (2012) Evolution of C_4 plants: a new hypothesis for an interaction of CO_2 and water relations mediated by plant hydraulics. *Phil Trans R Soc B* **367**: 583–600.

Osmond CB (1971) Metabolite transport in C_4 photosynthesis. *Aust J Biol Sci* **24**: 159–164.

Park OK (2004) Proteomics studies in plants. *J Biochem Mol Biol* **37**: 133–138.

Patel M, Siegel AJ, Berry JO (2006) Untranslated regions of *FbRbc*S1 mRNA mediate bundle sheath cell-specific gene expression in leaves of a C_4 plant. *J Biol Chem* **281**: 25485–25491.

Pearcy RW and Ehleringer J (1984) Comparative ecophysiology of C_3 and C_4 plants. *Plant Cell Environ* **7**: 1–13.

Pearlman SM, Serber Z, Ferrell JE (2011) A mechanism for the evolution of phosphorylation sites. *Cell* **147**: 934–946.

Peet MM and Kramer PJ (1980) Effects of decreasing source/sink ratio in soybeans on photosynthesis, photorespiration, transpiration and yield. *Plant Cell Environ* **3**: 201–206.

Peisker M (1986) Models of carbon metabolism in C_3–C_4 intermediate plants as applied to the evolution of C_4 photosynthesis. *Plant Cell Environ* **9**: 627–635.

Peri PL, Pastur M, Lencinas MV (2009) Photosynthetic response to different light intensities and water status of two main *Nothofagus* species of southern Patagonian forest, Argentina. *J For Sci* **55**: 101–111.

Perry RH, Cooks RG, Noll RJ (2008) Orbitrap mass spectrometry: instrumentation, ion motion and applications. *Mass Spectrom Rev* **27**: 661–699.

Peterhänsel C, Blume C, Offermann S (2012) Photorespiratory bypasses: how can they work? *J Exp Bot* **64**: 709–715.

Peterhänsel C and Offermann S (2012) Re-engineering of carbon fixation in plants–challenges for plant biotechnology to improve yields in a high-CO_2 world. *Curr Opin Biotechnol* **23**: 204–208.

Pfündel E, Nagel E, Meister A (1996) Analyzing the light energy distribution in the photosynthetic apparatus of C_4 plants using highly purified mesophyll and bundle-sheath thylakoids. *Plant Physiol* **112**: 1055–1070.

Pick TR, Bräutigam A, Schlüter U, Denton AK, Colmsee C, Scholz U, Fahnenstich H, Pieruschka R, Rascher U, Sonnewald U (2011) Systems analysis of a maize leaf developmental gradient redefines the current C_4 model and provides candidates for regulation. *The Plant Cell* **23**: 4208–4220.

Pimentel D, Berger B, Filiberto D, Newton M, Wolfe B, Karabinakis E, Clark S, Poon E, Abbett E, Nandagopal S (2004) Water resources: agricultural and environmental issues. *BioScience* **54**: 909–918.

Pimentel D, Houser J, Preiss E, White O, Fang H, Mesnick L, Barsky T, Tariche S, Schreck J, Alpert S (1997) Water resources: agriculture, the environment, and society. *BioScience* **47**: 97–106.

Pingali PL (2012) Green Revolution: impacts, limits, and the path ahead. *Proc Natl Acad Sci USA* **109**: 12302–12308.

Pitt JJ (2009) Principles and applications of liquid chromatography-mass spectrometry in clinical biochemistry. *Clin Biochem Rev* **30**: 19–34.

Plapinger RE and Wagner-Jauregg T (1953) A nitrogen-to-oxygen phosphoryl migration: preparation of dl-serinephosphoric and threoninephosphoric acid. *J Am Chem Soc* **75**: 5757–5758.

Popp J, Lakner Z, Harangi-Rákos M, Fári M (2014) The effect of bioenergy expansion: food, energy, and environment. *Renew Sustainable Energy Rev* **32**: 559–578.

Portis AR and Heldt HW (1976) Light-dependent changes of the Mg^{2+} concentration in the stroma in relation to the Mg^{2+} dependency of CO_2 fixation in intact chloroplasts. *Biochim Biophys Acta* **449**: 434–446.

Portis AR and Parry MAJ (2007) Discoveries in Rubisco (Ribulose 1, 5-bisphosphate carboxylase/oxygenase): a historical perspective. *Photosynth Res* **94**: 121–143.

Porubleva L and Chitnis PR (2000) Proteomics: a powerful tool in the post-genomic era. *Indian J Biochem Biophys* **37**: 360–368.

Postel SL (2000) Entering an era of water scarcity: the challenges ahead. *Ecol Appl* **10**: 941–948.

Potters MB, Solow BT, Bischoff KM, Graham DE, Lower BH, Helm R, Kennelly PJ (2003) Phosphoprotein with phosphoglycerate mutase activity from the archaeon *Sulfolobus solfataricus*. *J Bacteriol* **185**: 2112–2121.

Powell AM (1978) Systematics of *Flaveria*. *Ann Mo Bot Gard* **65**: 590–636.

Pressman E, Peet MM, Pharr DM (2002) The effect of heat stress on tomato pollen characteristics is associated with changes in carbohydrate concentration in the developing anthers. *Ann Bot* **90**: 631–636.

Pretty J (2008) Agricultural sustainability: concepts, principles and evidence. *Philos Trans R Soc Lond, Ser B: Biol Sci* **363**: 447–465.

Rachmilevitch S, Cousins AB, Bloom AJ (2004) Nitrate assimilation in plant shoots depends on photorespiration. *Proc Natl Acad Sci USA* **101**: 11506–11510.

Raines CA (2011) Increasing photosynthetic carbon assimilation in C_3 plants to improve crop yield: current and future strategies. *Plant Physiol* **155**: 36–42.

Raines CA, Harrison EP, Ölçer H, Lloyd JC (2000) Investigating the role of the thiol-regulated enzyme sedoheptulose-1, 7-bisphosphatase in the control of photosynthesis. *Physiol Plant* **110**: 303–308.

Rajeevan MS, Bassett CL, Hughes DW (1991) Isolation and characterization of cDNA clones for NADP-malic enzyme from leaves of *Flaveria*: transcript abundance distinguishes C_3, C_3–C_4 and C_4 photosynthetic types. *Plant Mol Biol* **17**: 371–383.

Ramakrishnan PS (2001) Increasing population and declining biological resources in the context of global change and globalization. *J Biosci* **26**: 465–479.

Rathlev T and Rosenberg T (1956) Non-enzymic formation and rupture of phosphorus to nitrogen linkages in phosphoramido derivatives. *Arch Biochem Biophys* **65**: 319–339.

Rawsthorne S, Hylton CM, Smith AM, Woolhouse HW (1988) Photorespiratory metabolism and immunogold localization of photorespiratory enzymes in leaves of C_3 and C_3–C_4 intermediate species of *Moricandia*. *Planta* **173**: 298–308.

Reed JE and Chollet R (1985) Immunofluorescent localization of phospho*enol*pyruvate carboxylase and ribulose 1, 5-bisphosphate carboxylase/oxygenase proteins in leaves of C_3, C_4 and C_3–C_4 intermediate *Flaveria* species. *Planta* **165**: 439–445.

Reynolds M, Bonnett D, Chapman SC, Furbank RT, Manès Y, Mather DE, Parry MAJ (2010) Raising yield potential of wheat. I. Overview of a consortium approach and breeding strategies. *J Exp Bot* **62**: 439–452.

Rhoades MM and Carvalho A (1944) The function and structure of the parenchyma sheath plastids of the maize leaf. *Bull Torrey Bot Club* **71**: 335–346.

Rigden DJ, Lamani E, Mello LV, Littlejohn JE, Jedrzejas MJ (2003) Insights into the catalytic mechanism of cofactor-independent phosphoglycerate mutase from X-ray crystallography, simulated dynamics and molecular modeling. *J Mol Biol* **328**: 909–920.

Ritchie RJ (2006) Consistent sets of spectrophotometric chlorophyll equations for acetone, methanol and ethanol solvents. *Photosynth Res* **89**: 27–41.

Rizal G, Acebron K, Mogul R, Karki S, Larazo N, Quick WP (2013) Study of flowering pattern in *Setaria viridis*, a proposed model species for C_4 photosynthesis research. *J Bot* **10**: 1–9.

Rocha AG, Mehlmer N, Stael S, Mair A, Parvin N, Chigri F, Teige M, Vothknecht UC (2014) Phosphorylation of *Arabidopsis* transketolase at Ser(428) provides a potential paradigm for the metabolic control of chloroplast carbon metabolism. *Biochem J* **458**: 313–322.

Roeske CA, Kutny RM, Budde RJ, Chollet R (1988) Sequence of the phosphothreonyl regulatory site peptide from inactive maize leaf pyruvate, orthophosphate dikinase. *J Biol Chem* **263**: 6683–6687.

Rosenzweig C, Iglesias A, Yang XB, Epstein PR, Chivian E (2001) Climate change and extreme weather events. Implications for food production, plant diseases, and pests. *Global Change Hum Health* **2**: 90–104.

Rosnow J, Yerramsetty P, Berry JO, Okita TW, Edwards GE (2014) Exploring mechanisms linked to differentiation and function of dimorphic chloroplasts in the single cell C_4 species *Bienertia sinuspersici*. *BMC Plant Biol* **14**: 34.

Ruiz-Ballesta I, Feria AB, Ni H, She YM, Plaxton WC, Echevarría C (2014) *In vivo* monoubiquitination of anaplerotic phospho*enol*pyruvate carboxylase occurs at Lys624 in germinating *Sorghum* seeds. *J Exp Bot* **65**: 443–451.

Sack L and Holbrook NM (2006) Leaf hydraulics. *Annu Rev Plant Biol* **57**: 361–381.

Sage RF (1999) Why C_4 photosynthesis. *In* Sage, RF, Monson, RK, eds, *C_4 plant biology*. San Diego, CA, USA: Academic Press, 3–16.

Sage RF (2004) The evolution of C_4 photosynthesis. *New Phytol* **161**: 341–370.

Sage RF, Cen YP, Li M (2002) The activation state of Rubisco directly limits photosynthesis at low CO_2 and low O_2 partial pressures. *Photosynth Res* **71**: 241–250.

Sage RF, Christin PA, Edwards EJ (2011) The C_4 plant lineages of planet Earth. *J Exp Bot* **62**: 3155–3169.

Sage RF and Kubien DS (2007) The temperature response of C_3 and C_4 photosynthesis. *Plant Cell Environ* **30**: 1086–1106.

Sage RF, Pearcy RW, Seemann JR (1987) The nitrogen use efficiency of C_3 and C_4 plants. III. Leaf nitrogen effects on the activity of carboxylating enzymes in *Chenopodium album* (L.) and *Amaranthus retroflexus* (L.). *Plant Physiol* **85**: 355–359.

Sage RF, Sage TL, Kocaçinar F (2012) Photorespiration and the evolution of C_4 photosynthesis. *Annu Rev Plant Biol* **63**: 19–47.

Sage TL and Sage RF (2009) The functional anatomy of rice leaves: implications for refixation of photorespiratory CO_2 and efforts to engineer C_4 photosynthesis into rice. *Plant Cell Physiol* **50**: 756–772.

Saigo M, Alvarez CE, Andreo CS, Drincovich MF (2013) Plastidial NADP-malic enzymes from grasses: unraveling the way to the C_4 specific isoforms. *Plant Physiol Biochem* **63**: 39–48.

Sato S (2006) The effects of moderately elevated temperature stress due to global warming on the yield and the male reproductive development of tomato (*Lycopersicon esculentum* Mill.). *HortResearch* **60**: 85–89.

Sato S, Peet MM, Thomas JF (2000) Physiological factors limit fruit set of tomato (*Lycopersicon esculentum* Mill.) under chronic, mild heat stress. *Plant Cell Environ* **23**: 719–726.

Scheeff ED, Eswaran J, Bunkoczi G, Knapp S, Manning G (2009) Structure of the pseudokinase VRK3 reveals a degraded catalytic site, a highly conserved kinase fold, and a putative regulatory binding site. *Structure* **17**: 128–138.

Schlenker W and Roberts MJ (2009) Nonlinear temperature effects indicate severe damages to US crop yields under climate change. *Proc Natl Acad Sci USA* **106**: 15594–15598.

Schlosser A, Pipkorn R, Bossemeyer D, Lehmann WD (2001) Analysis of protein phosphorylation by a combination of elastase digestion and neutral loss tandem mass spectrometry. *Anal Chem* **73**: 170–176.

Schmitt MR and Edwards GE (1981) Photosynthetic capacity and nitrogen use efficiency of maize, wheat, and rice: a comparison between C_3 and C_4 photosynthesis. *J Exp Bot* **32**: 459–466.

Schulze S, Mallmann J, Burscheidt J, Koczor M, Streubel M, Bauwe H, Gowik U, Westhoff P (2013) Evolution of C_4 photosynthesis in the genus *Flaveria*: establishment of a photorespiratory CO_2 pump. *The Plant Cell* **25**: 2522–2535.

Schürmann P and Buchanan BB (2008) The ferredoxin/thioredoxin system of oxygenic photosynthesis. *Antioxid Redox Signal* **10**: 1235–1274.

Schweppe RE, Haydon CE, Lewis TS, Resing KA, Ahn NG (2003) The characterization of protein post-translational modifications by mass spectrometry. *Acc Chem Res* **36**: 453–461.

Scrutton NS, Berry A, Perham RN (1990) Redesign of the coenzyme specificity of a dehydrogenase by protein engineering. *Nature* **343**: 38–43.

Searles PS and Bloom AJ (2003) Nitrate photo-assimilation in tomato leaves under short-term exposure to elevated carbon dioxide and low oxygen. *Plant Cell Environ* **26**: 1247–1255.

Seemann JR, Badger MR, Berry JA (1984) Variations in the specific activity of ribulose-1, 5-bisphosphate carboxylase between species utilizing differing photosynthetic pathways. *Plant Physiol* **74**: 791–794.

Seo J and Lee KJ (2004) Post-translational modifications and their biological functions: proteomic analysis and systematic approaches. *J Biochem Mol Biol* **37**: 35–44.

Shane MW, Fedosejevs ET, Plaxton WC (2013) Reciprocal control of anaplerotic phospho*enol*pyruvate carboxylase by *in vivo* monoubiquitination and phosphorylation in developing proteoid roots of phosphate-deficient harsh hakea. *Plant Physiol* **161**: 1634–1644.

Sharkey TD (1988) Estimating the rate of photorespiration in leaves. *Physiol Plant* **73**: 147–152.

Sheehy JE, Ferrer AB, Mitchell PL, Elmido-Mabilangan A, Pablico P, Dionora MJA (2008) How the rice crop works and why it needs a new engine. *In* Sheehy, JE, Mitchell, PL, Hardy, B, eds, *Charting New Pathways to C_4 Rice*. Singapore: World Scientific Publishing, 3–26.

Sheen J (1999) C_4 gene expression. *Annu Rev Plant Biol* **50**: 187–217.

Shirahashi K, Hayakawa S, Sugiyama T (1978) Cold lability of pyruvate, orthophosphate dikinase in the maize leaf. *Plant Physiol* **62**: 826–830.

Sinha NR and Kellogg EA (1996) Parallelism and diversity in multiple origins of C_4 photosynthesis in the grass family. *Am J Bot* 1458–1470.

Slack CR (1968) The photoactivation of a phosphopyruvate synthase in leaves of *Amaranthus palmeri*. *Biochem Biophys Res Commun* **30**: 483–488.

Slack CR, Hatch MD, Goodchild DJ (1969) Distribution of enzymes in mesophyll and parenchyma-sheath chloroplasts of maize leaves in relation to the C_4-dicarboxylic acid pathway of photosynthesis. *Biochem J* **114**: 489–498.

Smart DR, Ritchie K, Bloom AJ, Bugbee BB (1998) Nitrogen balance for wheat canopies (*Triticum aestivum* cv. Veery 10) grown under elevated and ambient CO_2 concentrations. *Plant Cell Environ* **21**: 753–763.

Solari FA, Dell'Aica M, Sickmann A, Zahedi RP (2015) Why phosphoproteomics is still a challenge. *Mol BioSyst* **11**: 1487–1493.

Sommer M, Bräutigam A, Weber APM (2012) The dicotyledonous NAD-malic enzyme C_4 plant *Cleome gynandra* displays age-dependent plasticity of C_4 decarboxylation biochemistry. *Plant Biol* **14**: 621–629.

Steen H, Jebanathirajah JA, Rush J, Morrice N, Kirschner MW (2006) Phosphorylation analysis by mass spectrometry: myths, facts, and the consequences for qualitative and quantitative measurements. *Mol Cell Proteomics* **5**: 172–181.

Stitt M and Heldt HW (1985) Generation and maintenance of concentration gradients between the mesophyll and bundle sheath in maize leaves. *Biochim Biophys Acta* **808**: 400–414.

Stitt M and Schulze D (1994) Does Rubisco control the rate of photosynthesis and plant growth? An exercise in molecular ecophysiology. *Plant Cell Environ* **17**: 465–487.

Stitt M and Zhu XG (2014) The large pools of metabolites involved in intercellular metabolite shuttles in C_4 photosynthesis provide enormous flexibility and robustness in a fluctuating light environment. *Plant Cell Environ* **37**: 1985–1988.

Svensson P, Bläsing OE, Westhoff P (2003) Evolution of C_4 phospho*enol*pyruvate carboxylase. *Arch Biochem Biophys* **414**: 180–188.

Taniguchi M and Sugiyama T (1990) Aspartate aminotransferase from *Eleusine coracana*, a C_4 plant: purification, characterization, and preparation of antibody. *Arch Biochem Biophys* **282**: 427–432.

Tanz SK, Tetu SG, Vella NGF, Ludwig M (2009) Loss of the transit peptide and an increase in gene expression of an ancestral chloroplastic carbonic anhydrase were instrumental in the evolution of the cytosolic C_4 carbonic anhydrase in *Flaveria*. *Plant Physiol* **150**: 1515–1529.

Taus T, Kocher T, Pichler P, Paschke C, Schmidt A, Henrich C, Mechtler K (2011) Universal and confident phosphorylation site localization using phosphoRS. *J Proteome Res* **10**: 5354–5362.

Tausta SL, Coyle HM, Rothermel B, Stiefel V, Nelson T (2002) Maize C_4 and non-C_4 NADP-dependent malic enzymes are encoded by distinct genes derived from a plastid-localized ancestor. *Plant Mol Biol* **50**: 635–652.

Tcherkez GG, Farquhar GD, Andrews TJ (2006) Despite slow catalysis and confused substrate specificity, all ribulose bisphosphate carboxylases may be nearly perfectly optimized. *Proc Natl Acad Sci USA* **103**: 7246–7251.

Thelen JJ, Miernyk JA, Randall DD (2000) Pyruvate dehydrogenase kinase from *Arabidopsis thaliana*: a protein histidine kinase that phosphorylates serine residues. *Biochem J* **349**: 195–201.

Thingholm TE, Jensen ON, Larsen MR (2009) Analytical strategies for phosphoproteomics. *Proteomics* **9**: 1451–1468.

Tholen D, Boom C, Noguchi KO, Ueda S, Katase T, Terashima I (2008) The chloroplast avoidance response decreases internal conductance to CO_2 diffusion in *Arabidopsis thaliana* leaves. *Plant Cell Environ* **31**: 1688–1700.

Tichy A, Salovska B, Rehulka P, Klimentova J, Vavrova J, Stulik J, Hernychova L (2011) Phosphoproteomics: searching for a needle in a haystack. *J Proteomics* **74**: 2786–2797.

Tilman D (1998) The greening of the green revolution. *Nature* **396**: 211–212.

Tilman D, Cassman KG, Matson PA, Naylor R, Polasky S (2002) Agricultural sustainability and intensive production practices. *Nature* **418**: 671–677.

Tokgoz S, Zhang W, Msangi S, Bhandary P (2012) Biofuels and the future of food: competition and complementarities. *Agriculture* **2**: 414–435.

Toney MD (2014) Aspartate aminotransferase: an old dog teaches new tricks. *Arch Biochem Biophys* **544**: 119–127.

Tosens T, Niinemets Ü, Westoby M, Wright IJ (2012) Anatomical basis of variation in mesophyll resistance in eastern Australian sclerophylls: news of a long and winding path. *J Exp Bot* **63**: 5105–5119.

Tovar-Méndez A, Miernyk JA, Randall DD (2003) Regulation of pyruvate dehydrogenase complex activity in plant cells. *Eur J Biochem* **270**: 1043–1049.

Tovar-Méndez A and Muñoz-Clares RA (2001) Kinetics of phospho*enol*pyruvate carboxylase from *Zea mays* leaves at high concentration of substrates. *Biochim Biophys Acta, Protein Struct Mol Enzymol* **1546**: 242–252.

Tsuchida H, Tamai T, Fukayama H, Agarie S, Nomura M, Onodera H, Ono K, Nishizawa Y, Lee BH, Hirose S (2001) High level expression of C_4-specific NADP-malic enzyme in leaves and impairment of photoautotrophic growth in a C_3 plant, rice. *Plant Cell Physiol* **42**: 138–145.

Ueno Y, Hata S, Izui K (1997) Regulatory phosphorylation of plant phospho*enol*pyruvate carboxylase: role of a conserved basic residue upstream of the phosphorylation site. *FEBS Lett* **417**: 57–60.

Ueno Y, Imanari E, Emura J, Yoshizawa-Kumagaye K, Nakajima K, Inami K, Shiba T, Sakakibara H, Sugiyama T, Izui K (2000) Immunological analysis of the phosphorylation state of maize C_4-form phospho*enol*pyruvate carboxylase with specific antibodies raised against a synthetic phosphorylated peptide. *Plant J* **21**: 17–26.

Uhrig RG, She Y-M, Leach CA, Plaxton WC (2008) Regulatory monoubiquitination of phospho*enol*pyruvate carboxylase in germinating castor oil seeds. *J Biol Chem* **283**: 29650–29657.

van Wijk KJ (2001) Challenges and prospects of plant proteomics. *Plant Physiol* **126**: 501–508.

Vasile AJ, Andreea IR, Popescu GH, Elvira N, Marian Z (2016) Implications of agricultural bioenergy crop production and prices in changing the land use paradigm—the case of Romania. *Land Use Policy* **50**: 399–407.

Vidal J and Chollet R (1997) Regulatory phosphorylation of C_4 PEP carboxylase. *Trends Plant Sci* **2**: 230–237.

Villen J and Gygi SP (2008) The SCX/IMAC enrichment approach for global phosphorylation analysis by mass spectrometry. *Nat Protoc* **3**: 1630–1638.

von Caemmerer S (2000) In Biochemical Models of Leaf Photosynthesis. Csiro Publishing, Collingwood, Victoria, Australia.

von Caemmerer S and Evans JR (1991) Determination of the average partial pressure of CO_2 in chloroplasts from leaves of several C_3 plants. *Funct Plant Biol* **18**: 287–305.

von Caemmerer S and Furbank RT (1999) Modelling C_4 photosynthesis. *In* Sage, RF, Monson, RK, eds, *C_4 plant biology*. San Diego, CA, USA: Academic Press, 173–205.

von Caemmerer S and Furbank RT (2003) The C_4 pathway: an efficient CO_2 pump. *Photosynth Res* **77**: 191–207.

Walker GH and Izawa S (1979) Photosynthetic electron transport in isolated maize bundle sheath cells. *Plant Physiol* **63**: 133–138.

Walker JL and Oliver DJ (1986) Glycine decarboxylase multienzyme complex. Purification and partial characterization from pea leaf mitochondria. *J Biol Chem* **261**: 2214–2221.

Walker RP, Acheson RM, Técsi LI, Leegood RC (1997) Phospho*enol*pyruvate carboxykinase in C_4 plants: its role and regulation. *Funct Plant Biol* **24**: 459–468.

Walker RP, Chen ZH, Acheson RM, Leegood RC (2002) Effects of phosphorylation on phospho*enol*pyruvate carboxykinase from the C_4 plant Guinea grass. *Plant Physiol* **128**: 165–172.

Walker RP and Leegood RC (1995) Purification, and phosphorylation *in vivo* and *in vitro*, of phospho*enol*pyruvate carboxykinase from cucumber cotyledons. *FEBS Lett* **362**: 70–74.

Walker RP and Leegood RC (1996) Phosphorylation of phospho*enol*pyruvate carboxykinase in plants. Studies in plants with C_4 photosynthesis and crassulacean acid metabolism and in germinating seeds. *Biochem J* **317**: 653–658.

Wang JL, Klessig DF, Berry JO (1992) Regulation of C_4 gene expression in developing amaranth leaves. *The Plant Cell* **4**: 173–184.

Wang JL, Turgeon R, Carr JP, Berry JO (1993) Carbon sink-to-source transition is coordinated with establishment of cell-specific gene expression in a C_4 plant. *The Plant Cell* **5**: 289–296.

Wang L, Czedik-Eysenberg A, Mertz RA, Si Y, Tohge T, Nunes-Nesi A, Arrivault S, Dedow LK, Bryant DW, Zhou W, Xu J, Weissmann S, Studer A, Li P, Zhang C, LaRue T, Shao Y, Ding Z, Sun Q, Patel RV, Turgeon R, Zhu X, Provart NJ, Mockler TC, Fernie AR, Stitt M, Liu P, Brutnell TP (2014) Comparative analyses of C_4 and C_3 photosynthesis in developing leaves of maize and rice. *Nat Biotechnol* **32**: 1158–1165.

Wang L, Peterson RB, Brutnell TP (2011) Regulatory mechanisms underlying C_4 photosynthesis. *New Phytol* **190**: 9–20.

Wang LH, Li DQ, Fu Y, Wang HP, Zhang JF, Yuan ZF, Sun RX, Zeng R, He SM, Gao W (2007) pFind 2.0: a software package for peptide and protein identification via tandem mass spectrometry. *Rapid Commun Mass Spectrom* **21**: 2985–2991.

Wang Y, Bräutigam A, Weber APM, Zhu XG (2014) Three distinct biochemical subtypes of C_4 photosynthesis? A modelling analysis. *J Exp Bot* **65**: 3567–3578.

Wang YH and Chollet R (1993) *In vitro* phosphorylation of purified tobacco-leaf phospho*enol*pyruvate carboxylase. *FEBS Lett* **328**: 215–218.

Wang YH and Chollet R (1993) Partial purification and characterization of phospho*enol*pyruvate carboxylase protein-serine kinase from illuminated maize leaves. *Arch Biochem Biophys* **304**: 496–502.

Wang YH, Duff SM, Lepiniec L, Crétin C, Sarath G, Condon SA, Vidal J, Gadal P, Chollet R (1992) Site-directed mutagenesis of the phosphorylatable serine (Ser8) in C_4

phospho*enol*pyruvate carboxylase from sorghum. The effect of negative charge at position 8. *J Biol Chem* **267**: 16759–16762.

Weber APM and Bräutigam A (2013) The role of membrane transport in metabolic engineering of plant primary metabolism. *Curr Opin Biotechnol* **24**: 256–262.

Weber APM and von Caemmerer S (2010) Plastid transport and metabolism of C_3 and C_4 plants—comparative analysis and possible biotechnological exploitation. *Curr Opin Plant Biol* **13**: 256–264.

Wedding RT, Black MK, Meyer CR (1990) Inhibition of phospho*enol*pyruvate carboxylase by malate. *Plant Physiol* **92**: 456–461.

Werdan K, Heldt HW, Milovancev M (1975) The role of pH in the regulation of carbon fixation in the chloroplast stroma. Studies on CO_2 fixation in the light and dark. *Biochim Biophys Acta* **396**: 276–292.

Wessinger ME, Edwards GE, Ku MSB (1989) Quantity and kinetic properties of ribulose 1, 5-bisphosphate carboxylase in C_3, C_4, and C_3–C_4 intermediate species of *Flaveria* (Asteraceae). *Plant Cell Physiol* **30**: 665–671.

Wierenga RK, Terpstra P, Hol WGJ (1986) Prediction of the occurrence of the ADP-binding *βαβ*-fold in proteins, using an amino acid sequence fingerprint. *J Mol Biol* **187**: 101–107.

Wiese S, Reidegeld KA, Meyer HE, Warscheid B (2007) Protein labeling by iTRAQ: a new tool for quantitative mass spectrometry in proteome research. *Proteomics* **7**: 340–350.

Wilkie SE and Warren MJ (1998) Recombinant expression, purification, and characterization of three isoenzymes of aspartate aminotransferase from *Arabidopsis thaliana*. *Protein Expr Purif* **12**: 381–389.

Wilkins MB (1992) Circadian rhythms: their origin and control. *New Phytol* **121**: 347–375.

Williams BP, Johnston IG, Covshoff S, Hibberd JM (2013) Phenotypic landscape inference reveals multiple evolutionary paths to C_4 photosynthesis. *eLife* **2**: e00961.

Williamson BL, Marchese J, Morrice NA (2006) Automated identification and quantification of protein phosphorylation sites by LC/MS on a hybrid triple quadrupole linear ion trap mass spectrometer. *Mol Cell Proteomics* **5**: 337–346.

Wingler A, Walker RP, Chen ZH, Leegood RC (1999) Phospho*enol*pyruvate carboxykinase is involved in the decarboxylation of aspartate in the bundle sheath of maize. *Plant Physiol* **120**: 539–546.

Woo KC, Anderson JM, Boardman NK, Downton WJS, Osmond CB, Thorne SW (1970) Deficient photosystem II in agranal bundle sheath chloroplasts of C_4 plants. *Proc Natl Acad Sci USA* **67**: 18–25.

Woodward FI (2002) Potential impacts of global elevated CO_2 concentrations on plants. *Curr Opin Plant Biol* **5**: 207–211.

Wyrich R, Dressen U, Brockmann S, Streubel M, Chang C, Qiang D, Paterson AH, Westhoff P (1998) The molecular basis of C_4 photosynthesis in *Sorghum*: isolation, characterization and RFLP mapping of mesophyll-and bundle-sheath-specific cDNAs obtained by differential screening. *Plant Mol Biol* **37**: 319–335.

Yang Z, Zhang H, Hung HC, Kuo CC, Tsai LC, Yuan HS, Chou WY, Chang GG, Tong L (2002) Structural studies of the pigeon cytosolic $NADP^+$-dependent malic enzyme. *Protein Sci* **11**: 332–341.

Ye J, Zhang Z, You C, Zhang X, Lu J, Ma H (2016) Abundant protein phosphorylation potentially regulates *Arabidopsis* anther development. *J Exp Bot* **67**: 4993–5008.

Yerramsetty P, Agar EM, Yim WC, Cushman JC, Berry JO (2017) An *rbc*L mRNA-binding protein is associated with C_3 to C_4 evolution and light-induced production of Rubisco in *Flaveria*. *J Exp Bot* **68**: 4635–4649.

Zelitch I (1968) Investigation on photorespiration with a sensitive ^{14}C-assay. *Plant Physiol* **43**: 1829–1837.

Zelitch I, Schultes NP, Peterson RB, Brown P, Brutnell TP (2009) High glycolate oxidase activity is required for survival of maize in normal air. *Plant Physiol* **149**: 195–204.

Zhang E, Brewer JM, Minor W, Carreira LA, Lebioda L (1997) Mechanism of enolase: the crystal structure of asymmetric dimer enolase− 2-phospho-D-glycerate/enolase −phosphoenolpyruvate at 2.0 Å resolution. *Biochemistry* **36**: 12526–12534.

Zhang G and Neubert TA (2009) Use of stable isotope labeling by amino acids in cell culture (SILAC) for phosphotyrosine protein identification and quantitation. *In* Graauw, M, ed, *Phospho-Proteomics. Methods in Molecular Biology*, Vol 527: Humana Press, 79–92.

Zhang XQ and Chollet R (1997) Phospho*enol*pyruvate carboxylase protein kinase from soybean root nodules: partial purification, characterization, and up/down-regulation by photosynthate supply from the shoots. *Arch Biochem Biophys* **343**: 260–268.

Zhang Y, Fonslow BR, Shan B, Baek MC, Yates JR (2013) Protein analysis by shotgun/bottom-up proteomics. *Chem Rev* **113**: 2343–2394.

Zhao Y and Jensen ON (2009) Modification-specific proteomics: strategies for characterization of post-translational modifications using enrichment techniques. *Proteomics* **9**: 4632–4641.

Zhu XG, Long SP, Ort DR (2010) Improving photosynthetic efficiency for greater yield. *Annu Rev Plant Biol* **61**: 235–261.

Ziska LH and Bunce JA (1997) Influence of increasing carbon dioxide concentration on the photosynthetic and growth stimulation of selected C_4 crops and weeds. *Photosynth Res* **54**: 199–208.

Appendix A

Putative phosphorylation sites identified in darkened and illuminated leaves of *Setaria viridis*.

Phosphorylation sites identified in darkened and illuminated leaves of *Setaria viridis* by tandem mass spectrometry. Peptide spectra were searched against NCBI and UniProtKB plant protein sequences using MASCOT (Table A) and SEQUEST (Table B). Phosphorylations were determined using PhosphoRS. Phosphorylation site localisation probabilities ($P > 0.75$ is significant) are indicated in parentheses to the right of the modified amino acid. Phosphopeptide significance is measured against an *E*-value (MASCOT) and Xcorr (SEQUEST), where *E*-value ≤ 0.05 or Xcorr ≥ 2.15, is significant. *Reoccurring phosphorylation sites; **phosphorylations identified by phosphopeptide enrichment. Time-points (TP): TP2, 7.5 h into the dark (shaded); TP3, 4 h into the light; TP4, 15.5 h into the light.

Table A. Proteins identified using MASCOT.

Protein	Accession	Coverage (%)	Phosphopeptide	Position in peptide	MH^+ (Da)	Monoisotopic mass (Da)	*E*-value	TP
PEPC	526117397	56.43	HHS(1)IDAQLR	Ser-3**	1156.53	1075.54	0.25786	TP3
PEPC	P04711	18.35	HHS(1)IDAQLR	Ser-3*	1156.53	1075.54	0.00432	TP3
PPDK	514750542	60.53	GGMT(1)SHAAVVAR	Thr-4**	1252.55	1155.57	0.00011	TP2
PPDK	Q6AVA8	23.97	GGMT(1)SHAAVVAR	Thr-4*	1252.55	1155.57	2.47E-06	TP2
PPDK	514750542	60.53	GGMT(0.98)S(0.02)HAAVVAR	Thr-4*	1236.56	1155.57	0.00005	TP2
PPDK	Q6AVA8	23.97	GGMT(0.98)S(0.02)HAAVVAR	Thr-4*	1236.56	1155.57	7.93E-07	TP2
PPDK	514750542	62.55	GGMT(0.97)S(0.02)HAAVVAR	Thr-4*	1236.56	1155.57	0.00865	TP3
PPDK	P11155	20.49	GGMT(1)SHAAVVAR	Thr-4*	1236.56	1155.57	0.00009	TP3

Table B. Proteins identified using SEQUEST.

Protein	Accession	Coverage (%)	Phosphopeptide	Position in sequence	MH^+ (Da)	Monoisotopic mass (Da)	Xcorr	TP
PGM	K3XFX0	51.79	S(0.92)GGIQILT(0.69)S(0.69)HT(0.69)LQPVPVAIGGPGLHPGV	S520*; T527*, S528 or T530	3373.65	3132.75	2.27	TP2
PGM	K3XFX0	84.16	AHGTAVGLPSDDDMGNS(1)EVGHNALGAGR	S109**	2785.21	2704.22	4.39	TP3
PGM	K3XFX0	79.05	AHGTAVGLPSDDDMGNS(1)EVGHNALGAGR	S109*	2801.20	2704.22	3.63	TP4
			AGKPLLDKS(0.96)GGIQILT(0.88)S(0.57)HT(0.57)LQPVPVAIG	S520*; T527*; S528 or T530	3934.99	3652.07	1.58	TP4
AlaAT	K3ZSX0	72.80	LLEAT(0.5)GIS(0.5)T(0.5)VPGS(0.5)GFGQKEGVFHLR	T424 or T428; S427 or S432	2760.31	2599.37	2.08	TP2
			KVLFDMGPPLSREVQLVS(0.91)FHT(53.9)VS(0.53)K	S285; T288 or S290*	2916.42	2713.45	2.56	TP2
			TVAEARS(0.94)KGITVR	S206*	1509.77	1386.78	2.67	TP2
AlaAT	K3ZSX0	79.50	VAS(0.88)IALS(0.24)PNVPGQIFMGVMVNPPKPGDIS(0.64)YLK	S322 or S326; S348	4149.03	3972.08	2.81	TP3
			LLEAT(0.5)GIS(0.5)T(0.5)VPGS(0.5)GFGQKEGVFHLR	T424 or T428; S427 or S432	2760.31	2599.37	2.75	TP3
			VLFDMGPPLSREVQLVSFHT(0.75)VS(0.75)K	T288; S290*	2746.32	2585.36	1.75	TP3
AlaAT	K3ZSX0	71.34	VAS(0.99)IALS(0.98)PNVPGQIFMGVMVNPPKPGDISYLKFAA	S322; S326	4149.04	3972.08	2.38	TP4
			TVAEARS(0.99)KGITVR	S206*	1509.78	1386.78	1.95	TP4
			IIFTNVGNPHALGQKPLT(0.96)FPR	T57	2442.27	2319.27	2.75	TP4
AlaAT	K4A868	64.44	AT(0.07)GAYS(0.46)HS(0.46)QG	T167*; S171 or	1667.80	1544.80	1.62	TP2
			AT(0.9)GAYSHSQGIKGLRDAIAAGIAS(1)R	T167*; S189*	2673.25	2470.29	3.33	TP2
AlaAT	K4A868	66.48	AT(0.92)GAYSHSQGIKGLRDAIAAGIAS	T167*; S189*	2673.26	2470.29	3.13	TP3
			SSDRFLFLFAMAAS(0.93)VAVE	S62	3005.52	2866.53	2.05	TP3

Protein	Accession	Coverage (%)	Phosphopeptide	Position in sequence	MH^+ (Da)	Monoisotopic mass (Da)	Xcorr	TP
AlaAT	K4A868	60.00	AT(0.92)GAYSHSQGIKGLRDAIAAGIAS(1)R	T167*; S189*	2673.25	2470.29	3.03	TP4
			DGFPANADDIFIT(1)DGAS(1)PGVHLMMQLLIR	T203; S207	3306.45	3113.52	3.08	TP4
AlaAT	K4A8B1	12.83	AT(0.93)GAYSHSQGIKGLRDAIAAGIAS(1)R	T167*; S189*	2673.25	2470.29	3.40	TP3
AAT	K3XHJ0	45.22	IISMRQQLFDALKS(0.86)R	S391	1901.96	1804.99	2.24	TP2
AAT	K3YSB2	76.20	KHMPFFDVAYQGFAS(0.48)GS(0.48)LDEDAFSVRLFVK	S275 or S277	3488.62	3407.65	2.58	TP2
			MAS(0.53)T(0.53)AAFAVS(0.81)S(0.77)PAASAVAARSKVHGGGK	S3 or T4; S10; S11	2827.24	2586.32	2.48	TP2
			SQLKRLARPMYS(0.98)NPPIHG	S341	2372.22	2291.23	2.08	TP2
AAT	K3YSB2	74.45	RGMEVFVAQS(0.98)YSKNLGLY	S300	2514.18	2433.20	2.53	TP3
AAT	K3YSM6	53.27	IAGNLNMEYLPMGGS(1)IK	S99	1887.87	1806.89	2.31	TP2
AAT	K3Z6L1	43.61	LGYLAAPKHFVS(0.99)ACGKIQS(0.75)QYTSGASSISQK	S266; S273	3486.62	3226.63	2.71	TP2
AAT	K3Z6L1	51.57	IS(0.55)YAAAMS(0.55)T(0.97)LQT(0.91)AMEKIKEAMALLRPPV	S387 or T393; T394; T397	3486.62	3203.70	2.23	TP4
AAT	K4AG31	68.75	LVVEAAT(1)S(1)VFQK	T22; S23	1493.67	1290.71	1.70	TP4
Enolase	K3XWW9	83.18	QKLGANAILAVS(1)LAVCKAGAMVK	S121*	2393.27	2255.28	2.83	TP2
Enolase	K3XWW9	80.49	LGANAILAVS(1)LAVCKAGAMV	S121*	2153.11	1999.12	1.52	TP3
Enolase	K3XWW9	55.16	LTDEIGQQVQIVGDDLLVT(0.99)NPT(1)RVAK	T334; T337	2982.47	2821.51	1.00	TP4
Enolase	K3Z681	75.06	QLVLPVPAFNVINGGSHAGNK	T179 or S183	4507.29	4442.29	4.71	TP2
			LAMQEFMILPT(0.45)GASS(0.45					
			LGANAILAVS(1)LAVCKAGAS(	S120*; S129*	2357.21	2097.22	1.55	TP2
Enolase	K3Z681	44.49	LGANAILAVS(1)LAVCKAGAS(	S120*; S129*	2357.20	2097.22	3.25	TP3
Enolase	K3Z681	66.97	LGANAILAVS(0.99)LAVCKAGA	S120*	2235.23	2097.22	2.08	TP3

Protein	Accession	Coverage (%)	Phosphopeptide	Position in sequence	MH^+ (Da)	Monoisotopic mass (Da)	Xcorr	TP
NADP-ME	K3XFH6	88.26	VWLVDSKGLIVSS(0.99)R	S429*	1638.86	1557.88	2.07	TP3
			LALYT(0.89)ALGGVRPS(0.6)ACLPIT(0.6)IDVGT(0.89)NNEELL	T263*; T282*; S271 or T277	4816.29	4476.33	3.05	TP3
NADP-ME	K3XFH6	90.77	QKVWLVDSKGLIVSS(0.67)R	S429*	1895.01	1814.03	2.37	TP4
			LALYT(0.71)ALGGVRPS(0.84)ACLPIT(0.71)IDVGT(0.71)NNEE	T263*; T282*; S271 or T277	4816.29	4476.33	3.53	TP4
			SHLVFNDDIQGTAS(0.96)VVLAGLLAS(0.96)LK	S360; S369	2802.30	2567.39	1.92	TP4
NADP-ME	K3XFW4	38.14	IWLVDS(1)KGLIVS(1)S(1)RK	S373*, S379*; S380*	1982.91	1699.99	0.85	TP2
NADP-ME	K3XFW4	69.83	GLIYPPFS(1)NIRKIS(1)AHIA	S541; S547	2711.37	2550.43	3.20	TP4
NADP-ME	K3XFW4	69.83	LLGGTLADHTFLFLGAGEAGTGIAELIALEIS(0.9)R	S354	3448.77	3325.78	3.60	TP4
NADP-ME	K3XG11	78.36	KIS(1)AHIAAAVAAKAYELGLA	S530; T548	2385.20	2224.26	2.39	TP2
			VWLVDSKGLIVS(0.5)S(0.5)R	S362 or S363	1638.86	1557.88	1.96	TP2
NADP-ME	K3ZRI5	37.40	IVVAGAGSAGIGVVNAAS(0.99)K	S357	1748.91	1667.92	1.59	TP3
			T(1)YRMFNDDVQGT(1)AGVAIAGLLGAVR	T302; T313	2925.36	2722.41	1.40	TP3
			KVKPDVILGLS(1)AVGGLFS(1)KEVLEALK	S435*; S442*	2912.55	2709.59	1.76	TP3
			RS(100.0)LAPDRLR	S11	1205.62	1082.62	1.38	TP3
NADP-ME	K3ZRI5	42.86	RLHLLLS(1)QHPREYVT(1)AECHRPVVLHK	S25; T33	3348.68	3130.70	2.68	TP4
			VKPDVILGLS(1)AVGGLFS(1)K	S435*; S442*	2742.46	2581.50	2.80	TP4
PEPC	K3XV32	88.69	FTAATLEHGMHPPVS(1)PKPEWS(1)LLQKHARIR	S702**	2484.16	2387.17	2.57	TP2
				S180*	1301.72	1220.74	0.71	TP2
			RLVT(0.5)ELGKS(0.5)K	T147 or S152	1210.66	1129.67	1.06	TP2
			LNIGS(1)RPAKR	S752	1191.64	1110.65	2.17	TP2

Protein	Accession	Coverage (%)	Phosphopeptide	Position in sequence	MH^+ (Da)	Monoisotopic mass (Da)	Xcorr	TP
PEPC	K3XV32	92.22	HHS(1)IDAQLR	S11**	1156.52	1075.54	1.28	TP3
			FTAATLEHGMHPPVS(1)PKPEW	S702**	2468.16	2387.17	2.16	TP3
PEPC	K3XV32	94.81	HHS(1)IDAQLR	S11**	1156.83	1075.54	2.24	TP4
			LLAPGKVS(1)EDDK	S25**	1393.66	1270.67	2.31	TP4
			RS(1)LLQKHAR	S180*	1230.65	1107.65	2.08	TP4
			VVLGYVRDKLYS(1)T(1)R	S378; T379	1828.88	1667.93	1.94	TP4
PEPC-2	K3YPN6	43.52	GGGPTHLAILSQPPDT(0.92)IH	T658	2346.16	2223.17	2.41	TP4
			LLAPGKVS(1)EDDK	S26**	1393.66	1270.67	2.31	TP4
			VT(1)LDLLEMVFAKGDPGIAAV	S820	2561.26	2464.28	1.97	TP4
PPDK	K3Z3Q6	46.03	GGMT(1)SHAAVVAR	T462**	1236.56	1155.57	3.33	TP2
	K3Z3Q6	87.07	GGMT(0.98)SHAAVVAR	T462**	1236.55	1155.57	2.31	TP2
PPDK			S(0.33)GAAVS(0.46)MPGMMDT(0	S104; T109 or	3510.52	3317.60	2.90	TP2
			.6)VLNLGLNDEVAAGLGAKS(0.	S134				
			AVRQMIMAPT(1)LELR	T593	1724.85	1627.88	1.68	TP2
			MVEPGHLDQLLHPQFENPS(1)A	S394	2646.19	2549.23	1.89	TP2
PPDK	K3Z3Q6	58.96	GGMT(1)SHAAVVAR	T462**	1236.55	1155.57	4.24	TP3
PPDK	K3Z3Q6	43.88	GGMT(1)SHAAVVAR	T462**	1236.56	1155.57	3.08	TP3
PPDK	K3Z3Q6	88.55	QLKVLANADTPEDALT(0.99)AR	T557	2005.99	1925.01	1.96	TP3
			GGMT(0.99)SHAAVVAR	T462**	1236.56	1155.57	2.71	TP3
PPDK	K3Z3Q6	91.16	GGMT(0.99)SHAAVVAR	T462**	1236.56	1155.57	2.99	TP4
			AIFEAAIAMT(0.88)NQGVQVFP	T704; T721	5586.83	5393.88	3.47	TP4
			EIMVPLVGT(0.88)PQELGNQVA					
			VFAALGKTIDYKIGT(0.89)MIE	T753**	2416.26	2335.29	3.19	TP4

Appendix B

Measuring chlorophyll content.

To normalise protein samples, chlorophyll content from harvested leaf sections was determined. Chlorophyll assays were performed following Arnon (1949) and Leegood (1993). 1.28 cm^2 leaf sections were placed in a test tube and submerged in 3 mL 80% (v/v) ethanol, and incubated in the dark at 70 °C for 35 min. Extra time was added to allow complete leaf bleaching. Chlorophyll content was determined spectrophotometrically at A_{652}. The instrument was blanked at A_{750} to correct for sample turbidity (Ritchie, 2006). Chlorophyll content was determined in 80% ethanol was calculated using equation A,

$$\text{Chl } a = A_{652} \times 27.8 \qquad \text{(A)}$$

To extract in 80% acetone, leaf tissue was ground to a fine powder in a liquid nitrogen chilled mortar and homogenised in 1 mL 80% chilled acetone. Plant lysate was transferred to an Eppendorf and centrifuged at high speed at 4 °C. Supernatant was collected into a light impermeable glass vial and placed on ice. The remaining pellet was further washed with acetone until completely bleached; the total volume per chlorophyll extract did not exceed 3.5 mL. Glass vials were removed from ice and let to equilibrate at room temperature before measuring chlorophyll. Chlorophyll *a* in 80% acetone was quantified spectrophotometrically at A_{652} and content in mg L^{-1} was determined using equation B,

$$\text{Chl } a \text{ mg L}^{-1} = \frac{A_{652} \times 1000}{34.5} \qquad \text{(B)}$$

NB. Protein extracts were normalised against the lowest whole protein concentration.